Manipulation of host nuclear function by Chlamydia trachomatis

Manipulation of host nuclear function by *Chlamydia trachomatis*

Oliver WF Martin

Institute of Structural and Molecular Biology,

Birkbeck, University of London

A thesis submitted for the degree of Doctor of Philosophy

August 2016

Declaration

I, Oliver Martin, declare that this thesis has been written by myself, and the work contained herein is my own except where explicitly stated otherwise in the text.

Abstract

Chlamydia trachomatis is an obligate intracellular bacterium, responsible for the most prevalent bacterial sexually transmitted infection and is the leading cause of acquired blindness worldwide. *Chlamydiae* survive and replicate within a specialised intracellular membrane-bound compartment known as the inclusion. Inclusion biogenesis requires manipulation of host processes by translocated bacterial effectors. Despite *Chlamydia* targeting at least one effector into the nucleus, surprisingly little is known about how and why the bacteria interact with this major organelle. The aim of the work presented in this thesis was to examine the consequences of *Chlamydia* infection on nuclear architecture, organisation and function.

Structurally, nuclei of cells infected with *C. trachomatis* become highly lobulated, reminiscent of both laminopathy and transformed cells. Analysis of the nuclear lamina (NL) demonstrated that lamin A/C is enriched at the inclusion-proximal face of the nuclear envelope (NE) and depleted elsewhere around the nuclear periphery. Lamin B is reduced and nuclear pore complexes (NPCs) are depleted in the inclusion-proximal lamin A/C-enriched region. Other NL scaffolding proteins including SUN proteins and emerin are unaffected. Transmission electron microscopy revealed a minimal distance of ~100 nm is maintained between the NE and inclusion membrane (IM), showing a classical membrane contact site does not form. Lamin A/C enrichment and NPC depletion occur independently of existing cellular NPC-free islands present in the NE, and are specific to *C. trachomatis* rather than *C. muridarum*.

Functionally, these infection-associated NE alterations are promoted by bacterial factors and can recover following induced bacterial killing or inclusion clearance. Host nuclear protein transport ceases in the NPC-depleted region, whereas host nuclear mRNA distribution is unaffected. Associated local changes in host chromatin architecture occur, since heterochromatin accumulates at the inclusion-proximal face of the nuclear periphery at NPC-depleted and lamin A/C-enriched zones. Lamin A/C changes are the driving force behind the NE modifications, as the NPC-depletion and heterochromatin accumulation is absent when cells lacking lamin A/C are infected with *C. trachomatis*. Remarkably, in these knockout cells, inclusions are larger and more bacterial progeny are produced.

Computationally, chlamydial proteins of unknown function that may be translocated to the nucleus or NE were identified. A tool was developed to generate a consensus secondary sequence from multiple available prediction software. Using this tool, the chlamydial proteome was searched for proteins similar in secondary structure to known cellular NE or NE-interacting proteins. Three proteins were identified, of which CT350 and CT384 are predicted to be type III secretion substrates. When ectopically expressed in HeLa cells, CT384 localised to the nucleus and resulted in aberrant nuclear architecture.

Taken together, the data demonstrate that *Chlamydia* profoundly manipulates nuclear architecture from within the inclusion, and via interactions at the inclusion-proximal region of the NE constructs a lamin A/C-enriched platform to drive localised redistribution of heterochromatin and changes in host gene expression.

Acknowledgements

Firstly thank you to my PhD supervisor, Dr. Richard Hayward. Your guidance and support has been invaluable throughout and your tireless commitment to ensuring I produce the best work I can, whilst under-appreciated at the time, has made me a better scientist and person. I wish you and everyone in the lab all the best for the future.

I thank Dr. Maud Dumoux, you are nothing short of one of the best people I have ever met, and I have no doubt I would not have reached this point without you. Thank you for always making time to answer questions for me, provide guidance and give pep talks. You have consistently gone above and beyond for me and everyone in the lab, to which I will always be grateful. You have made Hawkeye my favourite avenger.

To Charlotte and Ellie, you have been the best friends I could ask for and I am so thankful to have been in the lab and gone through it all with you guys. My best memories of this time will always be the sneaky coffee breaks (sorry Richard…), gossip, 'gates' and drinks that we have shared, and it just wouldn't have been as great without you both.

Thanks also go to all the other members of the Hayward lab who have come and gone throughout, especially Dr. Andrea Nans for inducting me into electron microscopy and for her thoughtful input.

Thank you to my second supervisor Dr. Maya Topf for your ideas, expertise and advice, and thank you to the Topf group for your support and help in turning an experimental biologist into, at least a partial, computational biologist.

Thank you to my thesis chair, Dr. Andy Osborne, for helping keep me on the right track and for your constructive criticism. I also thank the MRC for the opportunity and funding to make this PhD possible, and all the staff and students of the ISMB for making this such a friendly environment to work.

To Anna, thank you for always keeping me going, words can never express how much you mean to me and how thankful I am that you are always supporting me by my side. From the cups of tea to the endless encouragement, I don't know where I'd be without you.

Finally, I would like to thank my friends and family for their support and motivation, for those that are here at the end, and for the one who will forever be sorely missed.

Table of contents

List of Figures

List of Tables and Appendices

List of Abbreviations

53BP1	53 binding protein 1
Aac	Amino acid composition
ARM	Armadillo repeat
BAF	Barrier-to-autointegration factor
BAHD1	Bromo adjacent homology domain-containing protein 1
BSA	Bovine serum albumin
CEP170	Centrosomal protein 170 kDa
CERT	Ceramide transfer protein
CFTR	Cystic fibrosis transmembrane conductance regulator
cIAP-2	Cellular inhibitor of apoptosis protein 2
COMC	Chlamydial outer membrane complex
CPAF	Chlamydial protease-like activity factor
CTD	C-terminal domain
DEPC	Diethylpyrocarbonate
Derlin-1	Der1-like protein 1
DTT	Dithiothreitol
DMEM	Dulbecco's modified eagle medium
DMSO	Dimethyl sulphoxide
DP-1	Deleted in polyposis 1
DRAQ-5	1,5-bis{[2-(di-methylamino)ethyl]amino}-4,8-dihydroxyanthracene-9,10-dione
EB	Elementary body
EDMD	Emery-Dreifuss muscular dystrophy
EDTA	Ethylenediaminetetraacetic acid
ER	Endoplasmic reticulum
F-actin	Filamentous actin
FCS	Foetal calf serum
FG	Phenylalanine glycine
FISH	Fluorescent *in-situ* hybridisation
FOV	Field of view
FS	Freeze-substitution
GAG	Glycosaminoglycan
GEF	Guanine nucleotide exchange factor
H3K4	Histone 3 lysine 4
H3K9	Histone 3 lysine 9
HBSS	Hank's balanced salt solution
HCMV	Human cytomegalovirus
HEPES	4-(2-hydroxyethyl)-1-piperazineethanesulfonic acid
HGPS	Hutchinson-Gilford progeria syndrome
HMGB1	High-mobility group box 1
HMM	Hidden Markov model
HP1	Heterochromatin protein 1
hpi	Hours post infection
hTERT	Human telomerase reverse transcriptase
IFNγ	Interferon gamma
IFU	Inclusion forming unit
IM	Inclusion membrane
Inc	Inclusion membrane protein
INM	Inner nuclear membrane

IPAM	Inclusion protein acting on microtubules
KASH	Klarischt, ANC-1, and Syne homology
kDa	Kilodaltons
LAD	Lamina-associated domain
LAP2α	Lamina-associated polypeptide 2α
LBPA	Lysobisphosphatidic acid
LBR	Lamin B receptor
LC3	Light chain 3
LD	Lipid droplet
Lda	LD-associated
LEM	LAP2-emerin-MAN1
LGV	Lymphogranuloma venereum
LINC	Linker of nucleoskeleton and cytoskeleton
LntA	*Listeria* nuclear targeted protein A
LPS	Lipopolysaccharide
MAP1	Microtubule-associated protein 1
MAPK	Mitogen-activated protein kinase
MC	Membrane coat-like
MCS	Membrane contact site
MDM2	Murine double minute 2
MeCP2	Methyl CpG binding protein 2
MEF	Mouse embryonic fibroblast
MEM	Minimal essential medium
MHC	Major histocompatibility complex
MKL	Megakaryoblastic acute leukaemia factor-1
MLN64	Metastatic lymph node 64
Mlp1	Myosin-like protein 1
MOMP	Major outer membrane protein
MSA	Multiple sequence alignment
MTOC	Microtubule-organising centre
mTOR	Mammalian target of rapamycin
MVB	Multivesicular body
MYPT1	Myosin light chain 2 phosphatase
NE	Nuclear envelope
NL	Nuclear lamina
NLS	Nuclear localisation sequence
NOR	Nucleolar organiser region
NPC	Nuclear pore complex
NTD	N-terminal domain
NTR	Nuclear transport receptor
NUE	Nuclear effector protein
Nup	Nucleoporin
NXF1	Nuclear export factor 1
ONM	Outer nuclear membrane
ORF	Open reading frame
P/S	Penicillin/streptomycin
PAMP	Pathogen-associated molecular pattern
PARP-1	Poly(ADP-ribose) polymerase 1
pATM	Protein kinase ataxia telangiectasia mutated
PBS	Phosphate buffered saline
PcG	Polycomb group
PDGFR	Platelet derived growth factor receptor

PDI	Protein disulphide isomerase
PFA	Paraformaldehyde
PFI	Pore-free Island
pG	Penicillin G
PMA	Phorbol myristate acetate
PML	Promyelocytic leukaemia protein
Pmp	Polymorphic membrane protein
pRb	Retinoblastoma protein
PRC	Polycomb repressive complex
PRR	Pattern recognition receptor
RB	Reticulate body
rER	Rough endoplasmic reticulum
ROI	Region of interest
RPE-1	Retinal pigment epithelial cell
RT	Room temperature
SDS	Sodium dodecyl sulphate
SET	Su(var)3-9, Enhancer-of-zeste, Trithorax
SINC	Secreted inner nuclear membrane-associated *Chlamydia* protein
SIRT2	Sirtuin 2
Slc1	SycE-like chaperone 1
snRNP	Small ribonucleoprotein
SPG	Sucrose-phosphate-glutamic acid
SSC	Saline-sodium citrate
SSE	Secondary structure element
SNX	Sorting nexin
SUN	Sas1, UNC-84
T2S	Type II secretion
T3S	Type III secretion
Tarp	Translocated actin recruiting protein
Tat	Twin-arginine translocation
TCA	Tricarboxylic acid
THP-1	Human acute monocytic leukaemia cell
TLR	Toll-like receptor
Tpr	Translocated promoter region
WT	Wildtype

Chapter 1 – Introduction

1.1 *Chlamydia*

1.1.1 History and taxonomy

The *Chlamydiaceae* are a family of bacteria belonging to the *Chlamydiae* phylum that in turn consists of two genera, *Chlamydia* and *Chlamydophila,* whose members are obligate intracellular pathogens that infect vertebrates causing disease. Due in part to their biphasic lifecycle and obligate intracellular development, the taxonomy of the *Chlamydiaceae* has been difficult to define and remains controversial to the present day. Chlamydial organisms from trachoma patients were first described in 1907 as protozoa by Halberstaedter and von Prowazek, in what unknowingly became the first description of *Chlamydia trachomatis* (reviewed in Nunes and Gomes, 2014). *Chlamydophila psittaci* was then identified in 1930 after a worldwide pandemic of human psittacosis (Coles, 1930). However, *C. psittaci*, together with the causative agent of lymphogranuloma venereum (LGV), were incorrectly classified as viruses of the psittacosis-LGV as they could not grow on artificial media, and were not blocked by bacterial filters (reviewed in Nunes and Gomes, 2014). The trachoma causing agents were linked to the psittacosis-LGV viruses in 1942 by the discovery of a common (group) antigen (Rake, 1942). However it was not until 1966 that these organisms were classified as bacteria (Moulder, 1966), after studies showed they replicate by binary fission (Bedson and Gostling, 1954), and have cell envelopes comparable in structure to Gram-negative bacteria (Armstrong and Reed, 1964; Moulder, 1966).

Similarities in the morphology and lifecycle of these chlamydial organisms led to the creation of the genus *Chlamydia*. Within the genus, LGV and trachoma organisms were classified as *Chlamydia trachomatis*, and psittacosis organisms as *Chlamydia psittaci*, separated based on morphological and phenotypic differences. For example, *C. trachomatis* accumulates glycogen (Gordon and Quan, 1965) and is sensitive to sulphadiazine (Lin and Moulder, 1966), which is not the case for *C. psittaci*. Furthermore, *C. psittaci* propagates within multiple irregularly shaped compartments termed inclusions, whilst *C. trachomatis* propagates within a single spherical inclusion. The genus was further refined using DNA-based classification. Techniques such as DNA-DNA hybridisation and restriction endonuclease analysis led to the assignment of

new species into the *Chlamydia* genus such as *Chlamydia pneumoniae* (Grayston et al., 1989) and *Chlamydia pecorum* (Fukushi and Hirai, 1992). Proposed alterations to the taxonomy were made again in 1999, after phylogenetic analysis of the 16S and 23S ribosomal RNA genes revealed two major lineages of the *Chlamydiaceae*, *C. trachomatis*-like species and non-*C. trachomatis*-like species (Everett et al., 1999). Briefly, the 16S and 23S rRNA gene sequences varied by 4-7% and 7-9% respectively between the genera, whilst within the groups the variation was ≤ 5% and ≤ 3% for *Chlamydia* and *Chlamydophila* respectively (Everett et al., 1999). The *C. trachomatis*-like species remained under the genus *Chlamydia*, and include *C. trachomatis, C. suis* and *C. muridarum*, whilst *C. abortus*, *C. psittaci*, *C. caviae*, *C. felis*, *C. pneumoniae* and *C. pecorum* form the genus *Chlamydophila*. The scientific community remains divided on these proposed changes, with some suggesting that not only are the sequence homology boundaries for genera separation arbitrary, but also that *Chlamydiae* evolution is so divergent from other bacteria, and the *Chlamydiae* lifecycle so intractable to genetic exchange, that classification based on 16S rRNA sequence divergence alone is not applicable (Schachter et al., 2001; Stephens et al., 2009). Indeed, Stephens et al. (2009) suggest a single genus *Chlamydia* as depicted in Figure 1.1.

As the most significant human pathogen of the *Chlamydiaceae, C. trachomatis* is the focus of this thesis. This species is divided into two biovars, characterised by the clinical symptoms developed by the patient and the host tropism of the bacteria; trachoma and LGV. These biovars are divided into 19 serovars distinguishable by the specific antibodies produced by the patient. Serovars A-K comprise the trachoma biovar which infect epithelial surfaces such as the conjunctiva (serovars A-C), causing trachoma, and genital epithelial cells (serovars D-K), resulting in the archetypal urogenital *Chlamydia* infection. Serovars L1-L3 comprise the LGV biovar, which upon infection of urogenital epithelial cells can further penetrate into the lymphatic system, causing the disease of the same name, LGV.

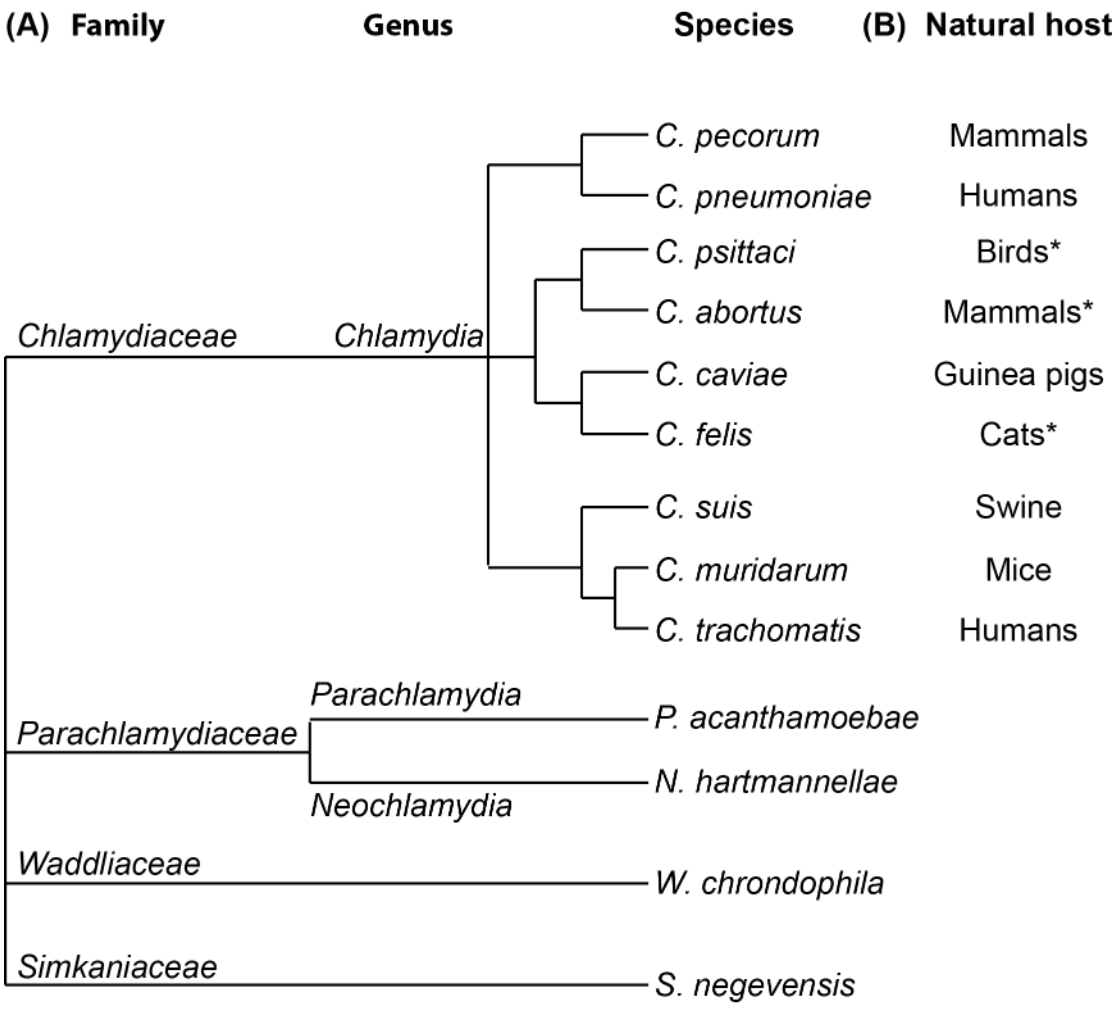

Figure 1.1. Revised taxonomic structure of the order *Chlamydiales*. (A) Taxonomy of *Chlamydiales* as described in Stephens et al., 2009. (B) The natural host of each *Chlamydia* species are presented. * indicates zoonotic transmission to humans can occur.

1.1.2 Epidemiology, pathology and treatment

Infections by members of the *Chlamydiaceae* cause a number of symptomatically distinct diseases dependent on the species, the strain and the host. The urogenital infection caused by *C. trachomatis* serovars D-K is the most common bacterial sexually transmitted infection in the world (Bébéar and de Barbeyrac, 2009), and as such represents a significant global health and economic burden. In 2012, the annual report of the UK National *Chlamydia* Screening Programme indicated that 7.7% of 15-24 year olds were positive for *Chlamydia* based on nucleic acid amplification tests (NCSP, 2012). Attempts to eradicate the disease have been hindered by the asymptomatic nature of the infection (up to 70% of cases in women and 50% in men), thus resulting in a significant asymptomatic carrier population (Stamm, 1999). Where symptomatic, *C. trachomatis* infection is characterised by cervicitis in women, and is frequently associated with endometriosis and pelvic inflammatory disease. Furthermore, reproductive complications such as ectopic pregnancy and neonatal pneumonia or conjunctivitis can occur. Chronic *C. trachomatis* infections have been linked to induction of squamous metaplasia in association with human papilloma virus infection, suggesting a synergistic effect in the development of cervical cancer (Silva et al., 2014). Urethritis occurs in men, which can progress to the upper genital tract causing epididymitis (Taylor Robinson and Thomas, 1980; Peipert, 2003). Reduced fertility has also been reported, although further studies have been conflicted (Idahl et al., 2007; Eggert Kruse et al., 2011). Dissemination beyond the epithelial layer occurs in *C. trachomatis* serovars L1-L3, resulting in LGV. In this variant, bacteria infect and spread systemically through the lymph nodes via macrophages, in some cases being isolated from the lower digestive tract (Zöllner et al., 1993). Initial symptoms of LGV often include a painless genital ulcer that goes unnoticed. Secondary and tertiary symptoms however can be much more severe, including inflammation of the lymph nodes that can progress to potentially permanent oedema and lymphatic obstruction (White, 2009).

Ocular infections caused by *C. trachomatis* serovars A-C result in trachoma, the leading global cause of preventable infectious blindness. Trachoma is endemic to large areas of the developing world, including sub-Saharan Africa, Asia, parts of the Middle East and South America. The disease most often occurs in low-income rural communities due to a lack of sanitation and the limited access to healthcare and water, and is thus classified as a neglected tropical disease by the World Health Organisation. Transmission occurs via direct contact or by flies that come into prior contact with the eyes or nose of infected persons. Blindness occurs

when recurrent infection results in chronic inflammation and scarring, leading to in-turning eyelashes (trichiasis) and subsequent damage to the cornea. In 2009, 40.6 million people were estimated to have active trachoma, of whom 8.2 million had already reached the stage of trichiasis (Mariotti et al., 2009).

C. pneumoniae is considered to be the second most significant human pathogen of the *Chlamydiaceae*, able to cause pneumonia. *C. pneumoniae* infection is also linked with various chronic conditions such as atherosclerosis and reactive arthritis (Zeidler and Hudson, 2014). Less common human pathogens include *C. psittaci*, a primarily avian-infecting species that causes potentially lethal respiratory psittacosis in humans (Knittler et al., 2014), and *C. abortus*, a primarily ruminant-infecting species that can colonise the placenta to cause abortion or pre-term labour (Baud et al., 2008). Other species cause significant veterinary problems, with *C. muridarum* infecting mice and hamsters, *C. suis* infecting pigs, *C. felis* infecting cats and *C. caviae* infecting guinea pigs.

Typical treatment for all species of *Chlamydia* involves the use of macrolide antibiotics such as azithromycin or tetracycline antibiotics like doxycycline. Antibiotic resistance is considered rare, despite significant selective pressure, although some incidences have been reported *in vivo* (Sandoz and Rockey, 2010). Screening programmes are in place in many developed countries to attempt to reduce the incidence of the sexually transmitted variant of the bacteria, although the impact and efficacy of these programmes has been somewhat limited. Vaccination is considered the favoured approach to reduce disease prevalence, however to date attempts to create a successful vaccine have been unsuccessful (Schautteet et al., 2011).

1.1.3 Lifecycle and mechanisms of pathogenicity

While the lifecycles, survival mechanisms and genetics of other bacterial pathogens have been extensively studied and elucidated, research into members of the *Chlamydiaceae* is comparatively less well developed. This can be largely attributed to the multiple challenges researchers face when studying *Chlamydiaceae*. Foremost of these difficulties is the obligate intracellular nature of the organism, which has until recently prevented traditional methods of genetic manipulation such as gene mutation or deletion commonly used to identify pathogen effectors (Wang et al., 2011; Ding et al., 2013; Agaisse and Derré, 2014; Bauler and Hackstadt, 2014). To circumvent this, many researchers have focused on investigating clinical strains

containing natural mutations, including Suchland and co-workers (2000), who characterised an inclusion membrane protein by identifying and sequencing *C. trachomatis* strains that formed multiple non-fusogenic inclusions as opposed to the single large inclusion characteristic of this species. A more recent study utilised chemical mutagenesis techniques and high-throughput sequencing to generate a library of *Chlamydia* mutants for phenotypic analysis. Analysis of 99 nonsense mutations in 84 open reading frames (ORFs) revealed that the metabolic pathways of *C. trachomatis* are remarkably plastic and that a number of uncharacterised secreted effector proteins (discussed later) are non-essential for infection (Kokes et al., 2015). These results were unexpected, as *C. trachomatis* possesses a small genome with just 894 ORFs (Stephens et al., 1998; Kalman et al., 1999) compared to 4554 ORFs in *Salmonella* (McClelland et al., 2001). During the course of this work, some genetic tools to transform *Chlamydia* have emerged, including the development of cloning vectors allowing both constitutive and inducible expression of fluorescent fusion-proteins and epitope-tagged chlamydial proteins (Wang et al., 2011; Ding et al., 2013; Agaisse and Derré, 2014; Bauler and Hackstadt, 2014). Tools to silence the expression of essential genes are yet to be developed, restricting the study of proteins such as virulence effectors using standard genetic methodology.

1.1.3.1 General overview of the *Chlamydia* lifecycle

A key factor in the genetic intractability of the *Chlamydiae* is their biphasic lifecycle, typically 30-72 hours in culture, dependent on strain and host cell (Fig 1.2). During entry and exit from the host cell, *Chlamydia* exists as small (~0.3 µm diameter), highly compact elementary bodies (EBs) that are metabolically inert. In order to grow and replicate, EBs differentiate into larger (~1.0 µm diameter), non-infectious reticulate bodies (RBs) that are metabolically active (Moulder, 1991). RBs replicate by binary fission within a single large inclusion inside the host cell. The lifecycle can be described in five steps: (1) EB attachment and entry into the host cell; (2) Transport of EB-containing vesicles to the peri-nuclear region and fusion into a single inclusion, and EB to RB differentiation; (3) inclusion modification and expansion and RB replication; (4) RB to EB redifferentiation; (5) bacterial release from the host cell by lysis or egress. Under conditions of bacterial stress persistence, described as a long-term viable but non-cultivatable growth stage, can occur (Hogan et al., 2004). *In vitro*, a persistent state can be induced by antibiotic treatment, amino acid depletion or interferon gamma (IFNγ) treatment, and frequently involves RBs becoming enlarged and progressively more aberrant (Clark et al., 1982; Coles et al., 1993; Beatty et al., 1994). Evidence for *in vivo* persistence also exists, with

multiple examples of morphologically aberrant chlamydial forms observed by electron microscopy (Nanagara et al., 1995; Skowasch et al., 2003).

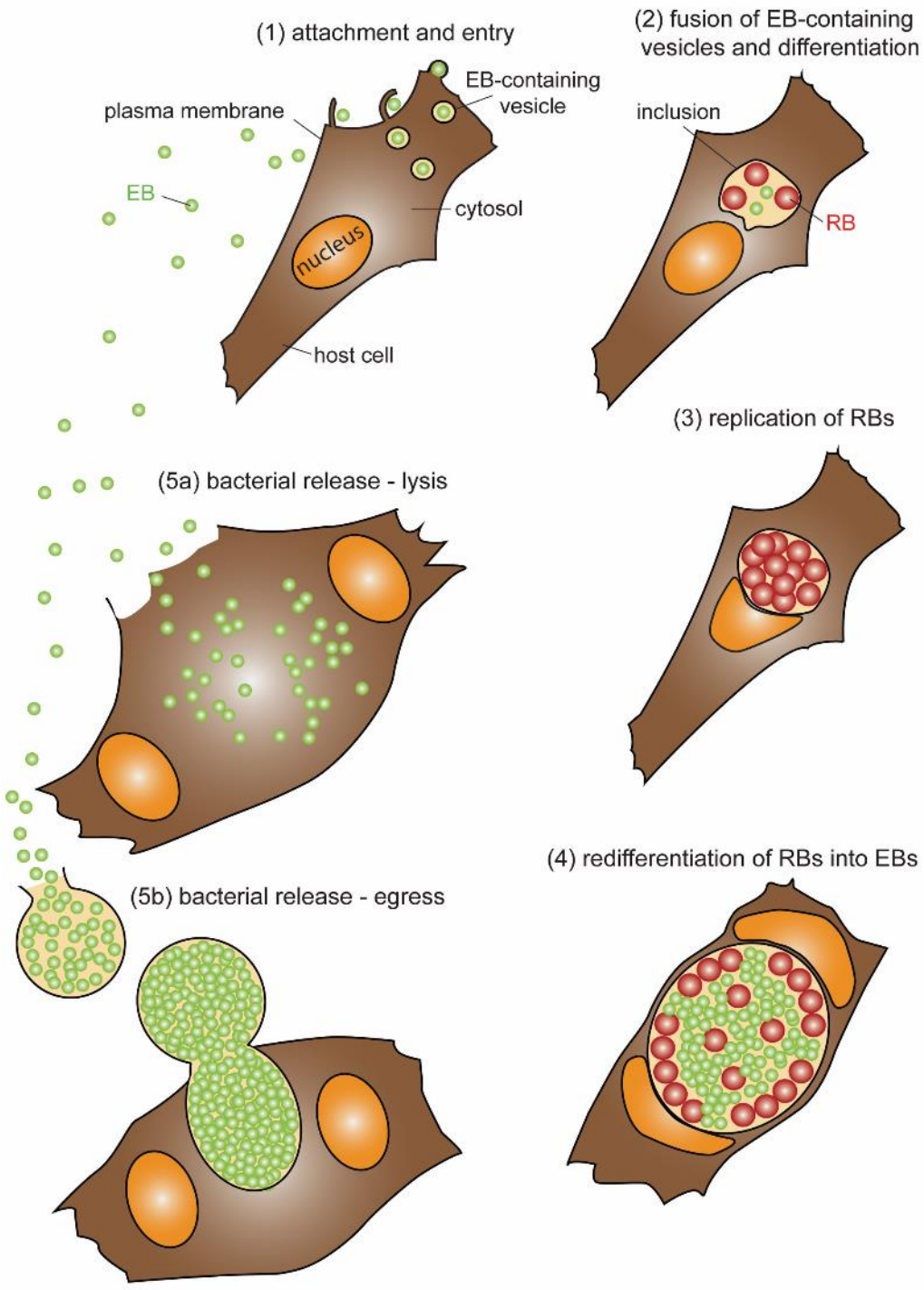

Figure 1.2. The biphasic life cycle of *C. trachomatis*. The life cycle of *C. trachomatis* can be described in five steps. (1) Elementary bodies (EBs, green spheres) attach to and enter cells, becoming encapsulated into vesicles (2) EB-containing vesicles migrate to and merge at the perinuclear region into a single inclusion and differentiate into reticulate bodies (RBs, red spheres) (3) RBs replicate and the inclusion begins to expand (4) RBs redifferentiate into EBs (5) Bacteria are released from the cell by lysis (5a) or inclusion egress (5b).

1.1.3.2 Secretion systems

A key component of the *Chlamydia* lifecycle is the utilisation of functional secretion systems (Wolf et al., 2006; Chen et al., 2010). Six secretion systems have been identified in Gram-negative bacteria to date, characterised by differences in the substrates of these systems and in the structure of the secretory apparatus (Costa et al., 2015). *Chlamydia* utilise both type II and type III secretion systems (Peters et al., 2007; Chen et al., 2010).

In type II secretion (T2S), periplasmic proteins secreted by the Sec-dependent pathway are secreted through the type II machinery to pass the outer membrane into the extracellular milieu (Korotkov et al., 2012). *Chlamydia* encodes many homologues of both Sec-dependent and T2S pathway proteins and chaperones, although the functionality of these homologues has not been demonstrated experimentally (Stephens et al., 1998; Karunakaran et al., 2003). However, experiments by Chen et al. (2010) showed the T2S pathway to be functional. Firstly, the N-terminal sequence of chlamydial protease-like activity factor (CPAF) is sufficient to direct export of mature PhoA, an enzyme active after translocation into the bacterial periplasm, in a heterologous system (Chen et al., 2010). This translocation was blocked in both *Escherichia coli* strains lacking the Sec-pathway chaperone SecB, and strains lacking the translocase complex subunit SecY, an essential component for translocase activity (Chen et al., 2010). Secondly, CPAF secretion is blocked in cells treated with arylomycin C16, a peptidase I inhibitor that prevents cleavage of the N-terminal signal sequence and so secretion of the protein (Chen et al., 2010). Indeed, T2S is vital for the *Chlamydia* lifecycle, as shown by attenuated growth of a *C. trachomatis* LGV-L2 variant bearing a point mutation in the T2S ATPase GspE (Snavely et al., 2014).

Chlamydial type III secretion (T3S) is better characterised than T2S. The T3S apparatus is composed of >20 proteins arranged to form an 'injectisome' that spans the bacterial envelope to inject, with the aid of chaperones, effectors directly into the host cell (Ghosh, 2004). In contrast to other Gram-negative bacteria, which have T3S genes clustered within a single locus located in a chromosomal pathogenicity island or virulence-associated plasmid (Winstanley and Hart, 2001), chlamydial T3S genes are distributed throughout the genome across at least six loci (Stephens et al., 1998; Hefty and Stephens, 2007). This suggests that *Chlamydia* T3S genes have not been recently acquired by horizontal gene transfer in a single evolutionary event. Phylogenetic analyses show the *Chlamydia* virulence T3S system evolved from an ancestral flagella T3S system modified to retain only the protein export function, and this may

represent a primordial system from which all T3S systems are derived (Kim, 2001; Peters et al., 2007). T3S systems are important for chlamydial development as demonstrated by inhibition with the small molecule inhibitor INP0400. Originally shown to block the T3S system in *Yersinia pseudotuberculosis*, INP0400 partially blocks entry of EBs, reduces intracellular RB replication and inhibits RB to EB differentiation (Muschiol et al., 2006; Wolf et al., 2006).

T3S systems are first utilised during entry, notably in delivery of translocated actin recruiting protein (Tarp) (discussed in 1.1.4). Surface projections on EBs were first observed in 1981 by Akira Matsumoto, and in 2008 Betts et al. demonstrated CdsF, a needle subunit protein, localised to the periphery of EBs. However, it was not until 2014 that the presence of these T3S systems was confirmed (Nans et al., 2014; Pilhofer et al., 2014). Using cryo-electron tomography, Nans et al. (2014) showed *C. trachomatis* EBs are polarised, with the periplasmic space in one hemisphere expanded to accommodate an array of 14-20 T3S systems. In the presence of host cells EBs orientate to align this T3S system array to face the target plasma membrane, which is proposed to allow the concentrated delivery of effector proteins to facilitate bacterial entry (Nans et al., 2014). These cryo-electron tomography studies were taken further to derive the *in situ* structure of the chlamydial T3S system (Nans et al., 2015). Upon contact with the host membrane, the needle of the chlamydial T3S system elongates by up to 2 nm, the basal body compacts by up to 5 nm, and the sorting platform (a structure where effectors are sequentially loaded for delivery) is stabilised (Nans et al., 2015). As such, these 'pump-action' conformational changes suggest the chlamydial T3S system behaves as a 'molecular syringe' to secrete effectors. The location of T3S system assembly is also important later in the *Chlamydia* lifecycle. At 22-24 hours post infection (hpi), the host rough endoplasmic reticulum (rER) is recruited to the inclusion periphery and rER proteins are enriched on and translocated into the inclusion. At these rER contact points, RBs assemble 'pathogen synapses', ordered arrays of 20-100 T3S systems in contact with the luminal face of the inclusion membrane that bridge the RB envelope to the rER in the host cytosol. These batteries of T3S systems, similar to the arrays observed during EB entry, likely ensure effector delivery at high local concentrations (Dumoux et al., 2012).

1.1.4 Attachment and entry

At the initiation of the chlamydial development cycle, *C. trachomatis* EBs attach to the host plasma membrane and induce their uptake into non-phagocytic mammalian cells. Initial

attachment is mediated by interactions between heparin sulphate-like glycosaminoglycans (GAGs) present on the host cell and the cysteine-rich protein OmcB of the chlamydial outer membrane complex (COMC) in the EB envelope (Zhang and Stephens, 1992; Moelleken and Hegemann, 2008). The COMC also comprises the major outer membrane protein (MOMP), chlamydial polymorphic membrane proteins (Pmps) and a number of hypothetical chlamydial proteins (Caldwell et al., 1981)). *C. trachomatis* is similar to other Gram-negative bacteria in having both an inner and an outer membrane, lipopolysaccharide (LPS), the afore-mentioned T3S systems, and a peptidoglycan layer (Liechti et al., 2014). However, it is the COMC that is the major determinant of structural integrity via disulphide-linked oligomers formed between MOMP, OmcA and OmcB (Hatch et al., 1984).

In addition to the interaction of GAGs and OmcB, multiple host cell receptors have been implicated in EB attachment. The high mannose oligosaccharide region of the *Chlamydia* MOMP mediates attachment through interactions with the host mannose receptor (Kuo et al., 1996). Chlamydial LPS is involved in *C. trachomatis* serovar E infection through binding of the cystic fibrosis transmembrane conductance regulator (CFTR), and *C. trachomatis* serovar E EBs also bind and colocalise with the oestrogen receptor (Ajonuma et al., 2010; Hall et al., 2011). The platelet derived growth factor receptor (PDGFR) has been linked to *C. muridarum* infection as phosphorylated PDGFRβ is recruited to entry sites (Elwell et al., 2008). Finally, cells depleted of protein disulphide isomerase (PDI) exhibited a >97% reduction in attachment of *Chlamydiae*, marking PDI as the only host protein identified as essential for attachment of multiple *Chlamydia* species (Abromaitis and Stephens, 2009).

After attachment, entry occurs via actin-dependent endocytosis. Upon EB binding to the host plasma membrane, the chlamydial protein Tarp is translocated across the plasma membrane by T3S systems (Clifton et al., 2004). This translocation is increased by the binding of chlamydial chaperone SycE-like chaperone 1 (Slc1) (Brinkworth et al., 2011). Following translocation into the host cell, Tarp is rapidly phosphorylated by host tyrosine kinases (Clifton et al., 2004). Phosphorylated-Tarp activates the Rac-dependent signalling cascade via binding of cellular Rac1 guanine nucleotide exchange factors (GEFs), resulting in Arp2/3 complex activation and actin reorganisation (Carabeo et al., 2004; Subtil et al., 2004; Jewett et al., 2006; Lane et al., 2008; Jiwani et al., 2012). Interestingly, Tarp phosphorylation is specific to *C. trachomatis*, indicating another mechanism for actin recruitment in other species of *Chlamydia*. This second mechanism is induced through the Tarp proline-rich C-terminal actin-binding domain, which promotes Tarp oligomerisation to mediate filamentous actin (F-actin)

nucleation and polymerisation (Jewett et al., 2006). Following entry, the T3S effector CT166 glycosylates Rac1 to inhibit further activation, thus ensuring a balanced uptake of *Chlamydia* into host-cells (Thalmann et al., 2010).

Recent cryo-EM studies by Nans et al. (2014) have shed considerable light on the mechanism of chlamydial entry. Three-dimensional reconstructions of *C. trachomatis* LGV2 EBs in contact with host cells showed a striking diversity of entry structures. EBs were visualised proximal to complex membrane ruffles, generating a macropinosome-like structure that could trap EBs prior to internalisation (Nans et al., 2014). EBs were also observed trapped under the bases of actin-rich filopodia in close association to the host cell membrane (Nans et al., 2014), representing an early entry structure and supporting previous live fluorescence and scanning electron microscopy data that showed *C. trachomatis* induce microvilli at entry sites (Carabeo et al., 2002). Lastly, curved membranes resembling phagocytic cups were observed that tightly zipper around individual EBs (Nans et al., 2014). Common to all of these ultrastructural snapshots of chlamydial internalisation are the ordered arrays of T3SSs, which were orientated towards and frequently in direct contact with the host plasma membrane. However, it remains unclear whether these intermediate states are interrelated or whether they represent independent entry pathways (Nans et al., 2014).

1.1.5 Formation of the inclusion and acquisition of soluble nutrients

1.1.5.1 Bacteria-containing vesicles migrate to the host centrosome

After entry into the host cell, internalised EBs differentiate into RBs and migrate to the peri-nuclear region. These vesicles do not acquire markers characteristic of the endocytic pathway as demonstrated by exclusion of early endosomal, late endosomal and lysosomal proteins (Fields and Hackstadt, 2002). Migration to the peri-nuclear region occurs via utilisation of the host microtubule motor, dynein, which transports bacteria-containing vesicles towards the minus-end of microtubules, resulting in their accumulation at the microtubule-organising centre (MTOC) (Clausen et al., 1997). Trafficking occurs independently of p50 dynamitin, the cargo-binding member of the dynactin complex, suggesting bacteria-containing vesicles migrate using a mechanistically distinct method to vesicular trafficking (Grieshaber et al., 2003). Instead, an inclusion membrane protein (Inc) (described in 1.1.5.2), CT850, is proposed to mediate interactions with dynein due to a number of lines of evidence. Firstly, when

exogenously expressed in uninfected cells, CT850 localises to the MTOC (Mital et al., 2010). Secondly, CT850 is expressed as early as 1 hour post infection when trafficking to the MTOC occurs (Belland et al., 2003). Thirdly, a yeast 2-hybrid system revealed an interaction between CT850 and the dynein light chain DYNLT1, and depletion of DYNLT1 disrupts inclusion positioning at the MTOC (Mital et al., 2015).

1.1.5.2 Inclusion membrane proteins mediate fusion of bacteria-containing vesicles and inclusion interactions

Once at the MTOC, fusion of bacteria-containing vesicles is dependent on modification of the vesicle membrane with the IncA protein (Hackstadt et al., 1999). First identified in *C. psittaci* as a serine/threonine phosphoprotein (Rockey et al., 1997), IncA has since been identified in *C. trachomatis* and is structurally similar to *C. psittaci* IncA (Bannantine et al., 1998). Mutations in *incA* result in strains that form multiple non-fusogenic inclusions as opposed to the characteristic single large inclusion (Suchland et al., 2000). IncA is proposed to use structural mimicry of the SNARE motif, a heptad repeat in the C-terminal region of eukaryotic SNARE proteins involved in compartment fusion, to aid in the fusion of *C. trachomatis*-containing vesicles in cells infected with multiple EBs (Delevoye et al., 2008). Expression of a mutant IncA lacking one or both of the SNARE-like domains in an *incA::bla* mutant of *C. trachomatis* LGV2 was insufficient to rescue homotypic fusion, whilst expression of wildtype (WT) IncA restored compartment fusion (Weber et al., 2016). IncA can also form complexes with host SNARE proteins Vamp3, Vamp7 and Vamp8 at the inclusion periphery, with these interactions proposed to permit fusion of cellular compartments with the inclusion membrane (Delevoye et al., 2008).

In addition to IncA, the inclusion is modified using T3S with up to 62 inclusion membrane proteins (Incs), the majority of which have as yet unknown functions (Rockey et al., 2002; Li et al., 2008; Dehoux et al., 2011). Incs are predicted to share a common motif of a hydrophobic domain of 40 amino acids with two, short (<100 residue) soluble domains protruding into the cytoplasm that mediate host-pathogen interactions (Bannantine et al., 2000). Recently, in a major study to identify protein-protein interactions between Incs and host proteins, Mirrashidi et al. (2015) expressed 58 of the 62 predicted *C. trachomatis* Incs, including the full-length proteins and the predicted cytoplasmic domains, individually in host cells. These Incs were then affinity purified and analysed by mass spectrometry to identify binding partners. Notably IncE was found to bind sorting nexin (SNX) 5 and SNX-6, components of the retromer. SNX5

and SNX6 depletion led to the production of increased infectious progeny, suggesting retromer-dependent trafficking restricts *Chlamydia* infection (Mirrashidi et al., 2015). Simultaneously, a quantitative proteomics approach taken by Aeberhard et al. (2015) also identified components of the retromer when *C. trachomatis* inclusions were isolated from cells.

IncB, CT101, CT222 and CT850 co-localise with members of the Src family of kinases at the inclusion membrane (Mital et al., 2010). Src family kinases are involved in a number of cellular signalling pathways that regulate functions including motility, apoptosis and membrane trafficking (Sandilands and Frame, 2008). IncB additionally forms round membranous vesicular compartments when ectopically expressed in HeLa cells, suggesting it may be important in influencing the membrane architecture of the inclusion (Mital et al., 2013). Further Incs include CT229, which interacts with the early endosome Rab GTPase protein Rab4A (Rzomp et al., 2006). Rab GTPases are important in regulation of various aspects of vesicular trafficking, including the formation, trafficking, docking and fusion of transport vesicles. *Chlamydiae* recruit a number of Rab GTPases to the inclusion during infection, and recruitment is species dependent. Rab1, Rab4 and Rab11 accumulate at *C. trachomatis*, *C. muridarum*, and *C. pneumoniae* inclusions, while Rab6 is associated solely with *C. trachomatis* inclusions and Rab10 associated with *C. muridarum* and *C. pneumoniae* inclusions (Rzomp et al., 2003). *C. trachomatis* development was not affected in cells expressing a mutant Rab4A protein however, suggesting additional Rab4 isoforms may perform redundant functions during infection (Rzomp et al., 2006). Additional Incs and their known pathogenic interactions with aspects of host cell biology, including hijacking of the host cytoskeleton, modulation of apoptosis and recruitment of host organelles to the inclusion, will be discussed in section 1.1.6.

1.1.5.3 Acquisition of soluble nutrients

After establishing an intracellular niche within the inclusion, *Chlamydiae* must acquire essential nutrients for subsistence and replication. Over the course of millennia *Chlamydia* species have lost the genes required to synthesise many metabolites including ATP, and instead evolved to scavenge these from the host cell (Saka and Valdivia, 2010). The inclusion is permeable to small ions such as Ca^{2+} and soluble molecules smaller than 520 Da, suggesting passive diffusion supports acquisition of nucleotides, tricarboxylic acid (TCA) cycle substrates and amino acids (Heinzen and Hackstadt, 1997). Energy parasitism is a key feature of

intracellular pathogens like *Chlamydia*. Analysis of whole-genome sequences from chlamydial species has revealed the presence of two ATP transporters, Npt1Ct for ATP import coupled to ADP export, and Npt2Ct for generic nucleotide import in a proton-dependent manner (Tjaden et al., 1999). Furthermore, host ATP and glucose production are upregulated during the replicative stages of *C. psittaci* infection (Ojcius et al., 1998). This increase could be an active and direct consequence of infection promoted by the pathogen, but may also be indicative of a passive stress response, whereby the host cell compensates for substrate loss to the bacteria (Ojcius et al., 1998). *C. trachomatis* inclusions also accumulate glycogen by a combination of bulk translocation from the host cytoplasm in association with the glycogen-binding enzyme Gys1 (Gehre et al., 2016), and by *de novo* synthesis by *Chlamydia*, which encodes a full complement of enzymes necessary for glycogenesis and glycogenolysis (Stephens et al., 1998; Lu et al., 2013; Gehre et al., 2016).

1.1.6 Manipulation of host cell processes by *Chlamydia*

1.1.6.1 Hijacking of the host cytoskeleton

Chlamydia uses Inc proteins to mechanically support the inclusion, which expands to occupy the majority of the host cytosol, by taking control of the host cytoskeleton. CT223, also termed inclusion protein acting on microtubules (IPAM), recruits and stimulates the centrosomal protein 170 kDa (CEP170) to hijack host microtubule organising activity. This leads to the formation of a microtubule cage and nest surrounding the inclusion to maintain cell and inclusion morphology, and so promote bacterial infectivity (Dumoux et al., 2015). Additionally, *C. trachomatis* remodels microtubules to coordinate Golgi stack recruitment to the inclusion (Al-Zeer et al., 2014), and intracellular growth of the bacteria is supported by microtubule-associated protein 1 (MAP1) light chain 3 (LC3), which is recruited to the inclusion periphery in a microtubule-dependent manner together with MAP1 subunit A and MAP1 subunit B (Al-Younes et al., 2011). Further cytoskeletal components are hijacked by *Chlamydia*, as F-actin and the intermediate filament protein vimentin form a network to encase and stabilise the inclusion (Kumar and Valdivia, 2008). The Inc protein inclusion membrane protein for actin assembly (InaC) is required for F-actin assembly at the inclusion by recruiting ADP-ribosylation factors and 14-3-3 proteins, and disruption of F-actin results in aberrant inclusion morphology and loss of inclusion integrity (Kumar and Valdivia, 2008; Kokes et al., 2015).

In addition to its role in regulating the cytoskeleton, CT223 also blocks cytokinesis as shown by a multi-nucleated phenotype observed in host cells when CT223 is ectopically expressed (Alzhanov et al., 2009). Indeed, up to 80% of HeLa cells infected with *C. trachomatis* are multi-nucleated by 40 hpi (Greene and Zhong, 2003; Brown et al., 2012). However, it is controversial whether chlamydial factors are required for multi-nucleation, as experiments by Sun et al. (2011) show polystyrene beads of a similar size to the inclusion are also sufficient to block cytokinesis.

1.1.6.2 Apoptosis and the immune response

Upon *Chlamydia* infection, many host cell responses are initiated. Pathogen-associated molecular patterns (PAMPs) like chlamydial LPS are recognised by pattern recognition receptors (PRRs) such as toll-like receptors (TLRs), which trigger an innate immune response (Joyee and Yang, 2008; Takeuchi and Akira, 2010). Transcription of cytokines and chemokines is induced, as well as the type I interferon response to activate cell-autonomous resistance mechanisms (Monroe et al., 2010; Barker et al., 2013). Further antimicrobials such as reactive oxygen species are also produced for recruitment of immune cells (Rusconi and Greub, 2011). Despite this initial immune activation, *Chlamydia* is a highly effective pathogen, able to manipulate immune signalling and apoptosis to prevent bacterial detection and host cell death (Zhong et al., 1999; Dong et al., 2005). NF-κB is a key host transcription factor involved in regulating the immune response during infection, and functions downstream from PRRs. NF-κB consists of a heterodimeric complex composed of two subunits, p50 (NF-κB1) and p65 (RelA) (Siebenlist et al., 1994). Under normal conditions, NF-κB is inactivated in complex with IκB in the cytosol. Upon degradation of IκB, the freed NF-κB complex can translocate to the nucleus to transcriptionally activate target genes involved in innate immunity and inflammation (Siebenlist et al., 1994). *Chlamydia* interferes with the NF-κB pathway via the action of two effectors, CT441 and Chladub1 (Lad et al., 2007a; Lad et al., 2007b; Le Negrate et al., 2008). CT441 is a tail-specific protease that inhibits NF-κB activation by direct proteolysis of the p65 subunit of NF-κB (Lad et al., 2007a; Lad et al., 2007b). Chladub1 binds to and inhibits the proteasomal degradation of IκB, and so prevents the subsequent activation and translocation of NF-κB to the nucleus (Le Negrate et al., 2008).

Chlamydia additionally manipulates antigen presentation. Major histocompatibility complexes (MHCs) class I and class II present bacterial antigens to $CD8^+$ and $CD4^+$ lymphocytes (Neefjes et al., 2011). The transcription factors RFX5 and USF-1 are degraded during infection, preventing

IFNγ-dependent induction of MHC II genes and both constitutive expression and IFNγ-dependent induction of MHC I genes (Zhong et al., 1999; Zhong et al., 2000). CD1d, an MHC-like protein complex, is also degraded preventing signalling to natural killer (NK) and NK T cells (Kawana et al., 2007). In addition to targeting host proteins, *Chlamydia* also degrades a subset of its own effectors to prevent them being used as substrates for antigen presentation (Jorgensen et al., 2011). These effectors include those translocated during invasion, such as Tarp, and inclusion membrane proteins expressed early after invasion, notably the well-characterised IncD (section 1.1.6.3) and IncE.

Chlamydia also counteracts host cell death to protect its intracellular niche by interfering with multiple apoptotic and necrotic pathways. Infected cells become resistant to various pro-apoptotic stimuli including DNA damaging agents such as etoposide and apoptosis-inducing molecules like tumour necrosis factor-α (Fan et al., 1998). Perhaps the most well studied mechanism for *Chlamydia* prevention of cell death is the degradation of pro-apoptotic BH3-only proteins, Bad, Bim and Puma during infection (Dong et al., 2005; Ying et al., 2005). This degradation results in reduced activation of Bax and Bak, and so inhibits cytochrome c release and caspase 3/9 activation (Fan et al., 1998; Fischer et al., 2001). IncG also contributes to the prevention of apoptosis. Phosphorylated IncG interacts with the host protein 14-3-3β, a phosphoserine-binding protein, via a conserved binding motif (Scidmore and Hackstadt, 2001). 14-3-3β sequesters the pro-apoptotic protein Bad at the inclusion membrane, thus the bacteria render the infected cell resistant to apoptotic stimuli (Verbeke et al., 2006). *C. trachomatis* also modulates pro-survival factors, up-regulating the cellular inhibitor of apoptosis protein 2 (cIAP-2) and the anti-apoptotic Bcl-2 family member Mcl-1 (Rajalingam et al., 2006; Rajalingam et al., 2008).

Although *Chlamydia* is effective at inhibiting apoptosis, infection can nevertheless result in necrotic cell death, leading to an inflammatory response. During necrosis, poly(ADP-ribose) polymerase 1 (PARP-1) induces the translocation of the pro-inflammatory mediator high-mobility group box 1 protein (HMGB1) to the cytosol, where it is released from the host cell after loss of plasma membrane integrity (Ditsworth et al., 2007). To reduce HMGB1 release, *Chlamydia* both degrades HMGB1 directly and cleaves PARP-1, preventing translocation of HMGB1 to the cytosol (Yu et al., 2010).

The majority of the cleavage and degradation events described in this sub-section were attributed to a single type II secreted protein, CPAF. However, a study by Chen et al (2012)

showed proteolysis of 11 of the host proteins identified as targets for CPAF was due to residual enzyme activity during sample processing. Of those proteins already described, Puma, Bim, Bak, p65/RelA and golgin-84 were not cleaved or degraded when urea was used to denature CPAF during sample processing (Chen et al., 2012). Despite this, CPAF activity is important for the chlamydial lifecycle, as *C.* trachomatis strains possessing loss-of-function mutations in the gene encoding for CPAF, *cpa*, display impaired generation of infectious EBs (Snavely et al., 2014).

1.1.6.3 Acquisition of lipids

Lipids are a crucial resource *Chlamydia* must appropriate from the host cell, and the bacteria accomplish this by manipulating host vesicular trafficking and by targeting organelles. The inclusion selectively interacts with exocytic vesicles travelling from the *trans*-Golgi to the plasma membrane to acquire sphingolipids such as ceramide and sphingomyelin (Hackstadt et al., 1995). Delivery of these sphingolipids involves the Golgi-associated protein Rab14, and is essential for expansion of the inclusion (Capmany and Damiani, 2010). Chlamydial infection also induces fragmentation of the Golgi apparatus via golgin-84 cleavage (Heuer et al., 2009). Depletion of Rab6a and Rab11a prevented golgin-84 cleavage, resulting in reduced lipid acquisition and inhibition of chlamydial development, whereas Golgi fragmentation prior to infection enhanced chlamydial propagation (Heuer et al., 2009; Lipinski et al., 2009). Multivesicular bodies (MVBs) are another major source of vesicle-derived lipids. MVB constituents CD63, metastatic lymph node 64 (MLN64) and lysobisphosphatidic acid (LBPA) are present in the lumen of the inclusion during *Chlamydia* infection, and inhibitors of MVB biogenesis reduce bacterial replication (Beatty, 2006). The GTPase Rab39a is important but not essential to mediate MVB-inclusion interactions, as Gambarte Tudela and colleagues (2015) showed MVB localisation at chlamydial inclusions is only reduced in cells depleted of Rab39a.

Chlamydia also acquire lipids from lipid droplets (LDs), intracellular organelles used to store neutral lipids such as triacylglycerides as a source of energy or material for membrane biosynthesis (Walther and Farese, 2012). LDs accumulate at the inclusion periphery and are subsequently translocated into the inclusion lumen (Kumar et al., 2006; Cocchiaro et al., 2008). At the inclusion membrane, LDs associate with four inclusion membrane proteins, IncA, IncG, Cap1 and CTL0882 (Saka et al., 2015). Translocation of LDs into the inclusion lumen is hypothesised to occur at IncA-enriched subdomains that can mediate membrane invagination of the inclusion (Cocchiaro et al., 2008). Remarkably, the global LD proteome is modified

during *C. trachomatis* infection, with enrichment of proteins related to lipid metabolism, biosynthesis and LD-specific functions (Saka et al., 2015). This modification, as well as recruitment to the inclusion membrane, may occur due to association of LDs with three chlamydial LD-associated (Lda) proteins, Lda1-3, which are translocated into the host cell and localise to LDs, directing their traffic to the inclusion by as yet uncharacterised interactions (Kumar et al., 2006).

As well as co-opting host organelles including the Golgi apparatus and lipid droplets, *Chlamydia* also targets the ER. IncD mediates recruitment of the ER to Golgi ceramide transfer protein CERT to the inclusion membrane, as well as the vesicle-associated membrane proteins VAPA and VAPB (Derré et al., 2011; Elwell et al., 2011; Agaisse and Derré, 2014). Depletion of either CERT or the VAP proteins led to a reduction in chlamydial growth, although the role of these proteins in *C. trachomatis* development was not determined. ER proteins, including ER-resident proteins calreticulin and PDI, and ER scaffolding proteins Rtn4b and its interacting protein deleted in polyposis (DP-1), are also recruited to the inclusion membrane in a wider recruitment of the host ER (Dumoux et al., 2012). Calreticulin, PDI and Der1-like protein 1 (derlin-1) also translocated into the lumen of the inclusion, often in close contact with the bacteria, suggesting ER membranes may be metabolised by *Chlamydia* to support growth. Indeed, an intact ER was found to be essential for inclusion biogenesis and chlamydial infectivity (Dumoux et al., 2012). However, the exact role of the ER in the infection cycle remains unknown.

1.1.6.4 Interactions with the nucleus

In addition to manipulating host organelles such as the ER, the Golgi apparatus and lipid droplets, *Chlamydia* infection is closely linked to the disruption of many nuclear processes that may prime cells for oncogenesis. For example, the tumour suppressor p53 is degraded from 24 hpi following ubiquitination by phosphorylated murine double minute 2 (MDM2), resulting in an enhancement of the apoptotic resistance of *Chlamydia*-infected cells (González et al., 2014). Disruption of p53 degradation stalls the redifferentiation of RBs into EBs, thus inhibiting the formation of infectious progeny (González et al., 2014). Furthermore, the telomerase catalytic subunit of human telomerase reverse transcriptase (hTERT) is transiently up-regulated during early infection in association with ceramide recruitment to the inclusion, as ceramides are known inhibitors of hTERT transcription (Wooten-Blanks et al., 2007; Padberg et al., 2013). This alters cellular aging and survival pathways both during and following infection,

contributing to the prevention of proliferative blocks and increasing host cell resistance to DNA damage-induced apoptosis (Padberg et al., 2013). These effects are important for *Chlamydia*, as infection also results in sustained upregulation of γH2AX, a marker for DNA double-strand breaks and H3K9me3, a marker for senescence-associated heterochromatin foci (Chumduri et al., 2013). Simultaneously, *Chlamydia* infection impairs the DNA damage response by inhibiting recruitment of phosphorylated nuclear protein kinase ataxia telangiectasia mutated (pATM) and tumour protein 53 binding protein 1 (53BP1) to DNA damage sites (Chumduri et al., 2013).

Chlamydia also translocates T3S effectors to the nucleus and nuclear envelope including NUE and CT311 in *C. trachomatis* infection, and SINC in *C. psittaci* infection. CT737, also named nuclear effector protein (NUE), contains an unusual nuclear localisation sequence (NLS), consisting of a C-terminal NLS and an internal NLS, resulting in its targeting to the host nucleus following translocation into the host cytosol (Pennini et al., 2010). NUE also contains a Su(var)3-9, Enhancer-of-zeste, Trithorax (SET) domain, a 130-residue amino acid sequence that mediates histone methyltransferase activity. Histone methylation modifies gene transcription dependent on the histone and lysine residue modified, as well as the number of methyl groups added. This modification to transcriptional activity occurs as methylation of these histones, as well as other post-translational modifications including acetylation, phosphorylation and citrullination, results in reduced or enhanced accessibility of the transcriptional machinery to chromatin (Tessarz and Kouzarides, 2014). For example, tri-methylation of histone 3 lysine 9 (H3K9) is associated with transcriptional silencing (Rea et al., 2000), whilst di- or tri-methylation of histone 3 lysine 4 (H3K4) is associated with active transcription (Schneider et al., 2004). NUE methylates eukaryotic histones H2B, H3 and H4 *in vitro*, suggesting *Chlamydia* can directly alter host gene transcription. Whilst the specific lysine residues modified and the resulting methylation state was not determined, NUE could be utilised by *Chlamydia* to, for example, inhibit transcriptional activation of genes related to the immune response. Rolando et al. (2013) demonstrated this possibility in *Legionella pneumophila*. Here, *Legionella* modifies host chromatin directly using the type IV secreted protein RomA, which is a SET domain-containing methyltransferase that methylates H3K14. Methylation of H3K14 reduces expression of innate immune genes, thus promoting *Legionella* pathogenesis (Rolando et al., 2013). *Listeria monocytogenes* also targets the host nucleus. Firstly, the bacterial surface-protein InlB triggers nuclear translocation of sirtuin 2 (SIRT2). SIRT2 deacetylates histone H3 at lysine 18 (H3K18), an enzymatic reaction associated with gene silencing (Eskandarian et al., 2013). Secondly, the *Listeria* nuclear targeted protein A (LntA) is translocated to the host

nucleus where it binds bromo adjacent homology domain-containing protein 1 (BAHD1), a nuclear protein involved in gene silencing and heterochromatin formation, to modulate the interferon response (Lebreton et al., 2014).

C. trachomatis translocates a second effector to the host nucleus, CT311, which accumulates in the nucleus late during the infection cycle but whose function is unknown (Lei et al., 2013). *C. psittaci* translocates an effector to the inner nuclear envelope, the secreted inner nuclear membrane-associated *Chlamydia* protein (SINC). Upon localisation at the inner nuclear envelope, SINC was identified in close proximity to 22 inner nuclear membrane proteins including the nucleoporin ELYS, lamin B1, emerin, MAN1, LAP1 and LBR. These proteins have diverse roles in the maintenance of nuclear shape and stability as well as chromatin tethering, and will be discussed in section 1.2. Remarkably, SINC accumulates in the nuclear envelope of non-infected cells, although the mechanism of transport and functional implications of this remain unclear (Mojica et al., 2015).

1.1.7 Exit from the host cell

Towards the latter stages of the *Chlamydia* lifecycle, RBs redifferentiate into EBs and exit from the host cell is initiated. A contact-dependent hypothesis has been proposed as the trigger for RB to EB differentiation. As the inclusion reaches the maximum size possible based on spatial constraints imposed by the host cell, dividing RBs in contact with the inclusion membrane begin to detach due to a decrease in the available space for T3S system contacts. This untethering of RBs is proposed to be a signal that triggers RB to EB redifferentiation (Wilson et al., 2006; Wilson et al., 2009). Progeny then exit the cell via two mechanisms, host cell lysis or extrusion of the whole inclusion. The former is mediated by cysteine-proteases which degrade the inclusion, nuclear and plasma membranes in an ordered sequence (Hybiske and Stephens, 2007). The final step in this lysis pathway, rupture of the plasma membrane, is dependent on an influx of extracellular calcium ions. The latter, extrusion of the inclusion, requires actin polymerisation, the actin nucleation factor N-WASP, RhoA and myosin II (Hybiske and Stephens, 2007). In this process, intact inclusions are released from the host cell, and residual bacteria may contribute to persistent bacterial infection (Beatty, 2007).

The exact molecular mechanisms that control which of these two exit pathways is employed are as yet unknown, however the inclusion membrane protein CT228 promotes extrusion by

association with a myosin light chain 2 phosphatase (MYPT1) (Lutter et al., 2013). Active MYPT1 is recruited peripherally around the inclusion early during infection, preventing activation of myosin light chain 2 to ensure premature release of the inclusion does not occur. Later during infection, inactive phosphorylated MYPT1 becomes enriched in Src-family kinase-rich microdomains and co-localises with phosphorylated myosin light chain 2, myosin light chain kinase, myosin IIA and myosin IIB. This favours the local activation of myosin light chain 2, engaging the myosin motor complex to promote egress of the intact chlamydial inclusion (Lutter et al., 2013).

1.2 The Nucleus

In the preceding section the extensive interactions between *Chlamydia* and major host organelles in infected cells, including the nucleus, have been outlined. Although interactions between *Chlamydia* and the nucleus have been characterised, much remains to be established about the relationship between the inclusion and this major organelle, especially given the close spatial proximity between the nucleus and inclusion at late stages of the infection cycle and the deformation of the nucleus that occurs due to pressure exerted by the expanding inclusion (Padberg et al., 2013; Brown et al., 2014; Sun et al., 2016). As *Chlamydia* manipulation of nuclear function is the focus of this thesis, the following section will summarise the functional architecture of the nucleus, how its structural integrity is maintained and how it is connected to the rest of the cell.

1.2.1 The nuclear envelope

1.2.1.1 General overview of the nuclear envelope

The nucleus is partitioned from the cytoplasm by the nuclear envelope (NE), a lipid bilayer deriving from and contiguous with the ER (Fig 1.3). The inner nuclear membrane (INM) and outer nuclear membrane (ONM) are spaced at a distance of 40-50 nm, and this double membrane is punctuated by nuclear pore complexes (NPCs) where the INM and ONM fuse to form the pore membrane (Prunuske and Ullman, 2006). The nucleus is connected from the nuclear lamina to the cytosolic cytoskeleton via the linkers of nucleoskeleton and cytoskeleton (LINC) complexes, consisting of SUN (Sas1, UNC-84) proteins in the INM linked to KASH proteins (Klarischt, ANC-1, and Syne Homology) in the ONM (Crisp et al., 2006; McGee et al.,

2006). Four KASH proteins are present in vertebrates (Starr and Fridolfsson, 2010). Nesprin-1 and Nesprin-2 (also known as SYNE1 and SYNE2 respectively) interact with F-actin via their N-terminal actin-binding domain, and Nesprin-3 and Nesprin-4 bind to plectin and kinesin-1, respectively (Razafsky and Hodzic, 2009; Roux et al., 2009; Starr and Fridolfsson, 2010). SUN proteins are integrated into the INM by transmembrane domains, with their N-termini exposed to the nucleoplasm and their C-termini protruding into the perinuclear space to enable binding to KASH proteins (Sosa et al., 2012). Of the five SUN proteins characterised, only SUN1 and SUN2 localise to the inner nuclear envelope and are able to bind the KASH proteins (Tzur et al., 2006). Together, SUN and KASH proteins form LINC complexes to connect the nucleus to intermediate filaments and microtubules, which is important for general cellular organisation, nuclear migration, anchorage and mechanosensing (Burke and Roux, 2009). As the focus of this thesis, the NPCs and nuclear lamina will now be described in more detail.

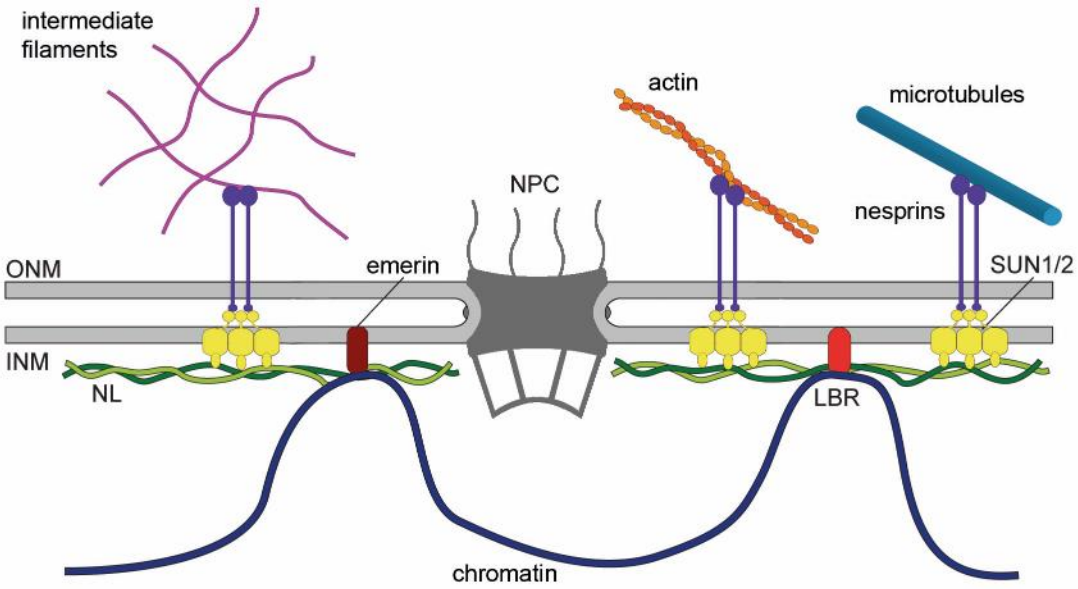

Figure 1.3. The nuclear envelope (NE). The nucleus is partitioned from the cytosol by a lipid bilayer known as the NE (light grey). The NE is connected to cytoskeletal components [actin (orange), microtubules (light blue), intermediate filaments (pink)] via nesprins (purple), which are KASH (Klarischt, ANC-1, and Syne Homology) proteins in the outer nuclear membrane (ONM). Nesprins interact with SUN (Sas1, UNC-84) proteins (yellow) in the inner nuclear membrane (INM) to form linkers of nucleoskeleton and cytoskeleton (LINC) complexes. SUN proteins interact with the nuclear lamina (NL) (green) composed of lamin A/C and lamin B. The NL tethers chromatin (dark blue) at the nuclear periphery in association with other INM anchored proteins such as emerin (dark red) and lamin B receptor (LBR) (light red). Transport through the NE occurs through nuclear pore complexes (NPCs) (dark grey), transmembrane multimeric assemblies embedded in the membrane where the INM and ONM connect.

1.2.1.2 The nuclear pore complexes

A major structural and functional component of the NE are the nuclear pore complexes (NPCs), 125 MDa macromolecular assemblies spanning the NE through which highly selective nucleocytoplasmic transport occurs (Reichelt et al., 1990). The number of NPCs per cell varies depending on cell type and cell cycle phase, but proliferating human cells have on average 2000-5000 pores per nucleus (Gerace and Burke, 1988). The NPC core is composed of two outer, two inner and one transmembrane ring, forming a pore through which transport occurs (Fig 1.4) (Alber et al., 2007). The rings are composed of eight asymmetrical repeat units termed 'spokes'. Between these spokes there are eight additional peripheral channels measuring 5-10 nm diameter. These channels were originally proposed to mediate passive diffusion of ions and small proteins, however more recent studies suggest they are equally involved in selective transport (Mohr et al., 2009). Two filamentous structures extend from the outer rings into the cytoplasm or nucleoplasm, the cytoplasmic filaments and the nuclear basket respectively.

NPCs are composed of approximately 30 proteins termed nucleoporins (Nups), the majority of which exist in multiples of eight, giving the NPCs pseudo-eightfold symmetry (Rout et al., 2000). Nups are divided into three categories: transmembrane Nups, structural Nups and phenylalanine-glycine (FG)-repeat containing Nups (Cronshaw et al., 2002). Transmembrane Nups anchor the NPC within the nuclear envelope. Structural Nups form the scaffold of the NPC and number approximately half of total NPC proteins. They comprise the outer rings, or Nup107 sub-complexes, the inner rings, and the linker Nups that bridge these rings. FG-Nups are present in the pore, the cytoplasmic filaments and the nuclear basket and number approximately one third of total NPC proteins. FG-Nups in the pore allow highly selective transport whilst simultaneously blocking diffusion of molecules greater than 30-40 kilodaltons (kDa) in size (Fried and Kutay, 2003).

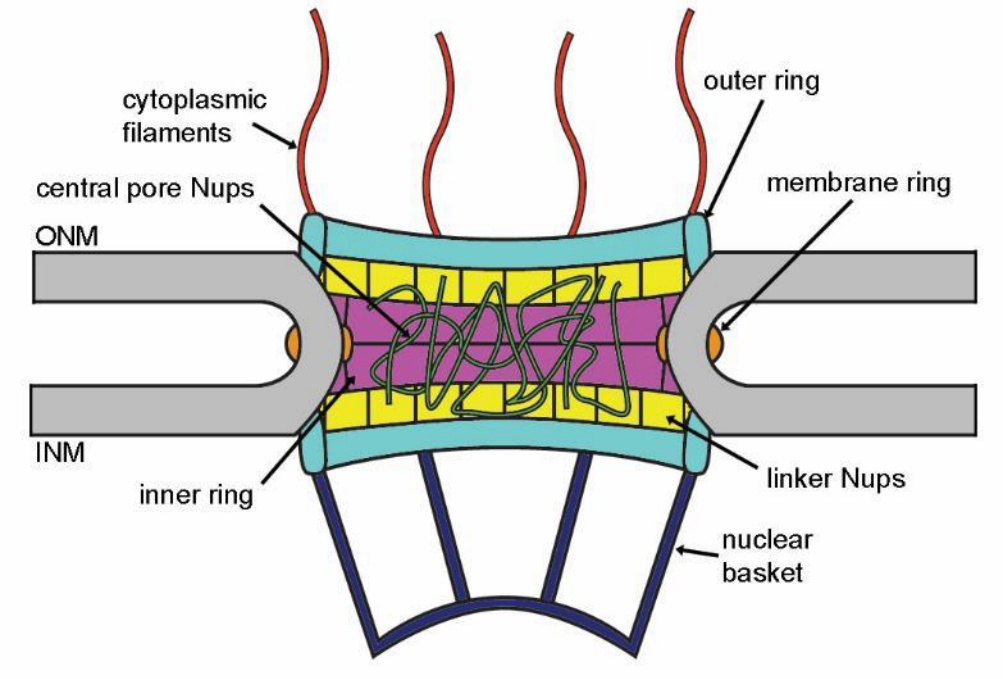

Figure 1.4. Structure of the nuclear pore complex. Nuclear pore complexes (NPCs) are macromolecular assemblies that span the nuclear envelope (grey) where the inner nuclear membrane (INM) and outer nuclear membrane (ONM) connect. The NPC is divided into three sections, the nuclear basket (dark blue), the cytoplasmic filaments (red) and the central channel through which transport occurs. Outer (light blue) and inner (purple) ring nucleoporins (Nups) provide a scaffold for the NPC architecture, connected by linker Nups (yellow). The membrane ring (orange) anchors the NPC within the nuclear envelope. Central pore Nups (green) mediate the selective transport of cargo into and out of the NPC.

Transport through the pore is mediated by nuclear transport receptors (NTRs), which recognise and subsequently bind to nuclear import or export signals on cargo proteins, often in conjunction with adaptor proteins (Pemberton and Paschal, 2005). The majority of these NTRs belong to the karyopherin family, including importin-β, importin-α and exportin-1. Nuclear-localisation sequences are typically composed of one or more clusters of basic amino-acid residues (Dingwall and Laskey, 1991). Several models have been proposed for the mechanism of transport through the pore, but no studies have been conducted to conclusively prove one hypothesis for transport over another (Walde and Kehlenbach, 2010). All models describe NTR binding to FG-Nups in the central pore and exclusion of molecules larger than ~5 nm (~40 kDa) by FG-Nups (Walde and Kehlenbach, 2010).

The filaments at the cytoplasmic face of the NPC are structurally disordered polypeptides that contribute to transport efficiency by providing docking sites for incoming cargo, or by promoting the release of nuclear export cargo into the cytoplasm during export (Strambio-De-Castillia et al., 2010). Among the proteins forming the cytoplasmic filaments, Nup214 and Nup358 are involved in nuclear protein import and export, as well as recruiting mRNA export factors such as Dbp5 and Gle1 (von Moeller et al., 2009; Noble et al., 2011). The nuclear basket is comprised of eight filaments extending from the outer nuclear ring converging to form a basket-like structure (Goldberg and Allen, 1992). The nuclear basket also contributes to nucleocytoplasmic transport. The major molecular component of the nuclear basket is translocated promoter region (Tpr) protein, which functions in the nuclear export of proteins and mRNA via interaction with the CRM1 export receptor (Ben-Efraim et al., 2009). Nup153 and Nup50 function in both import and export, with Nup153 providing a scaffold for Nup50 to bind and displace NLSs from NTRs, thus releasing cargo, or to bind export receptor-cargo complexes for transport through the pore (Guan et al., 2000; Matsuura and Stewart, 2005).

In addition to its role in nucleocytoplasmic transport, the nuclear basket has many additional nuclear functions. Studies in *Drosophila* have shown Nup153 and the Tpr homologue mammalian target of rapamycin (mTOR) bind to 25% of the genome in continuous domains extending from 10 kb to 500 kb. These nucleoporin-associated regions contain predominantly highly expressed genes, enriched with markers of active transcription such as histone H4 lysine 16 acetylation (Vaquerizas et al., 2010). Indeed, nuclear basket proteins such as Tpr establish heterochromatin exclusion zones to prevent the spread of self-propagating heterochromatin, and so gene silencing around the NPC (Shinkura and Forrester, 2002; Brown et al., 2014). These proteins further impact on chromatin structure by tethering certain genes for rapid

reactivation in a mechanism termed transcriptional memory. For example, in yeast *INO1* and *GAL1*, encoding inositol-3-phosphatase synthase and galactokinase 1 respectively, are retained at the NPCs in association with the Tpr homolog myosin-like protein 1 (Mlp1) for several generations (Tan Wong et al., 2009). Finally, some nuclear basket proteins interact with the DNA repair machinery. Deletion of Mlp1/Mlp2 in yeast prevents telomere anchoring at the NPC and so significantly reduces double-strand break repair (Galy et al., 2000).

1.2.1.3 The nuclear lamina

NPC positioning within the NE is linked to the nuclear lamina (NL), a thin (15-20 nm) type-V intermediate filament network closely associated with the nuclear face of the INM of eukaryotic cells (Gerace et al., 1978; Gerace and Burke, 1988). Lamins are composed of a long central α-helical domain, flanked by globular N-terminal (head) and C-terminal (tail) domains (Fisher et al., 1986). All these domains are required for lamins to self-assemble into higher-order structures consisting of a coiled-coil dimer formed by in parallel and in register interactions (Foeger et al., 2006; Ben-Harush et al., 2009). There are two types of lamins. B-type lamins include lamin B1 and lamin B2 (*LMNB1 and LMNB2* respectively), which are widely expressed in somatic cells, and lamin B3, a splice variant derived from *LMNB2* which is expressed in the testis only (Peter et al., 1989; Vorburger et al., 1989; Furukawa and Hotta, 1993). A-type lamins, which include the major lamins A and C widely expressed in somatic cells, the minor lamin AΔ10 weakly expressed in somatic cells, and lamin C2 expressed exclusively in the testis, are encoded by a single gene, *LMNA* (Lin and Worman, 1993; Wilson and Foisner, 2010). Originally proposed as a framework for the nuclear envelope, more recent evidence suggests the NL has major roles in chromatin organisation, gene transcription and DNA replication and repair (Amendola and van Steensel, 2014).

Mammalian genomes have ~1100-1400 lamina-associated domains (LADs), nucleotide sequences ranging from 10 kb to 10 Mb, which cover nearly 40% of the genome (Guelen et al., 2008). These LADs dynamically associate with the NL, and are enriched with histone modifications associated with transcriptional repression, including H3K9me3 and H3K27me3 (Towbin et al., 2012; Zullo et al., 2012). As such, the majority of chromatin anchored on the nucleoplasmic face of the NE is in the tightly packed heterochromatin form, limiting accessibility of transcription factors, and so gene expression can be modulated by re-localisation towards or away from the NL at the nuclear periphery (Finlan et al., 2008). Tethering of LADs at the nuclear periphery is proposed to occur by complexes formed between

chromatin-bound proteins, the NL, and transmembrane proteins localised in the INM including the lamin B receptor (LBR) and members of the LAP2-emerin-MAN1 (LEM)-domain protein family, emerin, lamina-associated-polypeptide 2 and MAN1 (Amendola and van Steensel, 2014). For example, LBR preferentially binds B-type lamins and tethers LADs by interacting directly with heterochromatin protein 1 (HP1) and methyl CpG binding protein 2 (MeCP2) (Makatsori et al., 2004; Olins et al., 2010; Babbio et al., 2012). Emerin binds lamin A, and tethers LADs by forming a ternary complex with the chromatin protein barrier-to-autointegration factor (BAF) (Lee et al., 2001).

In addition to tethering chromatin at the nuclear periphery, the NL provides structural and mechanical support essential to maintaining nuclear shape and stability (Dahl et al., 2004). Mechanical forces exerted on the nucleus emanate from cytoskeletal connections to lamins A and C via the LINC complexes, and so determine nuclear shape (Crisp et al., 2006). Through these connections, nuclear architecture can be manipulated to alter function in response to stimuli or forces exerted on the cell in a process termed mechanotransduction (Dahl et al., 2008). A-type lamins are the main proponents in providing mechanical support to the nucleus, as cells lacking lamin A/C but not lamin B1 exhibit reduced nuclear stiffness, misshapen nuclei, increased nuclear fragility and decreased cell viability under strain (Broers et al., 2004; Lammerding et al., 2006). Controlling nuclear shape and stiffness is critical for the cell. Extracellular or cytoskeletal forces can lead to the remodelling of chromatin and nuclear organisation (Booth-Gauthier et al., 2012; Iyer et al., 2012; Fedorchak et al., 2014). For example, mechanical forces applied to cells using magnetic particles induce a rapid decompaction of chromatin concomitant with actin remodelling (Iyer et al., 2012). Additionally, the G-actin-associated transcriptional cofactor megakaryoblastic acute leukaemia factor-1 (MKL), which modulates expression of genes related to cytoskeletal architecture and dynamics, is translocated to the nucleus upon application of force (Iyer et al., 2012).

1.2.2 The nucleoplasm and nuclear organisation

Within the nucleoplasm there exists a complex environment that ensures the multiple functions of the nucleus. In this section, the most relevant components and structures for this thesis will be presented.

1.2.2.1 Nucleoplasmic lamins

Whilst more than 90% of lamins are localised to the nuclear periphery, a sub-pool of A-type lamins are present in the nucleoplasm (Dorner et al., 2007). A-type and B-type lamins have an 18 amino acid farnesyl group-containing C-terminus which functions as a hydrophobic anchorage site for the nuclear membrane (Hozak et al., 1995; Moir et al., 2000). This C-terminal region is proteolytically cleaved in mature lamin A, allowing lamin A to untether from the nuclear periphery (Moir et al., 2000). A sub-fraction of lamin C, which lacks the farnesylated C-terminal region of lamin A, is also located in the nucleoplasm. Nucleoplasmic lamin A/C is predominantly associated with lamina-associated polypeptide 2α (LAP2α). These LAP2α-lamin A/C complexes bind the cell cycle and differentiation regulator retinoblastoma protein (pRb). LAP2α-lamin A/C is proposed to stabilise and lock pRb in an active hypo-phosphorylated state, thus repressing cell cycle progression (Johnson et al., 2004). LAP2α-lamin A/C complexes can also influence gene expression by interactions with the chromatin protein BAF (Dechat et al., 2004), as well as through interactions with nuclear actin and transcription regulators including c-Fos, SREBP1 and MOK-2 (Sasseville and Langelier, 1998; Dreuillet et al., 2002; Lloyd et al., 2002; Ivorra et al., 2006).

1.2.2.2 Chromosome territories

Perhaps the most important factor governing gene expression however is the organisation of the nucleus and genome as a whole. The mammalian genome is packaged into chromosomes, which are spatially organised within the interphase nucleus into chromosome territories. This compartmentalisation allows active and inactive genome regions to be separated from each other, and allows co-regulation of the activation or repression of the expression of specific genes (Cremer and Cremer, 2010). For instance, the gene-rich chromosome 19 is located in a central position in the nucleus, whilst the gene-poor chromosome 18 is located at the nuclear periphery (Croft et al., 1999). As previously discussed, transcriptionally repressive regions or heterochromatin are predominantly localised to the nuclear periphery, tethered by the nuclear lamina, but they are also associated with Polycomb group (PcG) bodies. PcG proteins are present in two complexes, polycomb repressive complex 1 (PRC1) and 2 (PRC2). PRC1 catalyses histone H2A ubiquitination, whilst PRC2 catalyses H3K27 di- and tri-methylation, resulting in transcriptional repression (Wang et al., 2004; Margueron and Reinberg, 2011). Transcriptionally active regions are termed euchromatin, and are localised towards the centre of the nucleus. Whilst heterochromatin is characterised by histone modifications such as

histone H3 lysine 9 methylation, euchromatin is marked by epigenetic modifications including histone H3 and H4 acetylation and histone H3 lysine 4 methylation (Shilatifard, 2006).

1.2.2.3 Nuclear speckles

Pre-mRNA splicing factors are organised into a multitude of punctate interchromatin granule clusters termed nuclear speckles, which are localised in the interchromatin regions of the nucleoplasm and number between 20-50 per nucleus (Spector, 1993). Proteins of the nuclear speckles include pre-mRNA splicing factors such as small ribonucleoproteins (snRNPs), transcription factors, 3'-end RNA processing factors and structural proteins such as Son, an essential protein in maintaining organisation of the aforementioned factors (Sharma et al., 2010; Spector and Lamond, 2011). Speckles are highly dynamic structures, varying in size, shape and number according to the levels of gene expression and other signals. Upon transcriptional inhibition, speckles become round and increase in size, suggesting they function in the storage or assembly of splicing factors (Melčák et al., 2000; Spector et al., 1991).

1.2.2.4 The nucleolus

Ribosomal RNA (rRNA) synthesis, processing and partial ribosome assembly all occurs at the nucleolus, the largest compartment of the nucleus. There are between 1 to 5 nucleoli per nucleus, formed around nucleolar organiser regions (NORs) (Spector, 1993). These NORs are 'chromosomal landmarks', consisting of tandemly repeated sequences of the ribosomal genes coding for 18S, 5.8S and 28S rRNA. The nucleolus is organised into three sub-domains, the fibrillar centres, the dense fibrillar component and the granular component. Ribosomal DNA transcription, rRNA processing and assembly of new ribosomal subunits occurs as a progression through these compartments (Fatica and Tollervey, 2002). Approximately 30% of nucleoli proteins are predicted to have a function related to the production of ribosomal subunits. The remaining proteins are predicted to be associated with the additional functions of the nucleoli, including regulation of RNA polymerase II transcription, cell cycle progression, DNA repair, the stress response and the biogenesis of ribonucleoprotein particles (Boisvert et al., 2007).

1.2.2.5 Cajal and promyelocytic leukaemia protein bodies

Other nuclear structures include the cajal bodies, of which there are typically 1-10 per nucleus, and the promyelocytic leukaemia protein (PML) bodies, of which there are typically 10-30 per nucleus (Gall, 2000). Cajal bodies are the site of pre-mRNA splicing factor biogenesis. The major protein of cajal bodies, coilin, is involved in the assembly and subsequent maintenance of cajal body structure, and acts as a binding factor for most of the cajal body interactions (Tucker et al., 2001). PML bodies are nuclear structures primarily made up of the protein PML (Maul et al., 2000). These structures have been functionally implicated in a number of cellular functions, including DNA repair, transcriptional regulation, cell senescence and apoptosis (Bernardi and Pandolfi, 2007).

1.3 Thesis aims

Throughout the course of its development cycle, *Chlamydia* interacts with and hijacks many host cell organelles, including the ER, the Golgi, the MVBs and LDs, to promote its intracellular lifestyle (Kumar et al., 2006; Heuer et al., 2009; Dumoux et al., 2012). In recent years, a number of studies have described the effects of *Chlamydia* infection upon the largest organelle in the host cell, the nucleus, such as the manipulation of histone methylation, the induction of DNA double-strand breaks and the depletion of the tumour suppressor p53 (Pennini et al., 2010; Chumduri et al., 2013; González et al., 2014). The inclusion is positioned in close spatial proximity to the host nucleus even in the earliest phase of *Chlamydia* development. The expanding inclusion exerts pressure on the nucleus leading to its deformation into a crescent shape (Padberg et al., 2013; Brown et al., 2014; Sun et al., 2016). Surprisingly, the implications of these observations have not been studied, especially given the emerging importance of chromosome positioning and the impact of mechanical forces on the regulation of gene transcription (Cremer and Cremer, 2010; Fedorchak et al., 2014). Thus, this thesis aims to examine and characterise in detail the relationship between the nucleus and the inclusion in infected cells.

Chapter 2 – Materials & Methods

2.1 Cell Culture

Unless otherwise stated all cell culture materials were purchased from Gibco (Invitrogen, Waltham, MA, USA). All sterile plasticware was purchased from Triple Red (Long Crendon, Buckinghamshire, UK). All centrifugation steps were performed using a Rotina 420R centrifuge (Hettich Lab Technology, Tuttlingen, Germany). Foetal calf serum (FCS) was decomplemented (50°C, 30 min) before use.

2.1.1 Cell lines and culture conditions

2.1.1.1 Cell lines

HeLa cervical epithelial cells were previously prepared in the laboratory and stored in liquid nitrogen. Cells were and grown and maintained in Dulbecco's modified eagle medium (DMEM) high glucose and GlutaMAX supplemented with 10% FCS and penicillin (100 units/ml) / streptomycin (100 µg/ml) (P/S) antibiotic mixture as recommended by the American Type Culture Collection (ATCC). $2x10^6$ cells were cultured to 70-90% confluence in 75 cm^2 tissue culture flasks in a humidified incubator at 5% (v/v) CO_2, 37°C before passage every 2-3 days. Human telomerase reverse transcriptase (hTERT) immortalised retinal pigment epithelial (RPE-1) cells (a gift from Dr. Emmanuel Boucrot, UCL) were cultured and maintained as with HeLa cells with one modification; the culture medium was altered to DMEM:F12 and supplemented with 0.25% (w/v) sodium bicarbonate. Human acute monocytic leukaemia (THP-1) cells (a gift from Dr. Kaila Srai, UCL) were cultured and maintained in RPMI-1640 medium supplemented with 10% FCS and P/S antibiotic mixture. Fresh media was added every 2-3 days and cells passaged every 7 days. Wildtype (WT) and *LMNA*$^{-/-}$ mouse embryonic fibroblasts (MEF) cells were a generous gift from Professor Brian Burke (A*STAR, Singapore) and grown and maintained in DMEM supplemented with 20% FCS, 1x Eagle's minimum essential medium (MEM) non-essential amino acids (Sigma Aldrich, St. Louis, MO, USA) and P/S antibiotic mixture. Cells were grown to 70-90% confluence and passaged.

2.1.1.2 Passage

Cells were passaged at 70-90% confluence (HeLa, RPE1, MEFs), or after 1 week (THP-1). For HeLa, RPE1 and MEF lines, cells were first washed in Hank's balanced salt solution (HBSS) to remove excess FCS. Cells were then dissociated from the flask using trypsin/EDTA solution [0.05% (w/v) trypsin, 200 µg/ml ethylenediaminetetraacetic acid (EDTA)] at 37°C for 5 min before collection in HBSS supplemented with 10% FCS. The resulting suspension was centrifuged (1200 rpm, 4°C, 10 min), and the cell pellet suspended in HBSS/FCS for counting and seeding in 75 cm^2 tissue culture flasks. For HeLa and RPE1 cell lines, $2x10^6$ cells were seeded, for MEF cell lines $1x10^6$ cells were seeded. As non-adherent cells, THP-1 cells were passaged first by centrifugation (1200 rpm, 4°C, 10 min), followed by resuspension in HBSS/FCS for counting and seeding ($1x10^6$ cells).

2.1.1.3 Counting and seeding

Following resuspension of cell pellet in HBSS/FCS, cells were counted. An equal volume of cell suspension was added to 0.4% (w/v) trypan blue solution. The resulting mixture was added to a KOVA Glasstic counting chamber (Hycor, Indianapolis, IN, USA) and the number of cells counted under a light microscope. Non-viable cells are permeable to trypan blue and so were not counted. Viable cells were counted and seeded, as outlined in Table 2.1 unless otherwise stated, in sterile cell culture plates and incubated for 18-24h [37°C, 5% (v/v) CO_2] to allow cell adherence. Prior to further experiments, THP-1 cells were differentiated by addition of phorbol myristate acetate (PMA) (Sigma Aldrich) to medium to 0.25 µM final concentration and incubated for 18-24 h [37°C, 5% (v/v) CO_2] to allow cell adherence.

Culture plate	**Cells/volume (ml) media added**
6 well plate	2.7×10^5 / ml
24 well plate	1.4×10^5 / ml
35 mm glass bottomed petri dish (MatTek Corporation, Ashland, MA, USA)	2×10^5 / ml
100 mm tissue culture dish	3×10^5 / ml
200 mm tissue culture dish	4×10^5 / ml

Table 2.1. Cell plating.

2.1.1.4 Coverslip preparation

Cells prepared for fluorescence microscopy were seeded on 12 mm glass coverslips (VWR) in a 24 well plate. Prior to seeding, cover slips were washed with 70% ethanol for 10 min then washed three times in excess HBSS.

2.1.1.5 Preparation of cells for live experiments

For live experiments, cells were seeded in glass-bottomed petri dishes. Immediately prior to live imaging, growth medium was removed, cells were washed in HBSS and medium was replaced with Fluorbrite DMEM supplemented with 10% (v/v) FCS.

2.1.2 *Chlamydia* infection

2.1.2.1 *Chlamydia* stocks

Chlamydia trachomatis serovar LGV2 stocks were prepared by Dr. Maud Dumoux (Birkbeck). HeLa cells were infected with *C. trachomatis* LGV2 (2.1.2.2) for 72 hours prior to collection by scraping in sucrose-phosphate-glutamic acid (SPG) buffer (220 mM sucrose, 17.4 mM Na_2HPO_4, 2.6 mM NaH_2PO_4, 20 mM L-glutamic acid). Bacteria were then released by repeatedly flushing the SPG medium through a 23g needle. The resulting EB-containing suspension was aliquoted and stored at -80°C.

2.1.2.2 Infection protocol

For infection medium, culture medium was prepared as normal except P/S was replaced with 25 µg/ml gentamicin. Adherent cells were infected with bacteria diluted in cell infection medium to achieve 90-100% infection across the population. Cells were centrifuged [900 rpm, room temperature (RT), 10 min] to synchronise infections and then incubated [37°C, 5% (v/v) CO_2, 90 min]. Finally, the medium was replaced 80 min later with fresh infection medium to remove any cell debris or dead bacteria.

2.1.3 Sample preparation for mEos2-importin-β import assay

Samples were prepared to study nucleocytoplasmic transport in living cells as described previously (Lowe et al., 2010), with the following modifications. Non-infected or *Chlamydia*-infected cells were washed for 3 x 2 min with phosphate buffered saline (PBS) (137 mM NaCl, 2.7 mM KCL, 8 mM Na_2HPO_4, 1.46 mM KH_2PO_4 in H_2O, pH 7.4), followed by a 2 min wash with permeabilisation buffer [50 mM 4-(2-hydroxyethyl)-1-piperazineethanesulfonic acid (HEPES), 50 mM KOAc, 8 mM $MgCl_2$, pH 7.3], followed by a 5 min permeabilisation with digitonin (Sigma Aldrich) at a concentration of 50 µg/ml supplemented with an energy regenerating system of 100 µM ATP (Roche), 100 µM GTP (Roche), 4 mM creatine phosphate (Roche) and 20 U/ml creatine kinase (Roche) in permeabilisation buffer. The digitonin was subsequently removed by washing for 3 x 3 min with transport buffer [20 mM HEPES, 110 mM KOAc, 5 mM NaOAc, 2 mM MgOAc, 2 mM dithiothreitol (DTT), pH 7.3]. After the final wash excess liquid was removed, the mEos2-importin-β reaction mix [importin-β (0.5 mM), RanGDP (5 µM), NTF2 (4 µM), 2 mM GTP, 0.1 mM ATP, 4 mM creatine phosphate, 20 U/ml creatine kinase in transport buffer] immediately added, and cells imaged live.

2.1.4 Transfections

Cells were seeded for 24 h prior to transfection using Turbofect (Thermofischer, Waltham, MA, USA), according to manufacturer's instructions with some modifications. Briefly, plasmid DNA (Table 2.3) was added to 50 µl DMEM with 0.7 µl Turbofect, mixed vigorously and incubated (RT, 15 min). The resulting solution constituted 1 volume of transfection mixture, and the number of volumes of transfection mixture added to cells was dependent on the cell culture dish used (Table 2.2). Medium was replaced with fresh culture/infection medium prior to addition of, and following 24 h incubation with transfection mixture. The amount of plasmid DNA added was determined by titration and observation of the number of successfully transfected cells (Table 2.3).

Culture plate	**Number of volumes of transfection mixture added per well**
6 well plate	3
24 well plate	1
35 mm glass bottomed petri dish	3

100 mm tissue culture dish	20
200 mm tissue culture dish	40

Table 2.2. Volumes of transfection mixture used per culture dish.

Encoded protein	Plasmid	Origin	Amount of DNA / 50 µl transfection mix (ng)
CT350-2xGFP	pEGFP-C2	this work	150 ng
CT384-2xGFP	pEGFP-C2	this work	300 ng
Nup37-3xGFP	pEGFP-C3	EUROSCARF, Frankfurt, Germany	300 ng
Nup85-3xGFP	pEGFP-C3	EUROSCARF, Frankfurt, Germany	300 ng
Pom121-3xGFP	pEGFP-C3	Dr. Guillaume Charras, UCL	300 ng
Sun1-GFP	pEGFP-C1	Professor Brian Burke (A*STAR, Singapore)	150 ng
Sun2-GFP	pEGFP-C1	Professor Brian Burke (A*STAR, Singapore)	150 ng
mEos2-importin-β	pCDNA3.1(+)	GenScript, Piscataway, NJ, USA	300 ng

Table 2.3. Constructs used for transfection of cells. EGFP: enhanced green fluorescent protein, produced either singularly (pEGFP-C1), in duplicate (pEGFP-C2) or in triplicate (pEGFP-C3) as an N-terminal fusion to the protein of interest. mEos: monomeric form of the photoactivatable fluorescent protein, Eos.

2.1.5 Polystyrene bead engulfment assay

Prior to incubation with cells, 15 µm diameter polystyrene beads (Polysciences, Warrington, PA, USA) were opsonised by incubation with human AB^+ sera [1:1 (v/v), 37°C, 1 h]. The bead/sera solution was then centrifuged (15,871 *g*, RT) using an Eppendorf 5424 benchtop centrifuge (Eppendorf, Hamburg), and the pelleted beads resuspended in PBS. Following PMA differentiation (section 2.1.3), THP-1 cells were incubated with 15 µm diameter opsonised polystyrene beads at a 2:1 cell to bead ratio for 48 h prior to fixation.

2.1.6 Drug treatments

2.1.6.1 Penicillin G

10,000 U/ml penicillin G stock solution was diluted to 10 U/ml final concentration as described by Dumoux *et al*. (2013) in culture or infection medium and the resulting medium added to cells at specified times.

2.1.6.2 Nigericin

5 mg nigericin sodium salt was dissolved in 6.7 ml dimethyl sulphoxide (DMSO) to yield a 1 mM stock solution. For treatment, nigericin solution was diluted in culture or infection medium to 1 µM final concentration and the resulting medium added to cells at specified times. This concentration was determined to be optimal previously (Andrew, 2014). Nigericin removal was performed by renewing medium with fresh culture or infection medium.

2.2 Fluorescence microscopy

2.2.1 Sample preparation

2.2.1.1 Preparation of fixed samples

Cells were fixed using paraformaldehyde (PFA) or methanol as required. For PFA fixation, growth medium was removed and cells were fixed in 4% (w/v) PFA diluted in PBS for 20 min at RT before the addition of an equal volume of neutralisation buffer (50 mM NH_4Cl in PBS) and incubation (4°C, minimum 1 h). For methanol fixation, growth medium was removed and cells were fixed in cold (-20°C) methanol (on ice, 3 min).

2.2.1.2 Permeabilisation

Fixed cells were washed in PBS prior to permeabilisation with either 0.05% (w/v) Triton X-100 dissolved in PBS (RT, 10 min) or cold (4°C) methanol/ethanol [1:1 (v/v), on ice, 5 min] before labelling.

2.2.2 Labelling

2.2.2.1 Antibody labelling

All antibodies were diluted in blocking buffer [1% (w/v) bovine serum albumin (BSA) (Sigma Aldrich) in PBS] as required using fixation/permeabilisation conditions shown in Table 2.4. Cells were washed in washing buffer [0.1% (w/v) BSA in PBS] prior to incubation with primary antibody (RT, 2 h). Following primary antibody incubation coverslips were washed with PBS and washing buffer before application of appropriate secondary antibodies as shown in Table 2.4 (RT, 1 h). Finally, cells were washed again as previously described and mounted in MOWIOL mounting medium [20% (w/v) MOWIOL 4-88 (Sigma Aldrich), 30% (v/v) glycerol in PBS] on glass microscope slides (VWR).

2.2.2.2 Fluorescent probe labelling

Fluorescent probes were diluted either alone in PBS or in conjunction with secondary antibodies as required. For double-stranded nucleic acid labelling, 1,5-bis{[2-(di-methylamino)ethyl]amino}-4,8-dihydroxyanthracene-9,10-dione (DRAQ-5) (Abcam, Cambridge, UK) at 5 mM stock concentration was diluted 1:1000 (v/v) in PBS.

2.2.2.3 Fluorescent *in-situ* hybridisation (FISH)

Oligonucleotide probes for FISH were designed and purchased from Sigma Aldrich. Probes consisted of a 5' AlexaFluor© 488-tagged, 30 base poly thymine (polyT) or poly adenine (polyA) oligonucleotide. FISH was conducted prior to antibody labelling. Cells were washed in PBS followed by washing in 2X saline-sodium citrate (SSC) buffer [diluted in H_2O from 20X SSC (Sigma Aldrich)]. Cells were then incubated in hybridisation buffer [4X SSC, 0.5 mM EDTA, 10% dextran sulphate, 10% deionised-formamide in diethylpyrocarbonate (DEPC) H_2O] mixed with 0.2 µM probe and incubated (37°C, 3 h). Cells were briefly washed in 2X SSC followed by PBS, before further labelling as required, and mounting.

Antibody	Host	Source	Fixation/permeabilisation	Dilution
FG-Nups (mAb414)	Mouse	Abcam	4% PFA / Triton X-100	1:2000
anti-Nup62	Mouse	BD Biosciences	4% PFA / Triton X-100	1:200
anti-Nup153	Mouse	Abcam	4% PFA / Triton X-100	1:100
anti-Lamin B1	Rabbit	Abcam	4% PFA / Triton X-100	1:200
anti-Lamin A/C	Mouse	Santa Cruz Biotechnology	4% PFA / Triton X-100	1:500
anti-Lamin A	Rabbit	Abcam	4% PFA / Triton X-100	1:500
anti-PDI	Rabbit	Sigma Aldrich	4% PFA / Triton X-100	1:500
anti-IncA	Mouse	Gift from Dr. Dan Rockey (Oregon State University)	4% PFA / Triton X-100	1:50
anti-H3K9me3	Rabbit	Abcam	methanol	1:500
anti-H3K4me3	Rabbit	Abcam	methanol	1:500
anti-CdsF	Rabbit	Gift from Dr. Kenneth Fields (University of Kentucky)	4% PFA / Triton X-100	1:100
anti-Emerin	Mouse	Abcam	4% PFA / Triton X-100	1:500
anti-*Chlamydia* spp.	Mouse	Argene (Now BioMérieux)	4% PFA / Triton X-100	1:300
AlexaFluor© conjugated secondary antibodies (488, 546, 633)	Goat	Invitrogen	4% PFA / Triton X-100; methanol	1:300

Table 2.4. Antibodies used for immunofluorescence.

2.2.3 Image acquisition and analysis

Unless otherwise stated, coverslips were observed using a confocal microscope (TCS SP5 AOBS; Leica Microsystems, Wetzlar, Germany) equipped with a 65 mW Argon laser, 1 mW HeNe 543 laser and a 10 mW HeNe 633 laser. Images were obtained sequentially using a 63x oil immersion objective (numerical aperture = 1.4) at 1024x1024 resolution with 400 Hz

scanning speed and a 2 frame average. z-sections were acquired at 0.33 µm intervals. Laser lines and emission windows were selected to avoid cross talk between channels in cells labelled with multiple antibodies. For GFP and AlexaFluor© 488, the 488 laser was selected and emission collected from 498 to 548 nm. For AlexaFluor© 546, the 543 laser was selected and emission collected from 555 to 633 nm. For AlexaFluor© 633 and DRAQ-5, the 633 laser was selected and emission collected from 660 to 746 nm. Image analysis was conducted using the open-source image processing package Fiji (Schindelin et al., 2012), a distribution of ImageJ (Schneider et al., 2012) and CellProfiler, an open-source image analysis software developed by Carpenter and co-workers (2006). In confocal images of *Chlamydia*-infected cells stained with DRAQ-5 to visualise DNA or anti-*Chlamydia* to visualise bacteria, the inclusion periphery was determined by tracing the edge of the inclusion using the bacterial DNA or bacteria respectively as a guide. In confocal images without DNA or *Chlamydia* staining, the inclusion position was traced by virtue of the exclusion of cellular markers upon overexposure. It should be noted that the inclusion periphery does not necessarily represent the true trajectory of the inclusion membrane.

2.2.3.1 Nuclear shape analysis

Maximum intensity projections of confocal xy-sections of HeLa cell nuclei labelled with lamin B1 were manually curated for the extent of lobulation. Nuclei were scored dependent on the number of invaginations of lamin B1 at the nuclear membrane, with single-lobed nuclei having no invaginations, bi-lobed nuclei having a single invagination and multi-lobed nuclei having multiple invaginations.

2.2.3.2 Intensity analysis of the nuclear envelope

To measure intensity of signal across the NE, the region of interest (ROI) was traced in Fiji using the 'segmented line' tool with a width of 5 pixels to match the thickness of the NE, and the 'Plot Profile' function was used, which displays a two-dimensional graph where the x-axis represents distance along the line and the y-axis the mean pixel intensity.

2.2.3.3 Quantification of the frequency of nuclear envelope alterations

The frequency of nuclear envelope alterations, including the lamin A/C 'patch', the FG-Nup 'gap', reduction in lamin B, and enrichment of H3K9me3, was manually curated in fixed non-

infected and infected HeLa/MEF cells. The lamin A/C patch was defined as an enrichment of lamin A/C staining on one face of the NE greater than 1 µm in diameter in both the xy and z dimensions, with at least 50% higher fluorescence intensity than the lamin A/C located on the distal face of the NE. The threshold of 50% was chosen to ensure differences in fluorescence are not due to natural variations. An FG-Nup gap was defined as a complete depletion of FG-Nup fluorescence intensity in the NE greater than 1 µm in both the xy and z dimensions. A lamin B reduction was defined as a region on one face of the NE greater than 1 µm in diameter in both the xy and z dimension, with at least 50% lower fluorescence intensity than the lamin B located on the distal face of the NE. For enrichment of H3K9me3, the requirement was for a region of enriched H3K9me3 on one face of the nucleus greater than 1 µm in both the xy and z dimensions with fluorescence intensity at least 50% higher than the H3K9me3 on the distal face of the nucleus.

2.2.3.4 Quantification of nuclear mRNA

Non-infected and *C. trachomatis* LGV2-infected RPE1 cells were prepared as described previously (section 2.1 and 2.2), and fixed and labelling for poly(A) mRNA and lamin B (section 2.7). Lamin B signal of nuclei in infected cells was identified using the 'IdentifyPrimaryObjects' function in CellProfiler to generate a mask covering the nuclear volume. Total intensity of poly(A) mRNA signal was then determined within this mask and calculated relative to area. The resulting average pixel intensity corrected for the area was then summed across the z-stack and divided by the number of z-sections to give mean nuclear pixel intensity per unit volume or mean nuclear voxel intensity.

2.2.3.5 Measuring inclusion size

Inclusion size was measured in infected cells labelled for *Chlamydia* as described by Dumoux et al. (2012). Briefly, the inclusion was segmented by applying grey level thresholding on wavelet-transformed images. B-Spline wavelets 'à trous' were used for convolution. A mask was created with the 'Fill Holes' option leading to the creation of a volume that represents the inclusion.

2.2.3.6 Measuring the roundness of inclusions

The roundness of inclusions (or contour ratio) was calculated from maximum intensity projections of confocal xy-sections of inclusions according to equation 1, where a perfect circle has a contour ratio of 1.

$$Contour\ ratio = \frac{4\pi x Area}{Perimeter^2}$$

Equation 1. Equation for the calculation of contour ratio.

2.3 Bacteria infectivity assay

2.3.1 Sample preparation

For quantification of infectivity in WT and *LMNA*$^{-/-}$ MEFs, an inclusion forming unit (IFU) assay was conducted. MEF cells were infected as previously described (section 2.2.2). At an appropriate time post infection, the infection medium was removed and cells and bacteria collected by scraping into SPG buffer (220 mM sucrose, 17.4 mM Na_2HPO_4, 2.6 mM NaH_2PO_4, 20 mM L-glutamic acid) prior to freezing at -80°C. After partial lysis by defrosting, cells containing bacteria were further lysed by flushing the SPG medium repeatedly through a 23g needle releasing *Chlamydia* into the medium. Bacteria were then diluted in infection medium and used to infect a fresh monolayer of HeLa cells prior to fixation at 24 hours post infection (hpi).

2.3.2 IFU quantification

Fixed HeLa cells were labelled with DRAQ-5 and anti-*Chlamydia* spp. antibody. The number of cells and inclusions were counted in duplicate across six randomly selected fields of view (FOVs) to calculate an average number of infections per FOV. This number was then multiplied by the dilution factor (1:20 for the cell layer, 1:2 for the infection medium) and a correction factor (area of coverslip / area of field of view) to obtain the IFU/ml.

2.4 Electron microscopy

Electron microscopy was conducted as described by Dumoux et al. (2012). Briefly, HeLa or RPE1 cells were cultured and infected directly on gold-coated copper membrane carriers with a 100 µm well depth (Leica) previously treated with DMEM/1% P/S for 3 days and FCS/1% P/S for 4 days. Cells were infected with *C. trachomatis* LGV2 as previously described. At 48 hpi, the membrane carriers were transferred to the Leica EM HPM100 for rapid freezing with liquid nitrogen at a pressure of 210,000 kilopascals and a cooling rate of approximately 25000 K/s. The frozen carriers were embedded in resin [freeze-substitution (FS)] using the Leica EM AFS2. Briefly, membrane carriers were incubated in dry acetone containing 0.2% uranyl acetate (FS cocktail) by warming from -160°C to -90°C. Samples were further warmed to -50°C while the FS cocktail was removed, and the samples washed in ethanol. Samples were then infiltrated with HM20 resin and the resin polymerised using UV light. The samples were finally warmed to RT and then sectioned using a Leica UC7 microtome. Sections were obtained at a 200 nm thickness and imaged using a Tecnai T10 microscope equipped with a Gatan 1k CCD camera.

2.5 Immuno (Western) blotting

2.5.1 Sample preparation

HeLa cells were seeded in 6 well plates and incubated for 18-24 h [37°C, 5% (v/v) CO_2] to allow cell adherence. Cells were infected as required and then detached by incubation in 500 µl versene (Gibco) [37°C, 5% (v/v) CO_2, 15 min]. An equal volume of HBSS/FCS was added, and the resulting cell suspension counted before centrifugation (1200 *g*, 10 min, 4°C). Cell pellets were suspended in 50 µl Laemmli buffer [125 mM Tris-HCL pH 6.8, 20% (v/v) glycerol, 4% (w/v) sodium dodecyl sulphate (SDS), 20% (v/v) β-mercaptoethanol, 0.02% (w/v) bromophenol blue] per million cells, boiled at 95°C for 10 min and stored (-20°C).

2.5.2 SDS-PAGE

Resolving and stacking gels were prepared as in Table 2.5. First, the resolving gel was pipetted into the 0.75 mm space in the gel caster. Propan-2-ol (VWR, Radnor, PA, USA) was added to ensure an even surface whilst the gel set. The propan-2-ol was then removed, the stacking gel

added and a 0.75 mm comb inserted. Once set, the gel was assembled in an electrophoresis tank, filled with migration buffer [25 mM Tris base, 192 mM glycine, 0.1% (w/v) SDS] and the comb removed. Samples were clarified (15,871 *g*, RT, 15 min) using an Eppendorf 5424 benchtop centrifuge prior to loading. Full-range rainbow molecular weight marker (Thermofischer) was added. Samples were electrophoresed at 30 mA per gel until the required separation of molecular weight markers was achieved.

Gel	**Recipe**
14% (resolving gel)	32% (v/v) ProSieve™ 50 gel solution (Lonza), 0.4 mM Trizma® hydrochloride pH 8.8, 0.1% (w/v) SDS, 0.15% (w/v) ammonium persulphate (APS), 2.15 mM N,N,N',N'-Tetramethylethylenediamine (TEMED) in H_2O
12% (resolving gel)	27% (v/v) ProSieve™ 50 gel solution, 0.4 mM Trizma® hydrochloride pH 8.8, 0.1% (w/v) SDS, 0.15% (w/v) APS, 2.15 mM TEMED in H_2O
10% (resolving gel)	23% (v/v) ProSieve™ 50 gel solution, 0.4 mM Trizma® hydrochloride pH 8.8, 0.1% (w/v) SDS, 0.15% (w/v) APS, 2.15 mM TEMED in H_2O
8% (resolving gel)	18% (v/v) ProSieve™ 50 gel solution, 0.4 mM Trizma® hydrochloride pH 8.8, 0.1% (w/v) SDS, 0.15% (w/v) APS, 2.15 mM TEMED in H_2O
5% (stacking gel)	4.5% (v/v) ProSieve™ 50 gel solution, 0.25 mM Trizma® hydrochloride pH 6.8, 0.2% (w/v) SDS, 0.1% (w/v) APS, 3.5 mM TEMED in H_2O

Table 2.5. Gel recipes.

2.5.3 Transfer

SDS-PAGE gels, 0.34 mm Whatmann blotting paper (Thermofischer) and nitrocellulose membrane (GE Healthcare, Little Chalfont, Buckinghamshire, UK) were equilibrated in transfer buffer [3.5 mM Tris base, 192 mM glycine, 20% (v/v) ethanol] at 4°C for 15 min. The cassette was then assembled as follows: foam, 3x filter paper, gel, membrane, 3x filter paper, foam. Transfers were run at 2 W per cassette (4°C, overnight).

2.5.4 Immunoblotting

Membranes were blocked in TBS-Tween (20 mM Tris HCL, 150 mM NaCl, 0.05% Tween-20) with 5% milk powder (w/v) (blocking solution) for 3 x 20 min at RT. Membranes were incubated with primary antibody diluted in blocking solution as required (Table 2.6) overnight at 4°C. Membranes were washed 3 x 20 min in TBS-Tween prior to incubation with goat anti-mouse HRP-coupled secondary antibody (1:10000, Invitrogen) (RT, 1 h). Membranes were washed again in TBS-Tween, dried, and incubated in enhanced chemiluminescence (ECL) detection reagent (GE Healthcare) prepared as per manufacturer instructions (RT, 5 min). Luminescence was detected using high performance chemiluminescence film (GE Healthcare) and the film was developed using a Compact X4 developing machine (Xograph Imaging Systems, Stonehouse, Gloucestershire, UK).

Antibody	Host	Source	Dilution
Anti-Lamin A/C [EPR4100]	Rabbit	Abcam	1:2000
Anti-γ-tubulin	Mouse	Abcam	1:2000

Table 2.6. Antibodies for immunoblotting. Primary antibodies for immunoblotting were diluted in blocking solution [5% milk powder (w/v) in TBS-Tween].

2.5.5 Quantification of lamin A/C protein levels

The developed film was digitally scanned to allow densitometry analysis. The density of bands in each lane was calculated by using the 'Plot Lanes' function in Fiji and measuring the area of each peak. The protein levels of lamin A and lamin C relative to γ-tubulin were calculated by dividing the area of the peaks corresponding to lamin A or lamin C by the area of the peak corresponding to γ-tubulin.

2.6 Remote sequence homology and fold recognition

For remote sequence homology detection, amino acid sequences of proteins of interest were submitted to the HHblits server (Remmert et al., 2011) using the HHblits UniProt20 hidden Markov model (HMM) database and default settings (three iterations, local alignment mode, MAC realignment threshold of 0.35). For fold detection, amino acid sequences of proteins of

interest were submitted to the HHpred homology detection and structure prediction server (Hildebrand et al., 2009) using the HHpred PDB70 HMM database and default settings (HHblits MSA generation method, three iterations, secondary structure scored, local alignment mode).

2.7 Identification of α-solenoid folds using secondary structure prediction

A tool for calculating and visualising consensus secondary structure prediction sequences from three secondary structure element (SSE) prediction software [Jpred (Cuff et al., 1998), Psipred (McGuffin et al., 2000), RaptorX (Källberg et al., 2012)] was written using the Python programming language. For each amino acid residue of the protein sequence of interest, the SSE type (helix, strand or coiled coil) and corresponding confidence value (scored from 0-9, with 9 being high confidence) are recorded and summed across the three prediction software. The SSE type with the highest confidence value is then selected as the consensus SSE for this position, and the confidence value of this consensus SSE is recalculated by dividing the sum of the confidence values for the SSE type by the maximum confidence value possible, which is 27 (3*9). The resulting consensus SSE sequence was output visually using the PostScript programming language for creating vector graphics. Code for the SSE consensus tool can be found in the appendix.

Parameters for identification of α-solenoid folds were then determined using the consensus SSE sequence of known α-solenoid fold-containing proteins (Nup85, Nup107, Nup133, Nup160, importin-β) which were determined to be minimally 450 amino acids in length, have a minimal uninterrupted sequence of alpha helix/loop residues of 200, and were comprised of over 90% α-helix/loop SSEs and over 40% α-helix SSEs.

2.8 Prediction of bacterial secretion

Amino acid sequences of proteins of interest were submitted to signal peptide [SignalP 4.0 (Petersen et al., 2011)] and type III secretion [EffectiveT3 (Arnold et al., 2009), BPBAac (Wang et al., 2011), ANN (Löwer and Schneider, 2009), T3_MM (Wang et al., 2013) and BEAN 2.0 (Dong et al., 2015)] prediction servers using default settings.

Chapter 3 – Examining the impact of infection with *C. trachomatis* on nuclear architecture

3.1 Introduction

Chlamydiae replicate within a membrane bound compartment termed an 'inclusion'. This inclusion localises to the peri-nuclear region in close proximity to the microtubule organising centre (Clausen et al., 1997). Briefly, as the infection progresses, the inclusion expands to occupy the majority of the host cytosol; recruiting, fragmenting or ingesting many cellular organelles including the endoplasmic reticulum (ER), the Golgi apparatus, multi-vesicular bodies and lipid droplets (as discussed in section 1.1.6) (Beatty, 2006; Kumar et al., 2006; Heuer et al., 2009; Dumoux et al., 2012). In HeLa cells, the infection cycle lasts 48-72 hours for *C. trachomatis* LGV2 (Andrew, 2014). In addition to targeting at least one type III effector, the histone methyltransferase NUE, to the nucleus (Pennini et al., 2010), *Chlamydia* infection also impacts upon cellular processes controlled by the nucleus, including inhibition of apoptosis by degrading p53, alteration of cellular aging pathways by upregulating hTERT and suppressing DNA double-strand break repair (Chumduri et al., 2013; Padberg et al., 2013; González et al., 2014). However, little is known about the mechanism of interactions with this major organelle.

Whilst images of late-stage *Chlamydia*-infected cells frequently show nuclei distorted into a crescent shape, any consequences of these changes have not been investigated (Padberg et al., 2013; Brown et al., 2014; Sun et al., 2016). Alterations to nuclear shape are associated with a number of pathologies and conditions, including laminopathies and cancer. In the laminopathies, lamina proteins are either mutated or mislocalised due to aberrant processing. These diseases are characterised by abnormal nuclear architecture, increased sensitivity to mechanical stress and alterations in gene expression (Burke and Stewart, 2002). For example, individuals with Hutchinson-Gilford progeria syndrome (HGPS) prematurely age due to a mutation in the *LMNA* gene, leading to an incompletely processed form of prelamin A known as progerin incorporating into the NL and altering the mechanical properties and organisation of the NL (Eriksson et al., 2003; Dahl et al., 2006). This results in nuclear shape abnormalities, aberrant organisation of heterochromatin and changes in the expression patterns of 352 genes (McCord et al., 2013). Additionally, nucleoplasmic progerin sequesters DNA replication and repair factors at foci leading to genomic instability (Musich and Zou, 2009), and reductions in

levels of nucleoplasmic lamin A/C result in impaired cell proliferation and down-regulation of extracellular matrix components (Vidak et al., 2015). The connection between aberrant nuclear shape and some cancers is less well established, but relates to the nuclear lamina as many tumours are characterised by down-regulation of A-type lamin expression (de las Heras et al., 2013). It is also interesting to note that abnormal nuclear shape is implicated in aging, in this case due to sporadic production of the HGPS lamin A isoform (Scaffidi and Misteli, 2006).

As exampled by the laminopathies, nuclear shape and function are therefore closely interrelated. Nuclear shape is determined by mechanical forces on the nucleus emanating from cytoskeletal connections to lamins A and C through the transmembrane LINC complexes. As a result of these connections, nuclear architecture can be manipulated to alter function in response to external stimuli or forces exerted on the cell in a process termed mechanotransduction. Indeed, these extracellular or cytoskeletal forces can induce distal remodelling of chromatin and nuclear organisation with subsequent impact on gene expression (Booth-Gauthier et al., 2012; Iyer et al., 2012; Fedorchak et al., 2014). Lamins are major determinants of structural and mechanical support in the nucleus, and the NL is further stabilised by lamin binding proteins such as emerin (Lammerding et al., 2005). Cells lacking lamin A/C, but not B-type lamins, exhibit reduced nuclear stiffness and increased nuclear and cellular fragility (Broers et al., 2004; Lammerding et al., 2006), whilst the aforementioned HGPS cells exhibit increased nuclear stiffness but also corresponding sensitivity to mechanical strain (Dahl et al., 2006). As might be expected, mutations in LINC complex proteins can also result in disease states due to interruption of nuclear-cytoskeletal connections. For instance, in Emery-Dreifuss muscular dystrophy (EDMD), mutations in the LINC complex proteins SUN1 and SUN2 contribute to increased disease severity (Meinke et al., 2014). Whilst nuclear shape is not known to be specifically manipulated by any intracellular pathogens, overexpression of the LINC complex protein SUN2 induces a multi-lobular nuclear shape similar to progeria cells that inhibits replication of certain HIV-1 and HIV-2 strains by blocking nuclear entry following reverse transcription (Donahue et al., 2016).

Therefore, given the importance of nuclear architecture in nuclear function, and the previously reported effect of the inclusion on the nucleus, the aim of this chapter is to examine in detail the impact of *Chlamydia* infection on nuclear shape and components of the nuclear envelope.

3.2 Assessment of nuclear shape in cultured mammalian cells

Prior to assessing the influence of chlamydial infection on nuclear architecture, it was first necessary to develop qualitative and quantitative approaches to study nuclear shape in cultured mammalian cell lines. The NE was visualised by confocal microscopy in fixed cells by labelling with an antibody raised against Lamin B1 and an appropriate AlexaFluor®-conjugated secondary antibody. In the majority of HeLa cells, nuclei were typically an ovoid shape with a uniform nuclear envelope (Fig 3.1A). However, a small proportion of cells exhibited bi-lobed or multi-lobed nuclei (Fig 3.1A). These non-ovoid shapes are typical in certain cell types, such as neutrophils, but have also been reported in HeLa cells, other transformed epithelial cell lines and aged cells (Scaffidi and Misteli, 2006; Imbalzano et al., 2013; Kawaguchi et al., 2015), and are dependent upon the nuclear lamina and cytoskeletal forces (Hoffmann et al., 2007; Olins et al., 2008). To assess nuclear shape, three nuclear morphologies were defined based on previously published studies: single lobed/ovoid, bi-lobed and multi-lobed, thus representing progressive distortion of nuclear shape (Goldman et al., 2004; Olins and Olins, 2004; Imbalzano et al., 2013). Cells that exhibited signs of apoptosis such as DNA fragmentation and membrane blebbing were excluded. When nuclear shape in cultured HeLa cells was assessed using these parameters, 75 ± 6.1% of nuclei are ovoid, 14 ± 4.5% are bi-lobed and 11 ± 1.7% are multi-lobed (Fig 3.1B). These approaches allowed the subsequent qualitative and quantitative analysis of nuclear architecture in *Chlamydia*-infected cells.

Figure 3.1. Assessment of nuclear shape in HeLa cells. Fixed HeLa cells were stained with anti-lamin B1 primary antibody and an AlexaFluor® 488-conjugated secondary antibody (grey) to visualise lamin B (A) Maximum intensity projections of confocal xy-sections of HeLa nuclei. Examples of single-lobed, bi-lobed and multi-lobed nuclei are shown. White arrowheads indicate points at which additional lobules can be observed. Scale bars, 10 µm. (B) Nuclei (n=200) were scored for the number of lobes based on the categories shown in (A). Error bars show standard deviation (***p<0.01 using Student's t-test between single lobed and bi/multi lobed).

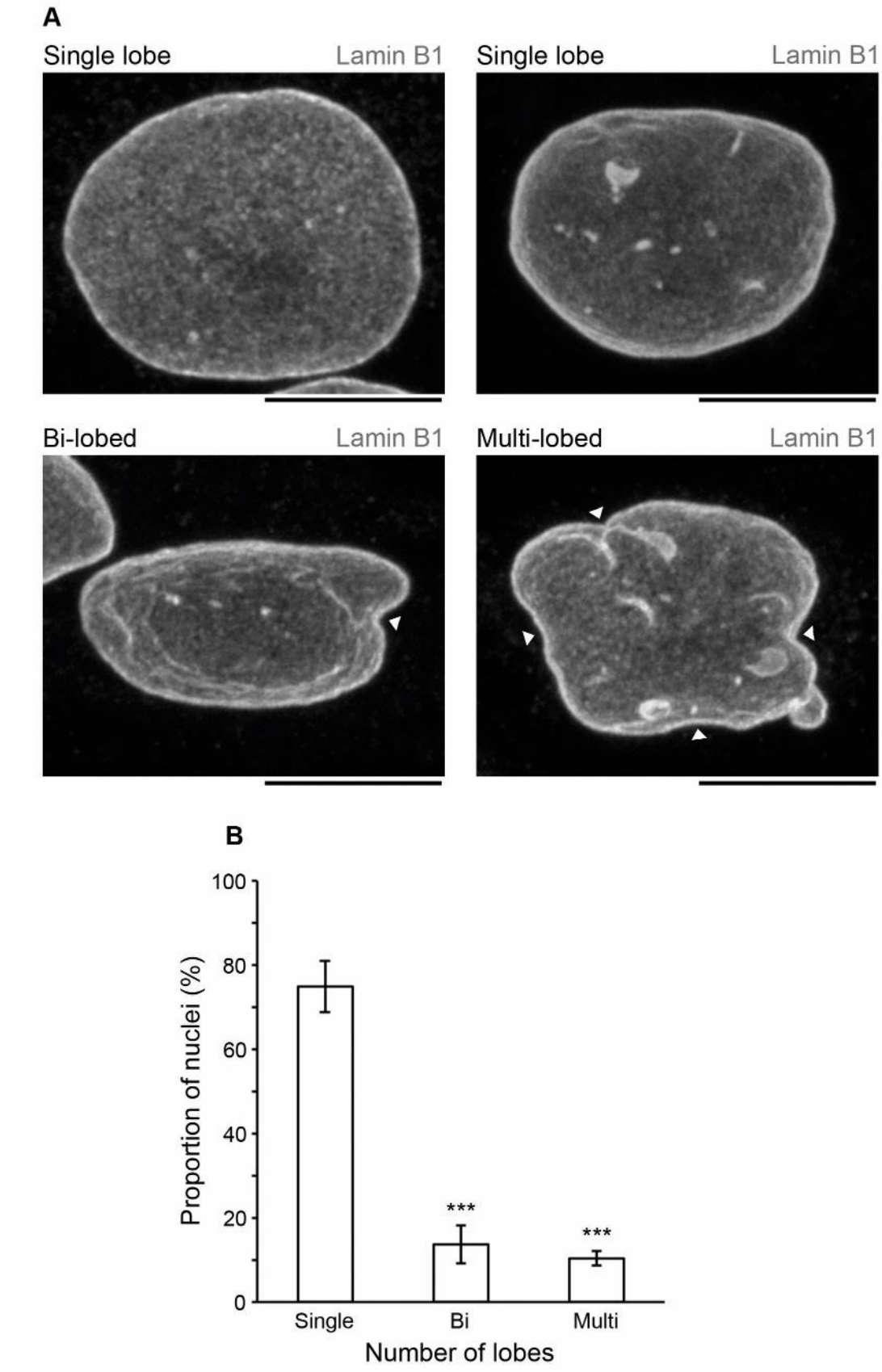
A
Single lobe
Lamin B1
Single lobe
Lamin B1
Bi-lobed
Lamin B1
Multi-lobed
Lamin B1
B
Proportion of nuclei (%)
100
80
60
40
20
0
***
***
Single
Bi
Multi
Number of lobes

3.3 Nuclear lobulation progressively increases during *Chlamydia* infection

Having characterised nuclear morphology in cultured HeLa cells, cells were infected with *C. trachomatis* LGV2 and nuclear shape identically quantified. The NE was visualised as previously with anti-Lamin B1, and an antibody raised against IncA, a *Chlamydia* inclusion protein, was used to visualise the inclusion membrane (IM). At 24 hours post infection (hpi), when the inclusion is relatively small, nuclear shape was distorted with an invagination of the NE adjacent to the inclusion (Fig 3.2A). As the infection progressed the inclusion expanded significantly causing the nuclei to become further distorted and crescent shaped (Fig 3.2B) (Brown et al., 2012). The inclusion-proximal face of the NE adopted a regular shape that closely followed the contours of, but did not co-localise with, the IM. However, the distal face of the NE was much more irregular, with multiple invaginations reminiscent of multi-lobed nuclei. Nuclear shape was therefore assessed using the morphology parameters described previously (Fig 3.2C).

At 24 hpi the proportion of nuclei with a single lobe was 52 ± 4.6%, significantly lower than non-infected HeLa cells. This value reduced further as the infection continued to progress, with just 37 ± 2.0% of nuclei being ovoid by 72 hpi. Correspondingly, the number of infected cells with bi- or multi-lobed nuclei increased during infection, with a trend from 24 to 72 hpi of an increasing proportion of multi-lobed nuclei. These data suggest that *Chlamydia* infection impacts upon nuclear shape more profoundly than previously thought with nuclei, in addition to distortion into a crescent shape, becoming increasingly lobulated.

Figure 3.2. Nuclear shape is distorted during chlamydial infection. HeLa cells were infected with *C. trachomatis* LGV2 and fixed at the indicated time post infection. Cells were double-stained with anti-IncA primary antibody and an AlexaFluor® 488-conjugated secondary antibody (grey, green) to visualise the inclusion membrane, and anti-lamin B1 primary antibody and an AlexaFluor® 546-conjugated secondary antibody (red) to visualise lamin B. (A) 24 hours post infection (hpi). (B) 48 hpi. (C) Nuclei at each time point post infection (n=100) were scored for the number of lobes based on the categories shown in Fig 3.1. White bars: single lobed, grey bars: bi-lobed, black bars: multi-lobed. NI: non-infected. Error bars show standard deviation (**$p<0.05$ using Student's t-test between NI single lobed and 24/48/72 hpi single lobed, and with a Q value greater than the critical Q value for significance to 0.05 using One-way analysis of variance (ANOVA) followed by post-hoc Tukey's honest significant difference (HSD) test).

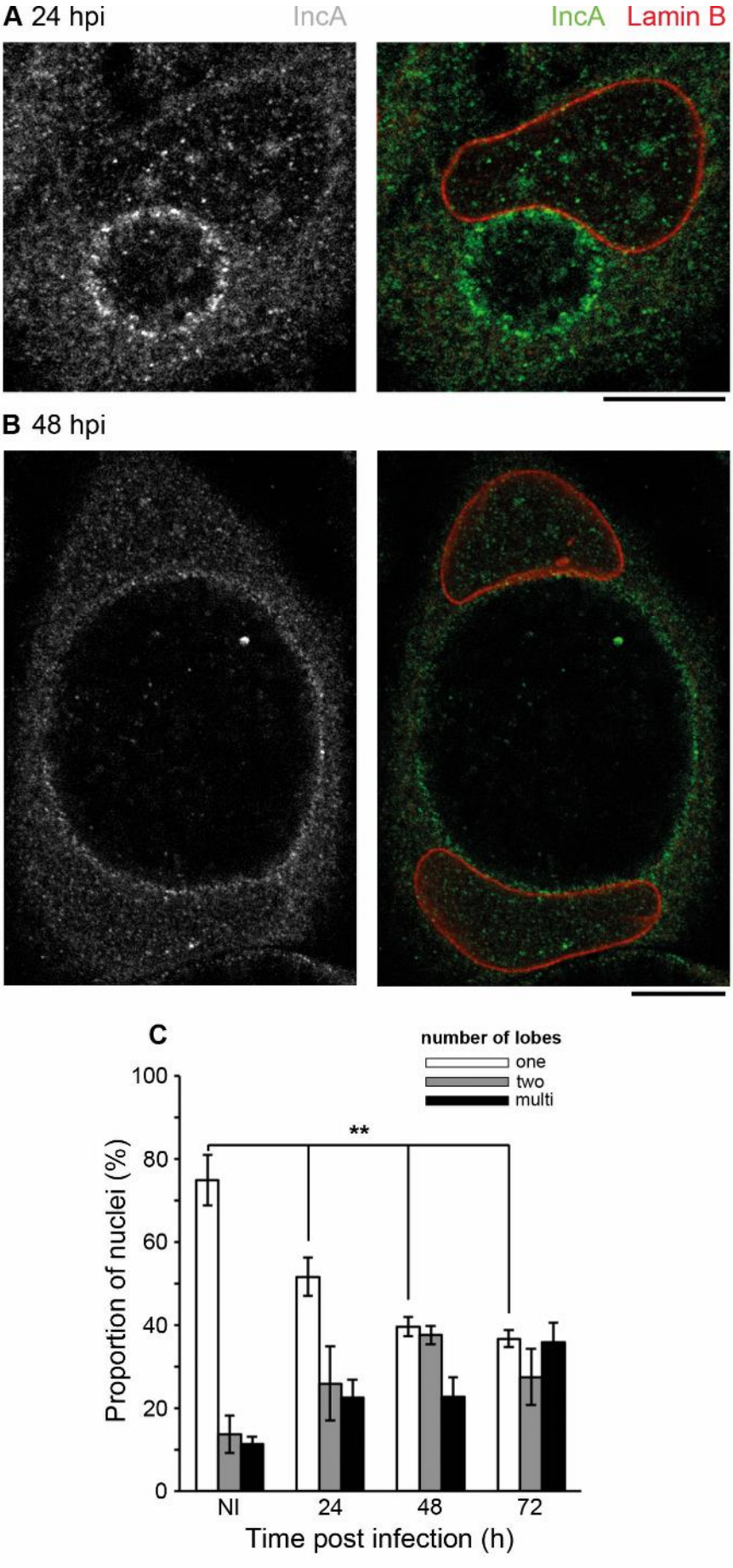
A 24 hpi
IncA
IncA Lamin B
B 48 hpi
C
number of lobes
one
two
multi
**
Proportion of nuclei (%)
100
80
60
40
20
0
NI
24
48
72
Time post infection (h)

3.4 A consistent distance is maintained between the inclusion membrane and nuclear envelope

The chlamydial inclusion contacts multiple host organelles, notably the ER, where it assembles a 'pathogen synapse' at which ordered arrays of type III secretion complexes link the bacterial envelope, the inclusion membrane and the rough ER (Dumoux et al., 2012). The outer nuclear membrane (ONM) of the NE also possesses ribosomes, and is contiguous with both the rough and smooth ER (Gerace and Burke, 1988). Given the biochemical similarity between the ONM of the NE and the ER and the close proximity of the inclusion membrane to the NE as the inclusion expands into and deforms the host nucleus, it is conceivable that *Chlamydia* may also establish an array of T3SS at this location to target effectors such as NUE directly into the nucleus.

To investigate this, chlamydial type III secretion complexes were labelled using an antibody raised against the major needle subunit protein, CdsF (Fig 3.3). DRAQ-5 was used to label double-stranded nucleic acids such as host and bacterial DNA and cytosolic RNA (Martin et al., 2005). Serial confocal z-sections showed that at 24 hpi, when the majority of the bacteria are metabolically active reticulate bodies (RBs), there is consistent labelling of CdsF around the IM but no specific polarisation towards the NE (Fig 3.3A). At 48 hpi, where there are significantly fewer RBs and more of the infectious, metabolically inactive elementary bodies (EBs), CdsF labelling became more irregular around the IM (Fig 3.3B). Whilst CdsF was still present at the IM adjacent to the NE, there was no apparent polarisation of CdsF facing the nucleus.

The lack of enrichment of T3S complexes suggests a pathogen synapse with the nucleus similar to that formed with the ER is unlikely. However, this does not exclude the existence of other membrane contact sites (MCSs). To investigate whether any evidence of contact sites exists, electron microscopy was used to observe phenomena that are not visible at the resolution of light microscopy. HeLa cells infected with *C. trachomatis* LGV2 were vitrified at 48 hpi by high-pressure freezing, freeze-substituted, embedded in HM20 resin, and observed by electron microscopy (Fig 3.4A). These higher resolution views showed that RBs do not specifically cluster adjacent to the nucleus or exhibit specific structural rearrangements. The inclusion-proximal face of the NE closely tracked the contours of the IM but did not come into contact, and a patch of increased electron density formed at the IM where the IM and NE are closely apposed (indicated by cyan arrows), suggesting the composition of the IM in this region is

altered. Intriguingly, the IM and NE appeared to be separated by a consistent distance. To quantify this, linear distances between the IM and NE at approximately 100 nm intervals were measured from the electron micrographs (Fig 3.4B). The average distance in 10 infected cells was 163 nm with a minimum distance of 104 nm and a maximum distance of 240 nm. This range of distances between cells was much larger than the range of distances for measurements within each cell, with an average standard deviation of 44.6 nm compared to 23.5 nm respectively, indicating that measurements within each cell are relatively more constant. However, it is difficult to draw conclusions from this difference as measurements were taken from single EM sections and not tomograms, and so the relative position in z between different sections, and therefore the relative z position of the NE in relation to the inclusion, is unknown.

Nonetheless, these distances far exceed the proximity of both the pathogen synapse and canonical MCSs, which are typically less than 30 nm (Dumoux et al., 2012; Helle et al., 2013). Taken together, these data suggest a classical MCS existing between the IM and the NE such as that seen between, for example, the ER and the mitochondria is unlikely (Helle et al., 2013), but the existence of increased electron density at the IM and a relatively constant distance between the IM and NE hint at the possibility of some form of novel junction.

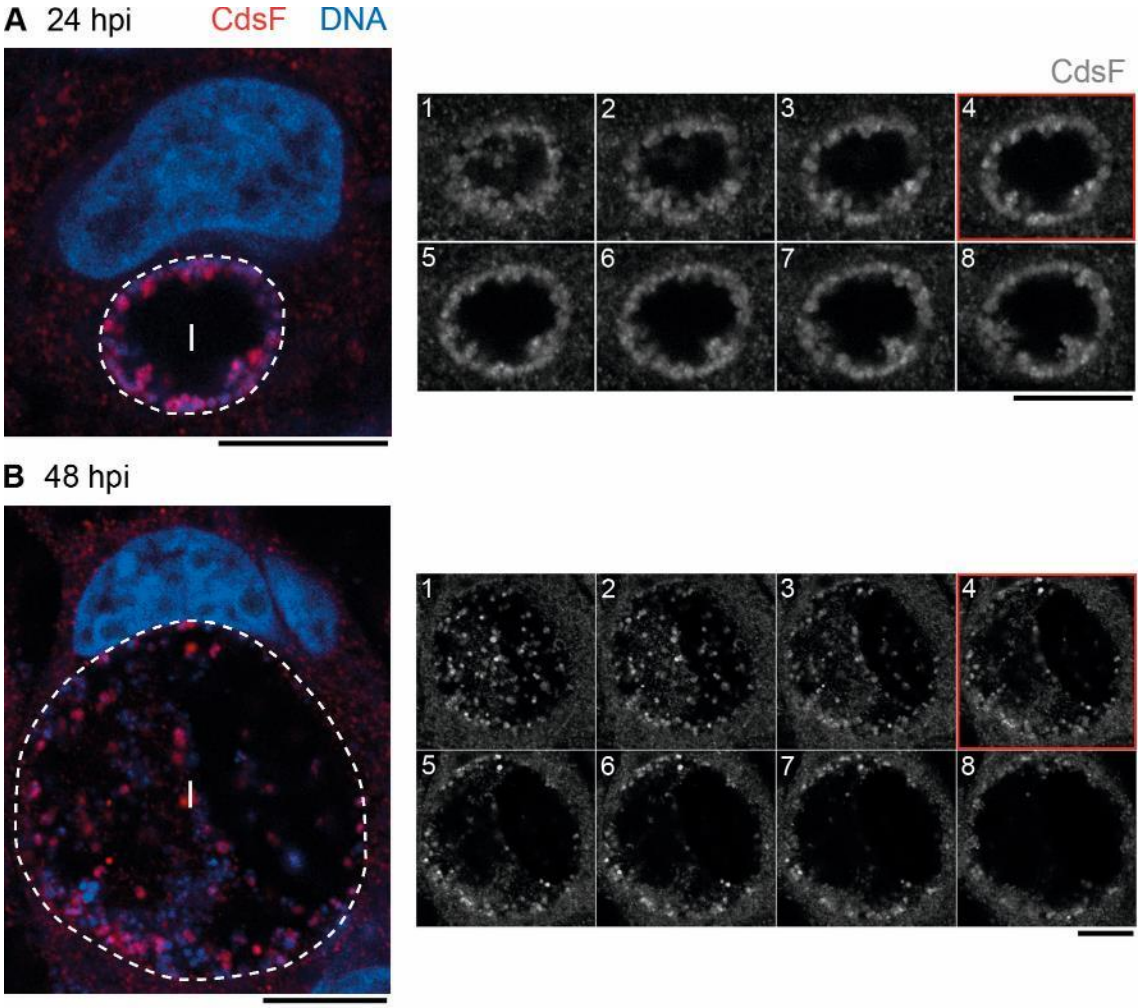

Figure 3.3. *Chlamydia* type III secretion systems are not enriched at the inclusion membrane proximal to the nucleus. HeLa cells were infected with *C. trachomatis* LGV2 and fixed at the indicated time post infection. The exposed needle of the chlamydial T3SS was labelled with an anti-CdsF primary antibody and an AlexaFluor® 546-conjugated secondary antibody (grey, red), and double-stranded nucleic acids stained with DRAQ-5 (blue). Left panels: confocal images of infected cells in the xy-plane, with the inclusion (I) periphery indicated by the white dashed line (Methods 2.8). Right panels: confocal xy-sections of the inclusion, ascending in the z dimension through the cell (1-8) with a step of 0.34 µm. Red borders indicate the sections equivalent to the left panels. (A) 24 hours post infection (hpi). (B) 48 hpi. Scale bars, 10 µm.

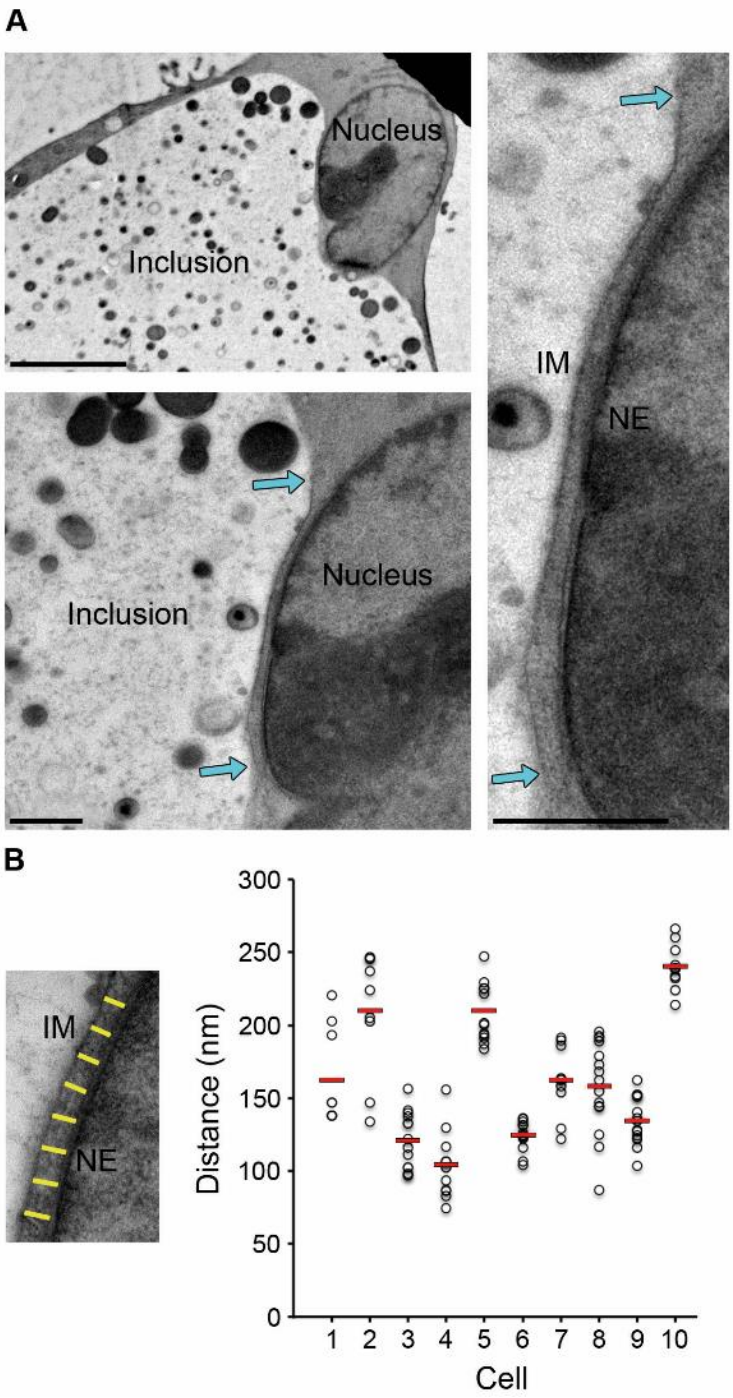

Figure 3.4. Electron microscopy reveals a consistent distance between the inclusion membrane and nuclear envelope. HeLa cells infected with *C. trachomatis* LGV2 were vitrified at 48 hours post infection by high-pressure freezing, negatively stained using uranyl acetate during freeze-substitution, embedded in HM20 resin and sectioned**.** (A) Upper left: transmission electron micrograph of a 200 nm thick section with an infected HeLa cell. Lower left and right: Magnifications of the inclusion and nucleus, showing a consistent distance between the inclusion membrane (IM) and the nuclear envelope (NE). Cyan arrows mark a region of increase electron density in the IM. Scale bars: upper, 5 µm; lower left, 1 µm; lower right, 0.2 µm. (B) Measurements of the linear distance perpendicular from the NE to the IM (left; yellow dashes) where the NE tracks the contours of the IM were taken at 100 nm intervals and plotted for each cell (n=10) (right), with white circles as the individual distance measurements and red dashes indicating mean distance.

3.5 Lamin A/C is enriched at the inclusion-proximal face of the NE during *Chlamydia* infection

The experiments presented so far have shown a pathogen synapse between the inclusion and nucleus similar to that observed between the inclusion and ER is not present, but a novel junction-like structure may exist (section 3.4). Additionally, gross nuclear architecture is distorted into a crescent structure and nuclei in infected cells become progressively lobulated at the inclusion-distal face of the NE (section 3.3). Lobulated nuclei are most frequently associated with immune cells such as granulocytes in which lamin A/C and lamin B levels are reduced (Olins et al., 2001), and the laminopathies, rare genetic disorders caused by mutations in genes encoding for the NL, classically *LMNA* which encodes lamin A/C (Goldman et al., 2004). It was therefore hypothesised that the NL might be altered during *Chlamydia* infection.

HeLa cells infected with *C. trachomatis* LGV2 were fixed and labelled to visualise lamin A/C and DNA. In non-infected cells, lamin A/C labelling was evenly distributed throughout the NE as expected from previous studies using this antibody (Fig 3.5) (Dreuillet et al., 2002; Reynolds et al., 2004). This was replicated at 24 hpi where labelling was again evenly distributed despite the inclusion-induced distortion in gross nuclear architecture (Fig 3.6). At 48 hpi and 72 hpi however, major changes to lamin A/C distribution occurred (Fig 3.7 and Fig 3.8). At the inclusion-proximal face of the NE, where the inclusion compresses the nucleus leading to the associated distortion of gross nuclear architecture, a 'patch' of enriched lamin A/C was formed. Around the remainder of the NE, lamin A/C levels appeared depleted compared to control cells. To confirm this, the intensity of lamin A/C fluorescence was measured around the NE in non-infected and infected cells and plotted relative to distance (Fig 3.9A). The lamin A/C levels were ~50% higher in non-infected cells compared to infected cells, except within the region of the NE in infected cells corresponding to the patch of enrichment, where lamin A/C levels were equal to or greater than lamin A/C levels around the NE of non-infected cells. It is also interesting to note that the reduction in lamin A/C levels on the inclusion-distal face of the NE occur in the same region of the NE where the nuclei is more lobulated, suggesting these two observations may be linked (section 3.3).

The frequency of the enriched patch of lamin A/C was quantified in control and infected cells. A lamin A/C patch was defined as an enrichment of lamin A/C staining on one face of the NE greater than 1 µm in diameter in both the xy and z dimension, with at least 50% higher

fluorescence intensity than the lamin A/C located on the distal face of the NE. In infected cells, enrichment of lamin A/C exclusively occurred in the NE adjacent to the inclusion membrane, suggesting proximity to the inclusion may be important in forming the lamin A/C patch. Quantification showed that the frequency of lamin A/C patches increases as infection progresses (Fig 3.9B). At 24 hpi, 7.1 ± 0.2% of cells had nuclei with lamin A/C patches compared to 1.3 ± 0.4% of nuclei in non-infected cells. At 48 hpi this frequency rose to 52.9 ± 2.5% and at 72 hpi to 72.1 ± 11.5%. Thus, during the mid-stage of infection at 24 hpi, where the majority of bacteria are in the RB form, lamin A/C patches begin to form, but at late (48 hpi) and very late stages (72 hpi), where the bacteria are increasingly differentiating back into EBs, the lamin A/C patches occur in approximately half and three quarters of all infected cells respectively. These data support the conclusion that lamin A/C patch occurrence is associated with the latter stages of the *Chlamydia* lifecycle.

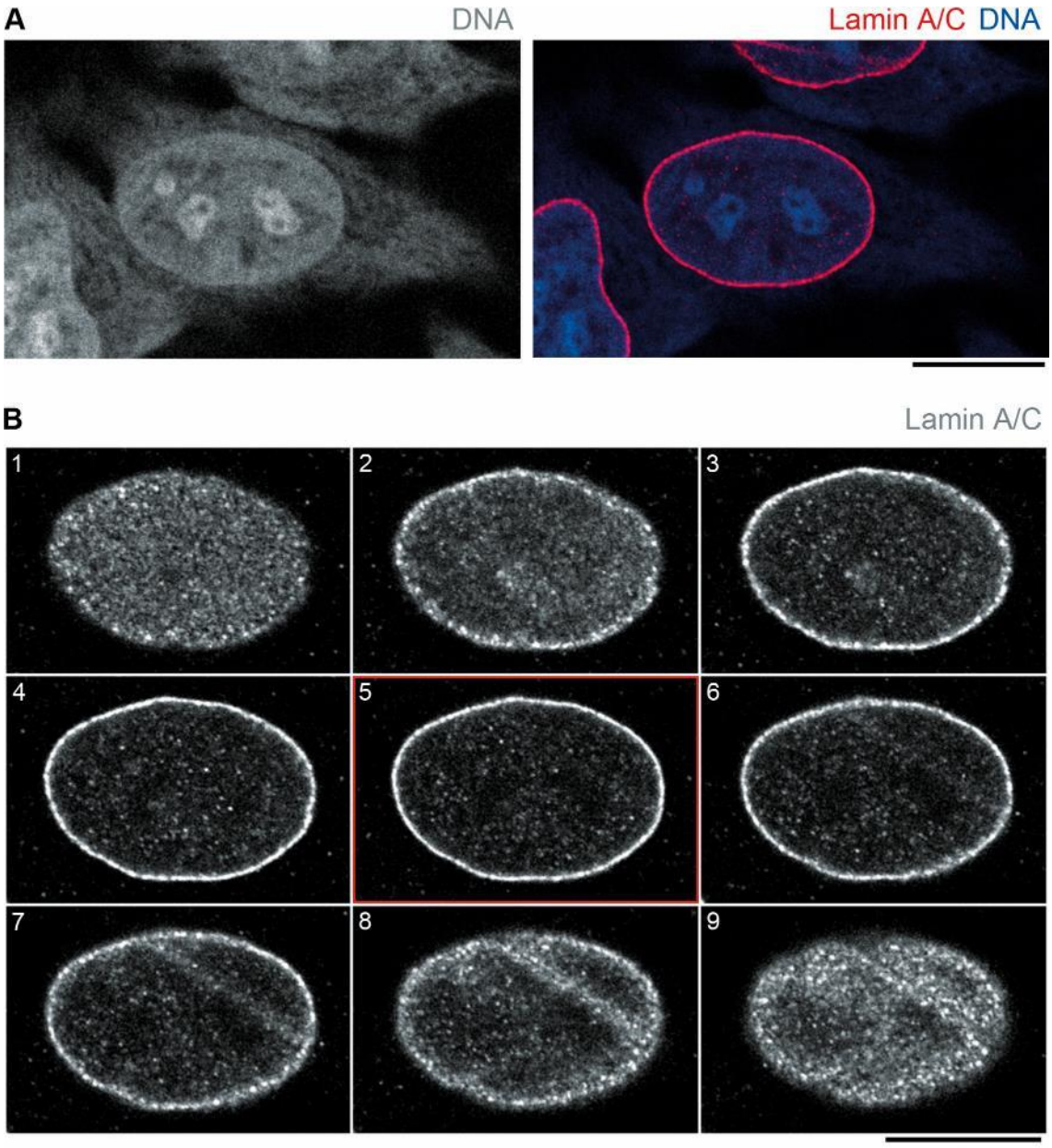

Figure 3.5. Lamin A/C is evenly distributed at the nuclear envelope in cultured HeLa cells. Fixed HeLa cells were double stained with anti-lamin A/C primary antibody and an AlexaFluor® 546-conjugated secondary antibody [red, grey (lower)] to visualise lamin A/C, and DRAQ-5 to visualise DNA [blue, grey (upper left)]. (A) Confocal images of a HeLa cell in the xy-plane. (B) Confocal xy-sections of the nucleus, ascending in the z dimension through the cell (1-9) with a step of 0.34 µm. The section equivalent to (A) is indicated with a red border. Scale bars, 10 µm.

Figure 3.6. Lamin A/C is evenly distributed at the nuclear envelope at 24 hours during chlamydial infection. HeLa cells were infected with *C. trachomatis* LGV2, fixed at 24 hours post infection (hpi) and double stained with anti-lamin A/C primary antibody and an AlexaFluor® 546-conjugated secondary antibody [red, grey (lower)] to visualise lamin A/C, and DRAQ-5 to visualise DNA [blue, grey (upper left)]. (A) Confocal images of an infected cell in the xy-plane, with the inclusion (I) periphery indicated by the white-dashed line (Methods 2.8). (B) Confocal xy-sections of the nucleus, ascending in the z dimension through the cell (1-12) with a step of 0.34 µm. The section equivalent to (A) is indicated by the red border. Scale bars, 10 µm.

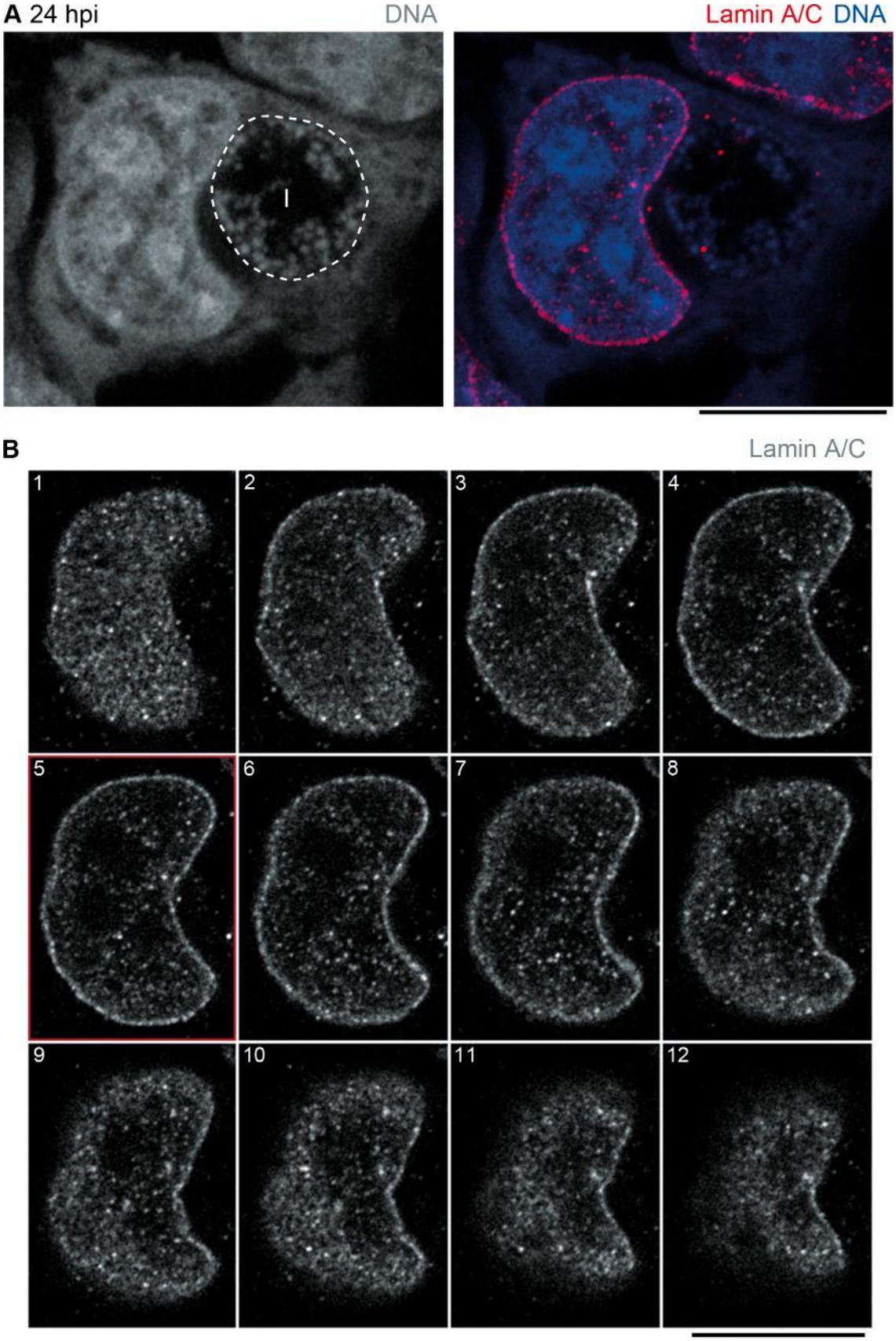
A 24 hpi
DNA
Lamin A/C DNA
I
B
Lamin A/C
1
2
3
4
5
6
7
8
9
10
11
12

Figure 3.7. Lamin A/C is enriched at the inclusion-proximal face of the nuclear envelope at 48 hours during chlamydial infection. HeLa cells were infected with *C. trachomatis* LGV2, fixed at 48 hours post infection (hpi) and double stained with anti-lamin A/C primary antibody and an AlexaFluor® 546-conjugated secondary antibody [red, grey (lower)] to visualise lamin A/C, and DRAQ-5 to visualise DNA [blue, grey (upper left)]. (A) Confocal images of an infected cell in the xy-plane, with the inclusion (I) periphery indicated by the white-dashed line (Methods 2.8). (B) Confocal xy-sections of the two nuclei, ascending in the z dimension through the cell (1-12) with a step of 0.34 µm. The sections equivalent to (A) are indicated by the red border. White arrows highlight areas of lamin A/C enrichment. Scale bars, 10 µm.

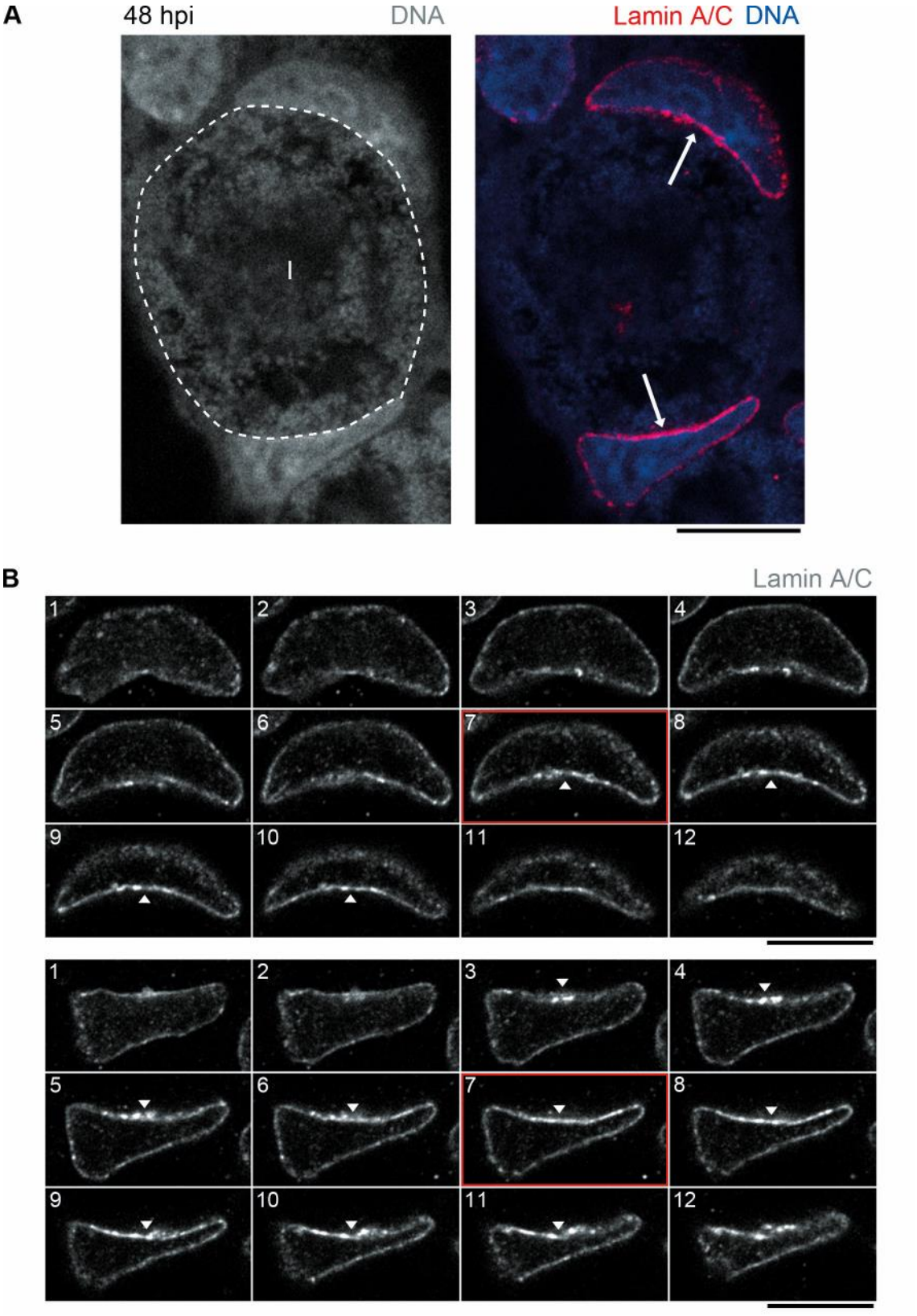
A
48 hpi
DNA
Lamin A/C DNA
B
Lamin A/C
1
2
3
4
5
6
7
8
9
10
11
12

Figure 3.8. Lamin A/C is enriched at the inclusion-proximal face of the nuclear envelope at 72 hours during chlamydial infection. HeLa cells were infected with *C. trachomatis* LGV2, fixed at 72 hours post infection (hpi) and double stained with anti-lamin A/C primary antibody and an AlexaFluor® 546-conjugated secondary antibody [red, grey (lower)] to visualise lamin A/C, and DRAQ-5 to visualise DNA [blue, grey (upper left)]. (A) Confocal images of an infected cell in the xy-plane, with the inclusion (I) periphery indicated by the white-dashed line (Methods 2.8). (B) Confocal xy-sections of the nucleus, ascending in the z dimension through the cell (1-15) with a step of 0.34 µm. The section equivalent to (A) is indicated by the red border. White arrows highlight areas of lamin A/C enrichment. Scale bars, 10 µm.

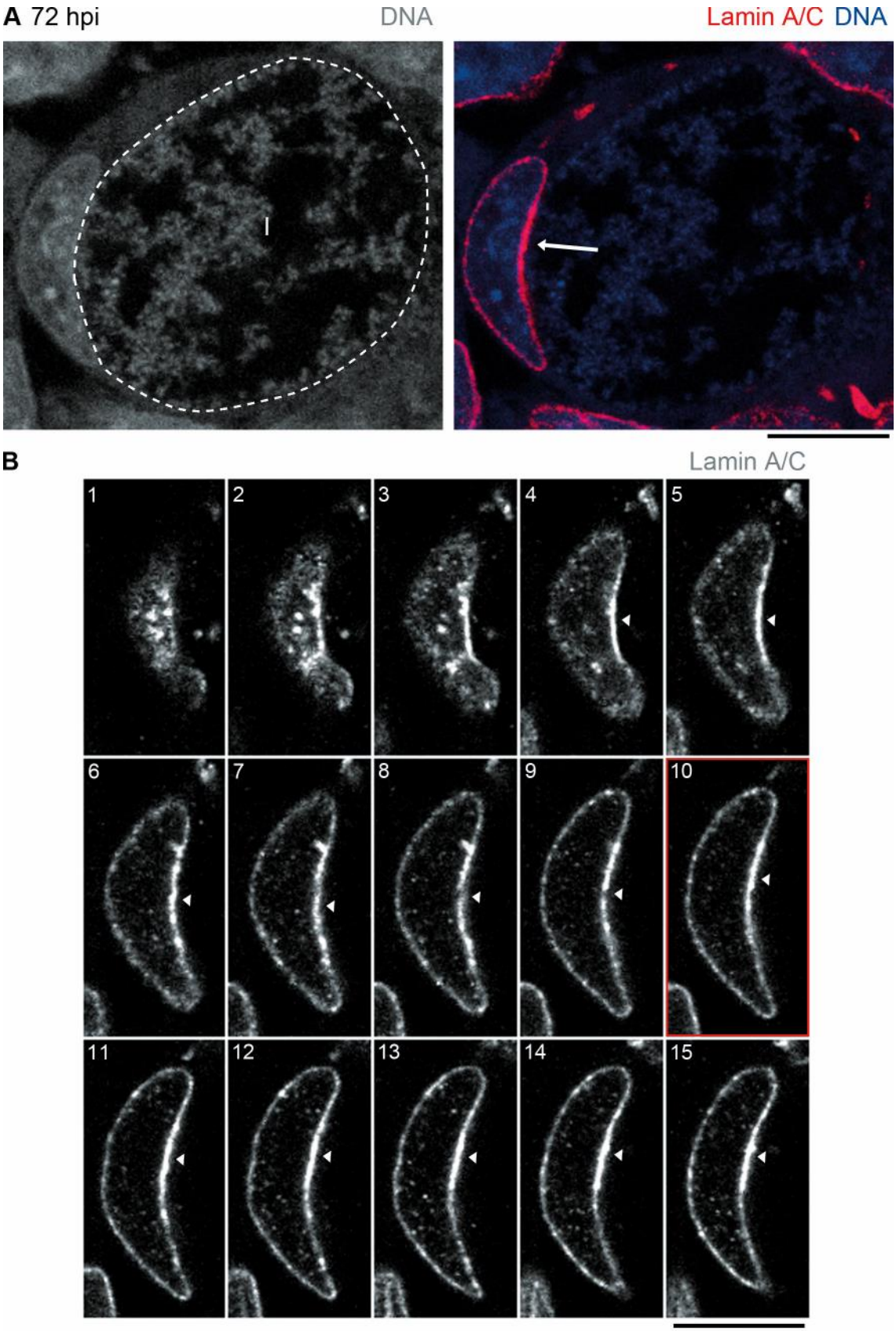
A 72 hpi
DNA
Lamin A/C DNA
I
B
Lamin A/C
1
2
3
4
5
6
7
8
9
10
11
12
13
14
15

Figure 3.9. Changes in lamin A/C distribution at the nuclear envelope occur more frequently late during chlamydial infection. (A) Fluorescence intensity was measured around the circumference of the nucleus starting at the inclusion-proximal face of the NE and averaged (n=10) across the nuclei of non-infected (grey) or late-stage (48 or 72 hours) infected (red) HeLa cells with patches of lamin A/C enrichment (defined as a region of lamin A/C on one face of the NE greater than 1 µm in diameter in both the xy and z dimensions with at least 50% higher fluorescence intensity than the lamin A/C located on the distal face of the NE). Shaded areas represent standard deviation. AU: Arbitrary units. (B) Histogram showing the proportion of non-infected (white bars) or *C. trachomatis* LGV2 infected (black bars) HeLa cells (n=150) exhibiting a lamin A/C patch scored at each time point. Error bars show standard deviation (**p<0.05, ***p<0.01 using Student's t-test as indicated).

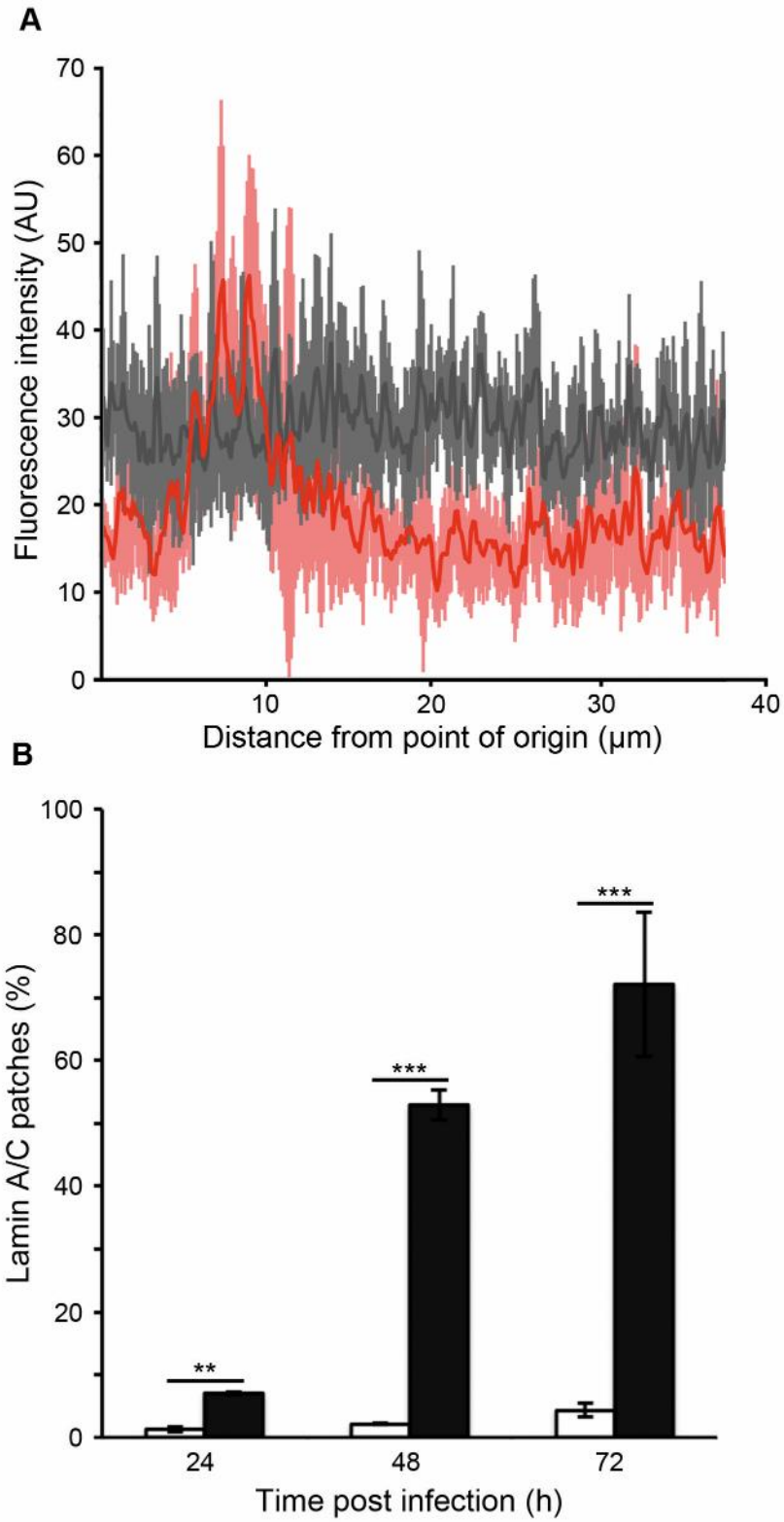
A
70
60
50
40
30
20
10
0
Fluorescence intensity (AU)
10
20
30
40
Distance from point of origin (µm)
B
100
80
60
40
20
0
Lamin A/C patches (%)
**
***
***
24
48
72
Time post infection (h)

3.6 Cellular lamin A/C levels are reduced in infected cells late during chlamydial infection

Quantification of fluorescence in the nuclei of infected cells containing the lamin A/C patch showed fluorescence is enriched at the inclusion-proximal face of the NE, and depleted elsewhere from the nuclear periphery (section 3.5). However, it is unclear as to whether this represents a net reduction in cellular lamin A/C in infected cells. To determine this, lamin A/C levels were examined by immunoblotting lysates collected from non-infected HeLa cells and comparing to lysates collected from *C. trachomatis* LGV2 infected HeLa cells at 24, 48 and 72 hpi (Fig 3.10A). Protein species were detected at ~76 kilodaltons (kDa) corresponding to lamin A, at ~68 kDa corresponding to lamin C, and at ~50 kDa corresponding to γ-tubulin. Qualitatively, lamin A and lamin C levels were reduced at 48 and 72 hpi, although levels were comparable in the non-infected cells and infected cells at 24 hpi. Despite this reduction, no cleavage products were detected, and no protein species were detected with molecular weights corresponding to aberrant splice variants such as progerin, the mutant form of lamin A detected in HGPS cells. To confirm the effect of *Chlamydia* infection on lamin A/C, the intensities of protein species were quantified by densitometry and normalised against γ-tubulin (Fig 3.10B). Surprisingly, at 24 hours the ratio of lamin A/C present in infected cells when compared to non-infected cells increases by approximately 0.1 for lamin A and 0.2 for lamin C. However, at 48 hours and 72 hours, both lamin A and lamin C are reduced compared to non-infected cells, with levels falling to 73 ± 9.8% and 81 ± 7.1% respectively at 48 hours, and 65 ± 10.7% and 83 ± 15.3% respectively at 72 hours. Thus, there is an overall reduction in lamin A/C levels in the host cell during the latter stages of infection with *C. trachomatis* LGV2.

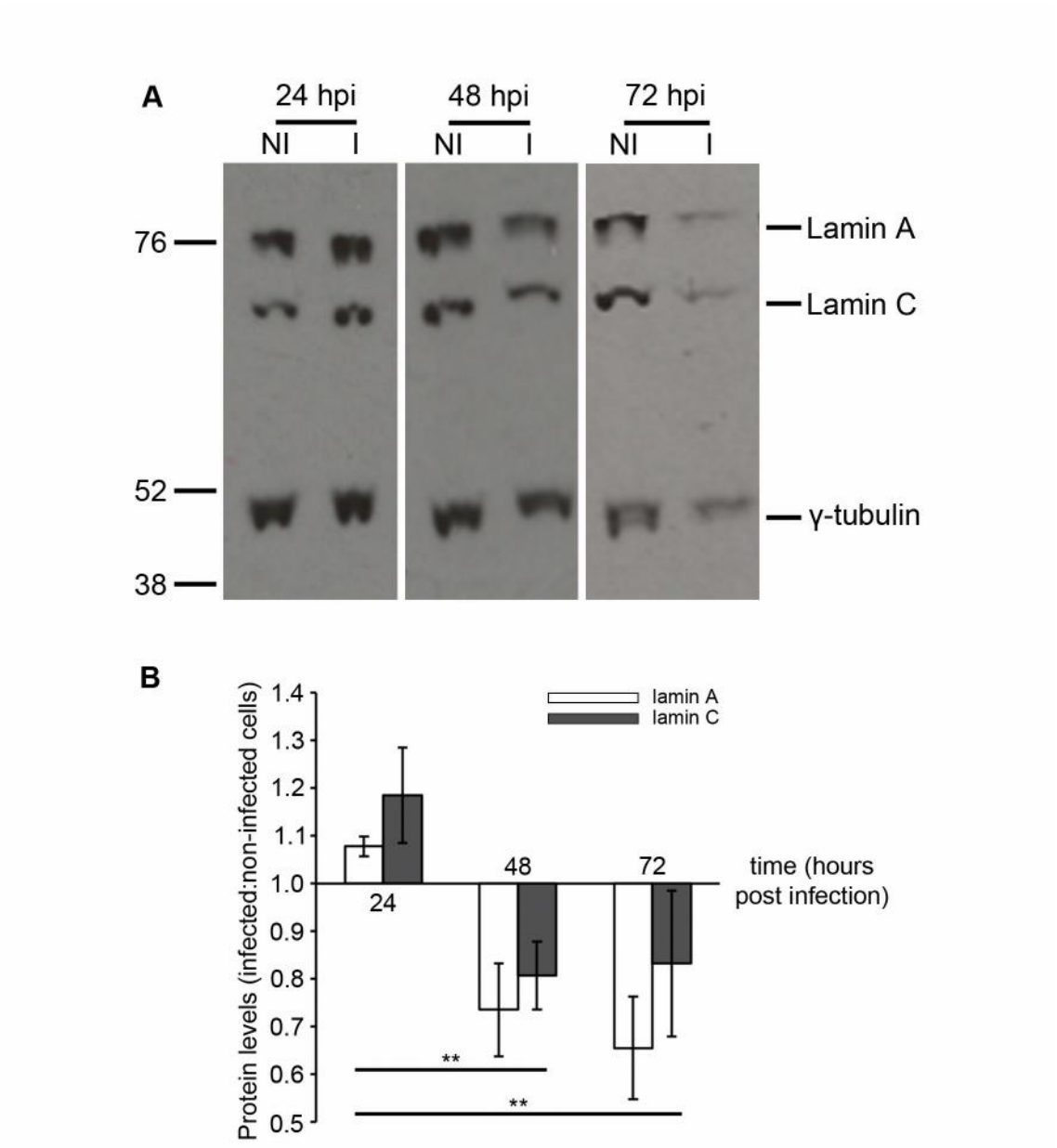

Figure 3.10. Cellular lamin A/C protein levels are reduced late during chlamydial infection. Lysates were prepared from non-infected or *C. trachomatis* LGV2-infected HeLa cells at 24, 48 and 72 hours post infection (hpi). (A) Proteins were separated by SDS-PAGE and analysed by immunoblotting using antibodies against lamin A/C and γ-tubulin. The position of the molecular weight markers are shown in kilodaltons (kDa, left). (B) Lamin A (white) and lamin C (grey) band intensity was quantified using ImageJ (average of two repeats), normalised relative to γ-tubulin and plotted as a ratio of mean levels in infected to non-infected cells. Error bars show standard deviation (**p<0.05 using Student's t-test between lamin A/lamin C at 24 hpi and lamin A/lamin C at 48 or 72 hpi, and with a Q value greater than the critical Q value for significance to 0.05 using One-way analysis of variance (ANOVA) followed by post-hoc Tukey's honest significant difference (HSD) test).

3.7 Lamin B is reduced at the inclusion-proximal face of the NE during *Chlamydia* infection

Given the changes described previously in A-type lamins (section 3.5), lamin B was re-examined to confirm whether or not any alterations to lamin B levels or localisation occur, and so determine whether all lamins are modified during infection or specifically lamin A/C. During *C. trachomatis* infection, at 24 hours, no discernible changes in lamin B fluorescence were observed relative to non-infected cells (Fig 3.11A). Later during infection, at 48 and 72 hours, lamin B fluorescence was partially depleted at the inclusion-proximal face of the NE (Fig 3.11B and C). Lamin B across the remainder of the NE was unchanged in comparison to control cells. For quantification, a 'lamin B reduction' was defined as a region on one face of the NE greater than 1 µm in diameter in both the xy and z dimension, with at least 50% lower fluorescence intensity than the lamin B located on the distal face of the NE. At 24 hpi there was no significant difference in the frequency of lamin B reduction compared to control. However, at 48 hpi and 72 hpi lamin B reduction occurred more frequently, in 16.5 ± 0.3% and 21.0 ± 4.5% of infected cells respectively (Fig 3.12). These data show that in addition to lamin A/C, lamin B is also affected late during *Chlamydia* infection at the inclusion-proximal region of the NE. However, whilst lamin A/C was enriched adjacent to the inclusion, lamin B was reduced, and lamin B around the rest of the NE was unaffected.

Figure 3.11. Lamin B is reduced at the inclusion-proximal face of the nuclear envelope late during chlamydial infection. HeLa cells were infected with *C. trachomatis* LGV2, fixed and double stained with anti-lamin B1 primary antibody and an AlexaFluor® 546-conjugated secondary antibody (red, grey) to visualise lamin B, and DRAQ-5 to visualise DNA (blue). Left panels: confocal images of infected cells in the xy-plane, with the inclusion (I) periphery indicated by the white dashed line (Methods 2.8). Right panels: confocal xy-sections of the midsection of the nuclei, ascending in the z dimension through the cell (1-6) with a step of 0.34 µm. Full z-stacks are available in the appendix. Red borders indicate the sections equivalent to the left panels. White arrows highlight areas of lamin B reduction. (A) 24 hours post infection (hpi). (B) 48 hpi. (C) 72 hpi. Scale bars, 10 µm.

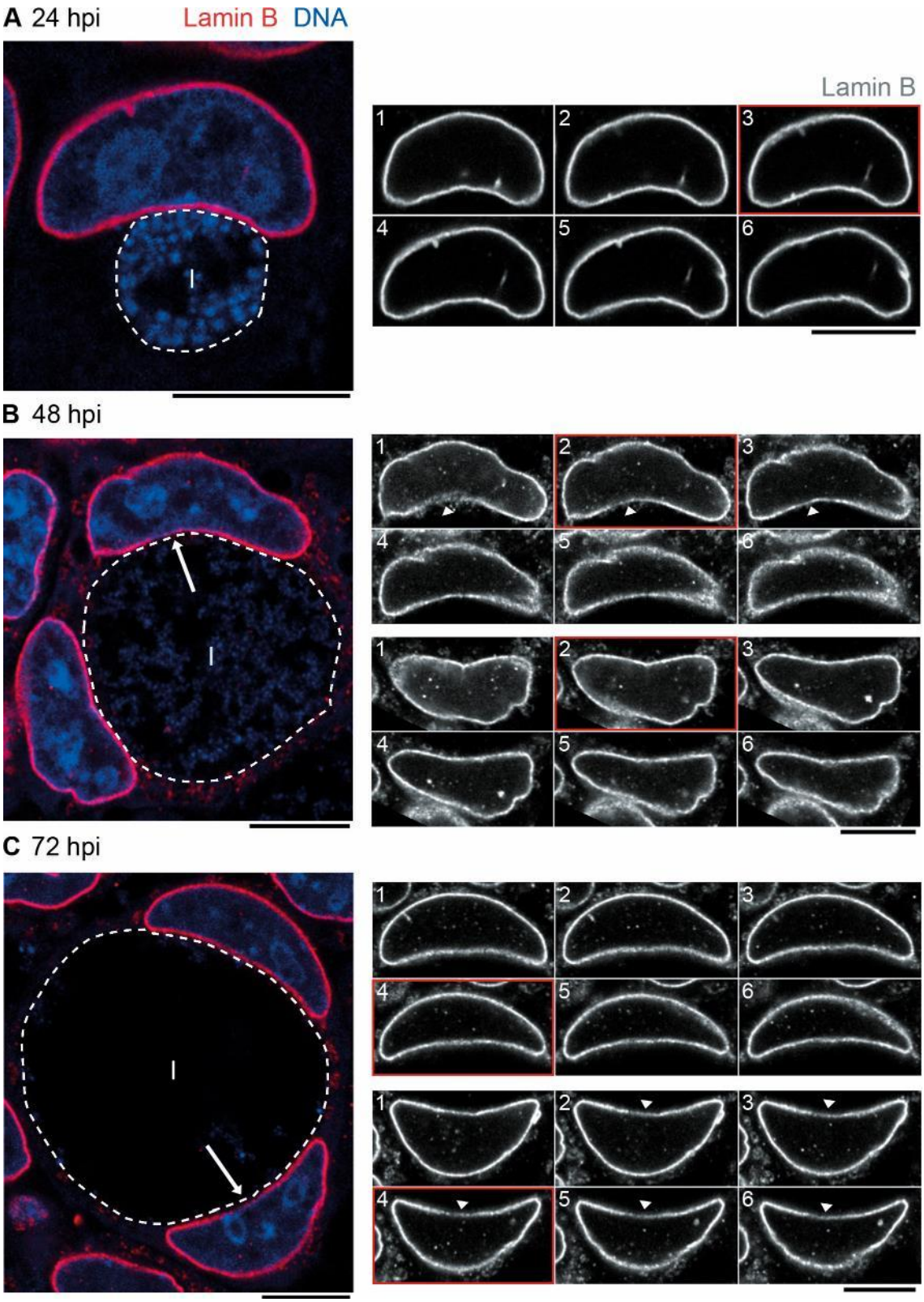
A 24 hpi
Lamin B DNA
Lamin B
1
2
3
4
5
6
I
B 48 hpi
C 72 hpi

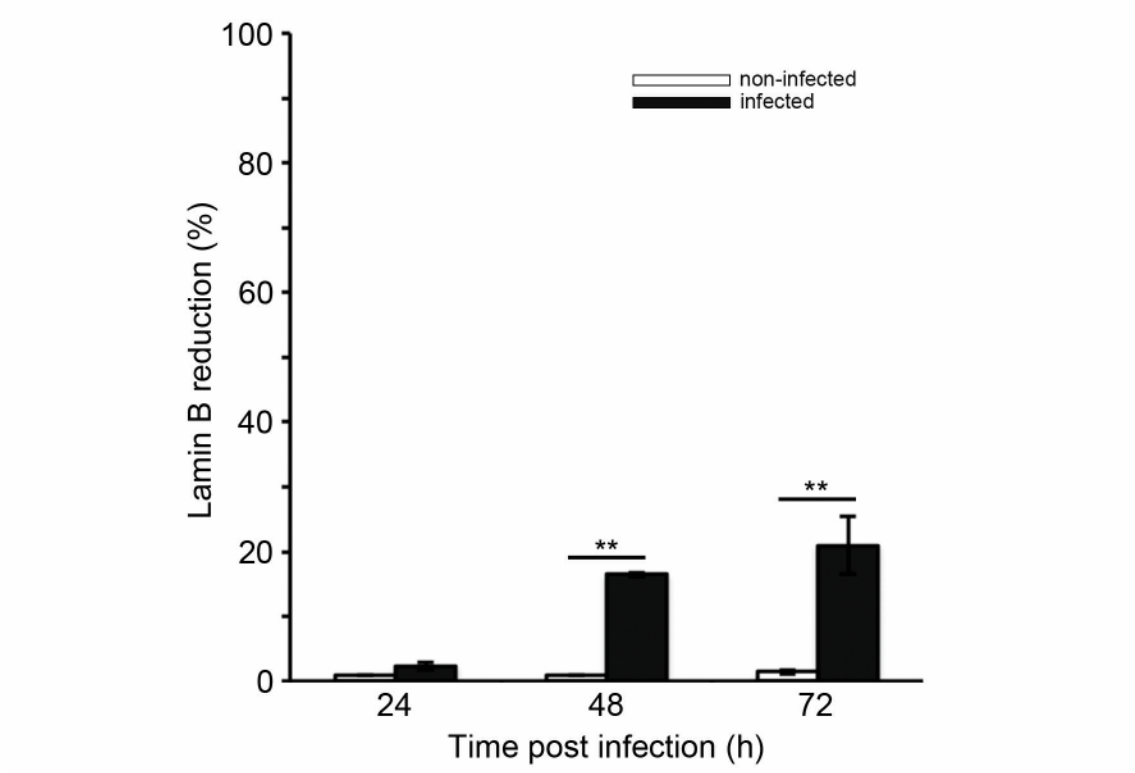

Figure 3.12. Reduction of lamin B occurs more frequently late during chlamydial infection. Histogram showing the proportion of non-infected (white bars) or *C. trachomatis* LGV2 infected (black bars) HeLa cells (n=150) exhibiting a reduction in lamin B scored at each time point. A lamin B reduction was defined as a region of lamin B on one face of the NE greater than 1 µm in both the xy and z dimensions with at least 50% lower fluorescence intensity than the lamin B located on the distal face of the NE. Error bars show standard deviation (**p<0.05 using Student's t-test as indicated).

3.8 Phenylalanine-glycine-repeat containing nucleoporins are depleted at the inclusion-proximal face of the NE during chlamydial infection

The nuclear lamina is essential for anchoring the nuclear pore complexes (NPCs) within the NE via direct interactions with nucleoporins (Nups), and ensures stable NPC positioning by counteracting dynein forces on the NPCs (Al Haboubi et al., 2011; Lussi et al., 2011; Guo and Zheng, 2015). RNA interference studies in *Caenorhabditis elegans*, which has only a single lamin gene, show lamin depletion causes changes in nuclear shape and clustering of NPCs (Liu et al., 2000). Additionally, distinct NE subdomains on the nuclear surface exist in proliferating mammalian cells termed 'pore-free islands', which are characterised by the depletion of NPCs and lamin B and an associated enrichment of lamin A/C (Maeshima et al., 2006). Given the importance of the NL in NPC positioning, and the previously demonstrated modifications to the NL in cells infected by *Chlamydia* (section 3.5), NPC distribution was investigated during chlamydial infection.

mAb414 is a widely used antibody that recognises epitopes in phenylalanine-glycine (FG) repeat regions, which are present in a subset of Nups in the cytoplasmic filaments, central pore and nuclear basket of the NPCs, allowing simultaneous labelling of multiple components of the NPCs (Davis et al., 1986). HeLa cells were therefore infected with *C. trachomatis* LGV2, fixed and labelled with mAb414 to visualise FG-Nups. Serial confocal z-sections of non-infected HeLa cells in the xy-plane show punctate FG-Nup labelling which was evenly distributed throughout the central z-sections, or midsection, of the NE, but absent in distinct regions of the nuclear surface consistent with pore-free islands (Fig 3.13). At 24 hpi, *C. trachomatis* LGV2 infection had no effects on FG-Nup distribution (Fig 3.14A). However, later during the chlamydial infection cycle, at 48 and 72 hpi, striking changes were observed. At this later stage there was a localised depletion in FG-Nup labelling, once again on the inclusion-proximal face of the NE, forming a 'gap' in the distribution of NPCs (Fig 3.14B and C). Similar to the lamin A/C patch and lamin B reduction, the gap in FG-Nups occurs in the central z-sections of the nucleus, distinct from the pore-free islands reported by Maeshima et al. (2006), which occur on the nuclear surface adjacent to the growth surface.

To quantify the frequency of FG-Nup depletion, an FG-Nup gap was conservatively defined as a complete depletion of FG-Nup fluorescence intensity greater than 1 µm in both the xy and z

dimensions. Consistent with the qualitative observations, at 24 hpi there was no significant difference in FG-Nup gap frequency compared to non-infected cells (Fig 3.15). At 48 and 72 hpi, FG-Nup depletion occurred in 21.3 ± 5.6% and 24.7 ± 9.7% of infected cells respectively, confirming NPC changes occur more frequently late in infection. These data show similarities to known cellular phenomena such as the pore-free islands. However in *C. trachomatis* infected cells the NPC gap is specifically adjacent to the chlamydial inclusion in the midsection of the NE, rather than on the nuclear surface.

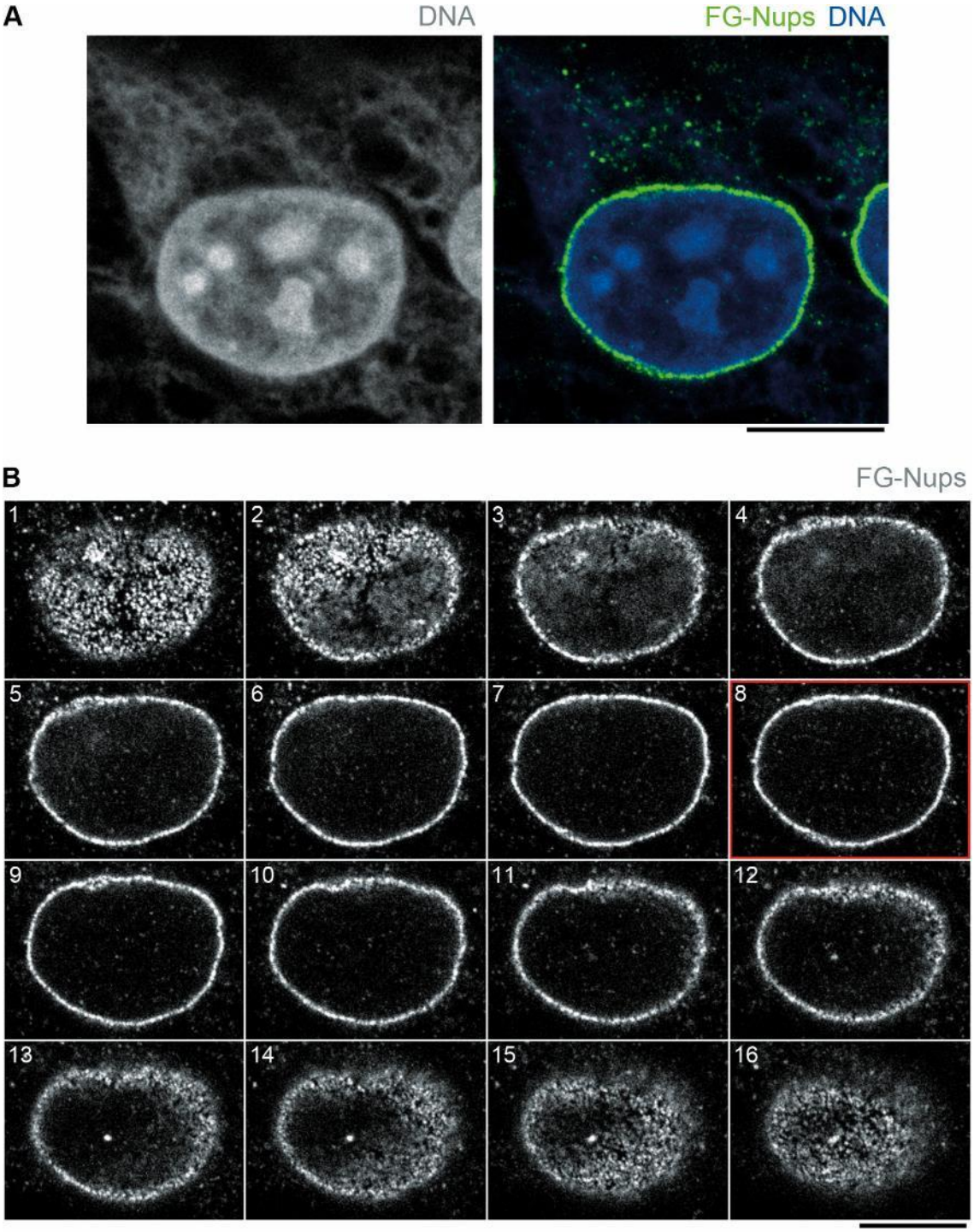

Figure 3.13. Phenylalanine-glycine repeat-containing nucleoporins (FG-Nups) are evenly distributed across the nuclear periphery in cultured HeLa cells. Fixed HeLa cells were double stained with mAb414 primary antibody and an AlexaFluor® 488-conjugated secondary antibody [green, grey (lower)] to visualise FG-Nups, and DRAQ-5 to visualise DNA [blue, grey (upper left)]. (A) Confocal images of a HeLa cell in the xy-plane. (B) Confocal xy-sections of the nucleus, ascending in the z dimension through the cell (1-16) with a step of 0.34 µm. The section equivalent to (A) is indicated by the red border. Scale bars, 10 µm.

Figure 3.14. Phenylalanine-glycine containing nucleoporins (FG-Nups) are depleted at the inclusion-proximal face of the nuclear envelope late during chlamydial infection. HeLa cells were infected with *C. trachomatis* LGV2, fixed and double stained with mAb414 primary antibody and an AlexaFluor® 488-conjugated secondary antibody (green, grey) to visualise FG-Nups, and DRAQ-5 to visualise DNA (blue). Left panels: confocal images of infected cells in the xy-plane, with the inclusion (I) periphery indicated by the white dashed line (Methods 2.8). Right panels: confocal xy-sections of the midsection of the nuclei, ascending in the z dimension through the cell (1-6) with a step of 0.34 µm. Full z-stacks are available in the appendix. Red borders indicate the sections equivalent to the left panels. White arrows highlight areas of FG-Nup depletion. (A) 24 hours post infection (hpi). (B) 48 hpi. (C) 72 hpi. Scale bars, 10 µm.

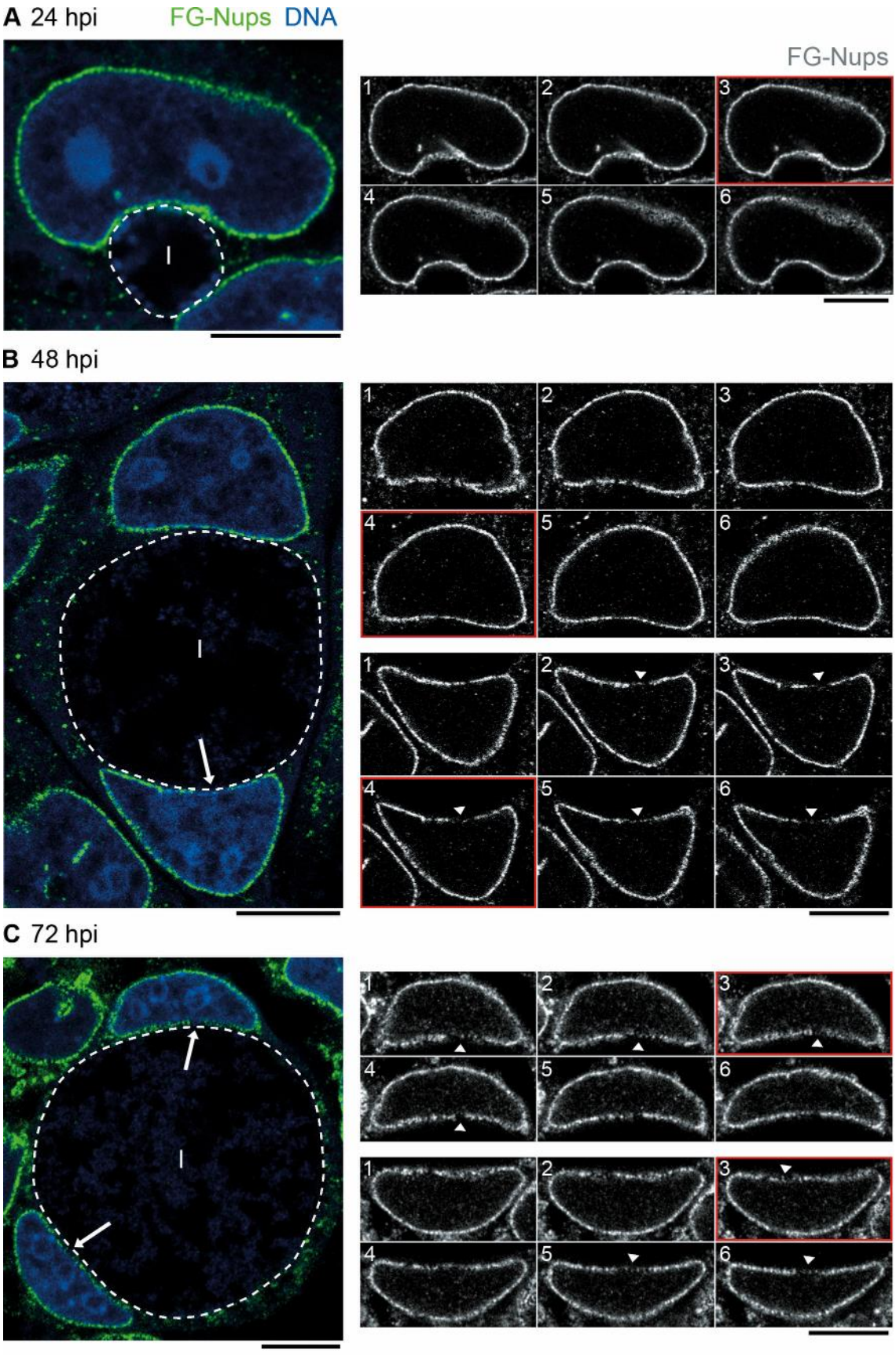
A 24 hpi
FG-Nups DNA
FG-Nups
B 48 hpi
C 72 hpi
I
1
2
3
4
5
6

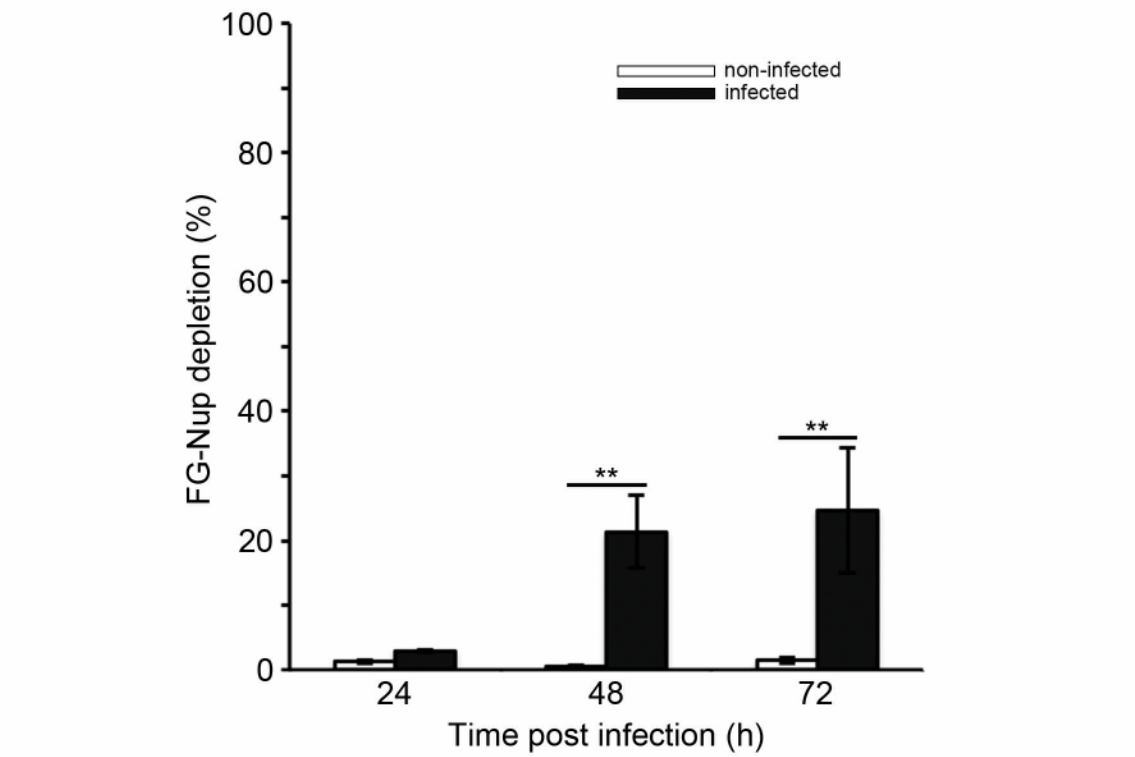

Figure 3.15. Depletion of phenylalanine-glycine containing nucleoporins (FG-Nups) occurs more frequently late during chlamydial infection. Histogram showing the proportion of non-infected (white bars) or *C. trachomatis* LGV2 infected (black bars) HeLa cells (n=150) exhibiting a depletion of phenylalanine-glycine containing nucleoporins (FG-Nups) scored at each time point. An FG-Nup depletion was defined as a complete depletion of FG-Nups fluorescence intensity greater than 1 µm in both the xy and z dimensions. Error bars show standard deviation (**p<0.05 using Student's t-test as indicated).

3.9 Specific components of NPCs are depleted during chlamydial infection

The previous experiments demonstrated FG-Nups are depleted at the inclusion-proximal face of the NE in 20-25% of late-stage *Chlamydia*-infected cells (section 3.8). As previously mentioned, mAb414 recognises epitopes in FG-repeat regions of NPC proteins, of which there are 13 FG-repeat containing Nups. To confirm these FG-Nups are being depleted, specific antibodies against representative FG-Nups were selected that recognise epitopes either within or away from the FG-repeat region. Anti-Nup153 recognises a region in the C-terminus of Nup153 that contains FG-repeats and so would also be recognised by mAb414, whereas anti-Nup62 recognises a region at the N-terminus of Nup62 that does not contain FG-repeats, and so would not be recognised by mAb414. Additionally, to confirm whether the depletion of FG-Nups represents modifications to existing nuclear pores or removal of nuclear pores entirely, Nups from other components of the NPCs that do not have FG-repeats were observed, such as members of the transmembrane ring or the outer ring/Y-complex. Experiments using antibodies to Nups from the outer ring were unsuccessful however as labelling was non-specific. Therefore an alternative method was undertaken, whereby mammalian expression constructs were used to transiently express components of the NPC in HeLa cells with fluorescent fusion proteins.

Images of control cells labelled with anti-Nup153 or anti-Nup62, or cells expressing Nup37-3xGFP (outer ring), Nup85-3xGFP (outer ring) or Pom121-3xGFP (transmembrane ring) are shown in Figure 3.16. Whilst Nup153, Nup62 and Pom121-3xGFP were evenly distributed across the midsection of the NE as expected, Nup37-3xGFP and Nup85-3xGFP localised incorrectly to the nucleoplasm and cytosol respectively. This was surprising as these constructs allowing the expression of structural Nups fused to fluorescent proteins have been shown previously to localise to the NE (Szymborska et al., 2013). Nevertheless, *C. trachomatis* LGV2 infected HeLa cells either expressing or labelled for the correctly localised Nup proteins were prepared (Fig 3.17). Gaps in the localisation of Nup153, Nup62 and Pom121-3xGFP can be observed at 48 hpi at the inclusion-proximal face of the NE, consistent with the FG-Nup labelling shown previously. The absence of Nup153 and Nup62 in this region suggest it is likely that all FG-repeat containing nucleoporins are depleted. Additionally, proteins were examined from each region of the NPC. Whilst Pom121 was the only protein not containing FG repeats that was successfully tested, it is a key nucleoporin in anchoring nuclear pores in the nuclear

envelope (Funakoshi et al., 2007). Therefore, as Pom121 was also depleted at the inclusion-proximal region of the NE, it is likely that entire nuclear pores are being removed in this region rather than a modification of a subset of components in existing NPCs.

Figure 3.16. Visualisation of individual components of the nuclear pore complexes. Cultured HeLa cells or HeLa cells transiently expressing Nup37-GFP, Nup85-GFP or Pom121-GFP fusion proteins were fixed and stained with DRAQ-5 to visualise DNA. (A) Nup62 was visualised by staining with anti-Nup62 primary antibody and an AlexaFluor® 488-conjugated secondary antibody. (B) Nup153 was visualised by staining with anti-Nup153 primary antibody and an AlexaFluor® 488-conjugated secondary antibody. (C) Nup37-GFP. (D) Nup85-GFP. (E) Pom121-GFP. Left panels: confocal images of HeLa cells in the xy-plane showing NPC components (green) and DNA (blue). Right panels: confocal xy-sections of the midsection of the nuclei showing NPC components (grey), ascending in the z dimension through the cell (1-6) with a step of 0.34 µm. Red borders indicate the sections equivalent to the left panels. Scale bars, 10 µm.

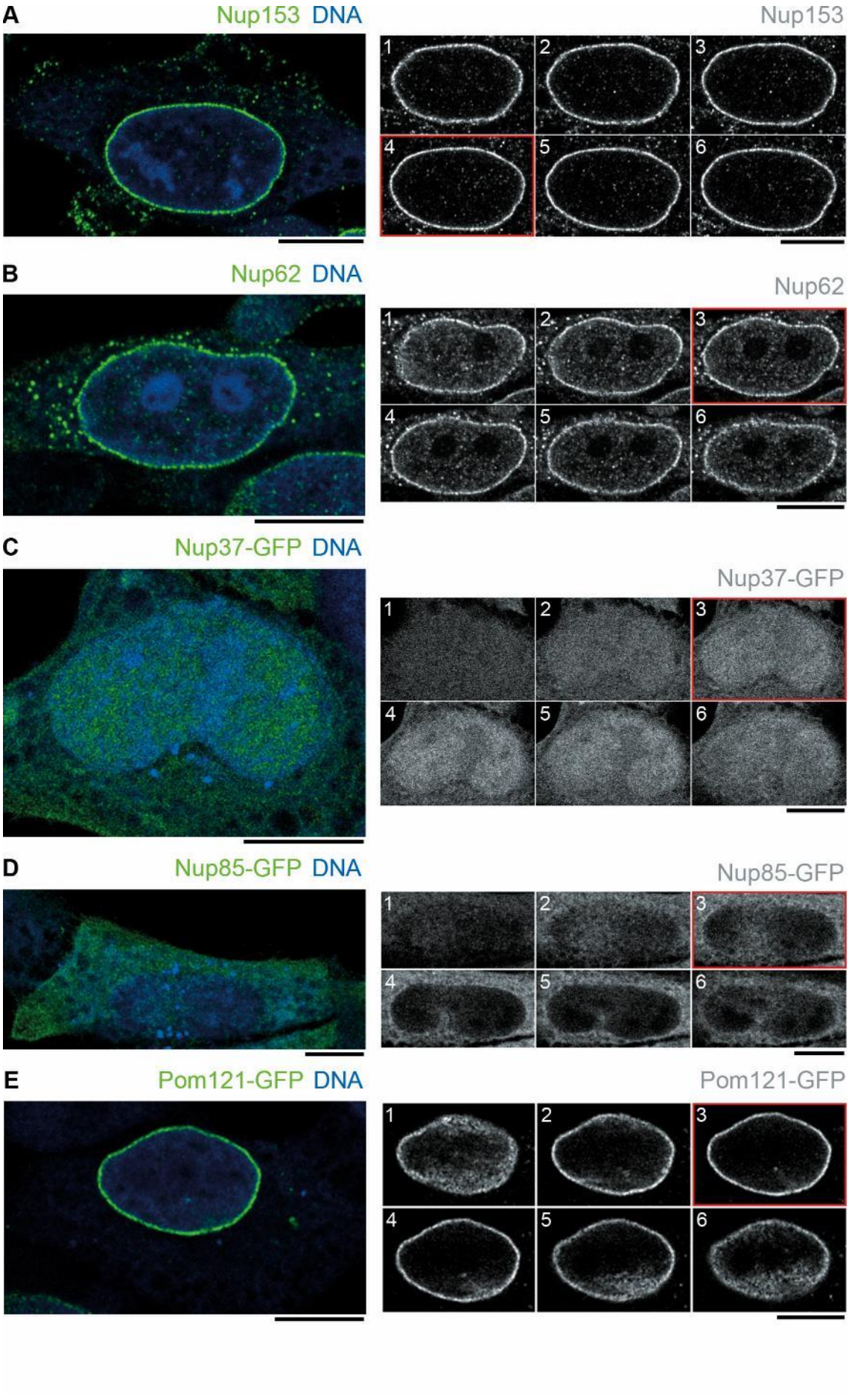
A
Nup153 DNA
Nup153
B
Nup62 DNA
Nup62
C
Nup37-GFP DNA
Nup37-GFP
D
Nup85-GFP DNA
Nup85-GFP
E
Pom121-GFP DNA
Pom121-GFP
1
2
3
4
5
6

Figure 3.17. NPC components are depleted at the inclusion-proximal face of the nuclear envelope during chlamydial infection. Cultured HeLa cells or HeLa cells transiently expressing Pom121-GFP fusion protein were infected with *C. trachomatis* LGV2 for 48 hours, fixed and stained with DRAQ-5 to visualise DNA. (A) Nup62 was visualised by staining with anti-Nup62 primary antibody and an AlexaFluor® 488-conjugated secondary antibody. (B) Nup153 was visualised by staining with anti-Nup153 primary antibody and an AlexaFluor® 488-conjugated secondary antibody. (C) Pom121-GFP. Left panels: confocal images of infected cells in the xy-plane showing NPC components (green) and DNA (blue). The inclusion (I) periphery is indicated by the white dashed line (Methods 2.8). Right panels: confocal xy-sections of the midsection of the nuclei showing NPC components (grey), ascending in the z dimension through the cell (1-6) with a step of 0.34 µm. Red borders indicate the sections equivalent to the left panels. White arrows indicate regions of NPC component depletion. Scale bars, 10 µm.

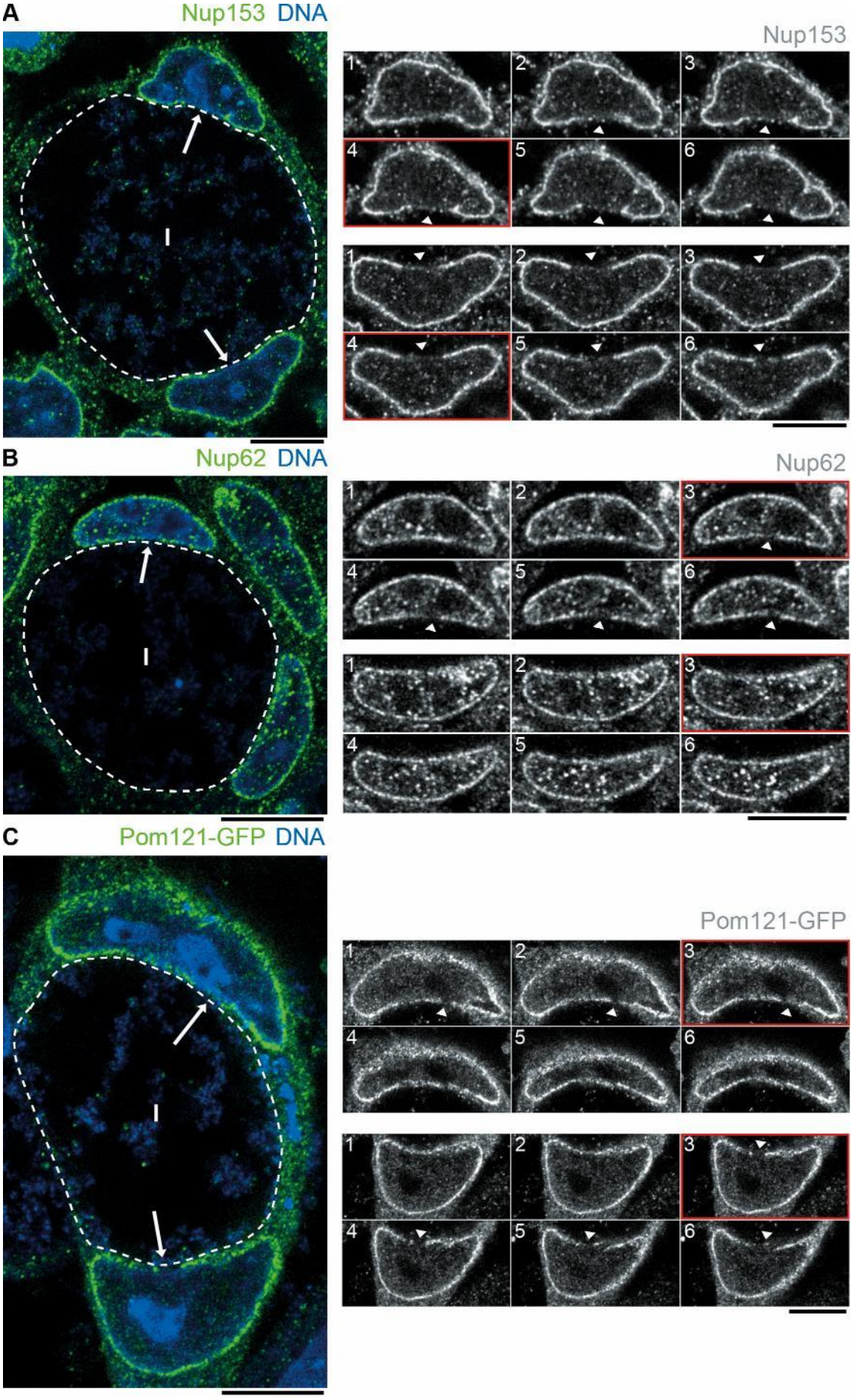
A
Nup153 DNA
Nup153
B
Nup62 DNA
Nup62
C
Pom121-GFP DNA
Pom121-GFP

3.10 Localisation of SUN proteins is unaffected during *Chlamydia* infection

Given the changes in nuclear shape observed during infection, it could be hypothesised that the protein levels or localisation of components of the LINC complex, such as the SUN proteins, could be also be impacted. LINC complexes mediate the physical connection between the nucleus and cytosolic cytoskeleton, and are therefore key in regulating nuclear-cytoplasmic communication in response to, for example, external stimuli, and also regulate nuclear position (Martins et al., 2012). Both of the two major SUN proteins, SUN1 and SUN2, interact with lamin A/C (Crisp et al., 2006; Haque et al., 2006), and SUN1 has a role in determining the distribution of the NPCs (Liu et al., 2007). Thus, it may follow that there could be a reduction in either SUN protein where lamin A/C is depleted, or a loss of SUN1 at the NPC depleted region. Due to the lack of commercial antibodies available against SUN proteins for use in immunofluorescence, SUN-GFP constructs previously used to study SUN protein function were utilised (Padmakumar et al., 2005; Liu et al., 2007; Lu et al., 2008). HeLa cells transiently expressing either SUN1-GFP or SUN2-GFP were infected with *C. trachomatis* LGV2, fixed and examined by confocal microscopy (Figs 3.18 and 3.19). In control cells both SUN-GFP proteins localised as expected to the NE (Figs 3.18A and 3.19A). However, no changes in localisation or fluorescence intensity could be observed in infected cells transiently expressing either SUN protein, suggesting these proteins are not remodelled during *C. trachomatis* infection (Figs 3.18B and 3.19B).

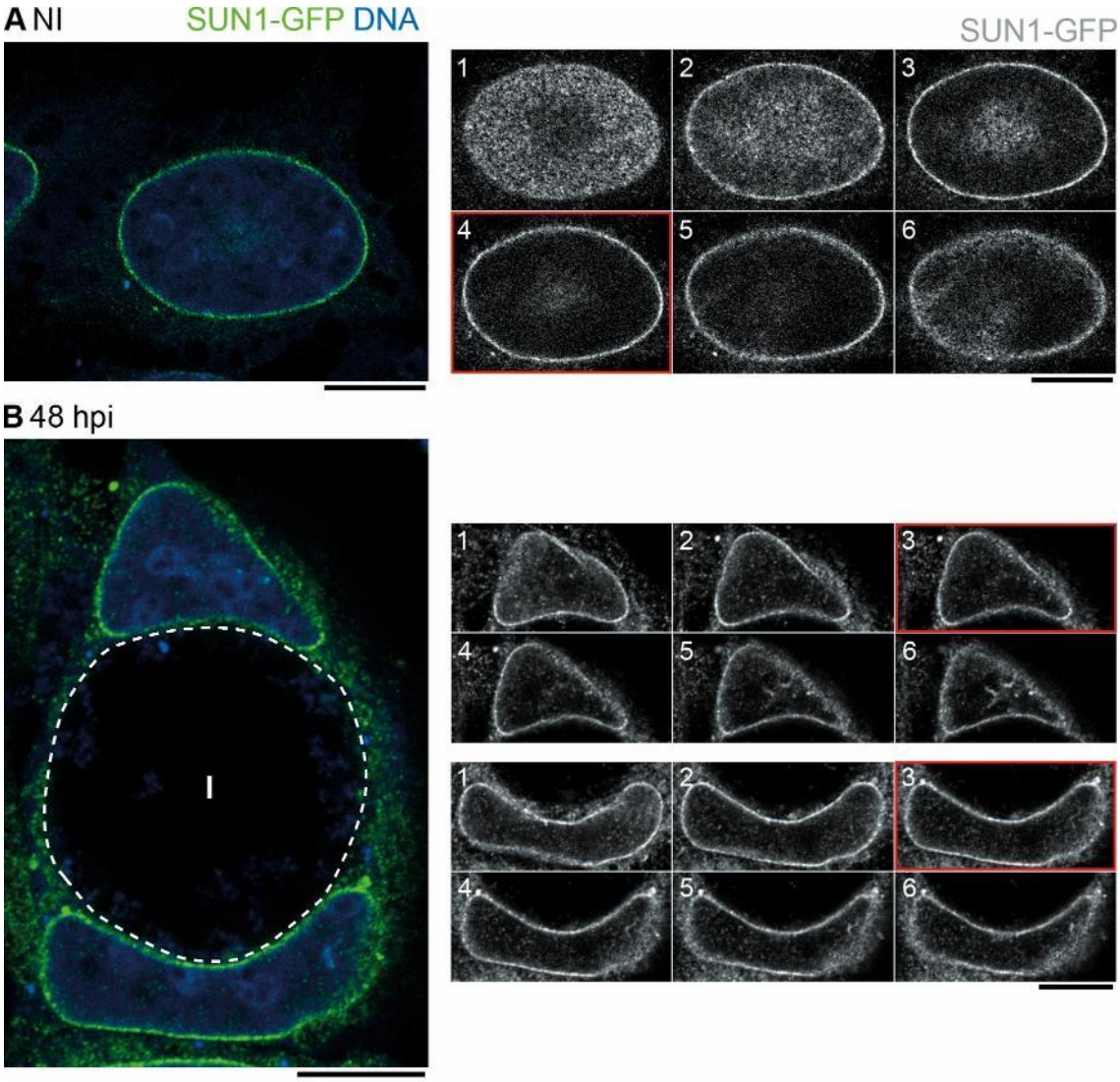

Figure 3.18 SUN1-GFP localisation is unaffected during chlamydial infection. (A) Non-infected (NI) or (B) 48 hour post infection (hpi) *C. trachomatis* LGV2 infected HeLa cells transiently expressing SUN1-GFP were fixed and stained with DRAQ-5 to visualise DNA. Left panels: confocal images of a non-infected and an infected cell in the xy-plane, showing SUN1-GFP (green) and DNA (blue). The inclusion (I) periphery is indicated by the white dashed line (Methods 2.8). Right panels: confocal xy-sections of the midsection of the nuclei showing SUN1-GFP (grey), ascending in the z-dimension through the cell (1-6) with a step of 0.34 µm. Red borders indicate the sections equivalent to the left panels. Scale bars, 10 µm.

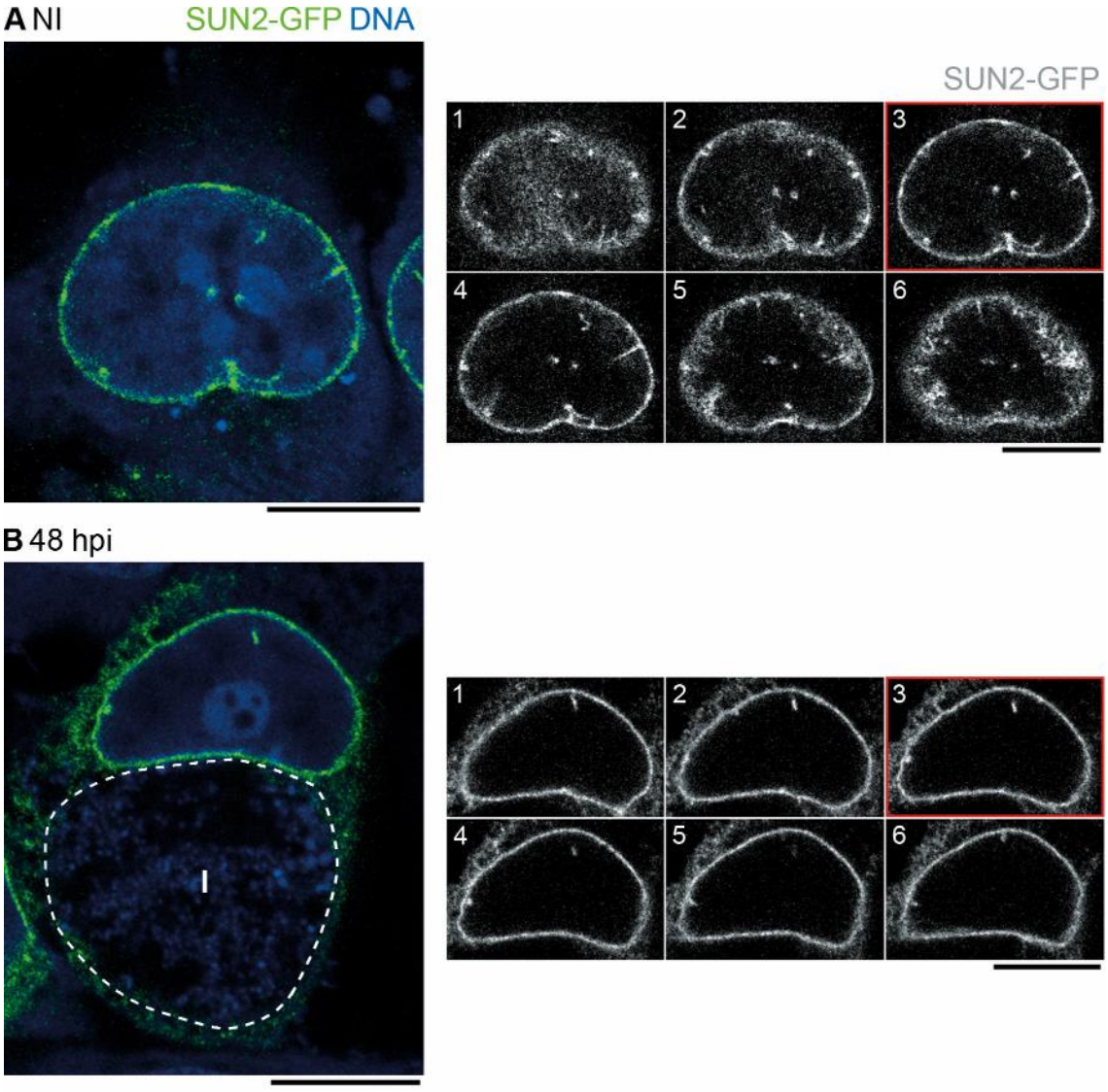

Figure 3.19 SUN2-GFP localisation is unaffected during chlamydial infection. (A) Non-infected (NI) or (B) 48 hour post infection (hpi) *C. trachomatis* LGV2 infected HeLa cells transiently expressing SUN2-GFP were fixed and stained with DRAQ-5 to visualise DNA. Left panels: confocal images of a non-infected and an infected cell in the xy-plane, showing SUN2-GFP (green) and DNA (blue). The inclusion (I) periphery is indicated by the white dashed line (Methods 2.8). Right panels: confocal xy-sections of the midsection of the nuclei showing SUN2-GFP (grey), ascending in the z-dimension through the cell (1-6) with a step of 0.34 µm. Red borders indicate the sections equivalent to the left panels. Scale bars, 10 µm.

3.11 Nuclear envelope alterations occur more frequently in multi-nucleated *Chlamydia* infected cells

The NE alterations occur with increasing frequency towards the latter stages of the *Chlamydia* lifecycle (Fig 3.9, 3.12 and 3.15). As described in chapter 1, proliferating *Chlamydia*-infected cells typically become multi-nucleated late during infection in cell culture due to a failure in cytokinesis at the end of the cell cycle. Whether this is a direct effect of *Chlamydia* infection, or an indirect effect caused by a large object occupying the majority of the cell remains to be determined (Alzhanov et al., 2009; Sun et al., 2011). Nevertheless, it is advantageous for *Chlamydia* to reside in a multi-nucleated cell. Multi-nucleated cells possess a higher Golgi content, allowing *C. trachomatis* to intercept Golgi-derived lipids faster than mono-nucleated cells, enhancing inclusion expansion and formation of infectious particles (Sun et al., 2016). Given that the NE alterations also occur more frequently late in infection when there are more multi-nucleated cells, it could be reasoned that there may be a relationship between multi-nucleation and NE alteration frequency.

The enrichment of lamin A/C and depletion of NPCs at the inclusion-proximal face of the NE were quantified separately in mono- and multi-nucleated cells, and the relative frequency compared (Fig 3.20). At both 48 and 72 hpi, lamin A/C patches and NPC gaps occurred more often in the multi-nucleated infected cells. At 48 hpi there was an ~1.5 fold increase in lamin A/C patch frequency in multi-nucleated infected cells compared to mono-nucleated infected cells, and an ~4 fold increase in NPC gap frequency. At 72 hpi there was an ~1.4 fold increase in lamin A/C patch frequency and an ~3 fold increase in NPC gap frequency. Notably, it was rare that more than one nucleus of a multi-nucleated infected cell had an enrichment in lamin A/C or depletion of NPCs, suggesting the nuclei are not identical. Taken together, these data indicate there is a relationship between multi-nucleation of infected cells and increased frequency of NE alterations.

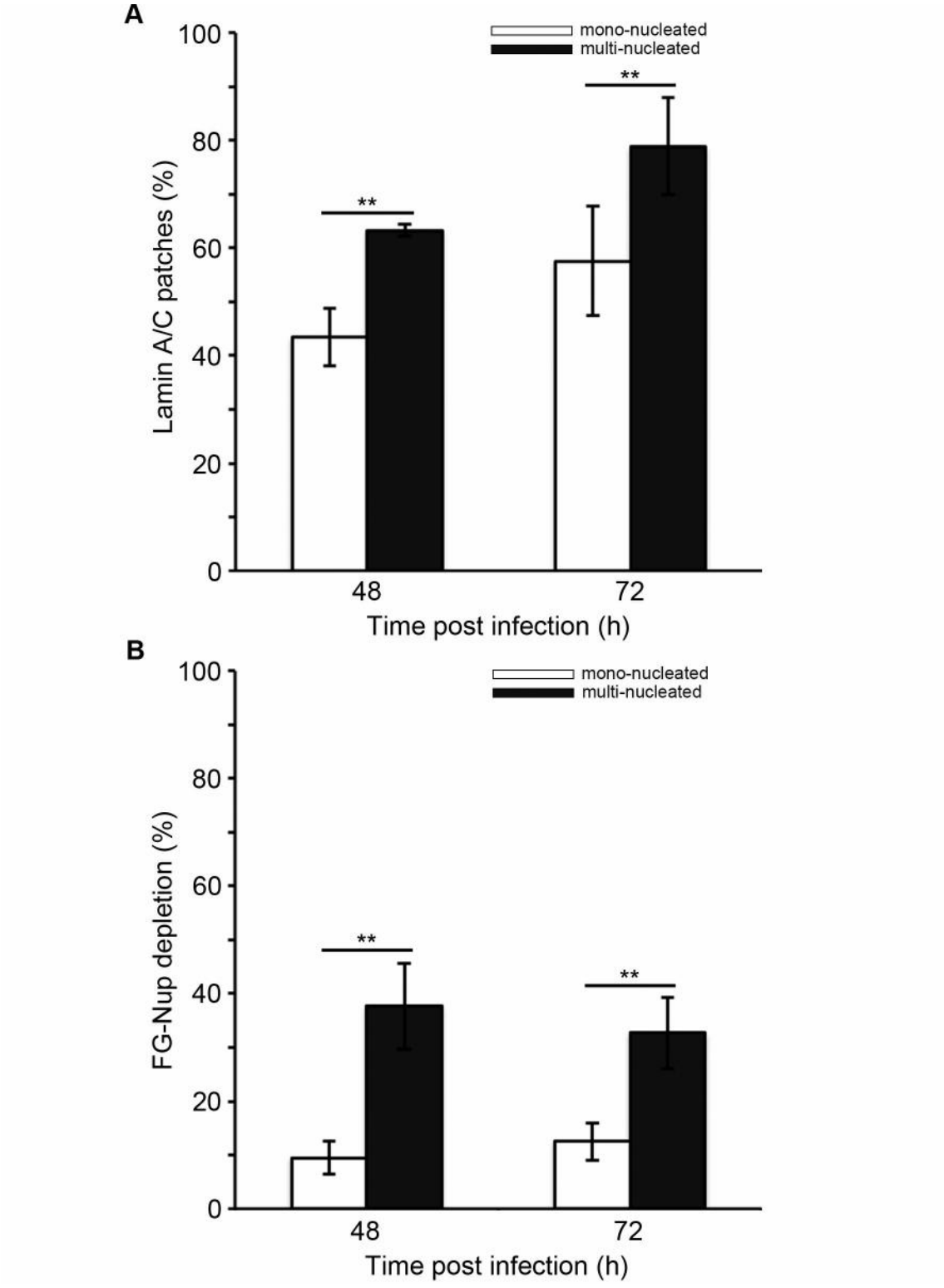

Figure 3.20 Nuclear envelope alterations occur more frequently in multi-nucleated *Chlamydia* infected cells. Histograms showing the proportion of mono-nucleated (white) or multi-nucleated (black) *C. trachomatis* infected cells (n=100) exhibiting an (A) lamin A/C patch or (B) FG-Nup depletion, scored at each time point. Error bars show standard deviation (**p<0.05 using Student's t-test as indicated).

3.12 Nuclear envelope alterations occur independently of host cell type and *Chlamydia trachomatis* serovar, but are dependent on *Chlamydia* species

Although HeLa cells are an accepted model for the *in vitro* reconstitution of chlamydial infection, it is important to determine whether the observed NE changes occur uniquely in this cell line. Additionally, variations may exist between *Chlamydia* serovar and species. For example, serovars A, D and L2 have significantly different Tarp proteins. Tarp from LGV serovars has two actin binding domains and up to nine tyrosine-rich repeat regions, whereas Tarp from serovars A and D have four and three actin binding domains respectively but only three tyrosine-rich repeat regions (Lutter et al., 2010). More significant differences exist between *C. trachomatis* and *C. muridarum*, although these species share similar gene number and order (Read et al., 2000). One of the best characterised of these variations is the differential response to IFN-γ. Human genital chlamydial strains can overcome the tryptophan-depleting effect of IFN-γ induced indoleamine 2,3-dioxygenase (IDO) expression in human epithelial cells by producing tryptophan synthase, whereas *C. muridarum* lack a functional tryptophan synthase (Roshick et al., 2006). Conversely in murine cells, *C. muridarum* can grow by interfering with IFN-γ-inducible p47 GTPases, whereas *C. trachomatis* does not (Nelson et al., 2005; Bernstein-Hanley et al., 2006). Thus, whether the NE alterations are *Chlamydia* species or strain dependent was also determined.

Retinal pigment epithelial 1 (RPE1) cells are a non-transformed hTERT immortalised cell line. RPE1 cells were chosen as they are karyotypically normal yet have similar infection kinetics to HeLa cells (Boiko et al., 2015; Ford, 2016). Cultured RPE1 cells infected with *C. trachomatis* LGV2 were fixed and labelled with anti-lamin A/C and mAb414 (Fig 3.21). Patches of lamin A/C enrichment and localised depletion of FG-Nup labelling were present in the NE adjacent to the inclusion in cells infected for 48 hours, consistent with observations in HeLa cells infected with *C. trachomatis* LGV2. These data suggest *C. trachomatis* LGV2 is able to induce NE alterations in RPE1 cells, despite them being an ocular cell type.

To investigate whether the NE alterations are specific to this species and/or serovar of *Chlamydia*, lamin A/C and NPC distribution were studied during infection with *C. trachomatis* serovar A, a trachoma causing serovar, and during infection with *C. muridarum*, a *Chlamydia*

species that naturally infects only mice and hamsters. In addition to other factors, the infection kinetics of *C. trachomatis* A and *C. muridarum* differ significantly from *C. trachomatis* LGV2. *C. trachomatis* A has a slower lifecycle, typically 72-96 hours, whilst *C. muridarum* has a faster lifecycle, lasting 30-42 hours (Lyons et al., 2005; Miyairi et al., 2006). Therefore, HeLa cells were prepared and infected with either *C. trachomatis* A or *C. muridarum* and fixed at time points approximately equivalent to 48 hpi during *C. trachomatis* LGV2 infection (72 and 30 hpi respectively). At 72 hpi during *C. trachomatis* A infection, lamin A/C patches and NPC gaps could be observed, which were similar in size and location to the NE alterations in cells infected with *C. trachomatis* LGV2 (Fig 3.22). However, at 30 hpi during infection with *C. muridarum*, the NE remains unchanged (Fig 3.23). Taken together, these data suggest NE alterations are specific to *C. trachomatis* but not *C. muridarum*, and NE alterations are not serovar specific.

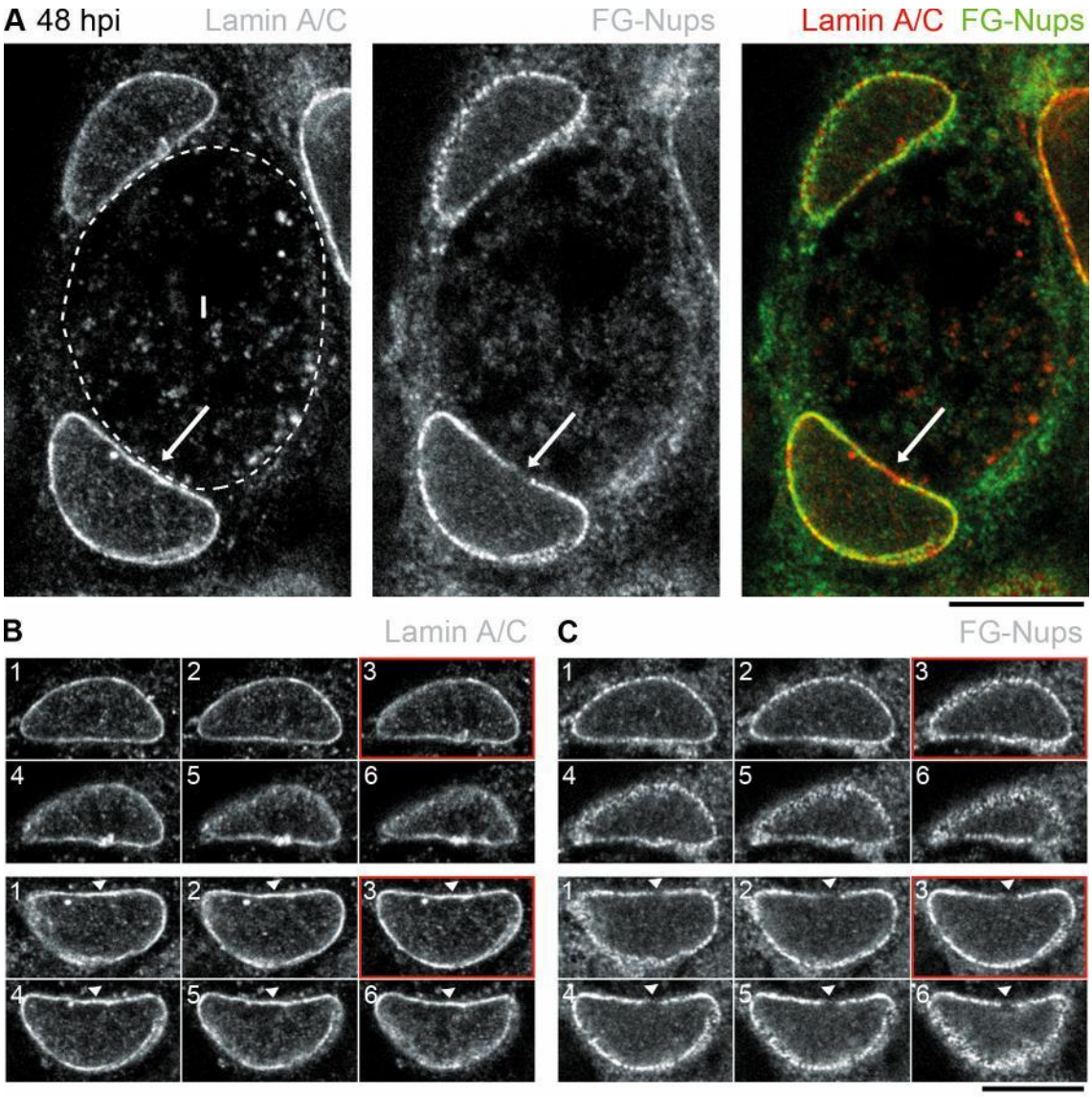

Figure 3.21. Nuclear envelope alterations occur in RPE1 cells infected with *C. trachomatis* LGV2. RPE1 cells were infected with *C. trachomatis* LGV2, fixed at 48 hpi and double stained with anti-lamin A/C primary antibody and an AlexaFluor® 546-conjugated secondary [grey (upper left, lower left), red] to visualise lamin A/C, and mAb414 primary antibody and an AlexaFluor® 488-conjugated secondary [grey (upper centre, lower right), green] to visualise phenylalanine glycine-containing nucleoporins (FG-Nups). (A) Confocal images of an infected cell in the xy-plane, with the inclusion (I) periphery indicated by the white-dashed line (Methods 2.8). (B) and (C) Confocal xy-sections of the midsection of the nuclei showing lamin A/C or FG-Nups, ascending in the z dimension through the cell (1-6) with a step of 0.34 µm. Red borders indicate the sections equivalent to (A). White arrows highlight areas of lamin A/C enrichment and FG-Nup depletion. Scale bars, 10 µm.

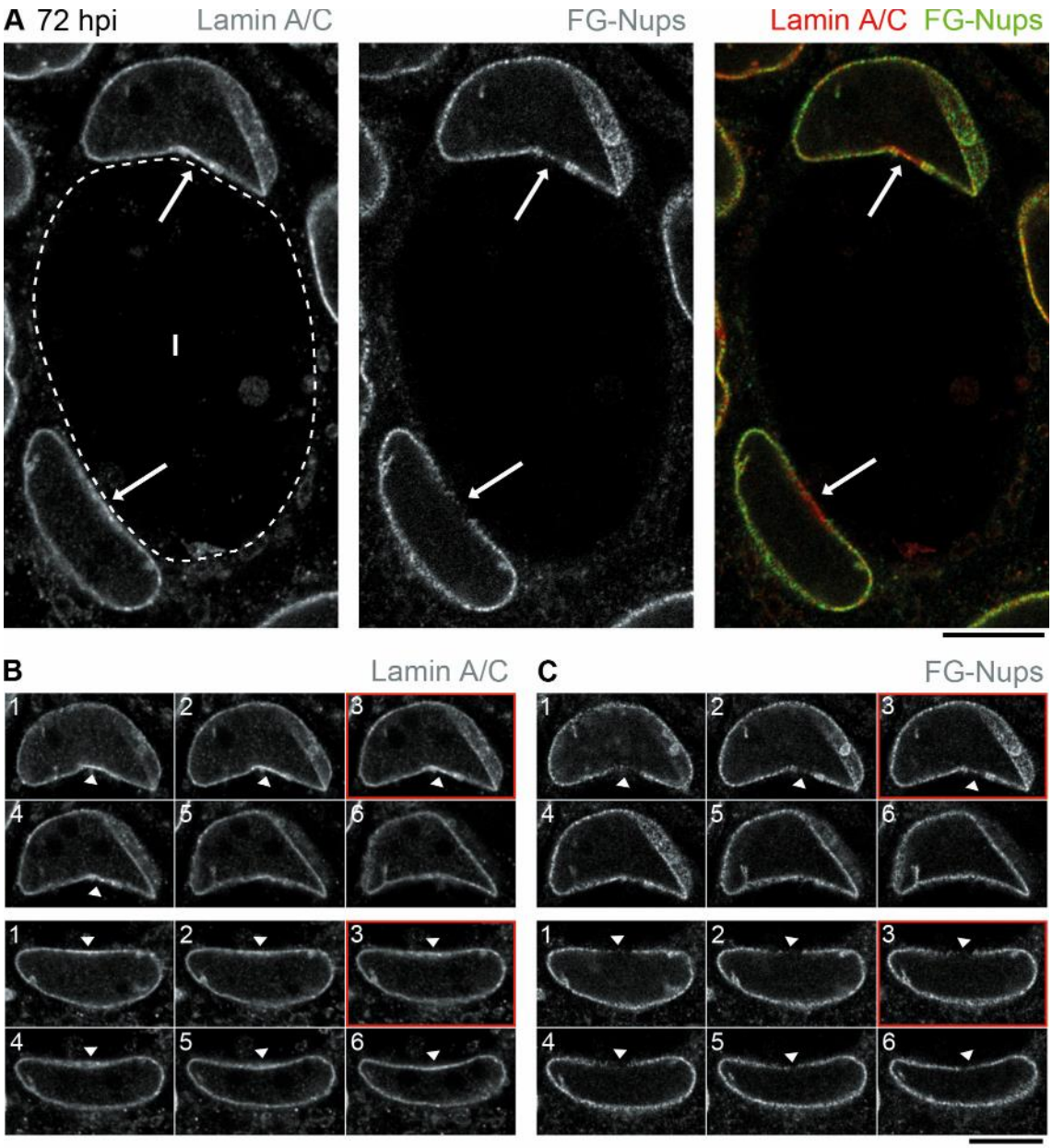

Figure 3.22. Nuclear envelope alterations occur in HeLa cells infected with *C. trachomatis* serovar A. HeLa cells were infected with *C. trachomatis* A, fixed at 72 hpi and double stained with anti-lamin A/C primary antibody and an AlexaFluor® 546-conjugated secondary [grey (upper left, lower left), red] to visualise lamin A/C, and mAb414 primary antibody and an AlexaFluor® 488-conjugated secondary [grey (upper centre, lower right), green] to visualise phenylalanine glycine-containing nucleoporins (FG-Nups). (A) Confocal images of an infected cell in the xy-plane, with the inclusion (I) periphery indicated by the white-dashed line (Methods 2.8). (B) and (C) Confocal xy-sections of the midsection of the nuclei showing lamin A/C or FG-Nups, ascending in the z dimension through the cell (1-6) with a step of 0.34 µm. Red borders indicate the sections equivalent to (A). White arrows highlight areas of lamin A/C enrichment and FG-Nup depletion. Scale bars, 10 µm.

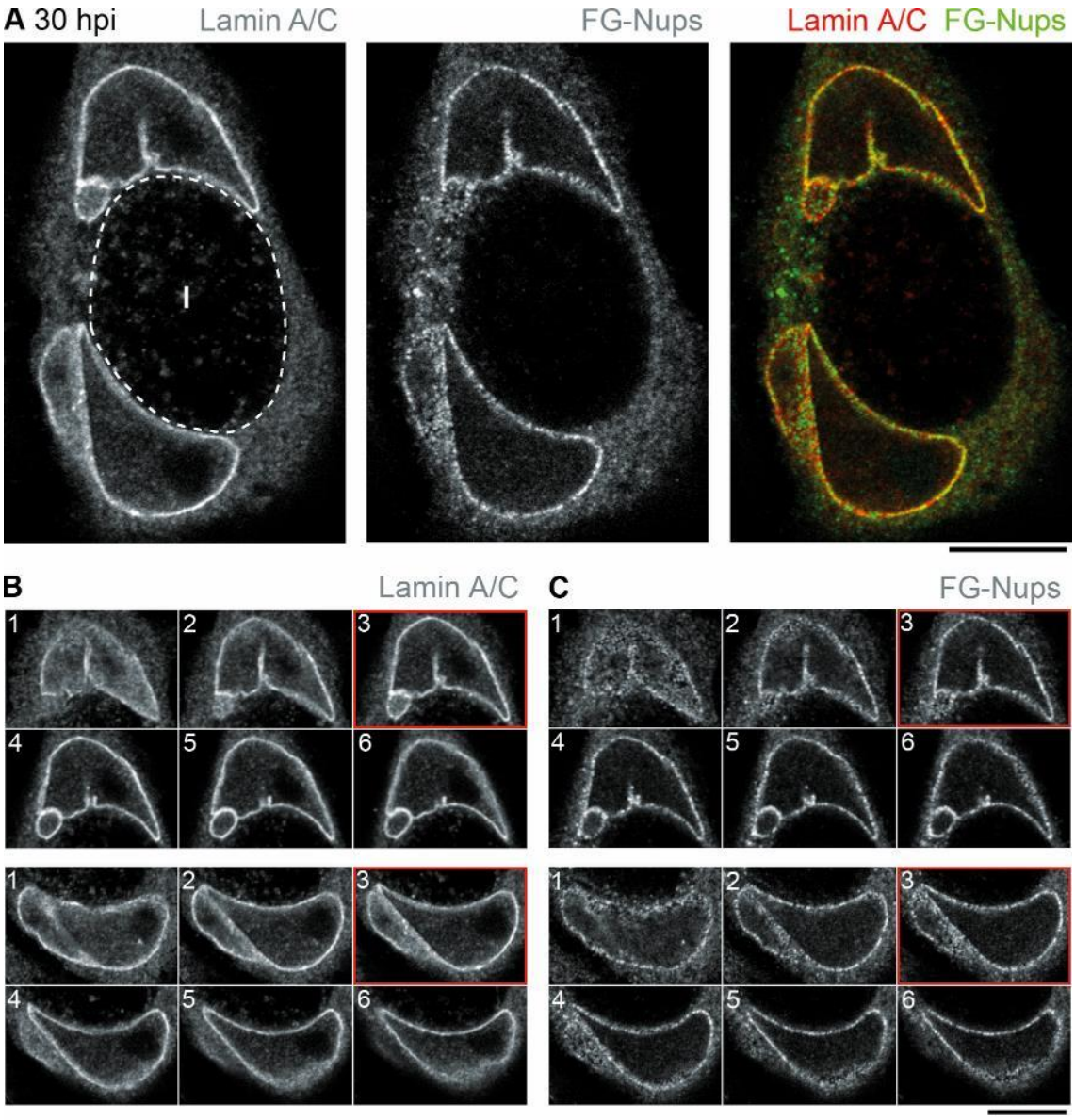

Figure 3.23. Nuclear envelope alterations do not occur in HeLa cells infected with *C. muridarum*. HeLa cells were infected with *C. muridarum*, fixed at 30 hpi and double stained with anti-lamin A/C primary antibody and an AlexaFluor® 546-conjugated secondary [grey (upper left, lower left), red] to visualise lamin A/C, and mAb414 primary antibody and an AlexaFluor® 488-conjugated secondary [grey (upper centre, lower right), green] to visualise phenylalanine glycine-containing nucleoporins (FG-Nups). (A) Confocal images of an infected cell in the xy-plane, with the inclusion (I) periphery indicated by the white-dashed line (Methods 2.8). (B) and (C) Confocal xy-sections of the midsection of the nuclei showing lamin A/C or FG-Nups, ascending in the z dimension through the cell (1-6) with a step of 0.34 µm. Red borders indicate the sections equivalent to (A). Scale bars, 10 µm.

3.13 Nuclear envelope alterations are independent of existing pore-free islands

The results presented in this chapter so far have demonstrated *Chlamydia trachomatis* infection causes aberrant nuclear architecture with increased lobulation of nuclei (section 3.3). These changes are concurrent with alterations to the nuclear envelope, including a lamin A/C patch, lamin B reduction and NPC gap which are adjacent to the inclusion, and a depletion of lamin A/C in the NE distal from the inclusion (sections 3.5-3.8). This arrangement of nuclear lamina and NPCs is strikingly similar to 'pore-free islands' (PFIs), previously observed in proliferating mammalian cells by Maeshima et al (2006). PFIs are characterised by the absence of NPCs and the enrichment of lamin A/C at the base or top of the nucleus. The NE alterations observed during chlamydial infection could therefore represent a rearrangement of existing PFIs towards to the inclusion periphery. To investigate this, cultured HeLa cells infected with *C. trachomatis* LGV2 were fixed and labelled to visualise lamin A/C and NPCs (Fig 3.24). In these cells, pore-free islands at the base of the nucleus could be observed, although lamin A/C fluorescence in these patches appeared unchanged, likely due to the reduction in lamin A/C in the NL not adjacent to the inclusion membrane (Fig 3.24A). In these same cells, both lamin A/C patches and NPC gaps could still be observed in the midsection of the nuclei adjacent to the inclusion (Fig 3.24A). To confirm this observation, the frequency of PFIs in non-infected cells versus infected cells was quantified and found to be similar (Fig 3.24B). These data suggest the *Chlamydia*-related NE alterations are not a rearrangement of existing PFIs, but instead co-exist with cellular PFIs.

Maeshima et al (2006) also noted that PFIs are characterised by enrichment in emerin, a lamina-associated inner nuclear membrane protein, and excluded from the ER that normally surrounds the nucleus (Maeshima et al., 2006). Interestingly, emerin was also identified as potentially interacting with SINC, the *C. psittaci* type III effector, although no homologous effectors have been identified in *C. trachomatis* (Mojica et al., 2015). Therefore, to verify the extent to which the *Chlamydia*-related NE alterations are reminiscent of PFIs, the localisation of emerin and an ER resident protein, protein disulphide isomerase (PDI) (Luz and Lennarz, 1996), was observed during chlamydial infection. HeLa cells were infected with *C. trachomatis* LGV2, fixed at 48 hpi and labelled for emerin or PDI. For emerin, labelling was evenly distributed across the base of nuclei in both non-infected and infected cells, in apparent contrast to the observations reported by Maeshima et al. (2006), and evenly distributed across

the central z-sections of the nuclei (Fig 3.25). As emerin was not enriched at the base of the nuclei as expected, it is not possible to conclude whether the *Chlamydia*-related NE alterations are similar or distinct from the PFIs in this aspect. For PDI, labelling was absent in the cytosol around the base of the nucleus in non-infected cells, similar to NPCs, but is present around the nucleus in the central z-sections, consistent with the pore-free island phenotype (Fig 3.26A). In infected cells this localisation was repeated, with PDI again absent in the cytosol around the base of the nuclei and present in the central z-sections proximal to the inclusion (Fig 3.26B). This suggests that the *Chlamydia*-related NE alterations not only coexist with the PFIs, but are also phenotypically distinct from the existing PFIs.

Figure 3.24. Nuclear envelope alterations which form during chlamydial infection are independent of existing pore-free islands. HeLa cells were infected with *C. trachomatis* LGV2, fixed at 48 hours post infection and double stained with anti-lamin A/C primary antibody and an AlexaFluor® 546-conjugated secondary (red) to visualise lamin A/C, and mAb414 primary antibody and an AlexaFluor® 488-conjugated secondary (green) to visualise phenylalanine glycine-containing nucleoporins (FG-Nups). (A) Left: confocal xy-section at the base of the cell, with the inclusion (I) periphery indicated by the white-dashed line (Methods 2.8) and pore-free islands in the nuclei indicated by yellow arrows. Right: confocal xy-section of the midsection of the same cell, with NE alterations indicated by the white arrows. Scale bars, 10 µm. (B) Histogram of the frequency of pore-free islands scored in infected cells and compared relative to non-infected cells at the same time point (n=100). Error bars show standard deviation.

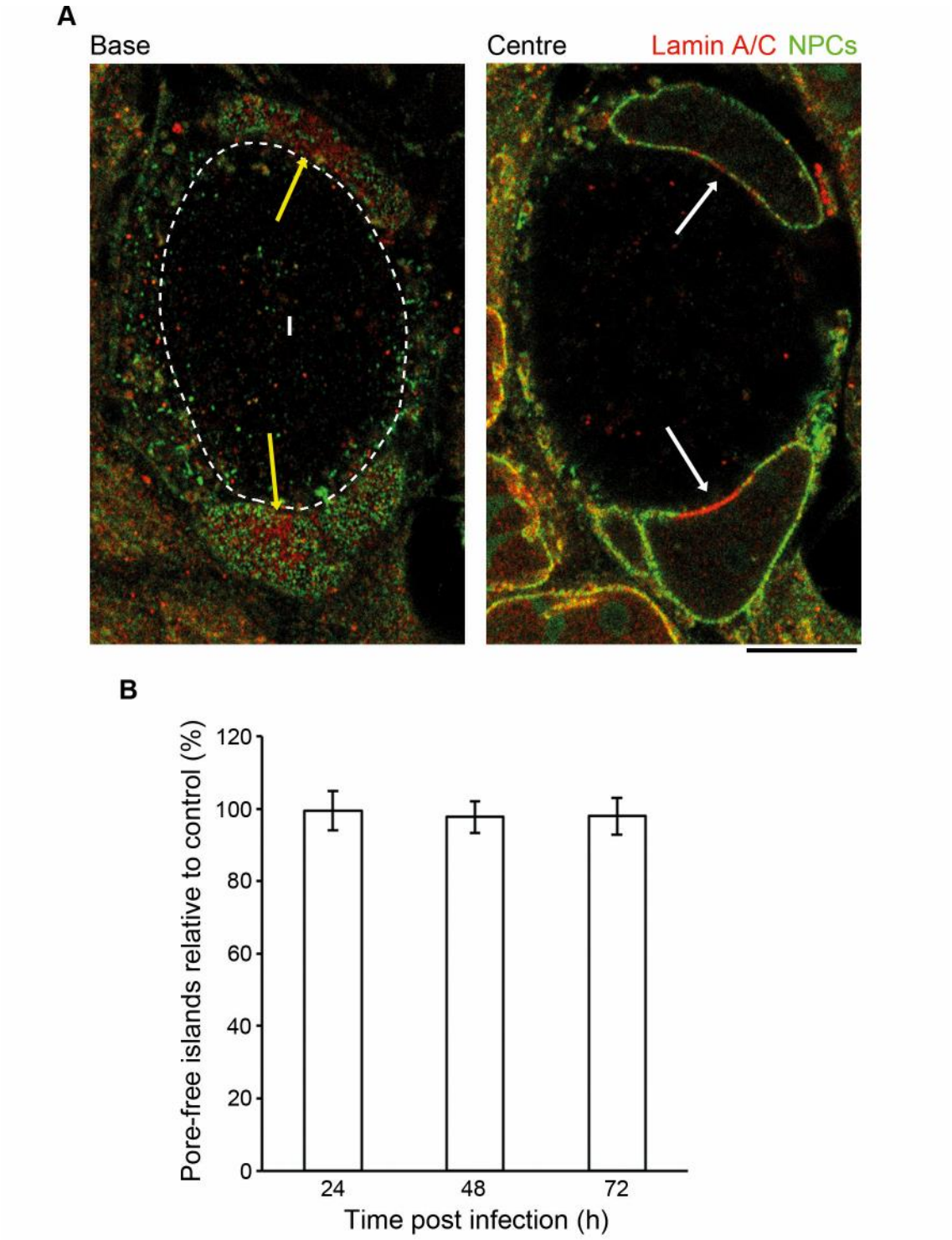
A
Base
Centre
Lamin A/C NPCs
I
B
Pore-free islands relative to control (%)
120
100
80
60
40
20
0
24
48
72
Time post infection (h)

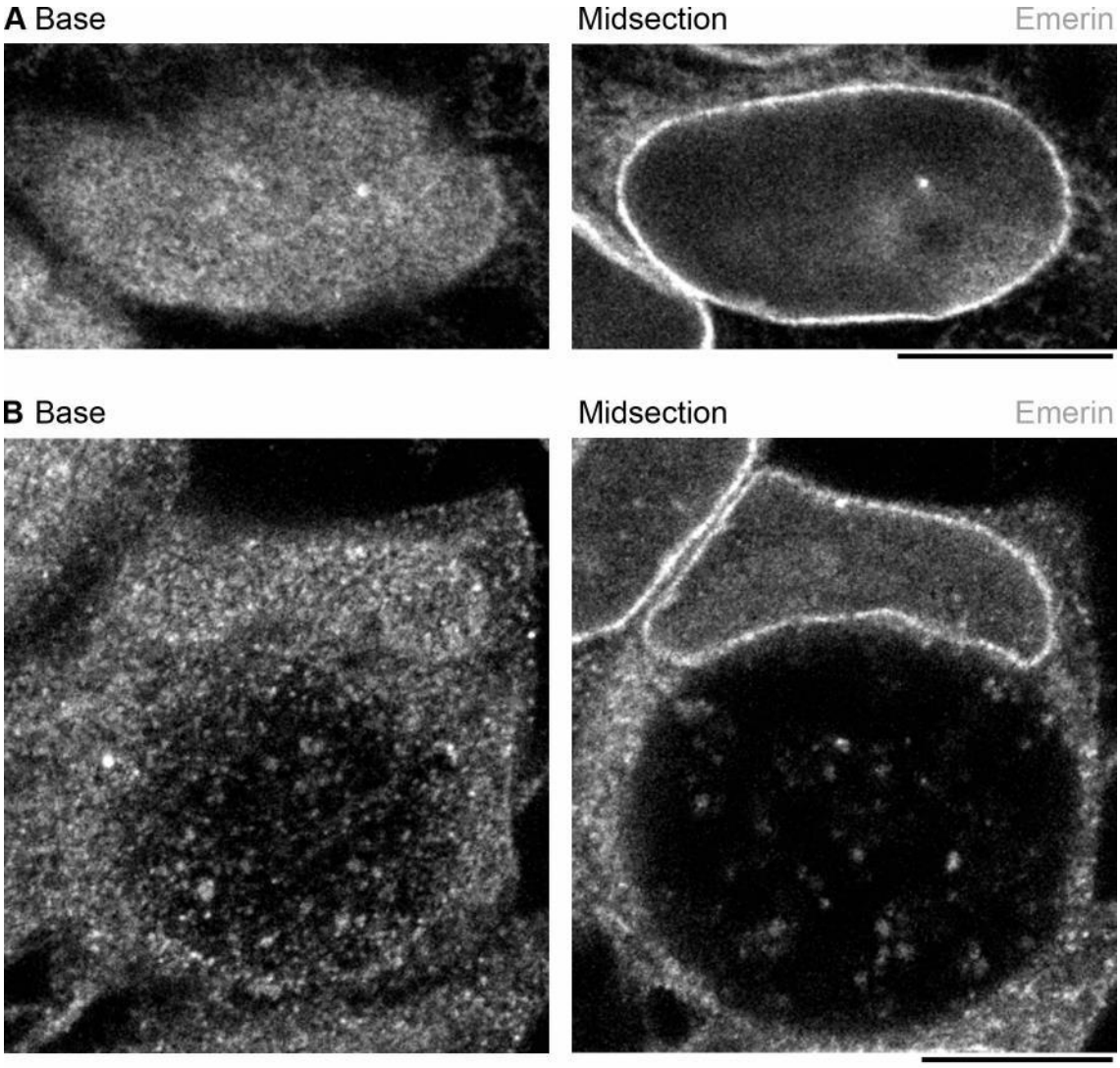

Fig 3.25 Pore-free island associated emerin changes could not be observed in non-infected or *Chlamydia*-infected HeLa cells. (A) Non-infected or (B) HeLa cells infected with *C. trachomatis* LGV2 for 48 hours were fixed and stained with an anti-emerin antibody and an AlexaFluor® 488-conjugated secondary (grey) to visualise emerin. Left panels: confocal xy-sections at the base of the cells. Right panels: confocal xy-sections of the midsection of the same cells. Scale bars, 10 μm.

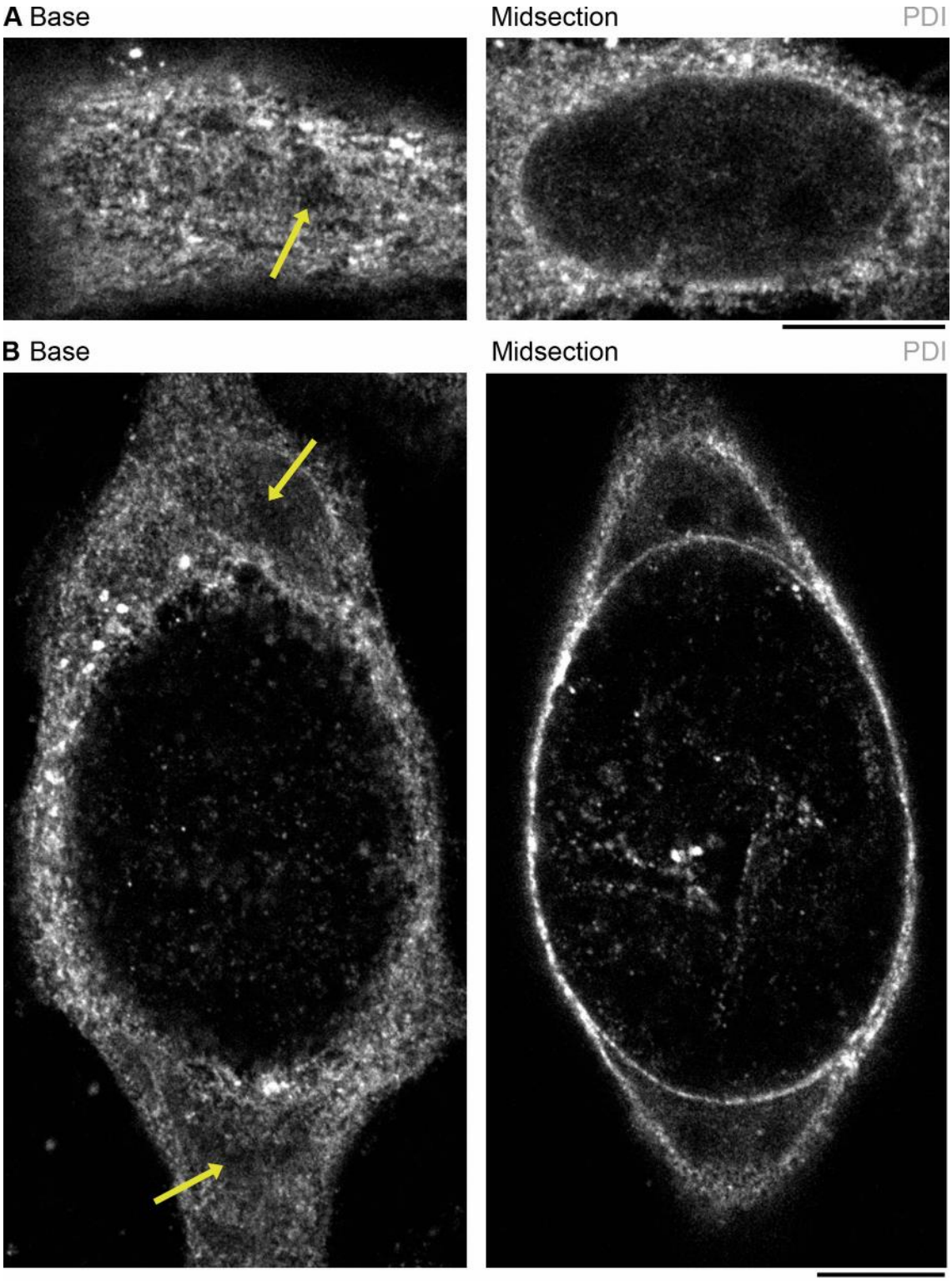

Fig 3.26 Pore-free island associated endoplasmic reticulum (ER) changes do not occur proximal to the inclusion in *Chlamydia*-infected HeLa cells. (A) Non-infected or (B) HeLa cells infected with *C. trachomatis* LGV2 for 48 hours were fixed and stained with an anti-protein disulphide isomerase (PDI) antibody and an AlexaFluor® 488-conjugated secondary (grey) to visualise the ER. Left panels: confocal xy-sections at the base of the cells, with regions of PDI exclusion indicated by yellow arrows. Right panels: confocal xy-sections of the midsection of the same cells. Scale bars, 10 µm.

3.14 Discussion

The data presented in this chapter establish a novel link between *Chlamydia* infection and nuclear architecture. Nuclear lobulation is increased at all stages of infection (Fig 3.2), and nuclear envelope changes occur with increasing frequency late during infection. These changes include an apparent enrichment in lamin A/C on the face of the NE close to the inclusion, termed a 'lamin A/C patch', with depletion in lamin A/C elsewhere in the NE (Figs 3.7-3.10). Additionally, a reduction in lamin B (Fig 3.11) and depletion of NPCs (or 'NPC gap') (Fig 3.14) is observed at the inclusion-proximal face of the NE with no disruption around the remainder of the NE. These changes coexist with and are independent of existing cellular pore-free islands (Figs 3.24 and 3.26), and occur in *C. trachomatis* but not *C. muridarum* (Fig 3.23).

Based on the frequency of occurrence, the lamin A/C patches appear to be more predominant than the lamin B reduction and NPC gap. Precedent exists for lamin A/C changes driving further alterations to the NE, such as in a subset of genetic diseases termed laminopathies. In the case of HGPS, a mutation in the prelamin A/C gene *LMNA* induces activation of a cryptic splice site, deleting 150 nucleotides at exon 11 and resulting in the production of a modified lamin A protein with a 50 amino acid deletion near the C terminus, termed LAΔ50 or progerin (Eriksson et al., 2003). Progerin incorporates into the NL, leading to the formation of a thicker and more stable lamin A/C network in HGPS cells, which, over time, results in increased lobulation of nuclei. Within these lobulated regions, lamin B is depleted and NPCs cluster, resulting in large areas of the NE depleted of NPCs (Goldman et al., 2004). These changes in the NE are remarkably similar to the alterations observed during infection with *C. trachomatis*. However, they differ in the positioning around the nuclear periphery. The lamin A/C patch, lamin B reduction and NPC gap occur proximal to the inclusion where the NE is uniform, away from the regions of lobulation on the inclusion-distal face of the NE where lamin A/C is depleted. Conversely, the changes to lamin B and NPCs in progeria cells occur within the lobulated regions, suggesting the underlying mechanisms are distinct (Goldman et al., 2004). The link between accumulation of lamin A/C and changes to other NE components is further supported by a cellular structure termed pore-free islands. PFIs are present on the nuclear surface of proliferating cells and are characterised by an area enriched in lamin A/C and depleted in lamin B and NPCs (Maeshima et al., 2006). It is therefore highly likely that the lamin A/C patch, lamin B reduction and NPC gap observed during chlamydial infection are inter-related, and this relationship will be explored in chapter 4.

At this stage, it is difficult to speculate on the mechanism by which infection with *Chlamydia* results in NE changes proximal to the inclusion. Given the similarities to previously observed cellular structures, it could be hypothesised that the lamin A/C patch is a host response to chlamydial infection rather than being driven by the pathogen. For example, the host nucleus could be strengthened in this region against the pressure of the expanding inclusion. However, a lamin A/C patch is not formed during *C. muridarum* infection, where the inclusion similarly distorts nuclear shape. Whilst it is necessary to examine the NE changes during *C. muridarum* infection of murine cells such as mouse embryonic fibroblasts (MEFs) to determine whether an atypical host cell type has any impact, these data suggest that bacterial factors present in *C. trachomatis* infection and not *C. muridarum* are required. Although the identity of bacterial factors is unknown, there is some evidence of a link between the NE alterations and cell division. Experiments showed the NE modifications occurred more frequently in multi-nucleated infected cells than in mono-nucleated infected cells, with a 1.5 fold increase in occurrence of the lamin A/C patch and a 3-4 fold increase in NPC gaps (Fig 3.19). This suggests that the NE alterations may be more prevalent following abortive cell division. During mitosis, the nuclear envelope breaks down and is reassembled, and as such represents an opportunity for *Chlamydia* to manipulate nuclear architecture with minimal energy, rather than during interphase where the NL is highly stable (Broers et al., 1999). Further evidence as to how the lamin A/C patch is formed lay in its positioning close to the inclusion. Transmission electron microscopy experiments revealed a relatively constant distance of ~160 nm is maintained between the NE and IM. This constant spacing between the IM and NE suggest there may be as yet unknown complexes bridging the gap.

In addition to the lamin A/C patch proximal to the inclusion, lamin A/C is also depleted from the remainder of the NL late during infection. This observation raises the possibility of an alternate model for the formation of the lamin A/C patch, where *Chlamydia* selectively destructs lamin A/C distal to the inclusion rather than stabilising or enriching lamin A/C proximal to the inclusion. Intriguingly, nuclear shape becomes more lobulated in the region of lamin A/C depletion. In granulocytes, increased lobulation correlates with reduced lamin A/C and lamin B levels (Olins et al., 2001), however lamin B levels remained constant in the region of lamin A/C depletion. Additionally, the increased lobulation of nuclei during chlamydial infection occurs as early as 24 hpi, whilst NE changes such as the lamin A/C patch, NPC gap and reduction in lamin A/C levels, do not occur until 48 hpi. Therefore, changes to nuclear shape precede NE alterations and so may, initially, be induced by other factors. Nuclear shape can be influenced by cytoskeletal forces transmitted through the LINC complexes (Maniotis et al.,

1997; Olins and Olins, 2004). During chlamydial infection, the cytosolic cytoskeleton is extensively remodelled, with Inc proteins such as IPAM hijacking host microtubule organising activity to form a microtubule cage and nest that surrounds the inclusion (Dumoux et al., 2015), and F-actin and the intermediate filament vimentin forming a network to encase the inclusion in association with the Inc protein InaC (Kumar and Valdivia, 2008; Kokes et al., 2015). These changes to the host cytoskeleton may therefore influence nuclear shape, resulting in the increased lobulation of nuclei observed during chlamydial infection.

Cytoskeletal forces can also result in remodelling of chromatin with effects on gene expression in a process termed mechanotransduction (Dahl et al., 2008). These forces are transmitted through the LINC complexes to the NL (Lombardi and Lammerding, 2011). The localisation of the SUN proteins, components of the LINC complex in the inner nuclear membrane, was not altered during chlamydial infection (Figs 3.18 and 3.19). However, the levels of NL proteins were modified, with a depletion of lamin A/C from the inclusion-distal face of the NE, and enrichment of lamin A/C and reduction of lamin B in the NE proximal to the inclusion. Thus, the cellular response to forces upon the nucleus, such as pressure exerted by the expanding inclusion, could be altered. For example, expression of the mechanosensitive genes *egr-1* and *iex-1* in response to mechanical strain in cells lacking lamin A/C is impaired (Lammerding et al., 2004). Functionally, the nuclear lamina is also important in the organisation and tethering of chromatin at the nuclear periphery via lamina associated domains (LADs) (Guelen et al., 2008). By constructing a patch of highly enriched lamin A/C whilst depleting lamin A/C elsewhere, infection with *C. trachomatis* could be resulting in a zone to enable manipulation of chromatin, and therefore gene expression and cellular processes.

Finally, the NPCs are depleted at the inclusion-proximal face of the NE (Fig 3.14). The primary function of the NPCs it to mediate the bidirectional transport of proteins between the cytosol and the nucleus, and to mediate export of mRNA. Nucleocytoplasmic transport may therefore be inhibited during chlamydial infection in the region of the NPC gap. Additionally, NPCs, like the nuclear lamins, are important in chromatin positioning at the nuclear periphery. Nuclear basket proteins such as Tpr form 'chromatin boundaries' to prevent the spread of heterochromatin gene silencing, and tether genes at the nuclear periphery for rapid reactivation (Shinkura and Forrester, 2002; Tan-Wong et al., 2009; Krull et al., 2010). Nuclear basket proteins also interact with the DNA repair machinery, which is of particular interest as *C. trachomatis* infection impairs the DNA damage response (Chumduri et al., 2013), and so depletion of NPCs may contribute to the malignant transformation of cells.

Chapter 4 – Determining the functional impact of modifications to the host nuclear envelope during infection with *C. trachomatis*

4.1 Introduction

The data presented in chapter 3 demonstrate that *Chlamydia* infection results in a number of alterations to nuclear architecture, including increased lobulation of the nucleus on the inclusion-distal face of the NE (Fig 3.2), enrichment in lamin A/C (termed a lamin A/C patch) at the inclusion-proximal face of the NE with depletion in the remainder of the NL (Figs 3.7-3.10), and an associated reduction in lamin B (Figs 3.11 and 3.12) and depletion of NPCs (termed an NPC gap) (Figs 3.14-3.15 and 3.17).

At this stage it is unclear whether these NE changes are directly induced by *Chlamydia* via the expression of virulence factors, or represent a host response to the presence of an exogenous compartment applying pressure to and distorting the host nucleus or nuclei. The NE changes occur in *C. trachomatis* but not *C. muridarum* (Fig 3.23), and during the infection cycle of both of these species the inclusion expands sufficiently to distort nuclear shape, suggesting the NE alterations are a *C. trachomatis* induced effect rather than a host response. However, further studies are required to confirm this conclusion, and so experiments will be conducted in this chapter to decipher more details about the mechanism by which the NE modifications occur.

The functional consequences of the NE changes for both the host and the bacteria are unknown. Although a number of pathogens, including *Chlamydia,* secrete effectors targeted to the nucleus (as discussed in 1.1.6.4), to date no other bacterial pathogens are known to specifically manipulate the composition of the NE. NPCs are essential for the specific transport of proteins between the nucleoplasm and the cytosol, and for the nuclear export of mRNA (Görlich and Kutay, 1999). Depletion of pores may therefore impact upon these processes on a local or global level. Experiments will therefore be undertaken in this chapter to investigate the impact of NPC depletion on protein transport and mRNA distribution in infected cells.

Additionally, the nuclear basket of NPCs is necessary for the formation of chromatin boundaries to prevent the spread of heterochromatin and tether highly expressed genes at the nuclear periphery for efficient mRNA export (Krull et al., 2010). Thus, chromatin organisation at the nuclear periphery may be impacted by depletion of NPCs. The NL and nuclear shape are also important for the regulation of chromatin organisation in the nucleus (Iyer et al., 2012; Zullo et al., 2012). Nuclear shape can be influenced by the composition of the NL as increased lobulation of the nuclei of neutrophils is accompanied by a reduction in lamin A/C and lamin B levels (Olins et al., 2001), and by cytoskeletal forces as microtubule depolymerisation reduces nuclear lobulation (Olins and Olins, 2004). Nuclear shape is inherently important in chromatin organisation due to the distribution of chromatin within chromosome territories, which allow the genome to be spatially organised within the interphase nucleus and active and inactive regions of the genome to be compartmentalised (Cremer and Cremer, 2010). Alterations to nuclear shape are therefore hypothesised to disrupt the distribution of chromosome territories and so impact the regulation of gene expression (Webster et al., 2009). The connection between the NL and chromatin positioning is better defined. Lamins tether chromatin to the nucleoplasmic face of the NE in the tightly packed heterochromatin form that associates with transmembrane proteins in the inner nuclear membrane such as emerin (Guelen et al., 2008; Amendola and van Steensel, 2014). Thus, the simultaneous enrichment of lamin A/C at the inclusion-proximal face of the NE and depletion of lamin A/C from the remainder of the NL may have a profound impact on chromatin organisation within the nucleus. Experiments to investigate whether chromatin organisation is altered during *Chlamydia* infection as a result of the NPC depletion, change in NL distribution and increased lobulation of the nucleus will therefore be conducted in this chapter.

4.2 Nuclear envelope alterations are independent of the size of the inclusion and require bacterial factors

The NE alterations occur more frequently towards the latter stages of the chlamydial life cycle (Figs 3.9, 3.12 and 3.15), when the inclusion is large and occupies the majority of the host cytosol. Conversely, early during infection when the inclusion is small, NE alterations do not occur (Figs 3.9, 3.12 and 3.15). It is therefore possible to conclude that the physical pressure of the inclusion on the nucleus induces a host-mediated reorganisation of lamin A/C towards the inclusion to strengthen this face of the nucleus against further distortion.

If NE alterations are related to physical pressure, one might expect a larger inclusion to cause a proportional increase in the size of lamin A/C patches and NPC gaps. To investigate this hypothesis, lamin A/C patch and NPC gap size was first measured in relation to inclusion size (Fig 4.1). The size of lamin A/C patches and NPC gaps were approximated as rectangles by measuring the longest distance in the xy dimension and multiplying by the length in the z dimension. Inclusion size was estimated by the average of two perpendicular measurements of diameter. The results showed the lamin A/C patches were significantly larger than the NPC gaps, at an average of 72.8 μm^2 compared to 19.1 μm^2 (Fig 4.1C). For both lamin A/C patches and NPC gaps, there was no correlation with corresponding inclusion diameter. Thus a larger inclusion was not associated with larger lamin A/C patches and NPC gaps, suggesting that it is unlikely the physical pressure exerted by the inclusion on the nucleus induces NE alterations (Fig 4.1A and B).

To further confirm that physical pressure alone is insufficient to cause NE alterations, experiments to simulate the inclusion size and nuclear distortion without the presence of bacterial factors were conducted. This approach was used by Sun et al (2011) to investigate multi-nucleation of cells following *Chlamydia* infection. The authors used CHO-IIA cells expressing an Fcγ receptor to ingest large polystyrene beads of a similar size to the *Chlamydia* inclusion, and showed that bacterial factors were not required to form multi-nucleated cells. For the experiments presented in this thesis, THP-1 macrophages were used to ingest polystyrene beads of a similar size to *C. trachomatis* LGV2 inclusions at 48 hpi. Polystyrene beads approximately 15 µm in diameter were opsonised with human AB^+ serum for one hour at 37°C. Beads were then incubated with THP-1 macrophages for 48 hours to allow ingestion and distortion of the nucleus, before fixation and labelling to visualise lamin A/C or NPCs (Fig 4.2A and B). Although the nuclei in bead-containing cells were clearly deformed to the crescent-like shape observed in *Chlamydia*-infected cells, no lamin A/C patches or NPC gaps were present. To confirm NE alterations still occur in this cell line, THP-1 macrophages were infected with *C. trachomatis* LGV2 for 48 hours, a time point when inclusions are similar in size to inclusions in HeLa cells at 48 hpi, before fixation and labelling for lamin A/C or NPCs (Fig 4.2C and D). As in HeLa cells, lamin A/C patches and NPC gaps were present in the central z-sections, or midsection, of the nucleus proximal to the IM. Quantification of the frequency of NPC gaps in infected THP-1 cells and THP-1 cells that have ingested polystyrene beads conclusively demonstrated that *C. trachomatis* infection is required for induction of NPC gaps (Fig 4.3). It can therefore be concluded that NE alterations are not exclusively associated with physical pressure and that bacterial factors are required.

Figure 4.1. The dimensions of the lamin A/C patch and NPC gap are independent of the size of the inclusion. HeLa cells infected with *C. trachomatis* LGV2 for 48 (white) or 72 hours (grey) were fixed and stained with anti-lamin A/C primary antibody and an AlexaFluor® 488-conjugated secondary antibody to visualise lamin A/C, or mAb414 primary antibody and an AlexaFluor® 488-conjugated secondary antibody to visualise NPCs. The dimensions of the lamin A/C patch and NPC gap were approximated by measuring the longest distance in the xy dimension and multiplying by the length in the z dimension. The inclusion size was estimated by averaging two perpendicular measurements of diameter. (A) Lamin A/C patch area versus inclusion diameter. (B) NPC gap area versus inclusion diameter. (C) Lamin A/C patch (red) and NPC gap (green) versus inclusion diameter.

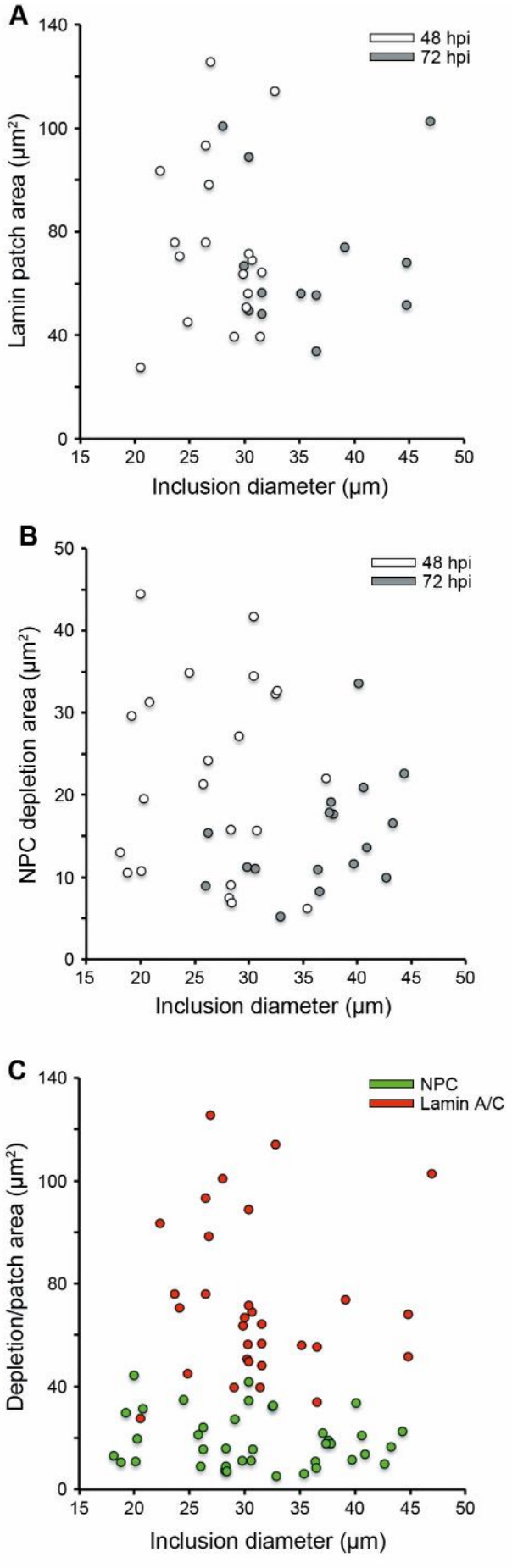
A
48 hpi
72 hpi
Lamin patch area (µm²)
Inclusion diameter (µm)
B
48 hpi
72 hpi
NPC depletion area (µm²)
Inclusion diameter (µm)
C
NPC
Lamin A/C
Depletion/patch area (µm²)
Inclusion diameter (µm)

Figure 4.2. Chlamydial factors are required for nuclear envelope modifications. THP-1 cells were incubated with human A/B serum opsonised polystyrene beads (A, B) or infected with *C. trachomatis* LGV2 for 48 hours (C, D) prior to fixation. Cells were then double stained with DRAQ-5 to visualise DNA (blue), and mAb414 primary antibody and an AlexaFluor® 488-conjugated secondary antibody (green) to visualise NPCs or anti-lamin A/C primary antibody and an AlexaFluor® 488-conjugated secondary antibody (red) to visualise lamin A/C. Left panels: confocal images of infected cells in the xy-plane, with the inclusion (I) periphery indicated by the white dashed line (Methods 2.8). Right panels: confocal xy-sections of the midsection of the nuclei, ascending in the z dimension through the cell (1-6) with a step of 0.34 µm. (A, B) THP-1 cells with ingested polystyrene beads visualised by differential interference contrast (grey). (C, D) *C. trachomatis* LGV2-infected THP-1 cells. White arrows highlight areas lamin A/C enrichment or NPC depletion. Scale bars, 10 µm.

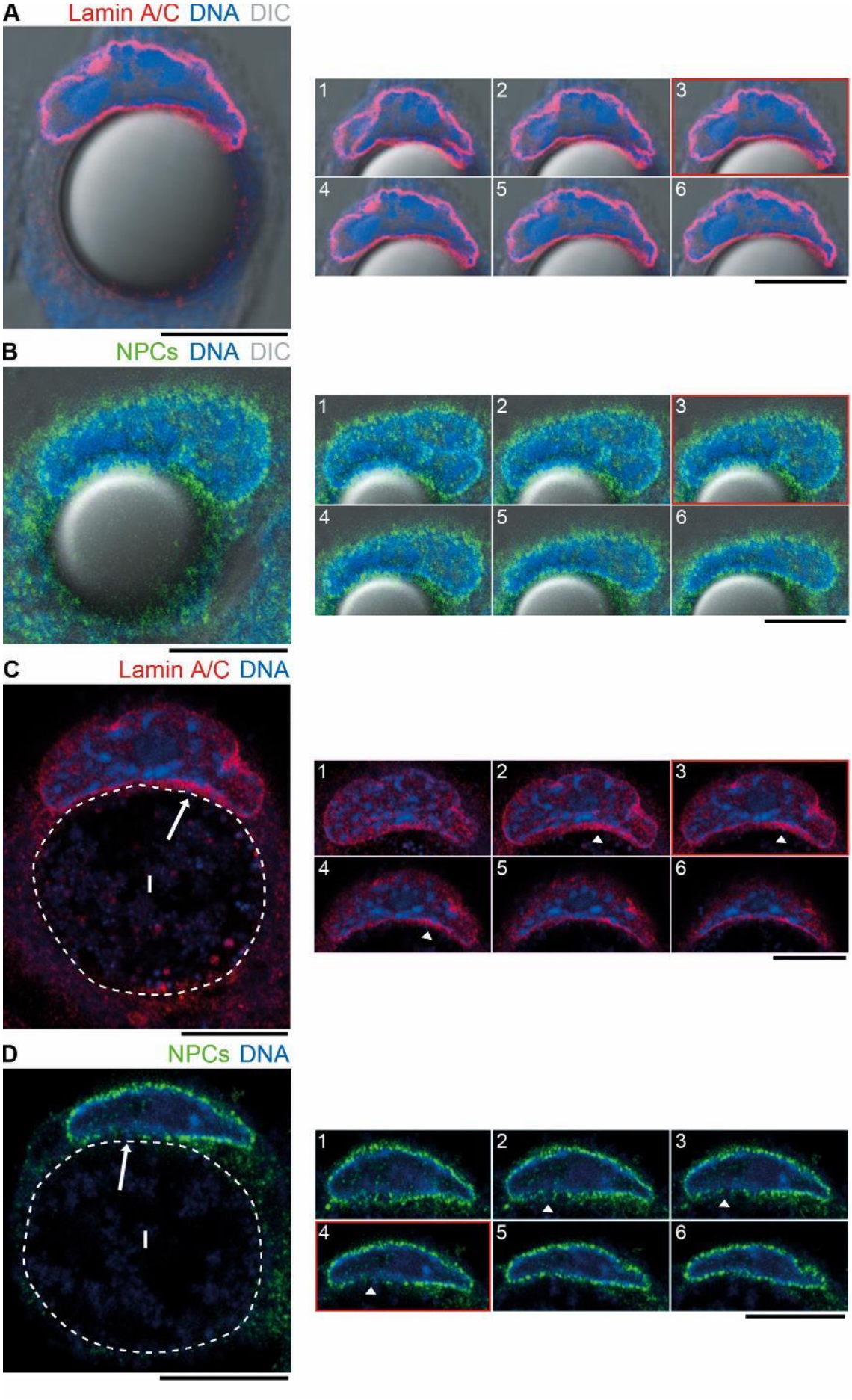
A
Lamin A/C DNA DIC
1
2
3
4
5
6
B
NPCs DNA DIC
1
2
3
4
5
6
C
Lamin A/C DNA
I
1
2
3
4
5
6
D
NPCs DNA
I
1
2
3
4
5
6

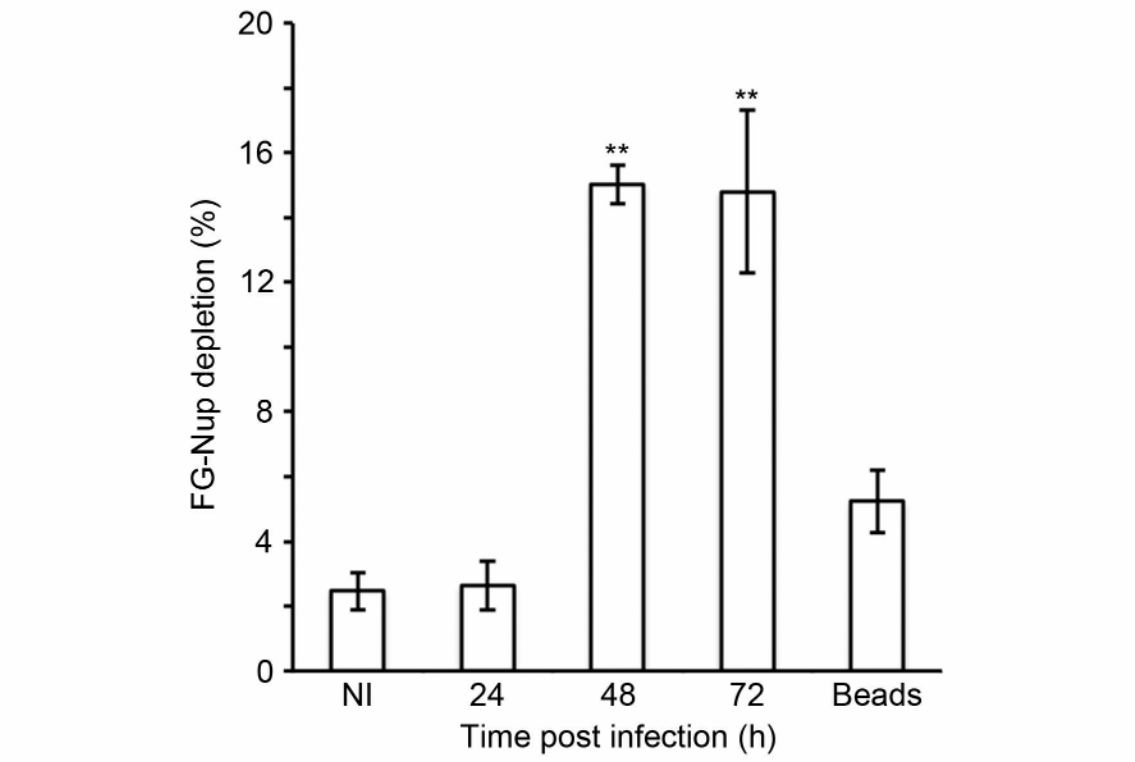

Figure 4.3. Chlamydial factors are essential for depletion of phenylalanine-glycine containing nucleoporins (FG-Nups). Non-infected (NI), *C. trachomatis* LGV2 infected (24, 48, 72 hours post infection) and polystyrene bead engulfing (Beads) THP-1 cells were fixed and stained with mAb414 primary antibody and an AlexaFluor® 488-conjugated secondary antibody to visualise NPCs. The frequency of the FG-Nup depletion, defined as a complete depletion of FG-Nups fluorescence intensity greater than 1 µm in both the xy and z dimensions, was scored as a proportion of total cells (n=100) for each time point or condition. Error bars show standard deviation (**p<0.05 using Student's t-test between NI and indicated).

4.3 *Chlamydia*-induced nuclear envelope modifications require a viable bacterial infection

The experiments presented previously demonstrated that nuclear envelope alterations are not induced by physical pressure distorting nuclear shape and require bacterial factors to be present in the host cell (section 4.2). Two scenarios therefore remain, that NE changes are a host response to *Chlamydia*, or that chlamydial effectors induce NE changes directly or indirectly. Penicillin G (pG) is a β-lactam antibiotic that causes RBs to become much larger (5-10 μm) and aberrant in morphology. These 'pG-forms' are unable to recover following withdrawal of pG and no longer express pre-16S rRNA, a marker of bacterial viability (Dumoux et al., 2013). However, the inclusion continues to expand as lysosomal compartments penetrate the inclusion to fuse with bacteria, so maintaining contact between the IM and NE and distortion of nuclear shape. Thus, pG was used as a tool to kill the bacteria at different stages of infection without clearing the bacteria from the cell, so maintaining the presence of bacterial factors that may stimulate a host response whilst inhibiting the expression of *Chlamydia* effectors.

HeLa cells were infected with *C. trachomatis* LGV2 for 48 or 72 hours before fixation, with pG added at 3, 24 or 48 hpi. Fixed cells were labelled for lamin A/C or NPCs (Fig 4.4A and B). As expected, bacteria became significantly larger and aberrant in treated cells, consistent with previous observations in the literature (Johnson and Hobson, 1977; Skilton et al., 2009; Dumoux et al., 2013). The frequency of the lamin A/C patch and NPC gap was quantified at each time point (Fig 4.4C and D) using parameters described previously (Methods 2.8.3). When pG was added at 3 hpi, a time point established in the literature to effectively kill the bacteria (Dumoux et al., 2013), the frequency of lamin A/C patch formation was dramatically reduced compared to non-treated infected cells to 14.2 ± 4.0% at 48 hpi and 12.5 ± 1.0% at 72 hpi, a 3.7- and 5.8-fold reduction respectively. Simultaneously, the frequency of NPC gap formation was reduced to levels close to that observed in non-infected cells, to just 3.8 ± 0.9% at 48 hpi and 4.7 ± 1.6% at 72 hpi, a 5.6 and 5.3-fold reduction respectively. pG was also added at 24 hpi, prior to NPC gap formation and when lamin A/C changes occur rarely, and at 48 hpi, when nuclear envelope changes have already occurred. When treated at 24 hpi, NE changes were again reduced compared to non-treated infected cells although not as significantly as when treated at 3 hpi. Lamin A/C patch frequency was reduced by 3.1- and 5.1-fold at 48 and 72 hpi, and NPC gap frequency was reduced by 2.7- and 3.2-fold. Treatment at 48 hpi had the smallest

effect, with lamin A/C patch and NPC gap frequency reduced by 1.7- and 1.5-fold respectively. In summary, there was a greater reduction in frequency when pG was added prior to occurrence of lamin A/C patches and NPC gaps, suggesting viable bacteria, and so chlamydial effectors, are required. Additionally, as there was little difference between treatment at 3 hpi and 24 hpi, it can be concluded that the effector or effectors required are secreted later during infection, after 24 hpi. As the frequency of lamin A/C patches and NPC gaps was not reduced to control levels, it is likely the antibiotic is not maximally efficient at killing the bacteria. There was a small but significant reduction in frequency when pG was added following the formation of lamin A/C patches and NPC gaps at 48 hpi, suggesting that constant release of an effector or effectors is required to maintain the NE changes.

Figure 4.4. Nuclear envelope changes require an active chlamydial infection. HeLa cells were infected with *C. trachomatis* LGV2 and treated with 10U/ml penicillin G (pG) at 3, 24 or 48 hours post infection (hpi) prior to fixation at 48 or 72 hpi. Fixed cells were then double stained with DRAQ-5 to visualise DNA (grey), and mAb414 primary antibody and an AlexaFluor® 488-conjugated secondary antibody (green) to visualise NPCs or anti-lamin A/C primary antibody and an AlexaFluor® 488-conjugated secondary antibody (red) to visualise lamin A/C. (A, B) *Chlamydia*-infected cells treated with pG at 24 hpi and fixed at 48 hpi. The inclusion (I) periphery is indicated by the white dashed line (Methods 2.8). (C) Lamin A/C patch or (D) NPC gap frequency was quantified (Methods 2.8.3) in untreated (-) cells or cells treated with pG, with non-infected (NI) cells used as a control. Error bars show standard deviation (**$p<0.05$ using Student's t-test between NI and indicated).

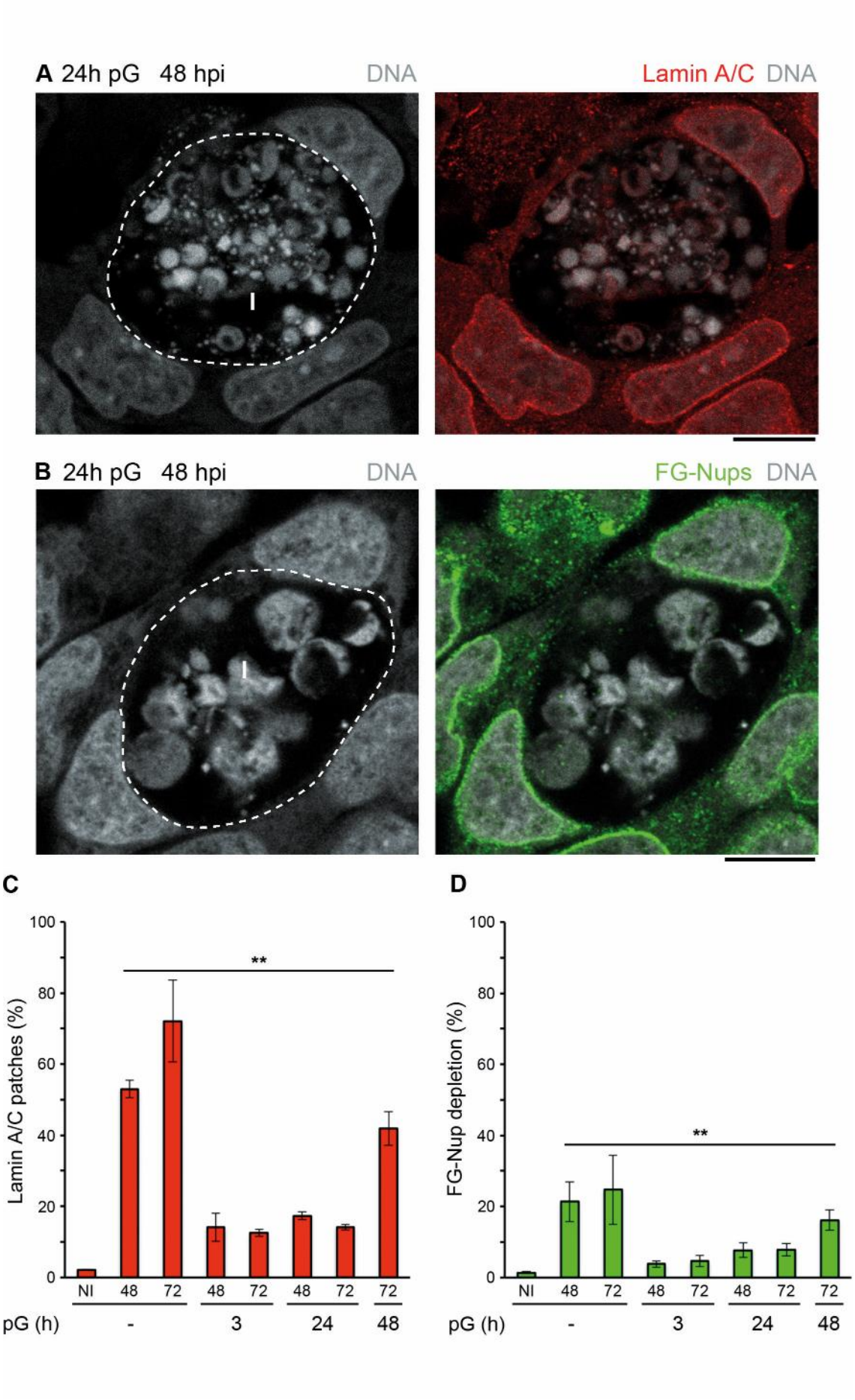
A 24h pG 48 hpi
DNA
Lamin A/C DNA
I
B 24h pG 48 hpi
DNA
FG-Nups DNA
I
C
Lamin A/C patches (%)
100
80
60
40
20
0
**
NI
48
72
48
72
48
72
72
pG (h)
-
3
24
48
D
FG-Nup depletion (%)
100
80
60
40
20
0
**
NI
48
72
48
72
48
72
72
pG (h)
-
3
24
48

4.4 Nuclear envelope damage is repaired after bacterial clearance

As demonstrated, treatment of *Chlamydia*-infected cells with pG antibiotics reduced the frequency of NE modifications (section 4.3). However, the frequency of the lamin A/C patches and NPC gaps did not return to levels present in non-infected cells. This suggests there may be permanent damage to the NE in infected cells. *Chlamydia* has been linked to cancer; both epidemiologically by a positive association with HPV-linked cervical cancers (Silva et al., 2014), and at a molecular level by perturbing chromatin, DNA double-strand break repair and cell cycle regulation (Introduction 1.1.6.4) (Chumduri et al., 2013; Padberg et al., 2013; González et al., 2014). If the NE changes are permanent it may represent a novel molecular mechanism by which *Chlamydia* is associated with cellular transformation. Indeed, studies have identified an association between both increased and decreased expression of lamin A/C in different cancer types (Wu et al., 2009; Kong et al., 2012; Bell and Lammerding, 2016).

One approach to studying whether NE damage is permanent would be to kill the bacteria late during infection and observe the frequency of NE alterations. However, pG treatment, while effectively killing the bacteria, does not immediately clear the large inclusion and aberrant bodies from the cell (Dumoux et al., 2013), and other antibiotics such as chloramphenicol or doxycycline do not function effectively late in infection when the majority of RBs have re-differentiated into EBs, and so would only be effective in subsequent infection cycles. Thus an alternative approach was required to clear the bacteria from the host cell. Nigericin is a potassium ionophore used in the Hayward laboratory by Andrew (2014) to investigate the role of potassium ions in *Chlamydia* development. An interesting unpublished observation was that nigericin, when added to late-stage *Chlamydia* infected cells, induced the ejection of inclusions, and so nigericin could potentially be applied as a tool to investigate NE modifications after the clearance of the inclusion from the previously infected cells. To confirm the efficiency of treatment, HeLa cells were infected with *C. trachomatis* for 48 hours prior to treatment with nigericin, and the proportion of infected cells compared to untreated infected cells fixed at the same time to determine the rate of inclusion clearance (Fig 4.5A). Inclusion clearance was progressive over time, with 18.7 ± 1.9% of inclusions cleared after 1 hour of treatment and 100% cleared after 48 hours.

To measure the effect of inclusion clearance on NE modifications, NPC gap frequency was scored. The frequency of NPC gaps was quantified in cells without inclusions (n=300) in duplicate (Fig 4.5B). A small but significant increase in NPC gap frequency from 1.4 ± 0.1% in the untreated population of cells to 4.2 ± 0.5% was initially observed after 6 hours of treatment, where 39.4% of inclusions had been cleared. The increase in NPC gap frequency remained stable from 6 to 24 hours after treatment, by which point 90.9% of inclusions had been cleared, and then declined to 1.5 ± 0.2% after 48 hours of treatment. There was therefore a short period of time where the NPC gap remained following clearance of inclusions, but NPC gap frequency then returned to levels observed in populations of cells that have never been infected. Thus, these data indicate the aberrant NPC distribution in infected cells returns to normal following inclusion clearance, and suggests there is no significant legacy of damage to NE composition following *Chlamydia* infection.

Figure 4.5 NPC gaps repair following nigericin-induced inclusion clearance. HeLa cells infected with *C. trachomatis* LGV2 were incubated with 1 μM nigericin at 48 hours post infection for 1, 6, 24 or 48 hours prior to fixation. Cells were then tripled stained with mAb414 primary antibody and an AlexaFluor® 488-conjugated secondary antibody to visualise NPCs, anti-*Chlamydia* primary antibody and an AlexaFluor® 546-conjugated secondary antibody (red) to visualise infected cells, and DRAQ-5 to visualise DNA. (A) The number of inclusions and nuclei were scored across 5 fields of view (totalling minimally 400 nuclei) in duplicate in nigericin-treated infected cells and compared to non-treated infected cells to determine the percentage of inclusion clearance following treatment. (B) The frequency of NPC gaps was quantified in cells without inclusions across 5 fields of view (totalling minimally 400 nuclei) in duplicate in non-treated (NT) and nigericin-treated populations of infected cells. Error bars show standard deviation (**$p<0.05$ using Student's t-test between (A) 24 and indicated or (B) NT and indicated).

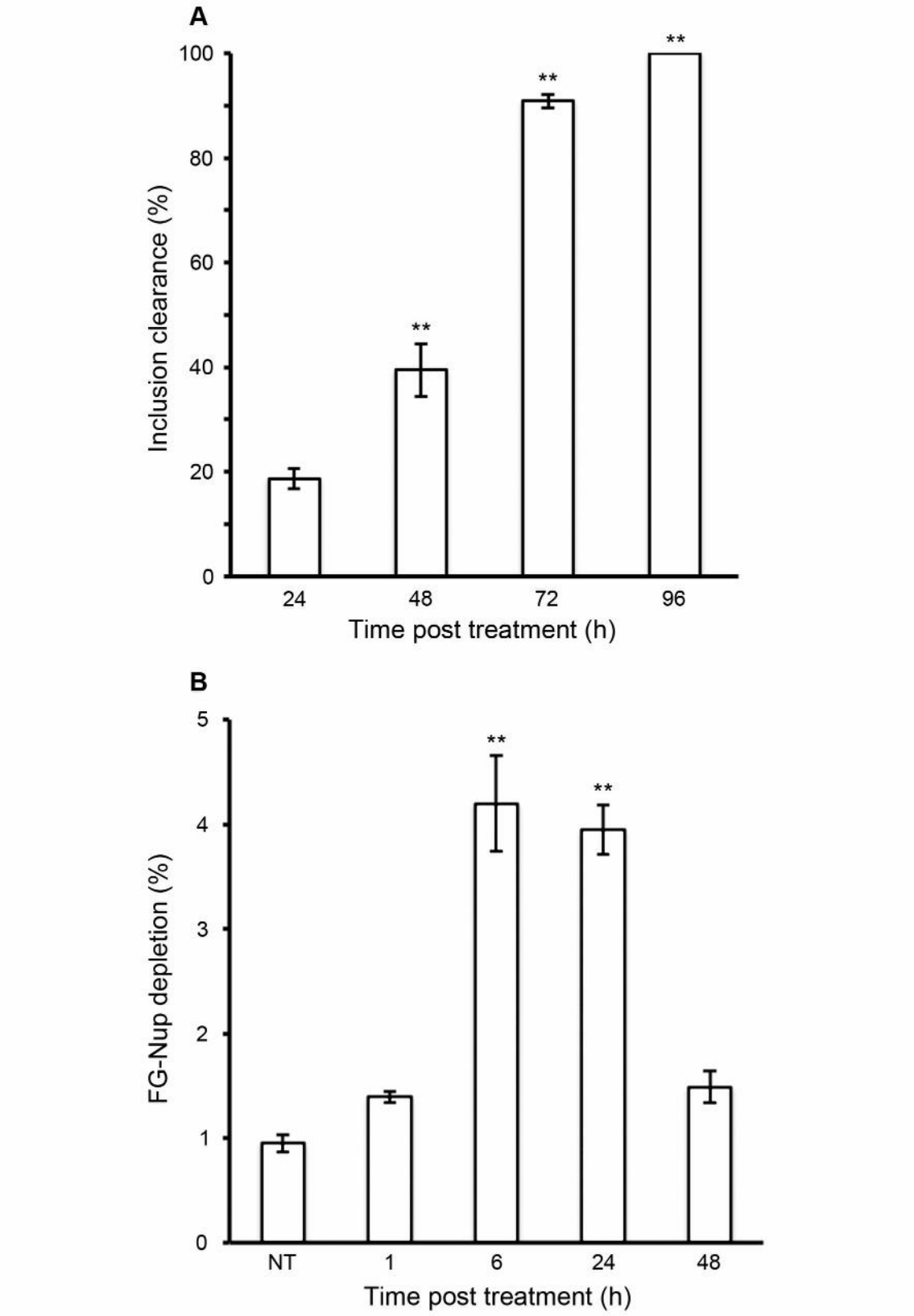
A
Inclusion clearance (%)
100
80
60
40
20
0
**
**
**
24
48
72
96
Time post treatment (h)
B
FG-Nup depletion (%)
5
4
3
2
1
0
**
**
NT
1
6
24
48
Time post treatment (h)

4.5 Host nucleocytoplasmic transport does not occur proximal to the inclusion membrane

The experiments presented in this chapter thus far have demonstrated that the modifications to the NE observed during infection with *C. trachomatis* are induced and maintained by bacterial effectors. However, the functional consequences of these NE changes were not investigated. Nuclear pore complexes mediate selective transport between the nucleus and the cytosol (Fried and Kutay, 2003). In chapter 3, it was shown that NPCs are depleted from the NE proximal to the IM (Figs 3.14 and 3.17). However, attempts to visualise the structural components of the pores were unsuccessful (Fig 3.16), although Pom121, a transmembrane Nup required for NPC assembly, was depleted (Stavru et al., 2006). Nevertheless, it is possible that the core scaffold of the NPCs is still present in these regions without the nuclear basket, central pore and cytoplasmic filaments, essentially forming a partial non-selective pore through which *Chlamydia* could efficiently target effectors into the nucleus. For molecules greater than 30-40 kDa in size, transport through the pore requires binding to a nuclear transport receptor such as importin-β, which shuttles between the nucleus and cytosol. The localisation of importin-β can therefore be analysed to determine whether nucleocytoplasmic transport occurs in the NE proximal to the inclusion, and so confirm whether pores are depleted in this region.

Ex-vivo approaches to study nucleocytoplasmic transport have used purified importin-β in conjunction with RanGDP and an energy regenerating system added to permeabilised cells to study nucleocytoplasmic transport at the NE (Lowe et al., 2015). In this study, Lowe et al. (2015) demonstrated importin-β accumulates at NPCs and traverses the pore in a Ran-dependent manner. To be able to study a subpopulation of transporter, a photo-convertible fluorescent protein such as mEos2, is used to visualise the protein of interest, importin-β (Lowe et al., 2015). Using this approach, the presence of nucleocytoplasmic transport (and so presence of NPCs) across the region of the NPC gap can be determined.

To study nucleocytoplasmic transport during chlamydial infection, the mEos2-importin-β assay was first reconstituted in cultured HeLa cells. Cells were cultured for 24 hours prior to semi-permeabilisation with digitonin, incubated with purified mEos2-importin-β and DRAQ-5 to stain DNA, and imaged live (Fig 4.6A). As expected (Lowe et al., 2015), mEos2-importin-β accumulated at the NE where it shuttles through the NPCs. The system was then transposed to

cells infected with *C. trachomatis* LGV2 for 48 hours (Fig 4.6B). Unexpectedly, mEos2-importin-β could not be introduced into infected cells, although present in neighbouring non-infected cells, indicating the infected cells were apparently not permeabilised by digitonin. Whilst not the focus of this thesis, and frustrating for the analysis of nuclear transport in infected cells, these data are intriguing. Digitonin permeabilises cell membranes by complexing with and precipitating cholesterol (Schulz, 1990), and therefore the resistance of *Chlamydia*-infected cells to digitonin-permeabilisation could indicate the cholesterol content of the plasma membrane has been dramatically altered.

As the permeabilisation method was unsuccessful, an alternative approach was adopted. A mammalian expression vector was engineered to express an mEos2-importin-β fusion protein (Methods 2.4). The vector was first tested by transiently transfecting cultured HeLa cells, fixing and staining DNA with DRAQ-5. mEos2-importin-β was distributed around the NE in a punctate distribution (Fig 4.7A), similar to distribution of purified mEos2-importin-β in permeabilised cells (Fig 4.6A). HeLa cells were then transfected with the mEos2-importin-β vector prior to infection with *C. trachomatis* LGV2 and fixation. At 48 hpi, when NE changes occur, a localised and striking depletion of mEos2-importin-β occurs at the inclusion-proximal face of the NE (Fig 4.7B). The location and size of the zone of mEos2-importin-β depletion is consistent with the depletion of NPCs described previously. These data suggest host nucleocytoplasmic transport is absent proximal to the inclusion, and further suggests that NPCs are not modified, but entirely absent.

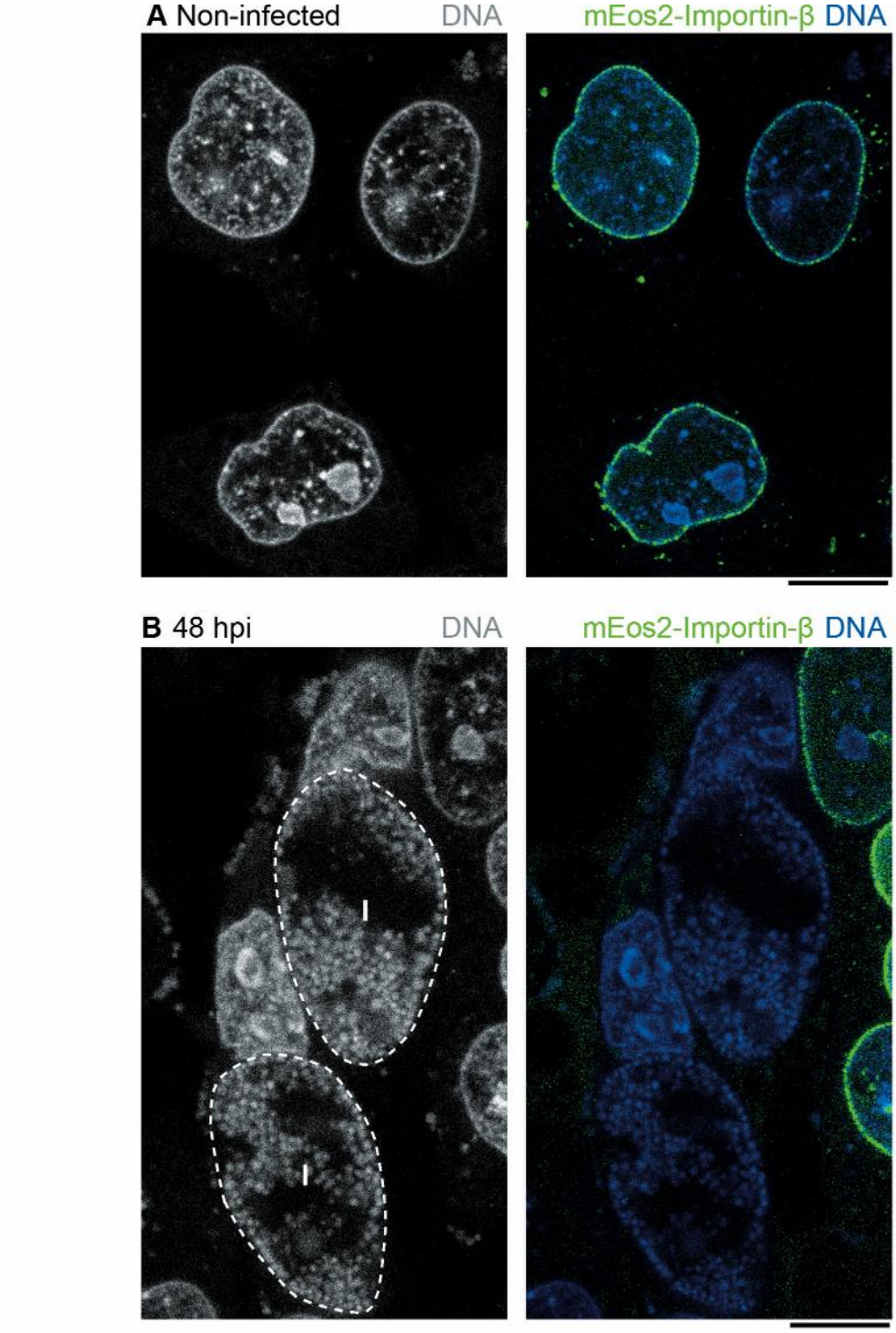

Figure 4.6 *Chlamydia*-infected cells are resistant to digitonin-permeabilisation. HeLa cells at 48 hours post infection (hpi) with *C. trachomatis* LGV2 were semi-permeabilised with digitonin, incubated with mEos2-importin-β (green) and stained with DRAQ-5 to visualise DNA (grey, blue) for live imaging. (A) Confocal images of non-infected cells in the xy-plane. (B) Confocal images of *Chlamydia*-infected cells in the xy-plane, with the inclusion (I) periphery indicated by the white dashed line (Methods 2.8).

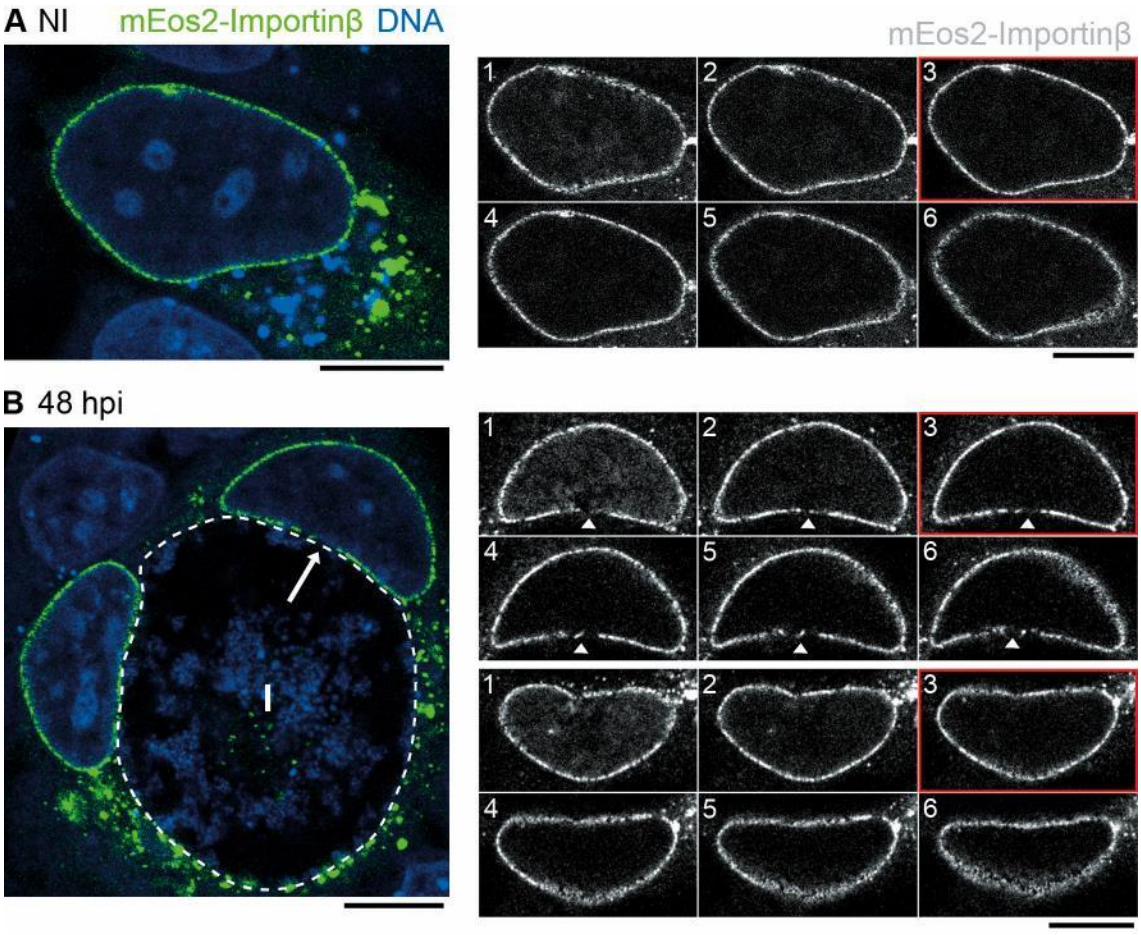

Figure 4.7. Transiently expressed importin-β is depleted at the inclusion-proximal face of the nuclear envelope during *Chlamydia* infection. HeLa cells transiently expressing mEos2-importin-β (green, grey) were infected with *C. trachomatis* LGV2, fixed and stained with DRAQ-5 to visualise DNA (blue). Left panels: confocal images of cells in the xy-plane, with the inclusion (I) periphery indicated by the white dashed line (Methods 2.8). Right panels: confocal xy-sections of the midsection of the nuclei, ascending in the z dimension through the cell (1-6) with a step of 0.34 µm. Red borders indicate the sections equivalent to the left panels. White arrows highlight areas of importin-β depletion. (A) Non-infected (NI) (B) 48 hours post infection (hpi). Scale bars, 10 µm.

4.6 Distribution of host nuclear messenger RNA appears unaffected during *Chlamydia* infection

In addition to mediating protein transport between the cytosol and the nucleus, NPCs are the conduit for the export of messenger RNA (mRNA) from the nucleus to the cytosol. The export of host mRNA is blocked during certain viral infections (Castelló et al., 2009; Kuss et al., 2013). For example, expression of poliovirus 2A protease in host cells induces cleavage of a number of FG-repeat containing Nups, including Nup62 and Nup98 in the central pore, and Nup153 of the nuclear basket. This results in inhibition of nuclear export and subsequent accumulation of poly(A) mRNA in the nucleus (Castelló et al., 2009). Moreover, addition of IFN-γ to cells infected with poliovirus partially prevented the cleavage of Nup98, thus preventing the inhibition of RNA nuclear export (Castelló et al., 2009). Adenoviruses, herpesviruses and vesiculoviruses also inhibit mRNA export, but instead target mRNA export factors such as nuclear export factor 1 (NXF1) (Kuss et al., 2013). Given that NPCs are entirely removed from the NE proximal to the inclusion, mRNA distribution was investigated during infection with *C. trachomatis*.

Fluorescent *in-situ* hybridisation (FISH) can be used to investigate mRNA distribution. FISH is a method developed in the 1980s to study localisation of DNA and chromosomes within the cell (Levsky and Singer, 2003). In more recent years, FISH techniques have taken advantage of the 3' end polyadenylation of messenger RNA (mRNA) to study mRNA localisation in the host cell (Castelló et al., 2009; Wickramasinghe et al., 2010). A 30 base poly-thymine (polyT) probe conjugated to a 5'-AlexaFluor 488 dye was used to visualise the pool of cellular polyadenylated mRNA. As a negative control, a 30 base poly-adenine (polyA) probe conjugated to a 5'-AlexaFluor 488 dye was also used. RPE1 cells were cultured and fixed prior to hybridisation of either polyT or polyA probes. RPE1 cells were used since they possess a normal karyotype and also exhibit lamin A/C patches and NPC gaps during chlamydial infection. In cells labelled with the polyT probe, fluorescence is localised predominantly to the nucleus, with the cytosol labelled weakly (Fig 4.8). The nuclear staining consists of many small punctate structures, similar to the pre-mRNA splicing regions in the nucleus, the nuclear speckles, in agreement with examples of poly(A) staining in the literature (Castelló et al., 2009; Wickramasinghe et al., 2010). As expected, the poly(A) probe exhibited near zero fluorescence. Mixing the probes at a 1:1 poly(T) to poly(A) ratio in a competitive inhibition assay also abrogated poly(A) mRNA

signal, suggesting the poly(A) probes competes with the poly(A) tail of mRNA by binding to the poly(T) probe. The poly(T) probe is therefore specifically detecting poly(A) mRNA.

With the assay optimised, poly(A) mRNA localisation in *Chlamydia*-infected cells was observed. Fixed *C. trachomatis* LGV2-infected RPE1 cells were hybridised with the poly(T) probe and labelled for DNA (Fig 4.9). Cytosolic mRNA levels appear unchanged during chlamydial infection. At 24 hpi, nuclear mRNA staining is similar to non-infected cells. However, later in infection, at 48 and 72 hpi, nuclear mRNA fluorescence intensity increases and the speckle-like localisation becomes more clustered. Polarisation of nuclear poly(A) mRNA to the inclusion-proximal face of the nucleus was not observed. From this qualitative analysis, the levels of nuclear poly(A) mRNA increase, suggesting nuclear export of mRNA is inhibited. However, it is also possible that the increase in poly(T) probe fluorescence in the nucleus is due to a compaction of nuclear volume as the inclusion expands and distorts nuclear shape. Therefore, quantification of nuclear poly(A) mRNA levels during infection is required that takes into account the nuclear volume.

RPE1 cells were infected with *C. trachomatis* LGV2, fixed prior to hybridisation with the poly(T) probe and labelled for lamin B. The nuclear periphery was detected using the lamin B fluorescence and a mask generated, within which the total intensity of poly(A) mRNA fluorescence was measured relative to the area of the nucleus (Fig 4.10A). The resulting average pixel intensity corrected for the area was then summed across the z-stack and divided by the number of z-sections to give the mean nuclear pixel intensity per unit volume or mean voxel intensity (Methods 2.8.4). The mean voxel intensity was averaged across the infected cell population and compared relative to non-infected cells at that time point (Fig 4.10B). The results show no significant difference between infected and control at any time points post infection. These data suggest there is no significant change in nuclear mRNA levels due to the removal of NPCs proximal to the IM, and therefore global mRNA export is not inhibited.

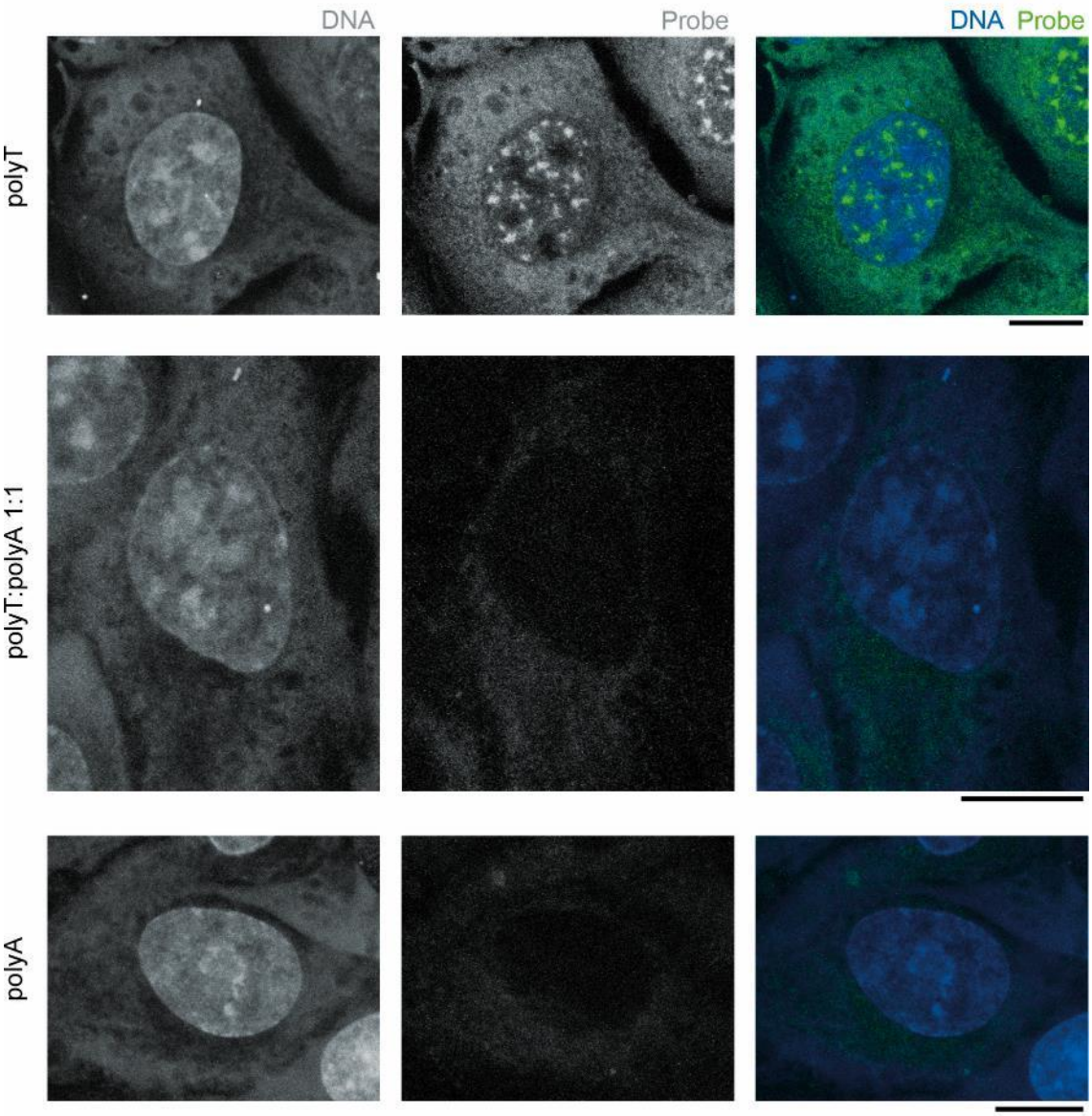

Figure 4.8. Optimisation of fluorescence *in-situ* hybridisation to visualise poly(A) mRNA. RPE1 cells were cultured and fixed prior to hybridisation with a 5'-AlexaFluor® 488-conjugated poly-thymine or poly-adenine probe [green, grey (centre panels)], or a 1:1 mixture of both probes. DNA [blue, grey (left panels)] was stained with DRAQ-5. Confocal images of all cells were acquired with identical laser power and photomultiplier voltage to ensure an accurate comparison of fluorescence intensity. Scale bars, 10 µm.

Figure 4.9. Nuclear poly(A) mRNA fluorescence is increased and clustered late during chlamydial infection. RPE1 cells were infected with *C. trachomatis* LGV2 and fixed prior to hybridisation with an AlexaFluor® 488-conjugated poly(T) probe (green, grey) to visualise poly(A) mRNA, and staining for DNA (blue) with DRAQ-5. Left panels: confocal images of cells in the xy-plane, with the inclusion (I) periphery indicated by the white dashed line (Methods 2.8). Right panels: confocal xy-sections of the midsection of the nuclei, ascending in the z dimension through the cell (1-6) with a step of 0.34 µm. Red borders indicate the sections equivalent to the left panels. (A) 24 hours post infection (hpi) (B) 48 hpi (C) 72 hpi. Confocal images of all cells were acquired with identical laser power and photomultiplier voltage to ensure an accurate comparison of fluorescence intensity. Scale bars, 10 µm.

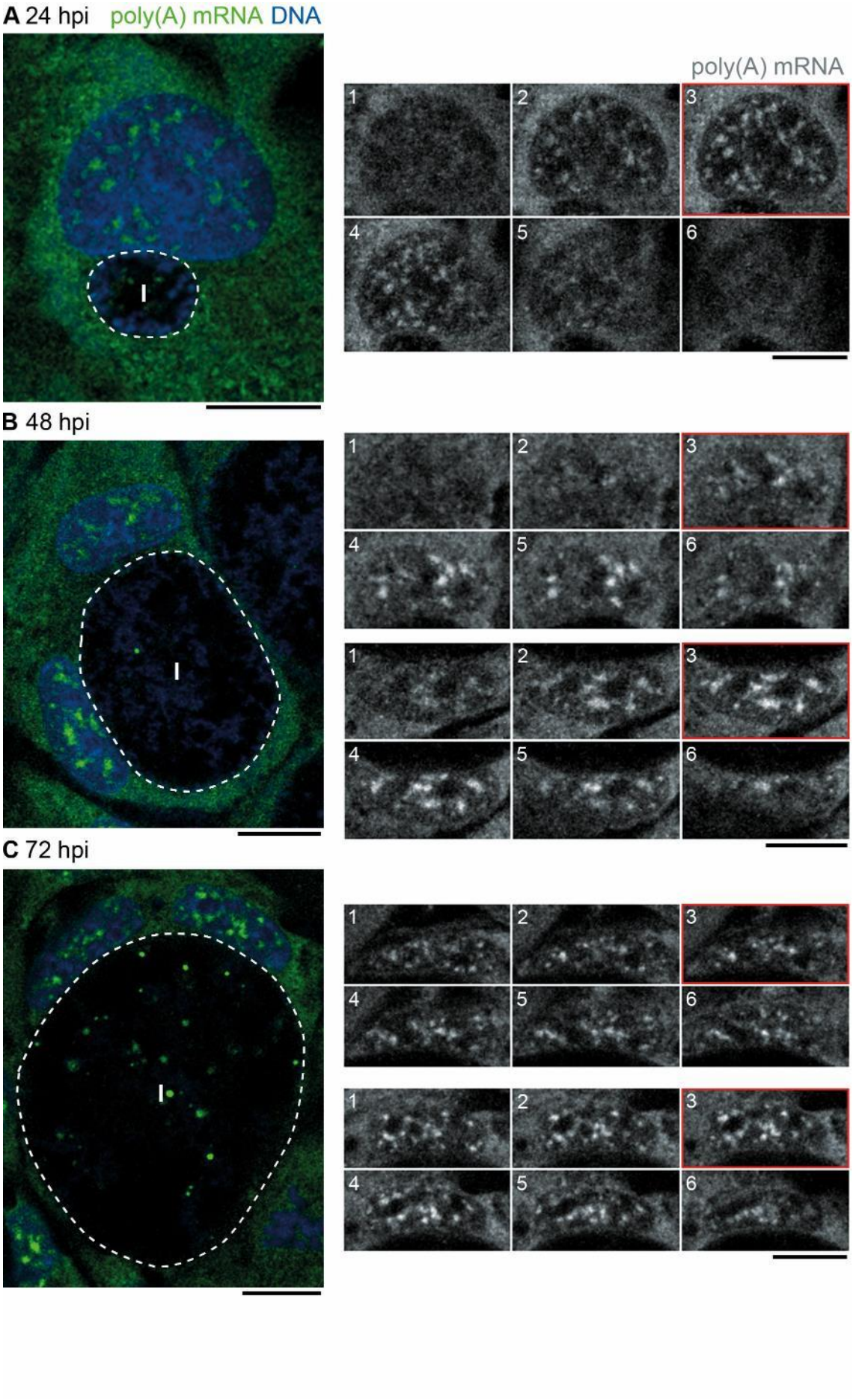
A 24 hpi poly(A) mRNA DNA
poly(A) mRNA
B 48 hpi
C 72 hpi
I
1
2
3
4
5
6

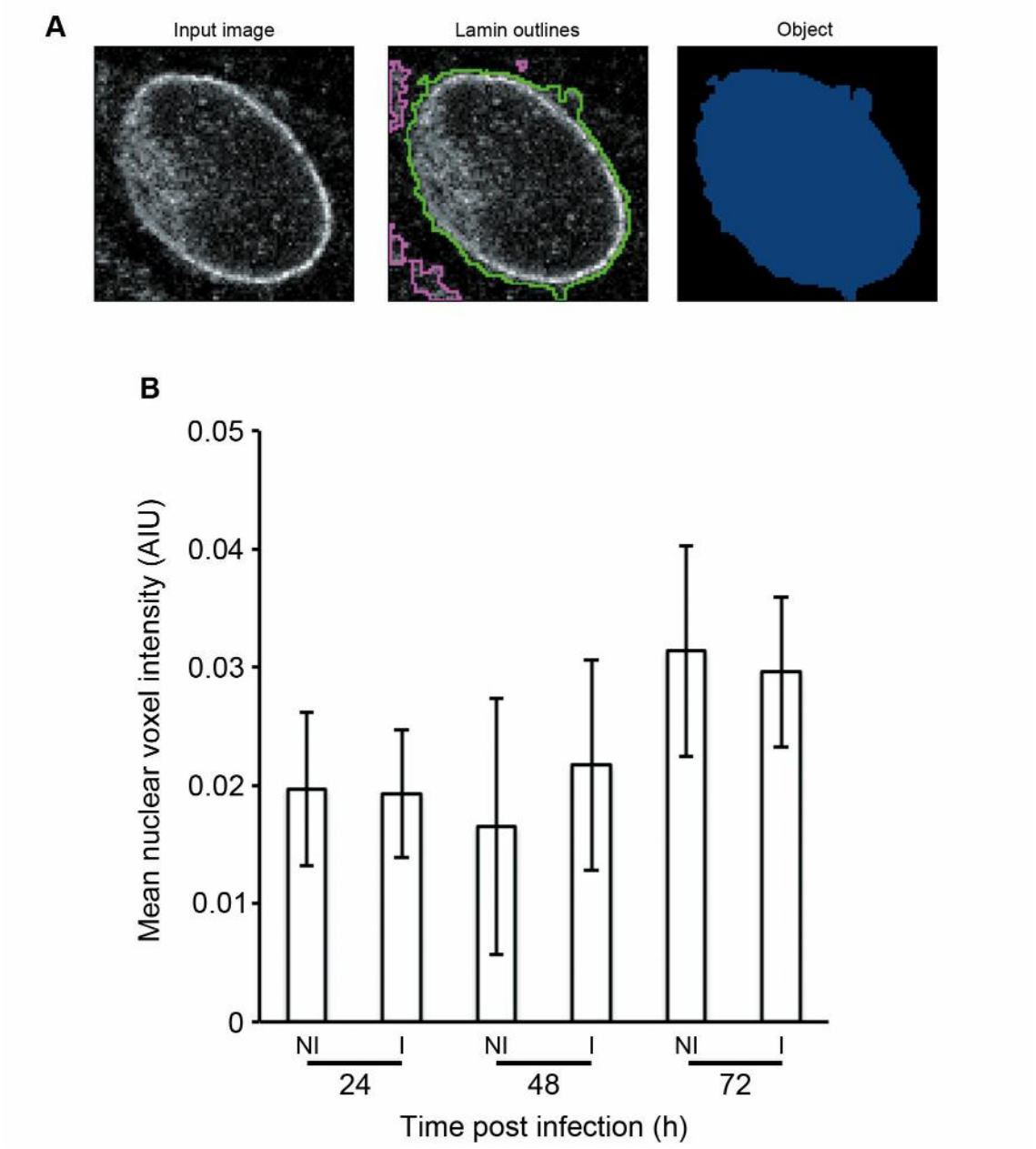

Figure 4.10. Total nuclear poly(A) mRNA levels remain constant during *Chlamydia* infection. RPE1 cells were infected with *C. trachomatis* LGV2 and fixed prior to hybridisation with an AlexaFluor® 488-conjugated poly(T) probe to visualise poly(A) mRNA and staining with anti-lamin B1 primary antibody and AlexaFluor® 546-conjugated secondary antibody to visualise lamin B. z-series were acquired for nuclei in non-infected (NI) or infected (I) cells (n=150) at 24, 48 or 72 hours post infection. (A) CellProfiler was used to automatically detect and convert the nuclear periphery from the lamin B fluorescence into a filled object representing the nuclear area. (B) Histogram showing the mean nuclear voxel intensity [measured in arbitrary intensity units (AIU)] in non-infected or infected cells (Methods 2.8.4). Error bars show standard deviation.

4.7 Heterochromatin accumulates on the face of the nucleus proximal to the inclusion

The nuclear basket of NPCs regulates chromatin organisation at the nuclear periphery by restricting heterochromatin, which is tethered by lamin A/C at the NE through lamina-associated domains in the genome, from spreading (Guelen et al., 2008; Krull et al., 2010). The lamin A/C alterations correlate with the NPC gap at the late stage of *Chlamydia* infection (Figs 3.9 and 3.15). Nuclear shape is also modified during chlamydial infection (Fig 3.2), becoming progressively lobulated which may influence chromosome positioning (Cremer and Cremer, 2010). Therefore, the positioning of chromatin in relation to the NPCs and lamin A/C was interrogated during infection with *Chlamydia*.

Histone modifications to individual chromatin domains lead to the condensation or de-condensation of chromatin structure, and thus restrict or allow access to transcription factors to repress or activate gene expression (Bártová et al., 2008). Histone modifications can therefore be used as markers for heterochromatin, the tightly packed transcriptionally repressed form of chromatin, or euchromatin, the loosely packed transcriptionally active form of chromatin (Bártová et al., 2008). Triple methylation of histone H3 lysine 9 (H3K9me3) is associated with constitutive heterochromatin (Rea et al., 2000), while triple methylation of histone H3 lysine 4 (H3K4me3) is associated with euchromatin (Schneider et al., 2004). Therefore, to investigate chromatin distribution during chlamydial infection, the localisation of histone markers H3K9me3 and H3K4me3 in non-infected and *C. trachomatis* LGV2-infected HeLa cells was examined.

In non-infected cells, H3K4me3 was distributed across the nuclear lumen (Fig 4.11A), consistent with euchromatin being localised distal to the nuclear periphery (Kimura, 2013). H3K9me3 was enriched towards the periphery of the nucleus and around the nucleoli (Fig 4.11B), as expected given the reported localisation of heterochromatin (Poleshko et al., 2013; Towbin et al., 2013). At 24 hpi with *C. trachomatis* LGV2, the distribution of H3K4me3 and H3K9me3 within the nucleus was similar to that of non-infected cells (Fig 4.12A and 4.13A). The distribution of H3K4me3 at 48 hpi also remained consistent, with no polarisation towards or away from the nuclear periphery (Fig 4.12B). However, changes were observed in the distribution of H3K9me3 at this time point, with an enriched patch of H3K9me3 appearing at the inclusion-proximal face of the NE, and H3K9me3 being depleted around the remainder of

the nuclear periphery (Fig 4.13B). These phenotypes are remarkably similar to the changes to lamin A/C during infection observed in chapter 3 (section 3.5), when an enrichment of lamin A/C is observed in the NE proximal to the inclusion, and lamin A/C is depleted elsewhere around the nuclear periphery. Indeed, when lamin A/C and H3K9me3 are co-labelled in cells infected with *C. trachomatis* LGV2 for 48 hours, the lamin A/C patch and H3K9me3 enrichment were present in close proximity (Fig 4.14).

The frequency of heterochromatin enrichment was then quantified. Enrichment in H3K9me3 was defined as a region on one face of the nucleus greater than 1 µm in the xy and z planes axis with at least 50% higher fluorescence intensity than the H3K9me3 at the opposing face of the nucleus. At 24 hpi just 2.0 ± 0.1% of infected cells had an enrichment of H3K9me3 at the luminal face of the nucleus proximal to the IM, whilst at 48 and 72 hpi 22.3 ± 3.2 and 27.8 ± 5.3% of infected cells showed enrichments respectively (Fig 4.15). These frequencies are very similar to the occurrence of the NPC gap, which occurred at 21.3% at 48 hpi and 24.7% at 72 hpi, rather than the lamin A/C patch, which occurred at 52.9% at 48 hpi and 72.1% at 72 hpi. Taken together, these data show heterochromatin localisation is modified late during chlamydial infection, with enrichment in heterochromatin observed in the region of the nucleus proximal to the inclusion.

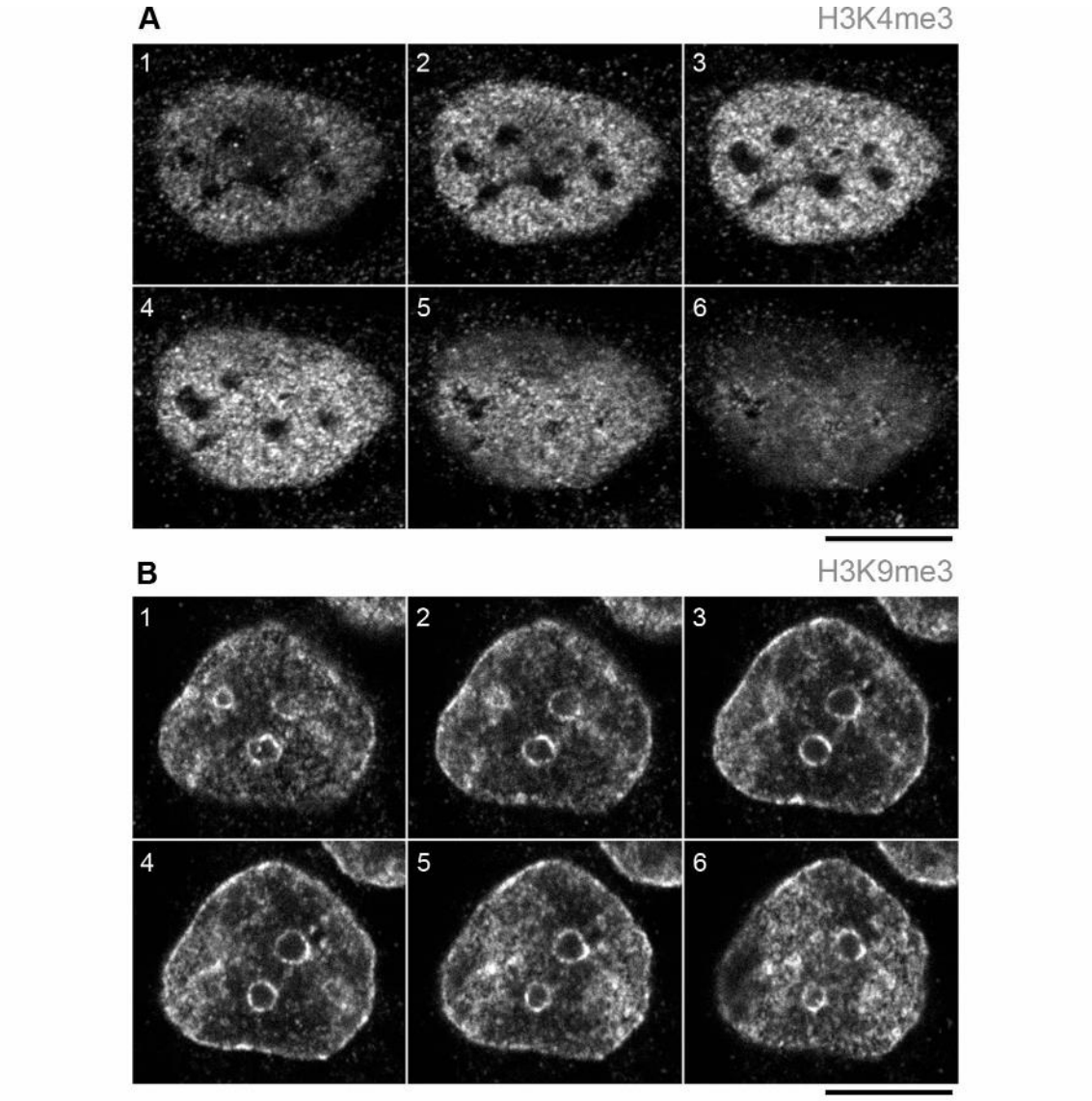

Figure 4.11. Distribution of euchromatin and heterochromatin in the nuclei of cultured HeLa cells. Fixed HeLa cells were stained with (A) anti-H3K4me3 primary antibody and an AlexaFluor® 488-conjugated secondary antibody (grey, upper) to visualise euchromatin or (B) anti-H3K9me3 primary antibody and an AlexaFluor® 488-conjugated secondary antibody (grey, lower) to visualise heterochromatin. Confocal xy-sections of nuclei ascend in the z dimension through the cell (1-6) with a step 0.34 µm. Scale bars, 10 µm.

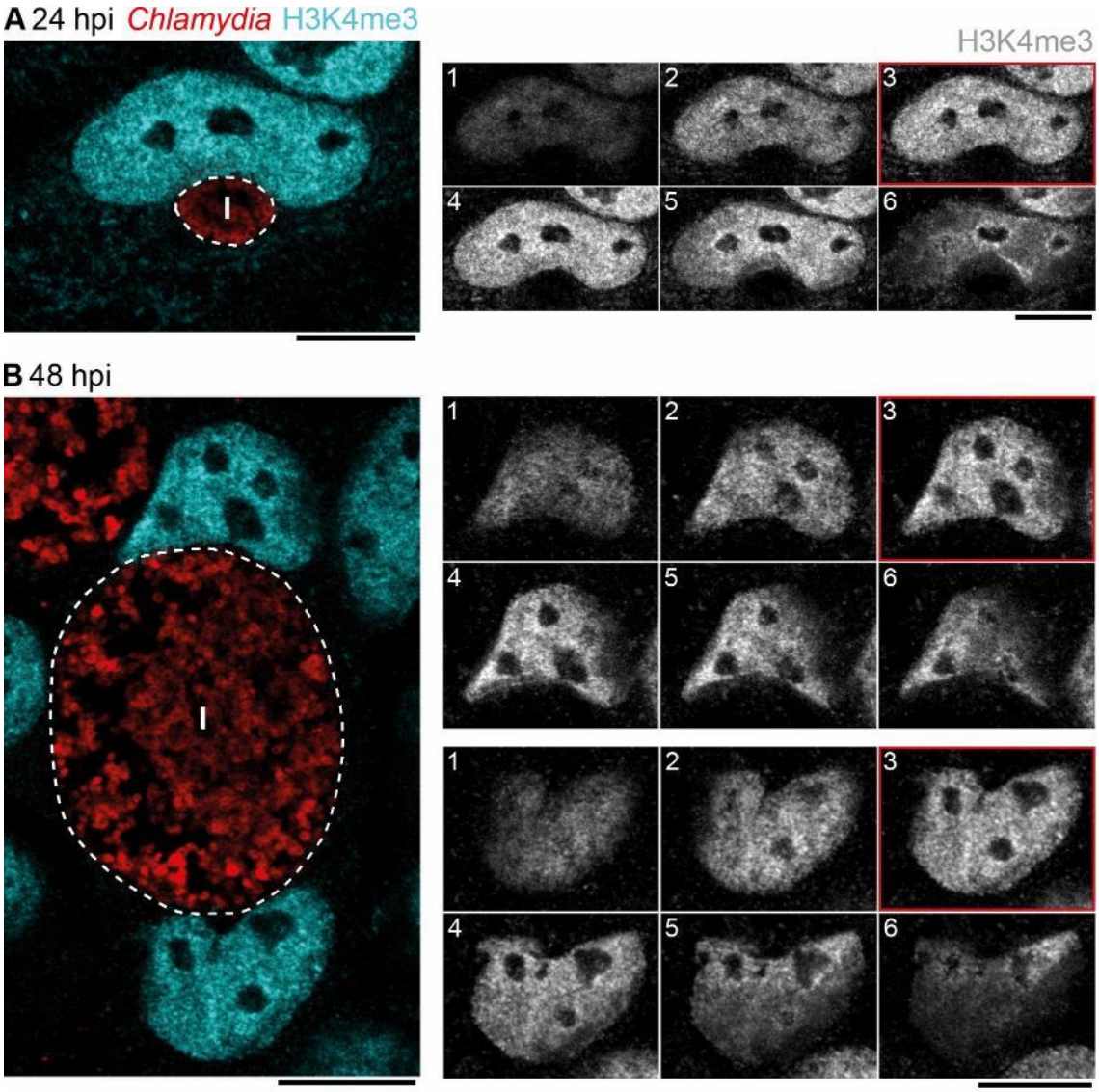

Figure 4.12. Euchromatin distribution is not polarised during infection with *Chlamydia*. HeLa cells were infected with *C. trachomatis* LGV2, fixed and double stained with anti-H3K4me3 primary antibody and an AlexaFluor® 488-conjugated secondary antibody (cyan, grey) to visualise euchromatin and anti-*Chlamydia* primary antibody and an AlexaFluor® 546-conjugated secondary antibody (red) to visualise bacteria. Left panels: confocal images of infected cells in the xy-plane, with the inclusion (I) periphery indicated by the white dashed line (Methods 2.8). Right panels: confocal xy-sections of the nuclei, ascending in the z dimension through the cell (1-6) with a step of 0.34 µm. Red borders indicate the sections equivalent to the left panels. (A) 24 hours post infection (hpi). (B) 48 hpi. Scale bars, 10 µm.

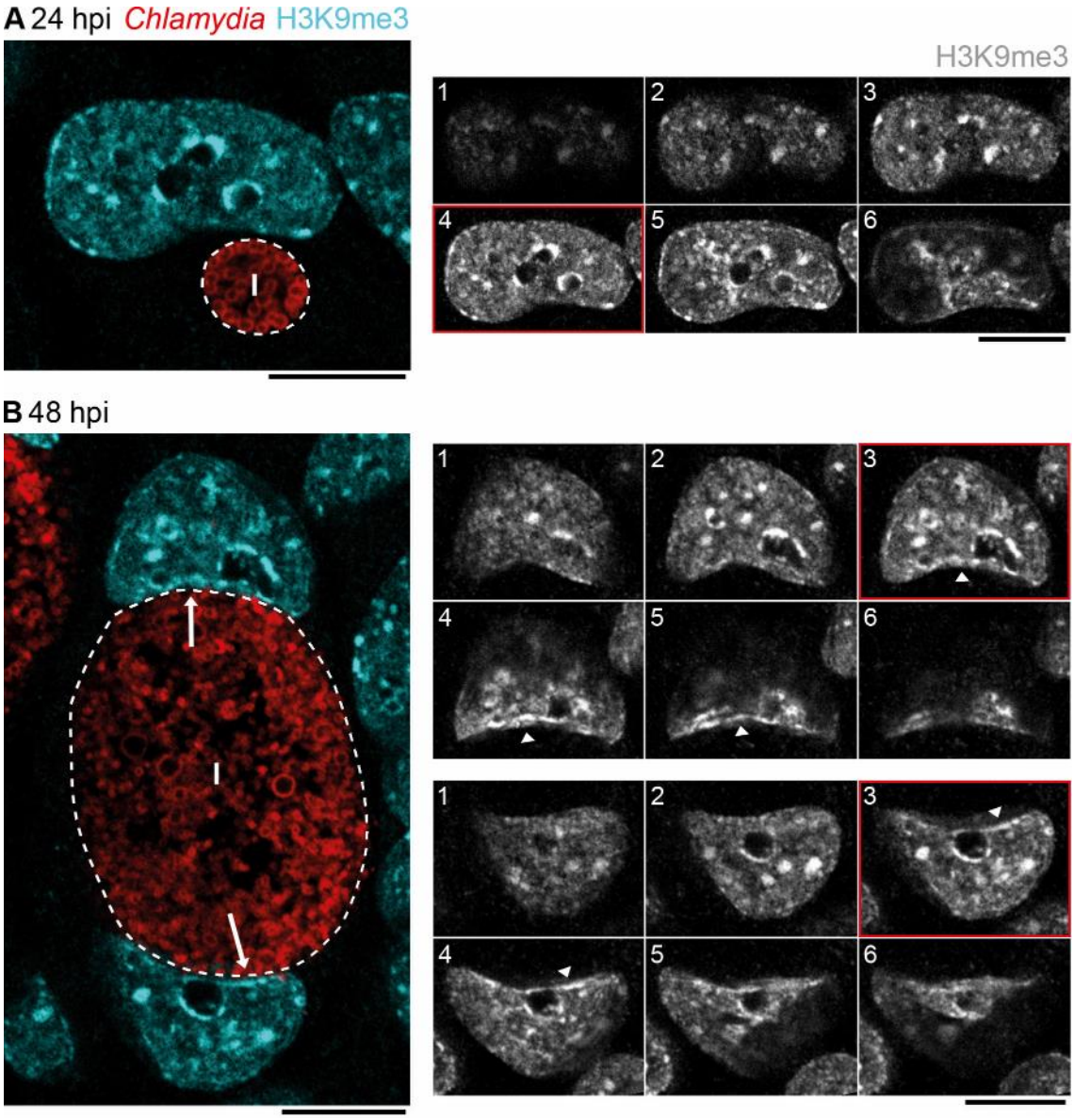

Figure 4.13. Heterochromatin accumulates at the inclusion-proximal face of the nucleus late during chlamydial infection. HeLa cells were infected with *C. trachomatis* LGV2, fixed and double stained with anti-H3K9me3 primary antibody and an AlexaFluor® 488-conjugated secondary antibody (cyan, grey) to visualise heterochromatin and anti-*Chlamydia* primary antibody and an AlexaFluor® 546-conjugated secondary antibody (red) to visualise bacteria. Left panels: confocal images of infected cells in the xy-plane, with the inclusion (I) periphery indicated by the white dashed line (Methods 2.8). Right panels: confocal xy-sections of the nuclei, ascending in the z dimension through the cell (1-6) with a step of 0.34 µm. Red borders indicate the sections equivalent to the left panels. (A) 24 hours post infection (hpi). (B) 48 hpi. Scale bars, 10 µm.

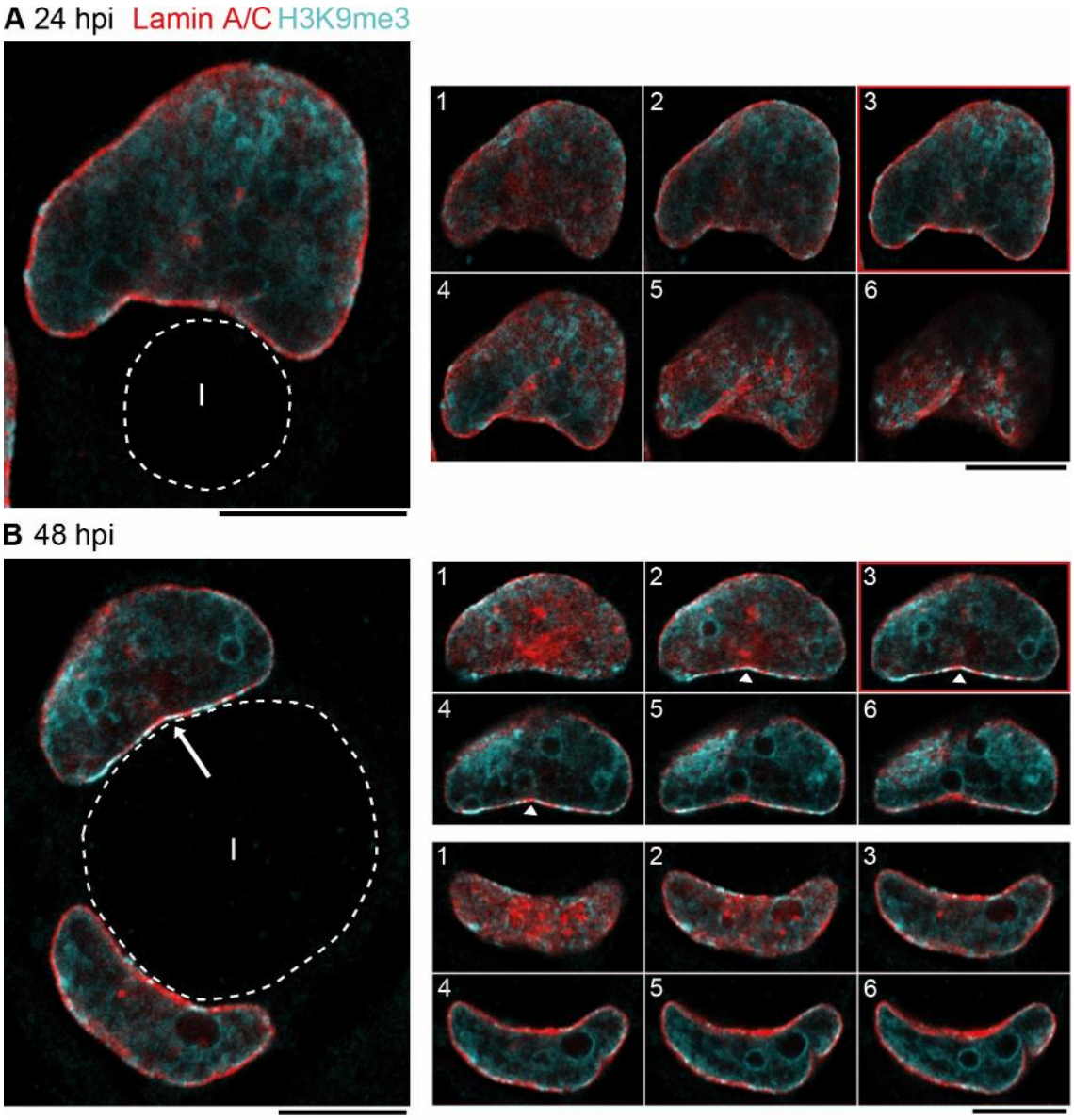

Figure 4.14. Heterochromatin and lamin A/C are enriched in close proximity at the inclusion-proximal face of the nuclear periphery late during chlamydial infection. HeLa cells were infected with *C. trachomatis* LGV2, fixed and double stained with anti-H3K9me3 primary antibody and an AlexaFluor® 488-conjugated secondary antibody (cyan, grey) to visualise heterochromatin and anti-lamin A/C primary antibody and an AlexaFluor® 546-conjugated secondary antibody (red) to visualise lamin A/C. Left panels: confocal images of infected cells in the xy-plane, with the inclusion (I) periphery indicated by the white dashed line (Methods 2.8). Right panels: confocal xy-sections of the nuclei, ascending in the z dimension through the cell (1-6) with a step of 0.34 µm. Red borders indicate the sections equivalent to the left panels. (A) 24 hours post infection (hpi). (B) 48 hpi. Scale bars, 10 µm.

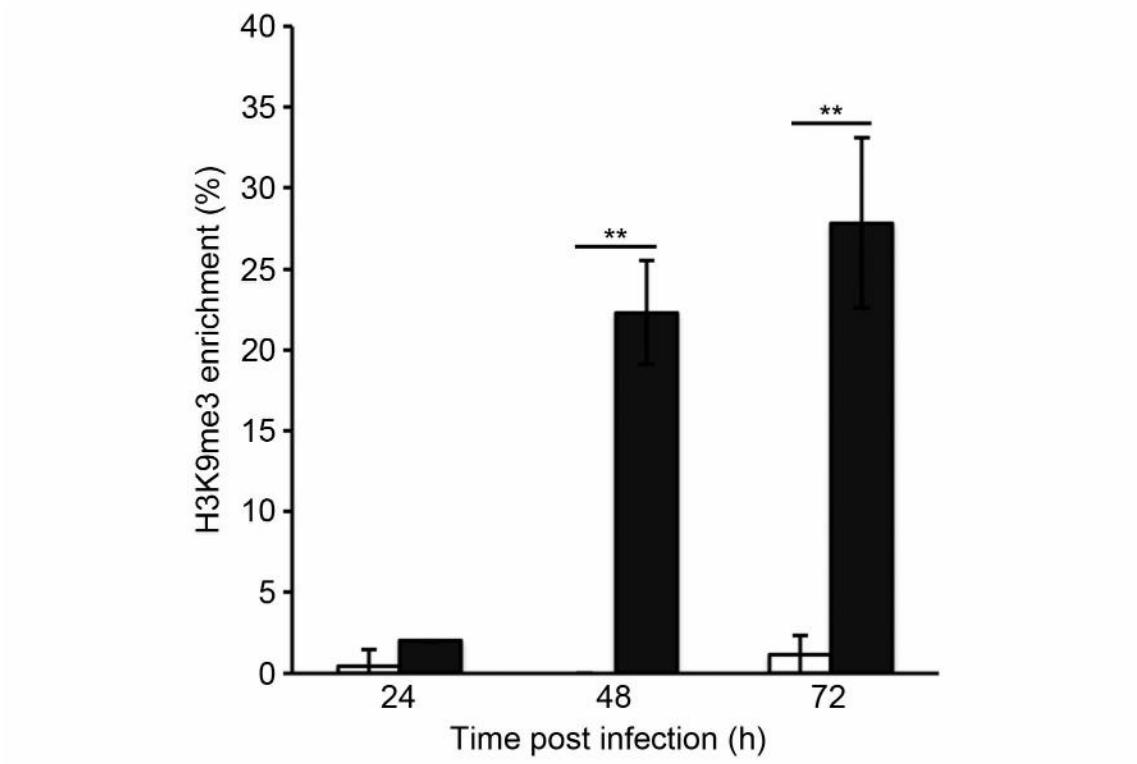

Figure 4.15. Enrichment of heterochromatin occurs more frequently late during chlamydial infection. Histogram showing the proportion of non-infected (white bars) or *C. trachomatis* LGV2 infected (black bars) HeLa cells (n=100) exhibiting an enrichment of heterochromatin scored at each time point. An enrichment of heterochromatin was defined as a region of H3K9me3 on one face of the nucleus greater than 1 µm in the xy and z planes with at least 50% higher fluorescence intensity than the H3K9me3 at the opposing face of the nucleus. Error bars show standard deviation (**p<0.05 using Student's t-test as indicated).

4.8 Lamin A/C is required for the depletion of NPCs and enrichment of heterochromatin observed during chlamydial infection

The nuclear lamina is essential for determining nuclear pore complex positioning within the NE (Liu et al., 2000; Guo and Zheng, 2015), and also tethers heterochromatin at the nuclear periphery by interacting with nucleotide sequences in the mammalian genome termed lamina-associated domains (Guelen et al., 2008). Furthermore, the increased lobulation of granulocyte nuclei is associated with a depletion of NL proteins (Olins et al., 2001). Given these NL functions, and given that the lamin A/C patch occurs in a significantly higher frequency of *Chlamydia*-infected cells than the depletion in NPCs or enrichment of heterochromatin (Figs 3.9, 3.15, 4.15), it was hypothesised lamin A/C may be at the origin of the NPC, heterochromatin and nuclear shape changes described previously (Figs 3.14, 4.13, 3.2).

Lamin A/C knockout fibroblasts were used to investigate this hypothesis. Mouse embryonic fibroblasts (MEFs), either WT or knockout for the gene encoding prelamin A/C (*LMNA*) by deletion of a region of *LMNA* from exon 8 to exon 11 [a generous gift from Professor Brian Burke (A*STAR, Singapore), created as described in Sullivan et al. (1999)], were infected with *C. trachomatis* LGV2, fixed and labelled for NPCs and lamin A/C or heterochromatin and lamin A/C. The absence of lamin A/C was verified by immunofluorescence, and the distribution of NPCs and heterochromatin analysed (Fig 4.16). In non-infected *LMNA*$^{-/-}$ MEFs, the absence of lamin A/C was clear. NPC levels appeared reduced in *LMNA*$^{-/-}$ MEFs compared to WT MEFs, but remained distributed around the entire nuclear periphery (Fig 4.16B). Heterochromatin was depleted from the nuclear periphery in *LMNA*$^{-/-}$ MEFs compared to WT MEFs (Fig 4.16D), as expected given the importance of lamin A/C in tethering heterochromatin at the NE (Solovei et al., 2013). The depletion of NPCs and enrichment of heterochromatin observed in the nuclei of *C. trachomatis*-infected HeLa cells (Figs 3.14 and 4.13) were present in *C. trachomatis*-infected WT MEFs (Figs 4.17A, 4.18A, 4.19A), confirming NE alterations occur independently of host cell line. However, neither the depletion of NPCs nor the enrichment of heterochromatin was observed in the *LMNA*$^{-/-}$ MEFs (Figs 4.17B, 4.18B, 4.19B), suggesting lamin A/C is required for these changes. The lobulation of nuclei in *C. trachomatis*-infected cells was also investigated in infected *LMNA*$^{-/-}$ MEFs, but no significant differences were observed compared to WT MEFs (Fig 4.20). These data support the conclusion that depletion of lamin A/C increases lobulation

of nuclei in infected cells, as lobulation of the nuclei of WT infected cells occurs in the NE distal to the inclusion where lamin A/C is depleted, and the nuclei of *LMNA*$^{-/-}$ MEFs are similarly lobulated in this region.

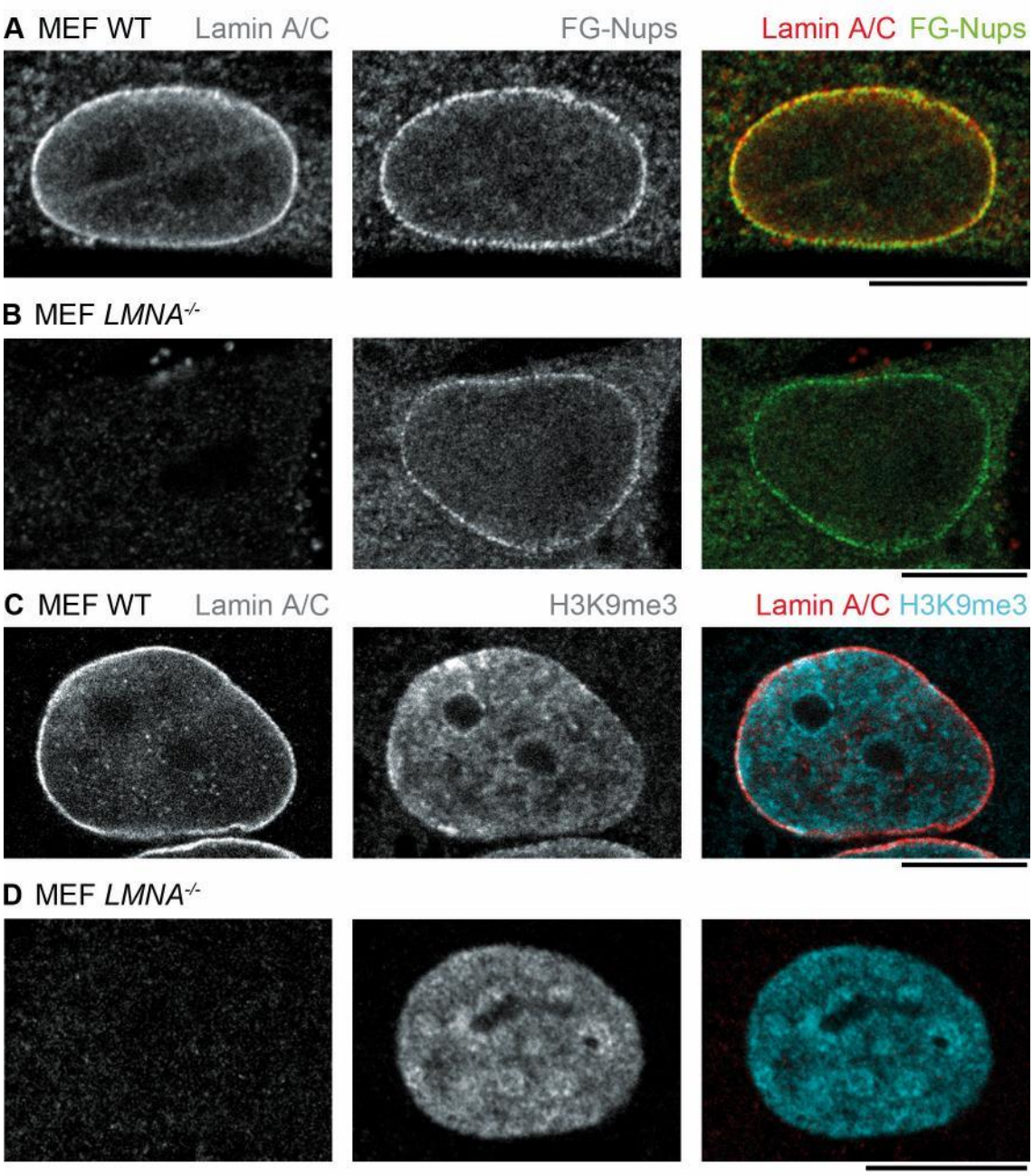

Figure 4.16. Distribution of nuclear pore complexes and heterochromatin in wildtype (WT) and *LMNA*-/- mouse embryonic fibroblasts (MEFs). Fixed (A, C) WT and (B, D) *LMNA*$^{-/-}$ MEFs were double stained with anti-lamin A/C primary antibody and an AlexaFluor® 546-conjugated secondary antibody [grey (left panels), red] to visualise lamin A/C, and either mAb414 primary antibody and an AlexaFluor® 488-conjugated secondary antibody [grey (A, B, centre panels), green] to visualise phenylalanine glycine-repeat containing nucleoporins (FG-Nups) or anti-H3K9me3 primary antibody and an AlexaFluor® 488-conjugated secondary antibody [grey (C, D, centre panels), cyan] to visualise heterochromatin. Scale bars, 10 µm.

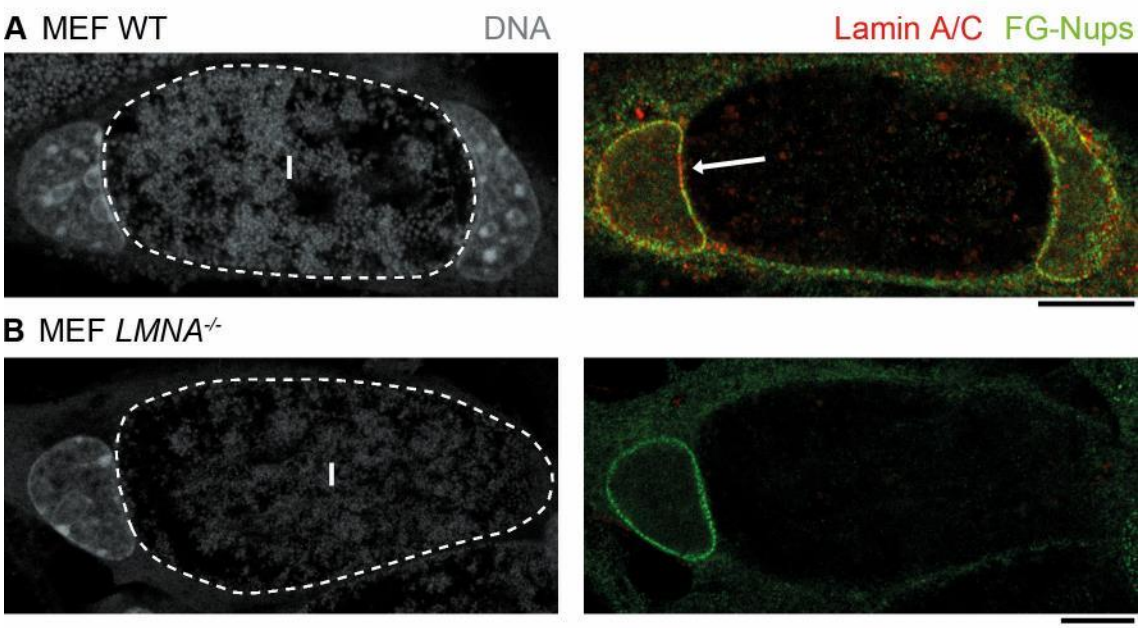

Figure 4.17. Lamin A/C is required for the *Chlamydia*-induced depletion of NPCs proximal to the inclusion. (A) WT or (B) *LMNA*$^{-/-}$ mouse embryonic fibroblasts (MEFs) were infected with *C. trachomatis* LGV2 for 48 hours, fixed and triple stained with mAb414 primary antibody and an AlexaFluor® 488-conjugated secondary antibody (green) to visualise phenylalanine glycine-repeat containing nucleoporins (FG-Nups), anti-lamin A/C primary antibody and an AlexaFluor® 546-conjugated secondary antibody (red) to visualise lamin A/C, and DRAQ-5 (grey) to visualise DNA. The inclusion (I) is indicated by a white-dashed line (Methods 2.8). A white arrow indicates an area of FG-Nup depletion and lamin A/C enrichment. Scale bars, 10 µm.

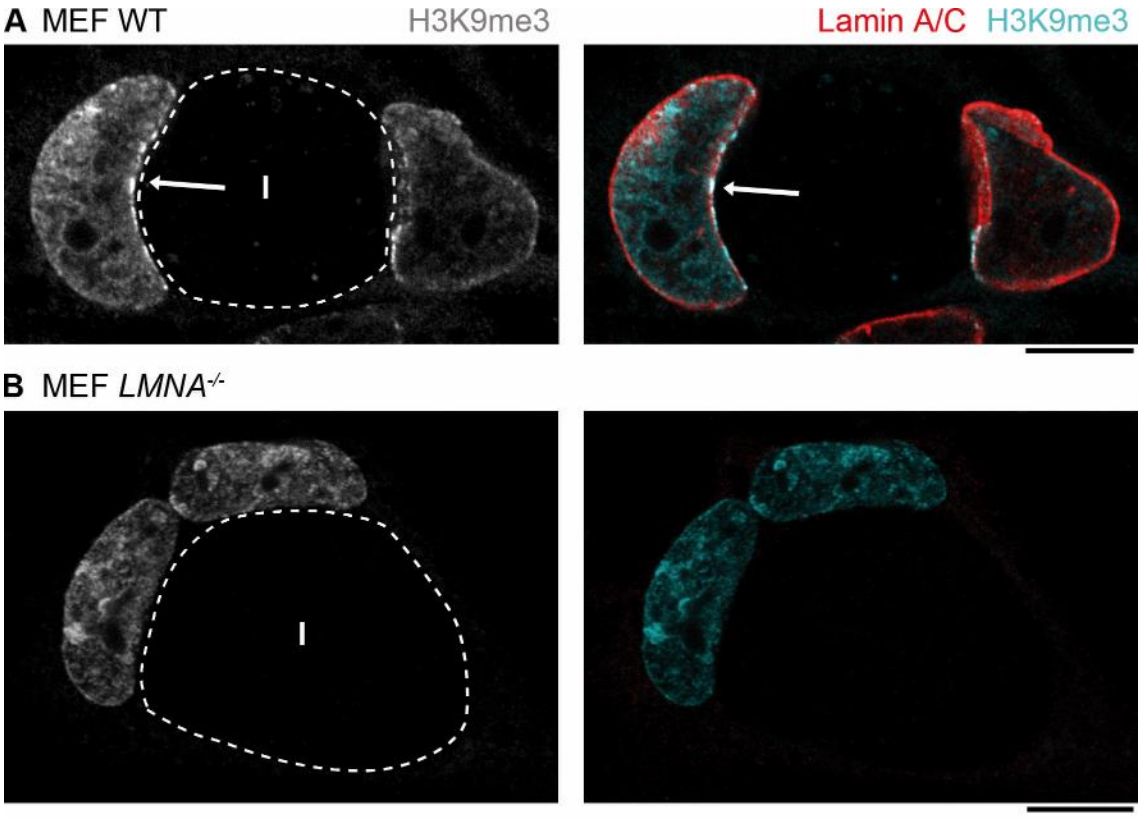

Figure 4.18. Lamin A/C is required for *Chlamydia*-induced enrichment of heterochromatin proximal to the inclusion. (A) WT or (B) *LMNA*$^{-/-}$ mouse embryonic fibroblasts (MEFs) were infected with *C. trachomatis* LGV2 for 48 hours, fixed and double stained with anti-H3K9me3 primary antibody and an AlexaFluor® 488-conjugated secondary antibody (grey, cyan) to visualise heterochromatin and anti-lamin A/C primary antibody and an AlexaFluor® 546-conjugated secondary antibody (red) to visualise lamin A/C. The inclusion (I) is indicated by a white-dashed line (Methods 2.8). A white arrow indicates an area enriched in heterochromatin and lamin A/C. Scale bars, 10 µm.

Figure 4.19. Quantification confirms lamin A/C is required for *Chlamydia*-induced nuclear envelope changes. WT (white bars) or *LMNA*$^{-/-}$ (black bars) mouse embryonic fibroblasts were infected with *C. trachomatis* LGV2, fixed at the indicated time post infection and stained with mAb414 primary antibody and an AlexaFluor® 488-conjugated secondary antibody to visualise phenylalanine glycine-repeat containing nucleoporins (FG-Nups) or anti-H3K9me3 primary antibody and an AlexaFluor® 488-conjugated secondary antibody to visualise heterochromatin. The proportion of cells (n=100) with (A) FG-Nup depletion or (B) H3K9me3 enrichment was scored according to previously defined parameters (Methods 2.8.4). Error bars show standard deviation (**p<0.05 using Student's t-test as indicated).

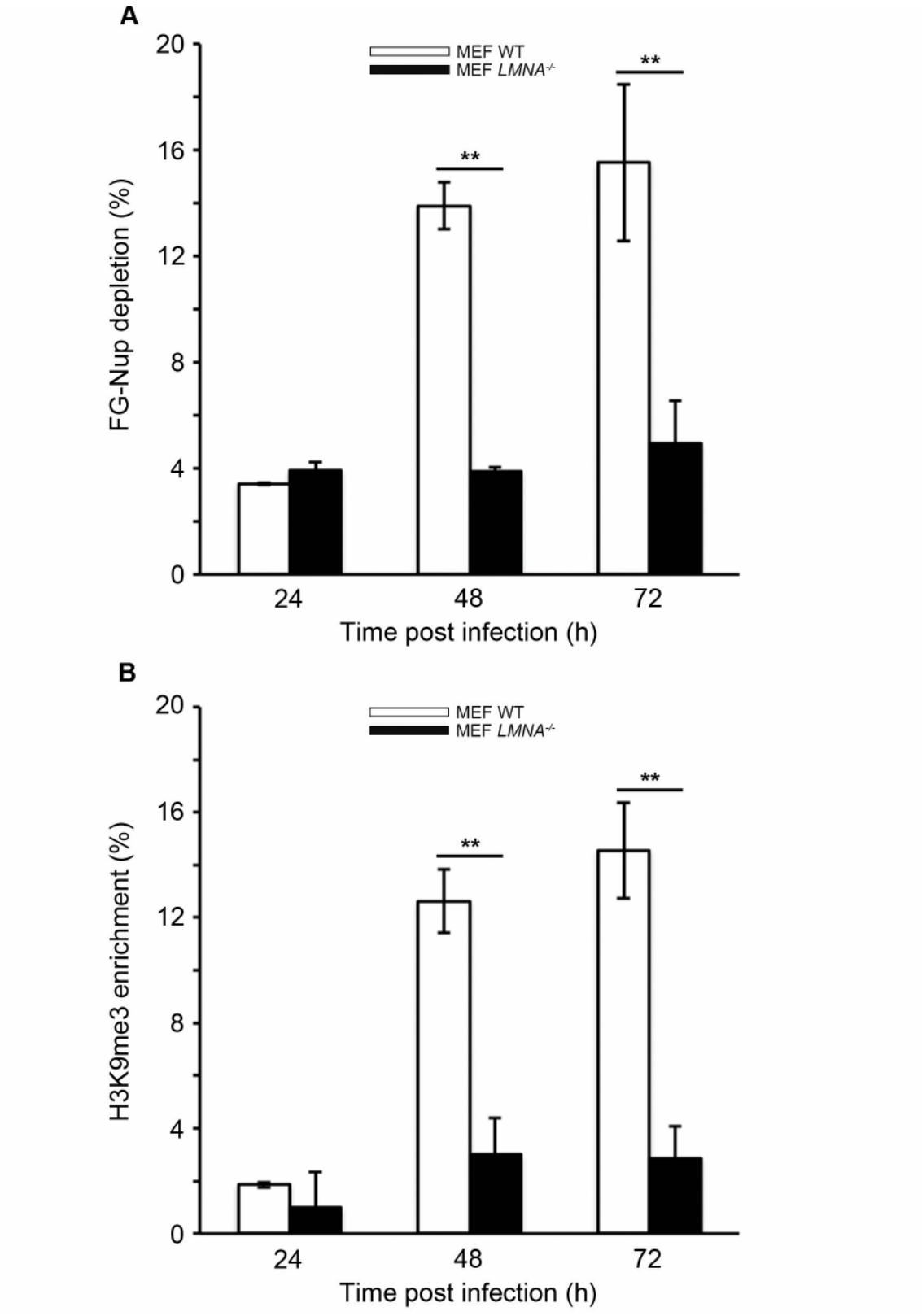
A
MEF WT
MEF LMNA-/-
FG-Nup depletion (%)
20
16
12
8
4
0
**
**
24
48
72
Time post infection (h)
B
MEF WT
MEF LMNA-/-
H3K9me3 enrichment (%)
20
16
12
8
4
0
**
**
24
48
72
Time post infection (h)

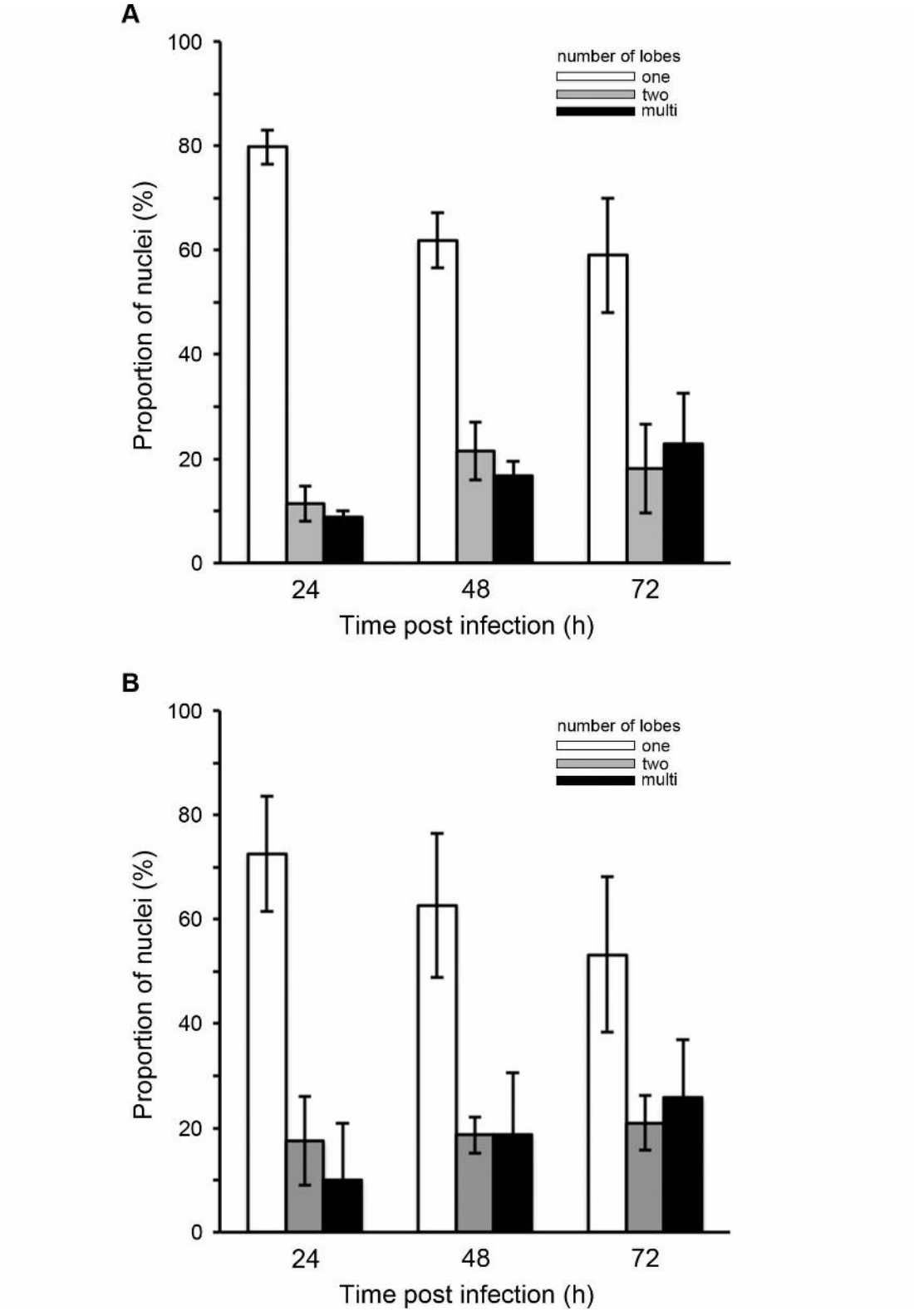

Figure 4.20. Lobulation of nuclei in *Chlamydia*-infected WT mouse embryonic fibroblasts (MEFs) is similar to *LMNA*-/- MEFs. (A) WT or (B) *LMNA*$^{-/-}$ MEFs were infected with *C. trachomatis* LGV2, fixed at the indicated time post infection and stained with mAb414 primary antibody and an AlexaFluor® 488-conjugated secondary antibody to visualise the nuclear envelope. Maximum projections of nuclei (n=100) at each time point were scored for the number of lobes according to previously defined parameters (Methods 2.8.1). White bars: single lobed, grey bars: bi-lobed, black bars: multi-lobed. Error bars show standard deviation.

4.9 *Chlamydia trachomatis* replicates faster in cells lacking lamin A/C

The experiments shown previously have demonstrated that lamin A/C is required for the enrichment of heterochromatin and depletion of NPCs observed during infection with *C. trachomatis* at the inclusion-proximal face of the nucleus (Figs 4.17-4.19). From scoring the frequency of NE modifications following penicillin G-killing of the bacteria, it was concluded that *C. trachomatis* specifically induces the enrichment of lamin A/C in a patch of the NE adjacent to the inclusion, likely through translocated effectors (Fig 4.4). Indeed, the lamin A/C patch occurs in 72.1 ± 11.5% of cells infected with *C. trachomatis* for 72 hours (Fig 3.9). Thus, formation of the lamin A/C patch and the subsequent effects on the NPCs and heterochromatin may be important for the chlamydial lifecycle. To investigate this, the size and shape of inclusions was measured in WT or *LMNA*$^{-/-}$ MEFs infected with *C. trachomatis* LGV2.

Maximum projections of *C. trachomatis*-infected cells were used to measure the roundness of inclusions or contour ratio. The data showed the contour ratio of inclusions in *LMNA*$^{-/-}$ MEFs was not significantly different than that of WT MEFs (Fig 4.21A), indicating inclusion shape does not change. Inclusion size was measured by automated reconstruction of the inclusion volume using the entire z-stack (Methods 2.8.5). Measurements of inclusion size were unsuccessful at 72 hpi, as it was not possible for the macro to differentiate between fluorescence at the inclusion periphery and fluorescence of EBs released from lysed cells. Nevertheless, the data showed inclusions in *LMNA*$^{-/-}$ MEFs were significantly larger than those of WT MEFs, with the difference being greatest at 48 hpi (Fig 4.21B). Taken together, these data suggest that inclusions are larger in cells lacking lamin A/C.

The increase in inclusion size in *LMNA*$^{-/-}$ MEFs may result in an increase in the number of infectious progeny produced during *C. trachomatis* infection. To investigate this, the number of EBs in *Chlamydia*-infected WT and *LMNA*$^{-/-}$ MEFs can be quantified by collecting bacteria at the time point of interest, infecting a second monolayer of cells and scoring the number of inclusions. The proportion of inclusions observed is then used to calculate the number of inclusion forming units (Methods 2.3.2). First, inclusion formation of *C. trachomatis* in WT and *LMNA*$^{-/-}$ MEFs was assessed to ensure any alterations in IFUs measured are not due to differences during chlamydial entry and early development up to 24 hpi (Fig 4.22A). No

significant difference occurred, and so bacteria infect both the WT and *LMNA*$^{-/-}$ MEFs equally. Subsequently, IFUs were recovered from the cell layer and growth media of *Chlamydia*-infected WT and *LMNA*$^{-/-}$ MEFs and quantified (Fig 4.22B and C). At 48 and 72 hpi, significantly more inclusions were formed from both the cell layer and the growth media collected from the *LMNA*$^{-/-}$ MEFs compared to the WT MEFs. Thus, ~7 fold at 48 hpi and ~6 fold at 72 hpi more bacterial progeny are produced when *Chlamydia* infects *LMNA*$^{-/-}$ cells. These data suggest *C. trachomatis* replicates faster in cells lacking lamin A/C.

Figure 4.21. Inclusion size, but not shape, is significantly altered in *LMNA*-/- mouse embryonic fibroblasts (MEFs). WT (white) or *LMNA*$^{-/-}$ (black) MEFs were infected with *C. trachomatis* LGV2, fixed at the indicated time post infection and double stained with anti-*Chlamydia* primary antibody and an AlexaFluor® 488-conjugated secondary antibody to visualise infected cells and DRAQ-5 to visualise DNA. (A) Inclusion roundness (or contour ratio, 4π x area/perimeter^2) was measured from maximum projections of inclusions (n=40). (B) Inclusion size was measured by automated reconstruction of the inclusion volume using the entire z-stack (Methods 2.8.5). Error bars show standard deviation (***$p<0.01$ using Student's t-test as indicated).

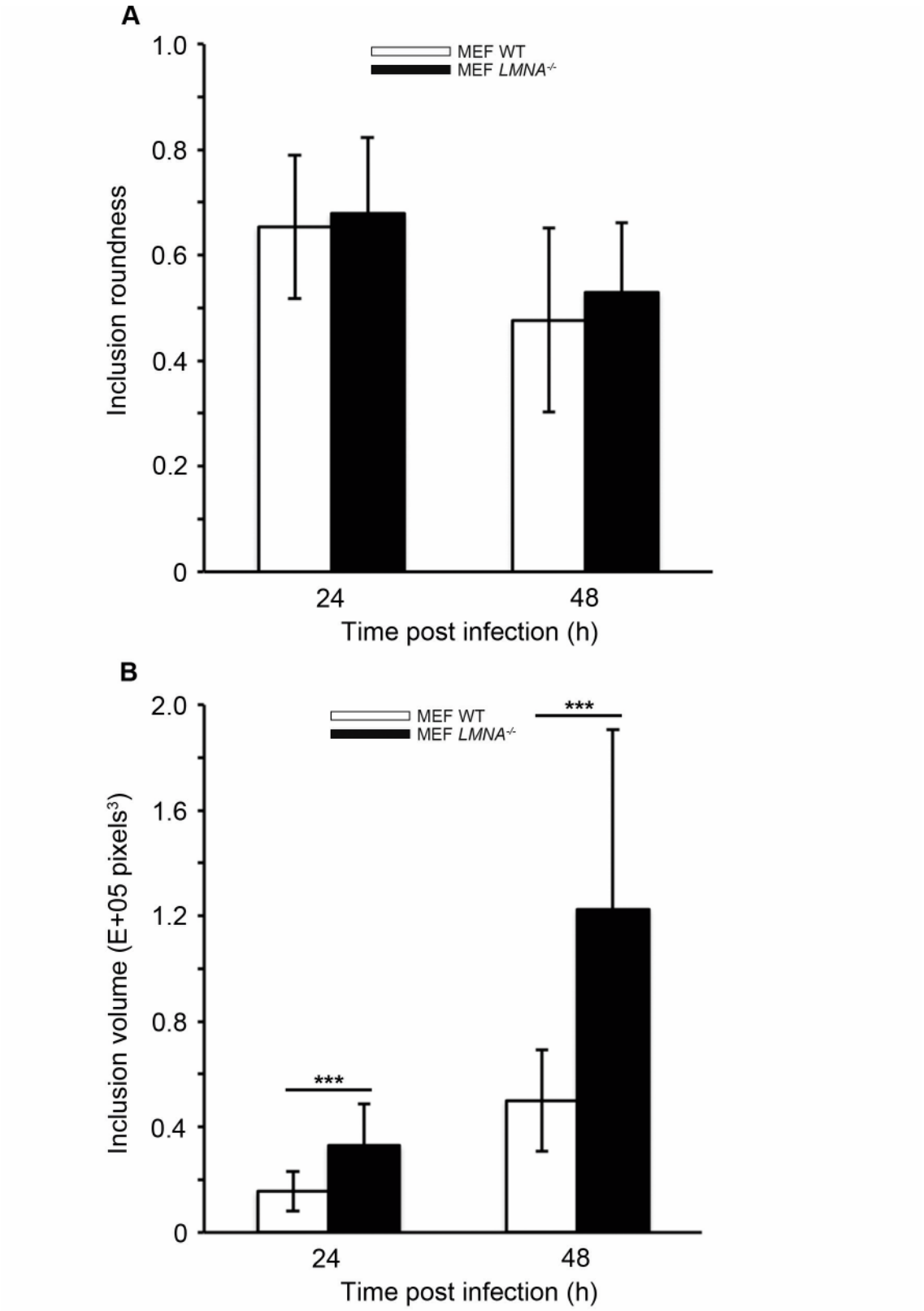
A
MEF WT
MEF LMNA-/-
Inclusion roundness
1.0
0.8
0.6
0.4
0.2
0
24
48
Time post infection (h)
B
MEF WT
MEF LMNA-/-
***
***
Inclusion volume (E+05 pixels3)
2.0
1.6
1.2
0.8
0.4
0
24
48
Time post infection (h)

Figure 4.22. Increased bacterial progeny are produced from *LMNA-/-* mouse embryonic fibroblasts (MEFs) compared to WT MEFs. (A) WT (white) or *LMNA*$^{-/-}$ (black) MEFs were infected with *C. trachomatis* LGV2, fixed at 24 hours post infection (hpi) and double stained with anti-*Chlamydia* primary antibody and an AlexaFluor® 488-conjugated secondary antibody to visualise infected cells and DRAQ-5 to visualise DNA. The number of inclusions was scored across 6 fields of view (n=300 cells) in duplicate and compared to the number of nuclei to determine the proportion of infected cells. (B) Cell layers or (C) growth medium collected at 48 or 72 hpi were lysed and diluted in fresh medium to infect a new layer of HeLa cells (Methods 2.9). After 24 hours, cells were fixed and labelled for *Chlamydia* and DNA. Inclusion-forming units (IFUs) were then quantified (IFU/ml). Error bars show standard deviation (***p<0.01 using Student's t-test as indicated).

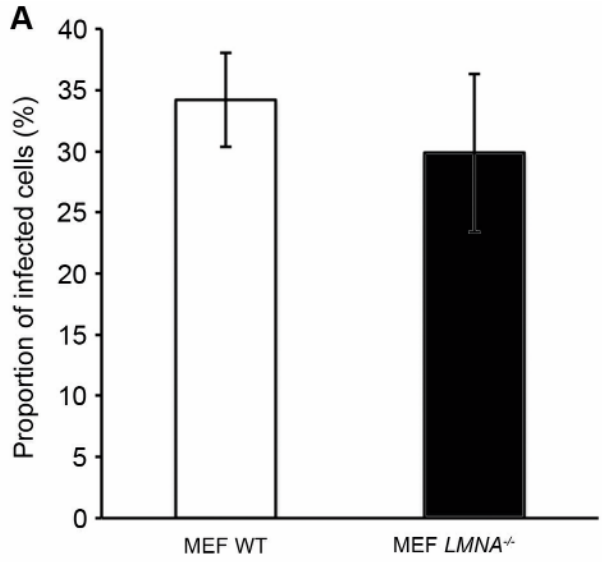
A
Proportion of infected cells (%)
40
35
30
25
20
15
10
5
0
MEF WT
MEF LMNA-/-

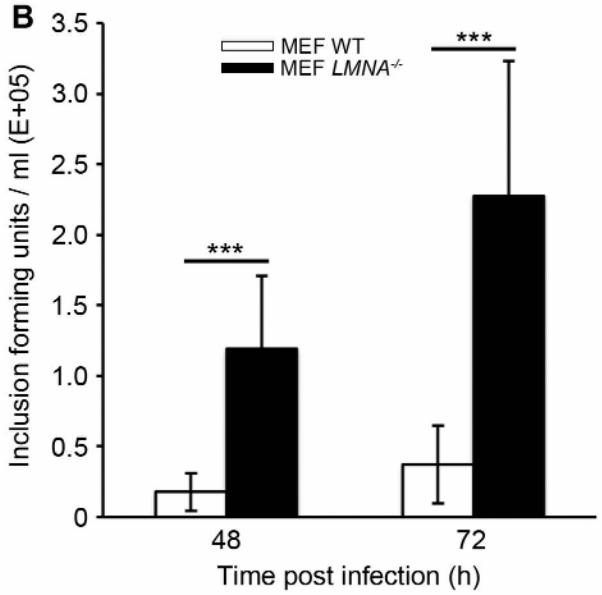
B
Inclusion forming units / ml (E+05)
3.5
3.0
2.5
2.0
1.5
1.0
0.5
0
MEF WT
MEF LMNA-/-
***
***
48
72
Time post infection (h)

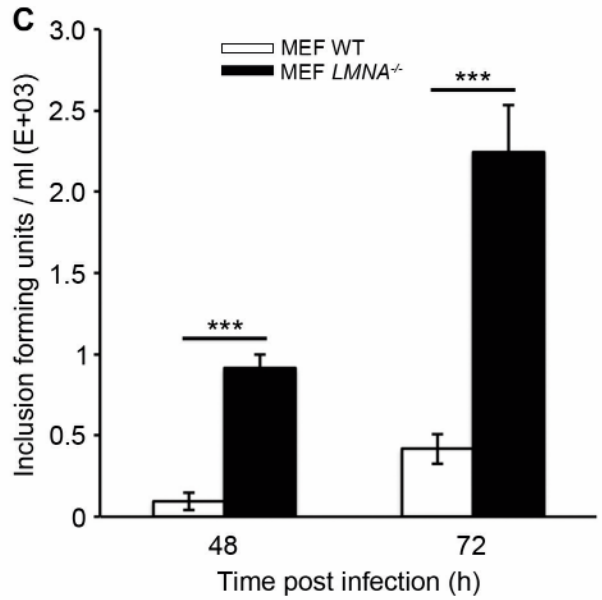
C
Inclusion forming units / ml (E+03)
3.0
2.5
2.0
1.5
1
0.5
0
MEF WT
MEF LMNA-/-
***
***
48
72
Time post infection (h)

4.10 Discussion

The data presented in this chapter establish that infection by *C. trachomatis* drives increased lobulation of nuclei, NPC depletion and heterochromatin reorganisation (Figs 4.13, 4.14 and 4.20) in a lamin A/C dependent manner (Figs 4.17-4.19). Although nuclear mRNA levels do not change during infection with *Chlamydia* (Figs 4.9 and 4.10), nuclear transport is absent proximal to the inclusion (Fig 4.7). The dimensions of the lamin A/C patch and NPC gap are independent of physical pressure on the nucleus (Fig 4.1), and the NE modifications are induced by bacterial factors (Figs 4.2, 4.3 and 4.4) and are repaired following inclusion clearance (Fig 4.5). Finally, the *Chlamydia* inclusion is larger and more progeny are produced when lamin A/C is depleted (Figs 4.21 and 4.22).

The mechanism by which *Chlamydia* simultaneously induces the lamin A/C patch whilst depleting lamin A/C from the remainder of the NL remains unknown, but the dual nature of these effects suggest multiple pathways or bacterial effectors will be necessary. The frequency of NE modifications was reduced to levels similar to that of non-infected cells following penicillin G-killing of the bacteria at 3 and 24 hpi (Fig 4.4), suggesting a bacterial effector is released after 24 hpi. Notably, expression of NUE, a *Chlamydia* effector targeted to the nucleus with histone methyltransferase activity, peaks at 24-40 hpi (Belland et al., 2003). Viable bacteria are required to maintain the NE changes, as there is an immediate reduction in the frequency of lamin A/C patches and NPC gaps following bacterial killing at 48 hpi (Fig 4.4), and NPC gap frequency returns to levels observed in control cells within 24 hours of inclusion clearance (Fig 4.5). This time frame correlates with the time taken for HeLa cells to complete the cell cycle, indicating the NE may be being repaired following reassembly after mitosis. Immunoprecipitation experiments were attempted to determine whether any *Chlamydia* effector or effectors could be detected interacting with lamin A/C, and also to determine whether lamin A/C interacts with additional host proteins during infection. However, extraction of lamin A from the cell lysate was unsuccessful, and so modifications to the immunoprecipitation protocol may be required before these experiments can be completed.

Following confirmation that the phenotypes observed during *Chlamydia* infection are bacterially driven, the major focus of this chapter was to determine the functional implications of the NE changes during *Chlamydia* infection. Host nucleocytoplasmic transport does not occur proximal to the inclusion (Fig 4.7), agreeing with previous observations that suggested

NPCs are entirely removed from this region. The lack of importin-β in regions where there are no NPCs indicates that the NTR must 'sense' NPCs through which it can traverse, rather than aggregate across the entire nuclear periphery. mEos2-importinβ can be photo-converted using a 405 nm laser to emit red fluorescence rather than green, and therefore could be used to study whether NPC transport is affected elsewhere in the NE by monitoring the half-life of red molecules at the NE. If transport is faster, the time taken for red molecules to be imported into the nucleus and replaced at the NE by green molecules will be reduced (Lowe et al., 2015). Using this experimental model, it can therefore be determined whether the cell compensates for a significant region of the NE becoming impermeable during chlamydial infection. From the FISH experiments, one can conclude that the cell can compensate, as there were no detectable changes to the global cellular nuclear poly(A) mRNA levels during infection (Fig 4.10). This suggests the local abrogation of nucleocytoplasmic transport proximal to the inclusion does not affect the overall distribution of mRNA, and that there is no block in mRNA export such as that reported during poliovirus infection (Castelló et al., 2009).

Following these experiments into the impact of depletion of NPCs, the potential consequences of the lamin A/C patch were investigated. H3K9me3, a marker for heterochromatin, was observed enriched towards the inclusion-proximal face of the nucleus, in close proximity to the lamin A/C patch, and depleted around the remainder of the nuclear periphery (Figs 4.13 and 4.14). At this stage, it is unknown whether this enrichment represents a redistribution of existing heterochromatin, or whether chromatin is being condensed proximal to the inclusion to the heterochromatin state and de-condensed elsewhere around the nuclear periphery. If the former, this would necessitate a reorganisation of chromosome territories within the nucleus which would not necessarily indicate a change in gene expression. However, if the latter, then the accessibility of transcription factors to genes proximal to the inclusion would be limited, which would reduce expression of genes in this region. Given that lamin A/C is required for these changes (Fig 4.18), it is more likely that *Chlamydia* utilises the chromatin tethering functions of lamin A/C as a means to reorganise chromatin distribution close to its intracellular niche. Indeed, as the nuclear basket proteins of NPCs are important in preventing the spread of heterochromatin (Shinkura and Forrester, 2002), one might hypothesise NPCs must be removed in this region for heterochromatin to be so highly enriched, as is observed. The accumulation of heterochromatin further distinguishes the *Chlamydia*-induced nuclear envelope changes from those observed in HGPS cells, where the increased thickness of the NL due to incorporation of LAΔ50 results in a loss of a peripheral heterochromatin (Goldman et al., 2004).

One of the most interesting avenues of research arising out of these observations of heterochromatin distribution during infection is to identify genes residing in this transcriptionally repressive region of chromatin. FISH could be used to investigate this, possibly by studying the positioning of chromosome territories to determine whether specific chromosomes are redistributed into this region. Further questions exist in the increased size of the inclusion and increased production of infectious progeny in cells lacking lamin A/C (Fig 4.22). Firstly, why does *Chlamydia* construct or stabilise this patch of lamin A/C with subsequent alterations to NPC and heterochromatin distribution, when simply depleting lamin A/C entirely allows the bacteria to replicate in much greater numbers? *Chlamydia* is clearly capable of depleting lamin A/C, as both immunofluorescence and immunoblotting experiments presented in chapter 3 show total levels of lamin A/C are reduced late in infection. It could therefore be concluded that *Chlamydia* may be sacrificing increased replication to control other factors, for example, genes related to the immune response may be located in the heterochromatin enriched region. Secondly, how does the lack of lamin A/C lead to a larger inclusion and so increase bacterial replication? Lamin A/C contributes to the shape and stiffness of the nucleus, therefore nuclei lacking lamin A/C may be more flexible. This could allow the inclusion to expand into and displace the nucleus to a greater degree, and so increase the space available within the inclusion for the bacteria to replicate. It would be interesting to study the effect of the opposite phenotype, enrichment of lamin A/C, on *Chlamydia* infection and whether this results in reduced inclusion size and bacterial replication.

Chapter 5 – Identification of chlamydial proteins that are targeted to and interact with the host nucleus

5.1 Introduction

The experiments presented thus far have focused on identifying changes to the host nucleus following *Chlamydia* infection. However, the bacterial proteins responsible for the changes described in chapters 3 and 4 remain unknown. NUE, a SET-domain containing protein with histone methyltransferase activity targeted to the nucleus (Pennini et al., 2010), is a candidate for interacting with heterochromatin, but further effectors are likely required to mediate other changes such as the simultaneous enrichment and depletion of lamin A/C from different regions of the NE. Major advances have been made over the course of this work in tools for the genetic modification of *Chlamydia* (Wang et al., 2011; Ding et al., 2013; Agaisse and Derré, 2014; Bauler and Hackstadt, 2014). However, as these tools are only now becoming widely available, it is particularly important to first gather as much information as possible about potential effector proteins to guide future experiments. Therefore, a computational approach was adopted to narrow the list of potential *Chlamydia* effector proteins that may be interacting with components of the host nucleus.

Many pathogens, including *Chlamydia*, utilise molecular mimicry to host proteins to interfere with and subvert host biological processes. This mimicry can occur on a predominantly functional level, whereby bacterial effectors develop distinct folds with no sequence similarity to eukaryotic proteins, yet have molecular surfaces that mirror host protein surfaces and so functionally mimic host processes (Stebbins and Galan, 2001). For example, *Salmonella* SptP induces hydrolysis of GTP to inhibit Rac1 and Cdc42 signalling, mimicking the function of host GTPase activating proteins to restore normal cytoskeletal architecture following bacterial internalisation (Fu and Galán, 1999; Stebbins and Galán, 2000). Alternatively, pathogen molecular mimicry can occur on a more structural level, whereby bacterial effectors adopt eukaryotic folds. For example, the chlamydial protein IncA is proposed to use structural mimicry to the SNARE motif, a eukaryotic motif involved in vesicle fusion, to aid in the fusion of *C. trachomatis*-containing vesicles in cells infected with multiple EBs (Delevoye et al., 2008). Furthermore, NUE contains a SET domain, a 130-residue domain found in eukaryotic histone methyltransferases (Pennini et al., 2010). In this chapter, the hypothesis that structural

mimicry of eukaryotic folds by pathogens could be exploited to identify new *Chlamydia* effectors that may be structural homologues of host nuclear proteins was explored.

Remote protein homology detection servers such as HHpred predict homologous structures from proteins that share less than 20% primary sequence similarity with the target (Söding et al., 2005). This is particularly important for *C. trachomatis*, since at the time of publication of the genome sequence it was reported 28% of predicted proteins have no similarity to any other sequences deposited in GenBank (Stephens et al., 1998), probably due to the evolutionary distance of the *Chlamydiaceae* from other pathogens (Stephens et al., 1998; Clarke, 2011). HHpred can detect such remote homologues by creating and comparing hidden Markov models (HMM) of sequence profiles (Söding, 2005). HMMs are statistical models that consider all possible combinations of matches, mismatches and gaps to generate an alignment of a set of sequences (Mount, 2004). Thus information, such as amino acid frequencies at certain positions and position-specific probabilities for insertions and deletions can be incorporated into the prediction (Söding, 2004; Söding et al., 2005). Additionally, HHpred incorporates the prediction of secondary structure elements (SSEs) into the alignment algorithms, allowing the detection of structural homologues from even more remote sequences.

It is also important when considering potential *Chlamydia* effectors to identify whether the proteins are translocated into the host cell and are therefore capable of acting as effectors. *Chlamydia* utilise both type II and type III secretion systems to translocate effectors into the host cell. Computational prediction can be used as a first step to determine whether proteins are likely to be secreted by either of these systems. T2S substrates of Gram negative bacteria contain an N-terminal signal peptide for delivery to the general secretory pathway or twin-arginine translocation (Tat) system machinery to allow translocation across the cytoplasmic membrane into the periplasmic space (Voulhoux et al., 2001; Filloux, 2004). However, the exact signal by which these substrates are then targeted to the T2S system is unknown, although protein folding is required suggesting the signal may be conformation dependent (Voulhoux et al., 2000; Korotkov et al., 2012). For the prediction of T3S substrates, numerous features are taken into account in addition to the N-terminal sequence, including position-specific amino acid composition profiles and the C-terminal sequence, which is required for secretion of some T3S effectors such as *Salmonella* SipC (Chang et al., 2005; Arnold et al., 2009; Wang et al., 2011; Dong et al., 2015).

The aim of this chapter is to use remote protein homology detection and structure prediction approaches in combination with available secretion prediction algorithms to identify *Chlamydia* effector proteins that may be targeted to or interact with the host nucleus, and so may be candidates for contributing to the nuclear reorganisation reported in the previous chapters.

5.2 Remote sequence homology and fold recognition reveals *Chlamydia* encodes proteins that are possible structural mimics of host nucleoporins and nuclear transport receptors

Whilst the *Chlamydia* effector protein NUE is targeted to the nucleus, the nuclear localisation signal is atypical (Pennini et al., 2010), and so exactly how NUE enters the host nucleus remains unknown. One possibility is that *Chlamydia* secretes proteins capable of mimicking the nuclear transport receptors (NTRs) such as importin-β, which transport cargo into the nucleus (Pemberton and Paschal, 2005). NTRs share a common fold, an α-solenoid, which consists of many repeats of α-helices packed together to form an elongated super-helix or 'solenoid' (Kobe and Kajava, 2000). Various repeat motifs in α-solenoids have been defined, including Armadillo (ARM), HEAT and ankyrin repeats, which differ subtly in their helical arrangement (Andrade et al., 2001; Mosavi et al., 2004). For example, the ARM repeat consists of three helices, whilst the ankyrin repeat consists of two α-helices separated by long loop regions (Kobe and Kajava, 2000). In NTRs, the α-solenoid fold provides a large surface area for protein-protein interactions (Andrade et al., 2001). However, the α-solenoid fold is not unique to NTRs. For example, the scaffold A subunit of protein phosphatase 2A, a serine/threonine phosphatase which regulates the function of many proteins including Akt, p53 and c-Myc, is a HEAT repeat-containing α-solenoid (Seshacharyulu et al., 2013). Furthermore, structural NPC components share the α-solenoid fold, in this case conferring flexibility to the pore to allow expansion during transport of large cargo (Andrade et al., 2001; Devos et al., 2006). Given that NPCs are depleted in the NE proximal to the inclusion, it could be speculated that *Chlamydia* could encode α-solenoid effectors that mimic the NPCs to form 'chlamydial' pores in this region of the NE, allowing efficient transport of chlamydial effectors into the nucleus. Remarkably, a predicted α-solenoid protein is targeted to the host nucleus during infection with the obligate intracellular bacteria *Anaplasma phagocytophilum*, which infects neutrophils (Caturegli et al., 2000). The AnkA protein contains 11 ankyrin repeat domains which is predicted to confer an α-solenoid fold, and can bind DNA and nuclear proteins with likely

effects on host gene expression (Park et al., 2004). Thus, attempts were made to identify *Chlamydia* proteins containing an α-solenoid fold.

HHblits is a prediction software for the identification of remote sequence homology (Remmert et al., 2011). In brief, HHblits first converts the query sequence, or multiple sequence alignment (MSA), to an HMM profile sequence (as described in section 5.1). It then searches an HMM database, created by clustering all homologous sequences from the UniProt database with a minimum pairwise sequence identity of 20% (Hauser et al., 2013), for other HMMs below a threshold expect value (E-value), the number of hits one can expect to detect by chance for a given database size. These HMMs are then added to and merged with the query HMM sequence and this new HMM profile is used for the next iteration. Iterations repeat until the specified number of cycles or until no new hits are found, at which point the resulting identified proteins are displayed. However, when α-solenoid containing Nups such as Nup85 and Nup107, or NTRs such as importin-β and importin-α are input into HHblits, no *Chlamydia* proteins were identified despite identification of 10,000 homologous sequences.

Given this initial result, an alternative approach was undertaken. Members of the *Planctomycetes-Verrucomicrobia-Chlamydiae* (PVC) superphylum (excluding the *Chlamydiae*) express 'membrane coat-like' (MC) proteins which consist of an α-solenoid followed by a β-propeller fold (Santarella-Mellwig et al., 2010). These MC proteins are found in all eukaryotes, and two Nups adopt this fold, Nup133 and Nup160 (Devos et al., 2004). In bacteria of the PVC superphylum, MC proteins are controversially proposed to allow a compartmentalised cell plan, and as such these bacteria have been suggested to reflect an intermediary in eukaryogenesis (Santarella-Mellwig et al., 2010; McInerney et al., 2011; Devos, 2012). Importantly, as these are prokaryotic proteins, they may have closer sequence homology to *Chlamydia* proteins than the eukaryotic α-solenoids searched such as Nup85 and importin-β, and so may reveal *Chlamydia* proteins with similar folds. Thus, amino acid sequences of all MC proteins of PVC superphylum species detected by Santarella-Mellwig et al. (2010) (Appendix 5.1) were input into HHblits to detect *Chlamydia* proteins. A subset of these proteins is listed in Table 5.1.

From the 47 MC proteins input into HHblits, six proteins from *C. trachomatis* were identified (Table 5.2). Of these hits, three proteins were identified multiple times, CT234, CT350 and CT384. The highest probability identification (90.91%) of CT234 was from a hypothetical *Planctomyces maris* protein. The probability score of an identified protein represents the

probability to be a true positive, defined to be either globally homologous or locally similar in structure to the query protein. The highest probability identifications of CT350 (98.40%) and CT384 (96.57%) were from a hypothetical *Blastopirellula marina* protein. The remaining proteins, CT198, CT599 and CT780 were identified with homology to just one of the query sequences, the *Rhodopirellula baltica* protein probable L-sorbosone dehydrogenase, with probabilities of 28.15%, 27.51% and 59.99% respectively. As these probability scores were significantly lower than the other proteins, CT198, CT599 and CT780 were excluded at this stage.

To confirm whether CT234, CT350 and CT384 have α-solenoid folds, amino acid sequences were submitted to the HHpred homology detection and structure prediction server (Table 5.3) (Söding, 2005). HHpred calculates the probability of a template to be a true positive using the same parameters as for HHblits. Both CT350 and CT384 were predicted with 99.8% and 99.91% probability respectively to be structurally homologous to protein phosphatase 2A regulatory subunit A, an α-solenoid protein. CT234 was predicted to have two domains, the N-terminal domain matching a transmembrane protein, the multidrug transporter MDFA, and the C-terminal domain matching an artificial α-solenoid GFP binding protein, bGFP-A. Homology was also detected between the three chlamydial proteins and other α-solenoid proteins, including importin-β, transportin-1 and β-catenin. Additionally, InterPro domain assignments predict CT350, CT384 and the C-terminal domain of CT234 to have an ARM-like helical domain, which occur in α-solenoid structures (Andrade et al., 2001). These data therefore suggest *C. trachomatis* encodes at least three proteins that adopt an α-solenoid fold.

Species	Gene Identifier (IMG database)	Encoded protein name
Verrucomicrobium spinosum	642333382	hypothetical protein
Rhodopirellula baltica	637434028	similar to glucose dehydrogenase-B
Pedosphaera parvula	642472080	hypothetical protein
Planctomyces maris	641112091	hypothetical protein
Lentisphaera araneosa	641131688	hypothetical protein
Gemmata obscuriglobus	642225569	hypothetical protein
Chthoniobacter flavus	642911643	heme-binding protein
Blastopirellula marina	638979470	hypothetical protein

Table 5.1. Subset of membrane coat-like (MC) proteins of the *Planctomycetes-Verrucomicrobia-Chlamydiae* (PVC) superphylum used for remote homology detection. Gene identifiers of genes encoding for MC proteins detected by Santarella-Mellwig et al. (2010) correspond to entries in the Integrated Microbial Genomes & Microbiome Samples (IMG) database, available at https://img.jgi.doe.gov. A full list of MC proteins used for remote homology detection is available in Appendix 5.1.

Protein	Instances identified	IMG gene identifier of best match	Probability (%)	E-value	Sequence identity
CT198	1	637438335	28.15	88	23%
CT234	22	641112478	90.91	0.027	26%
CT350	73	638979470	98.40	1e-09	18%
CT384	62	638979470	96.57	9.3e-05	18%
CT599	1	637438335	27.51	96	23%
CT780	1	637438335	59.99	13	29%

Table 5.2. *Chlamydia* proteins identified by remote sequence homology to bacterial membrane-coat like (MC) proteins. MC proteins identified in Santarella-Mellwig et al. (2010) were input into HHblits. Instances identified refer to the number of times the chlamydial protein was detected as homologous to an MC protein. Gene identifiers correspond to entries in the Integrated Microbial Genomes & Microbiome Samples (IMG) database, available at https://img.jgi.doe.gov. The probability, expect value (E-value) and sequence identity are listed for the best match. The probability of an identified protein to be a true positive (globally homologous or locally similar in structure to the query protein) was calculated by comparing the amino acid distributions between columns from the query protein alignment and columns from the identified protein template alignment together with probabilities for insertions and deletions at each position, position specific gap penalties and secondary structure information. The expect value (E-value) is the expected number of false positives with a higher probability than the identified protein when scanning the database. The sequence identity is the percentage of characters which match exactly between the query and the identified protein.

Protein	Top predicted structure	Probability (%)	E-value	Sequence identity	InterPro Domain assignment
CT234 NTD	Multidrug transporter MdfA	99.85	3.6E-18	11%	Major facilitator superfamily domain
CT234 CTD	bGFP-A/EGFP complex	99.90	1.4E-21	16%	Armadillo-like helical domain
CT350	Protein phosphatase 2A regulatory subunit A	99.80	8.4E-18	14%	Armadillo-like helical domain
CT384	Protein phosphatase 2A regulatory subunit A	99.91	1.9E-21	11%	Armadillo-like helical domain

Table 5.3. Structural predictions of identified chlamydial proteins. Amino acid sequences of CT234, CT350 and CT384 were submitted to HHpred and InterPro. CT234, predicted to contain two domains, was submitted separately for the N-terminal domain (NTD) and C-terminal domain (CTD). The top predicted structures with over 50% coverage of the input sequence are shown. The probability, expect value (E-value) and sequence identity are listed for the best match. The probability of an identified protein to be a true positive (globally homologous or locally similar in structure to the query protein) was calculated by comparing the amino acid distributions between columns from the query protein alignment and columns from the identified protein template alignment together with probabilities for insertions and deletions at each position, position specific gap penalties and secondary structure information. The expect value (E-value) is the expected number of false positives with a higher probability than the identified protein when scanning the database. The sequence identity is the percentage of characters which match exactly between the query and the identified protein. For each sequence, InterPro predicted a single domain.

5.3 Proteome-wide identification of α-solenoid folds using secondary structure prediction

The previous method, although successful in identifying three predicted α-solenoid proteins encoded by *Chlamydia*, is dependent on a degree of sequence homology between the MC proteins and chlamydial proteins. Given this requirement, it is unknown as to whether *Chlamydia* encodes further α-solenoid proteins that are not sufficiently homologous at the level of primary sequence to be detected. Thus, an alternative, broader approach was adopted to determine the entire repertoire of chlamydial α-solenoid proteins. With just 894 coding genes, *C. trachomatis* has a relatively small genome compared to other prokaryotes, more readily allowing whole proteome approaches to catalogue specific protein folds. α-solenoid proteins have a distinct secondary structure sequence, consisting of repeats of ~10-20 α-helical residues separated by ~3-8 coil residues. This repeating pattern can be exploited to identify proteins likely to have this fold in *Chlamydia*.

First, a tool for calculating and visualising the consensus secondary structure prediction sequences of proteins was written using the Python programming language (for code, see Appendix 5.2). The tool creates a consensus SSE sequence from the SSE predictions and confidence values of three available SSE prediction algorithms: Jpred, Psipred and RaptorX (Cuff et al., 1998; McGuffin et al., 2000; Källberg et al., 2012). For each amino acid residue of the protein sequence of interest, the SSE type (helix, strand or coil) and corresponding confidence value (scored from 0-9, with 9 being high confidence) are recorded and summed. The SSE type with the highest confidence value is then selected as the consensus SSE for this position, and the confidence value of this consensus SSE is recalculated by dividing the sum of the confidence values for the SSE type by the maximum confidence value possible, which is 27 (3*9). For example, if Psipred and RaptorX predict an α-helix at a certain position with confidence values of 8 and 7 respectively, whilst Jpred predicts a β-strand with confidence value of 5, the consensus SSE will be an α-helix with a confidence of 15/27. The consensus sequence is then output using the PostScript language to a visual format, where residue type is indicated by colour and confidence is indicated by bar height.

By visualising the consensus SSE sequences of a group of proteins with similar structures, parameters can be devised from the recurring SSE features to filter the chlamydial proteome to identify proteins with similar SSE sequences, such as α-solenoids. The consensus sequence

of the SSE predictions of structural Nups and NTRs are depicted in Figure 5.1. The results showed two distinct SSE patterns corresponding to the domains of human structural NPC proteins described previously (Devos et al., 2006), with proteins forming either a β-propeller fold (Nup37, Nup43, Sec13, Seh1), an α-solenoid fold (Nup85, Nup107), or a combination of both (Nup133, Nup160). Additionally, the NTR importin-β also formed an α-solenoid fold. The α-solenoid fold in the Nups and NTRs was minimally 450 amino acids in length, was comprised of over 90% α-helix or loop SSEs and over 40% α-helix SSEs, and had a minimal uninterrupted sequence of α-helix and/or loop residues of 200 (Fig 5.1). These observations were therefore used as parameters to filter the chlamydial proteome to identify NPC- or NTR-like α-solenoid proteins.

First, each protein sequence of the predicted *C. trachomatis* D/UW-3/CX proteome were analysed by PsiPred, Jpred and RaptorX to acquire SSE predictions (Fig 5.2). The secondary structure consensus tool was then run to determine an SSE consensus for each protein. Using the parameters for the identification of α-solenoids defined previously, the proteome was then filtered to identify all potential α-solenoids proteins. In total, 55 proteins remained from the 894 sequences examined (Appendix 5.3). The SSE predictions of these proteins were then manually curated to remove proteins unable to adopt an α-solenoid that had been detected despite filtering (Fig 5.3). For example, whilst the SSE sequence of CT641 is of sufficient length and composition to meets the previously defined parameters, it is comprised of extensive α-helical regions rather than alternating α-helical and coil repeats characteristic of α-solenoids, and so was excluded (Fig 5.3A). Conversely, the SSE sequence of CT350 consists of alternating α-helical and coil repeats and so was accepted (Fig 5.3B). After curation, just 12 potential α-solenoid proteins remained (Fig 5.3C). These 12 proteins were then submitted to HHpred and InterPro, and only three proteins, CT234, CT350 and CT384, were predicted to contain an α-solenoid fold by both algorithms. The consensus SSE prediction of these proteins is shown in Figure 5.4. All three of these proteins were identified using the previous method, supporting the prediction that they adopt an α-solenoid fold, and suggesting no further α-solenoid proteins are present in the predicted *Chlamydia* proteome.

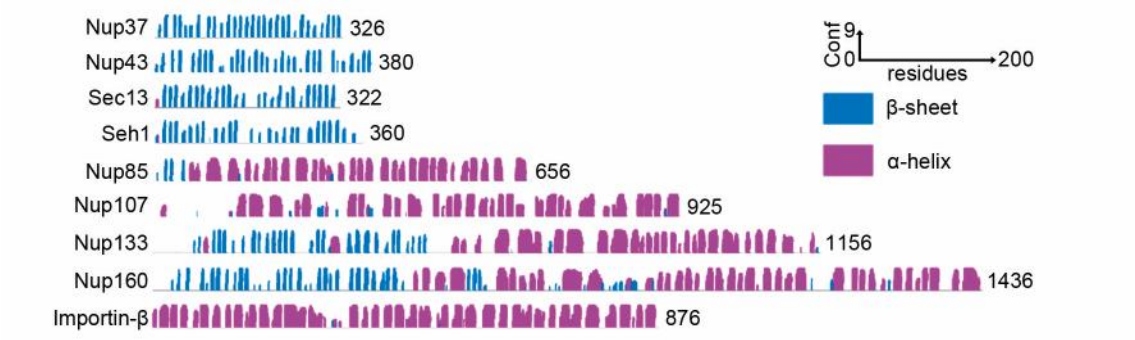

Figure 5.1. Graphical representation of consensus secondary structure sequences of a subset of structural Nups and importin-β. The consensus secondary structure sequence and confidence (bar height) was determined from three prediction algorithms, PsiPred, Jpred and RaptorX. β-sheets are represented in blue, α-helices in pink, whilst coil residues are not shown. Vertical scale bar, confidence (Conf) scored from 0-9. Horizontal scale bar, residue number.

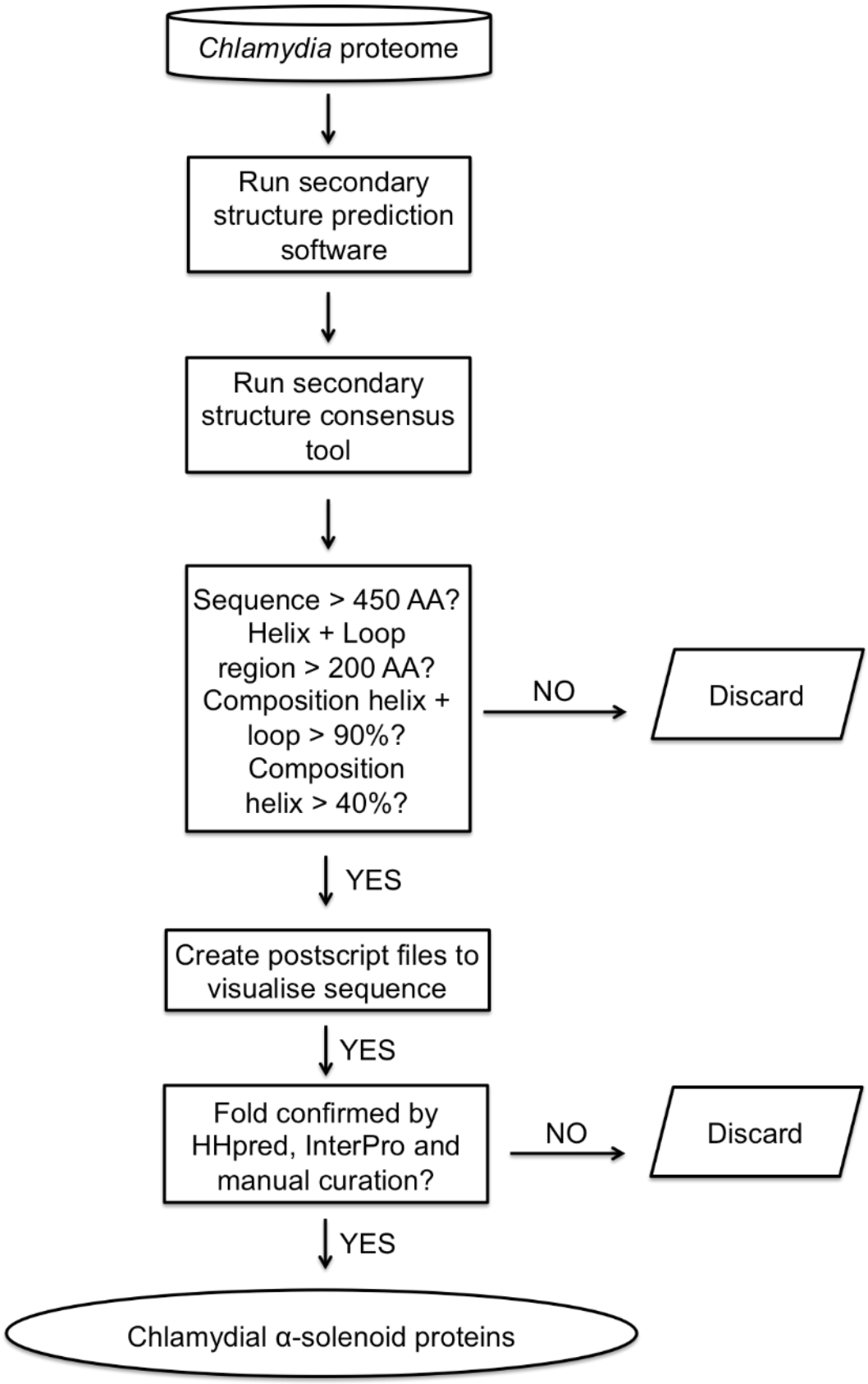

Figure 5.2. Workflow used to identify chlamydial proteins with α-solenoid fold. Parameters for filtering the chlamydial proteome were determined based on the secondary structure sequence of α-solenoids from NPC proteins and NTRs.

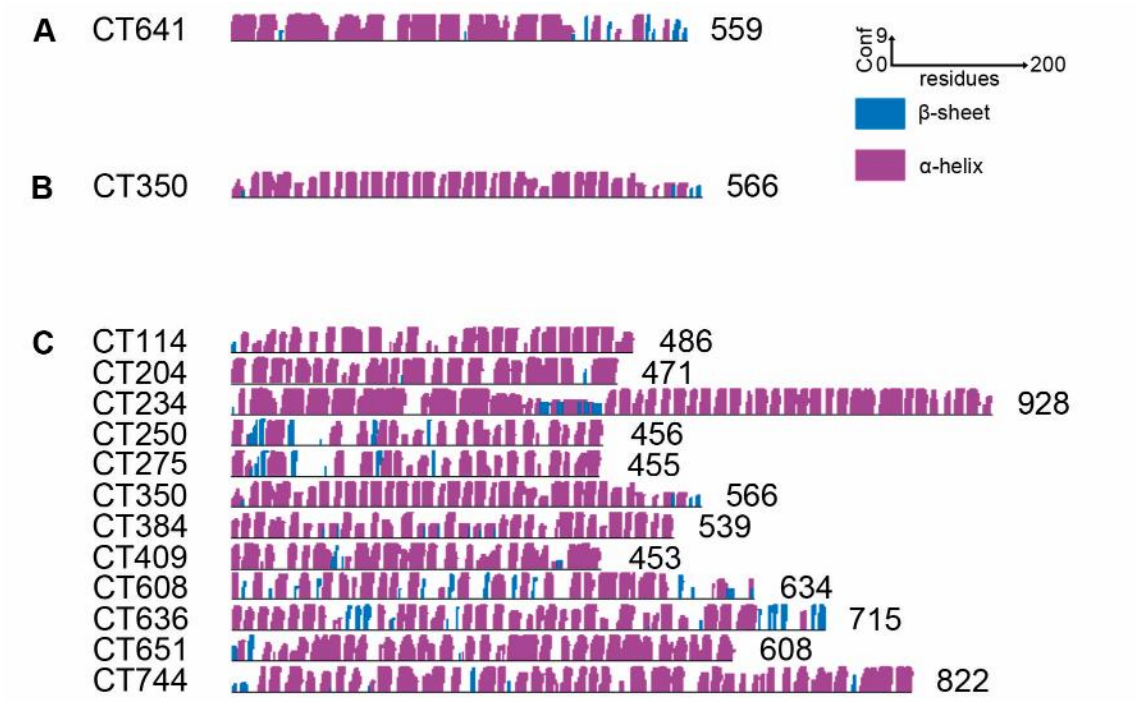

Figure 5.3. Consensus secondary structure sequences of the predicted α-solenoid proteins in the *C. trachomatis* proteome. The consensus secondary structure element (SSE) sequence was determined for each protein in the *C. trachomatis* proteome from three prediction algorithms, PsiPred, Jpred and RaptorX. The SSE sequences were then filtered for proteins with an α-solenoid fold using parameters (as defined in Figure 5.2) devised from analysis of the secondary structure sequence of structural Nups and importin-β. Following filtering, 55 proteins remained (Appendix 5.3). Sequences were then manually curated to remove incorrect hits such as (A) CT641, which is comprised of extensive α-helical regions rather than alternating α-helical and coiled coil repeats characteristic of α-solenoids as in (B) CT350. Following curation, 12 SSE sequences remained, corresponding to the chlamydial proteins in (C). β-sheets are represented in blue, α-helices in pink, whilst coil residues are not shown. Vertical scale bar, confidence (Conf) scored from 0-9. Horizontal scale bar, residue number.

Protein	Top predicted structure (>50% sequence coverage)	Probability (%)	E-value	Sequence identity (%)	InterPro Domain assignment
CT114	No detected structures	-	-	-	C-terminal tetratricopeptide-like helical domain
CT204	NADC family transporter	100.00	7.7E-39	20	Sodium/sulphate symporter
CT234 NTD	Multidrug transporter MdfA	99.85	3.6E-18	11	Major facilitator superfamily domain
CT234 CTD	bGFP-A/EGFP complex	99.90	1.4E-21	16	Armadillo-like helical domain
CT250	Chromosomal replication initiator protein DNAA	100.00	8.3E-52	25	P-loop containing nucleoside triphosphate hydrolase
CT275	Chromosomal replication initiator protein DNAA	100.00	3.1E-50	32	P-loop containing nucleoside triphosphate hydrolase
CT350	Protein phosphatase 2A regulatory subunit A	99.80	8.4E-18	14	Armadillo-like helical domain
CT384	Protein phosphatase 2A regulatory subunit A	99.91	1.9E-21	11	Armadillo-like helical domain
CT409	Arginine/agmatine antiporter	99.96	2.4E-27	14	Sodium/alanine symporter
CT608	DNA helicase II	100.00	2.4E-73	38	P-loop containing nucleoside triphosphate hydrolase
CT636	No detected structures	-	-	-	No detected domains
CT651	Cell division cycle protein 16 homolog	100.00	7.9E-30	10	No detected domains
CT744	Pre-mRNA-processing factor 6	99.97	1.7E-25	11	No detected domains

Table 5.4. Structural predictions of predicted chlamydial α-solenoid proteins. Amino acid sequences of chlamydial α-solenoid proteins (Fig 5.3C) were submitted to HHpred and InterPro. CT234, predicted to contain two domains, was submitted separately for the N-terminal domain (NTD) and C-terminal domain (CTD). The top predicted structures with over 50% coverage of the input sequence are shown. The probability, expect value (E-value) and sequence identity are listed for the best match. The probability of an identified protein to be a true positive (globally homologous or locally similar in structure to the query protein) was calculated by comparing the amino acid distributions between columns from the query protein alignment and columns from the identified protein template alignment together with probabilities for insertions and deletions at each position, position specific gap penalties and secondary structure information. The expect value (E-value) is the expected number of false positives with a higher probability than the identified protein when scanning the database. The sequence identity is the percentage of characters which match exactly between the query and the identified protein. The InterPro domains with the great sequence coverage are shown.

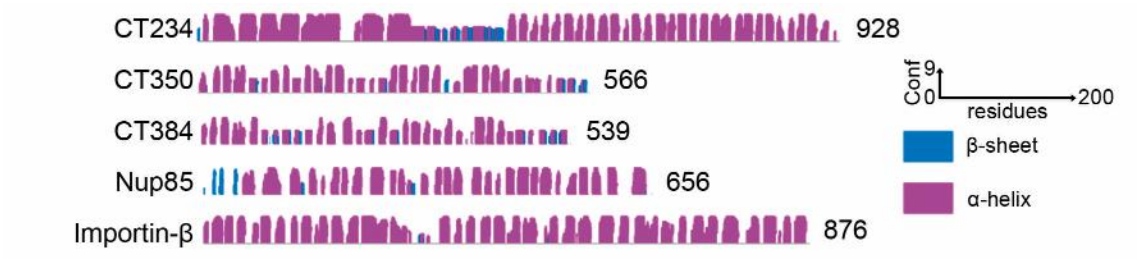

Figure 5.4. Graphical representation of consensus secondary structure sequences of identified chlamydial proteins. The consensus secondary structure sequence and confidence (bar height) was determined from three prediction algorithms, PsiPred, Jpred and RaptorX. β-sheets are represented in blue, α-helices in pink, whilst coil residues are not shown. Nup85 and importin-β are shown for comparison. Vertical scale bar, confidence (Conf) scored from 0-9. Horizontal scale bar, residue number.

5.4 Prediction of bacterial protein secretion

In order for a *Chlamydia* protein to be a bacterial effector, it must first be secreted by the pathogen. *Chlamydia* has two known secretion pathways involved in the translocation of virulence effectors, the type II secretion pathway and the type III secretion pathway.

For T2S, effectors possess an N-terminal signal peptide for translocation across the bacterial cytoplasmic membrane into the periplasmic space via the Sec or Tat pathways, and are subsequently exported by the double-membrane-spanning T2S system (Voulhoux et al., 2001; Filloux, 2004; Costa et al., 2015). SignalP is an algorithm that uses a neural-network based method trained and tested separately on eukaryotes, Gram-positive and Gram-negative bacteria for the prediction of signal peptides from amino acid sequences for translocation into the periplasmic space (Petersen et al., 2011). SignalP can therefore be used to predict chlamydial proteins targeted for secretion via T2S, and is the highest performing N-terminal signal peptide prediction method according to two independent assessments (Choo et al., 2009; Petersen et al., 2011; Sperschneider et al., 2015). SignalP outputs a score between 0 and 1.0, with the authors recommending scores above 0.45 as indicating sufficient selectivity and sensitivity for a positive prediction (Petersen et al., 2011).

For type III secretion, five algorithms exist for the prediction of secretion, EffectiveT3 (Arnold et al., 2009), ANN (Löwer and Schneider, 2009), BPBAac (Wang et al., 2011), T3_MM (Wang et al., 2013) and BEAN 2.0 (Dong et al., 2015). EffectiveT3, ANN and BPBAac use machine learning approaches that take into account N-terminal sequence features such as amino acid composition (Aac), frequency of SSEs and G+C content of the primary DNA sequence (Arnold et al., 2009; Löwer and Schneider, 2009; Wang et al., 2011). EffectiveT3 and ANN apply a sliding window approach, varying the start and length of the sequence during the learning and testing procedure, in order to determine the region of the N-terminus to analyse (Arnold et al., 2009; Löwer and Schneider, 2009). EffectiveT3 outputs a probability score from 0 to 1, with 0.95 considered to be the minimum for a positive prediction. ANN uses a threshold as the decision boundary for classification of output as positive or negative for T3S, with values above 0.4 indicating a sufficient true positive to false positive ratio to be predicted as T3S. BPBAac adopts a different approach, identifying distinct position-specific Aac profiles using the first 100 amino acids of the N-terminus (Wang et al., 2011). BPBAac is scored from 0 to 1.0, with the authors suggesting a score of 0.5 as minimal for a positive prediction with selectivity of over 95%

(Wang et al., 2011). T3_MM calculates and compares the absolute composition of each species of amino acid across a 100 amino acid N-terminal region between T3S and non-T3S proteins, and also sequentially calculates and compares the probability of each amino acid at the current position based on the amino acid at the preceding position between T3S and non-T3S proteins (Wang et al., 2013). From these values, a likelihood ratio (R) of a sequence being a T3S or a non T3S protein is determined. A minimal R value of 0 is suggested as a cut-off, at which point proteins are predicted as effectors with 89.6% selectivity and 90.9% sensitivity (Wang et al., 2013). Finally, BEAN 2.0 combines a sequence alignment-based predictor, which searches the training dataset for the most similar sequence to the query, a domain based-predictor, which scans and compares the Pfam domains of the query protein to the Pfam domains of the training dataset, and a machine-learning predictor, which analyses the Aac separately for the N-terminal 2-51 amino acids, 52-121 amino acids and C-terminal 50 amino acids and compares to the training dataset (Dong et al., 2015). Bean 2.0 also recommends a minimal score of 0 as a cut-off for positive prediction of T3S, although the significance of this value was not described (Dong et al., 2015). Independent studies to determine which of these algorithms performs the best with regards to sensitivity and selectivity have not been conducted, therefore all five algorithms were used in parallel.

To determine which of the identified α-solenoid proteins are predicted to possess a signal peptide for translocation through the Sec or Tat pathways, or are likely to be exported by a type III secretion system, amino acid sequences of CT234, CT350 and CT384 (see Appendix 5.4) were analysed using the six prediction algorithms described previously (Table 5.5). CT234 was not predicted by any of the algorithms to be secreted. CT350 was predicted to have a signal peptide for translocation to the bacterial periplasm using SignalP 4.0, and predicted by ANN and BEAN 2.0 to be secreted by T3S. It is unknown whether a protein can be secreted by both the Sec/Tat machinery and T3S systems, but as this has never been reported it is unlikely. CT384 was predicted by EffectiveT3 and ANN to be secreted by T3S. ANN was the only algorithm that predicted both of these proteins to be T3S, with CT384 scoring 0.920 and CT350 scoring 0.430. Whilst neither of these two proteins were predicted to be secreted using BPBAac, both scores were close to the author-suggested cut-off of 0.5 at 0.401 for CT350 and 0.455 for CT384. Additionally, both proteins scored close to the cut-off of 0 when analysed by T3_MM, with CT384 scoring -0.101 and CT350 scoring -0.187. Taken together, these data suggest that CT234 is unlikely to be secreted by *Chlamydia*, whilst both CT350 and CT384 could be chlamydial effector proteins.

Protein	Type II secretion	Type III secretion				
	SignalP 4.0	EffectiveT3 1.0.1	BPBAac	ANN	T3_MM	Bean 2.0
CT234	0.130	0	-0.963	0.040	-0.564	-0.303
CT350	0.676	0	0.401	0.430	-0.187	0.00651
CT384	0.147	0.998	0.455	0.920	-0.101	-0.346

Table 5.5. Prediction of secretion of *C. trachomatis* α-solenoid containing proteins. Cells shaded yellow scored above the author-suggested cut-offs for the algorithm (for a detailed explanation of the scoring method of each algorithm, refer to section 5.4). SignalP 4.0 cut-off = 0.570, EffectiveT3 1.0.1 cut-off = 0.95, BPBAac cut-off = 0.5, ANN cut-off = 0.4, T3_MM cut-off = 0.0, Bean 2.0 cut-off = 0.0.

5.5 CT384-GFP is enriched in the nucleus when expressed in host cells

To determine the localisation of potential effector proteins in bacterial pathogens, antibodies can be raised against the protein of interest to observe protein localisation at endogenous levels. Alternatively, tagged constructs can be used to transform the bacteria and the localisation of the protein observed by immunofluorescence labelling. However, chlamydial proteins typically have poor antigenicity, and genetic tools to transform *Chlamydia* are not yet widely available. To circumvent these issues, the protein of interest can be ectopically expressed as a fusion protein with GFP in the host cell. Although this is more artificial than expression by the bacteria, it is frequently used in the field as an alternative approach for determining initial localisation, and so allowing further functional studies to be conducted.

Mammalian expression vectors encoding for CT350-GFP and CT384-GFP were used to transfect HeLa cells, with vector encoding for GFP alone used as a control. GFP alone was distributed across the cell, with enrichment at the nucleus in some cells, whilst other cells had no nuclear enrichment (Fig 5.5A). Both CT350-GFP and CT384-GFP appeared enriched in the nucleus of transfected cells, and the nucleus in these cells appeared more lobulated and the nucleoli distorted (Fig 5.5B and C). To confirm nuclear enrichment of CT350-GFP and CT384-GFP in transfected cells, fluorescence intensity was quantified in the nucleus and in the cytosol, and the mean nuclear fluorescence intensity relative to cytosolic fluorescence intensity plotted as a histogram (Fig 5.6). For GFP, the ratio of mean nuclear fluorescence to mean cytosolic fluorescence was 1.37 ± 0.41. For CT350-GFP and CT384-GFP, the ratio of mean nuclear fluorescence to mean cytosolic fluorescence was 1.70 ± 0.42 and 2.39 ± 0.54 respectively. The difference in the relative nuclear fluorescence between GFP and CT350-GFP was not statistically significant ($p>0.05$) when the datasets were compared using the Student's t-test, whilst the difference in the relative nuclear fluorescence between GFP and CT384-GFP was statistically significant ($p<0.05$).

Taken together, these data suggest that the remote sequence homology, SSE prediction and fold recognition approaches were successful in identifying chlamydial proteins capable of localisation to the nucleus when expressed in eukaryotic cells. Further experiments to identify which host proteins are interacting with these chlamydial proteins and the localisation of these chlamydial proteins during infection will shed further light on their function.

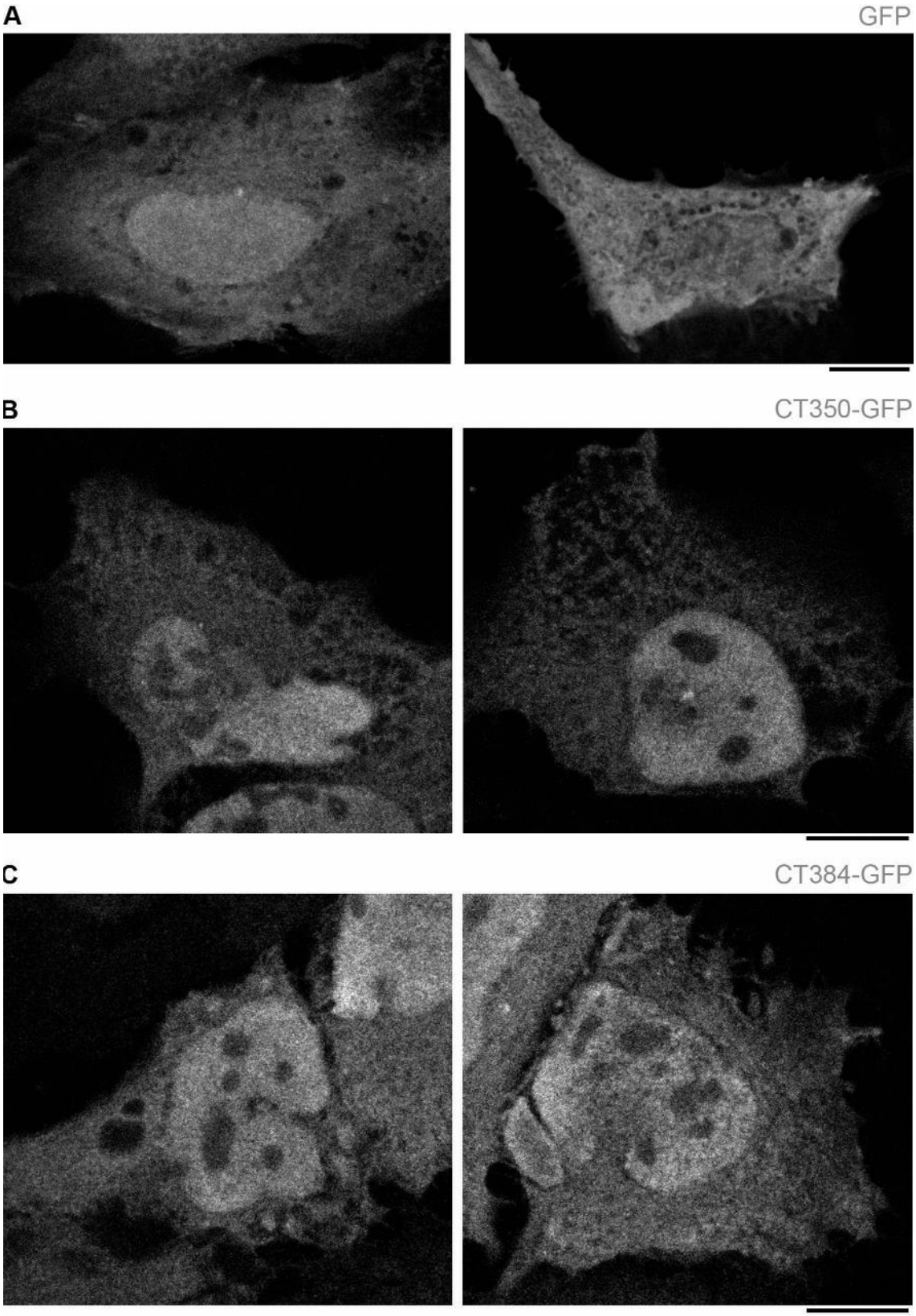

Figure 5.5. Preliminary data suggests chlamydial α-solenoid proteins localise to the nucleus when ectopically expressed in HeLa cells. HeLa cells transiently expressing mammalian expression vector encoding for (A) GFP, (B) CT350-GFP or (C) CT384-GFP were fixed and viewed by confocal microscopy. Scale bars, 10 µm.

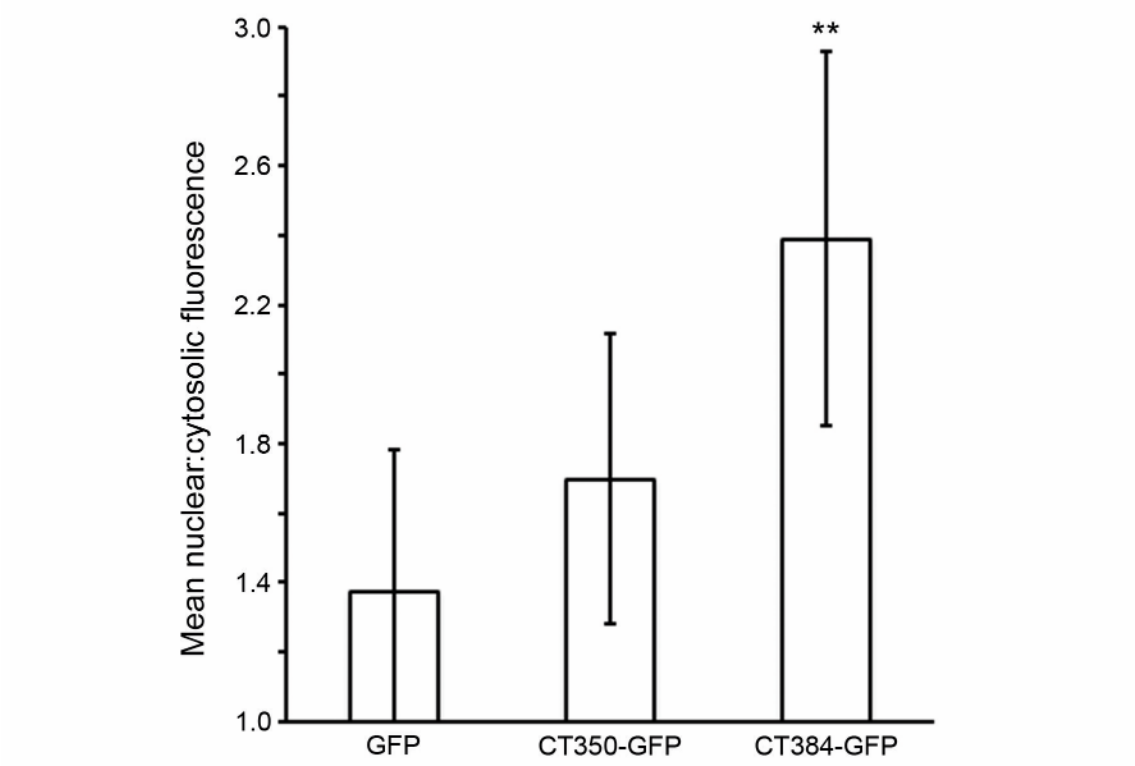

Figure 5.6. CT384-GFP is significantly enriched at the nucleus when ectopically expressed in HeLa cells. HeLa cells transiently expressing GFP, CT350-GFP or CT384-GFP were fixed and viewed by confocal microscopy. Fluorescence intensity of maximum intensity projections of confocal xy-sections was measured in the nucleus and in the cytosol (n=10) of transfected cells, and the mean ratio of nuclear to cytosolic fluorescence signal plotted as a histogram. Error bars show standard deviation (**$p<0.05$ using Student's t-test between GFP and CT350-GFP/CT384-GFP).

5.6 Discussion

In this chapter, computational methods have been used to identify chlamydial proteins structurally similar to structural NPC or NTR proteins that localise to the nucleus when ectopically expressed in host cells. The first of these methods used remote sequence homology and fold recognition (Tables 5.1-5.3), whilst the second used a proteome-wide approach, taking advantage of the common SSE features of structural NPC proteins and NTRs to identify similar folds in proteins encoded by *C. trachomatis* (Figs 5.2-5.4 and Table 5.4). Both methods identified three proteins: CT234, CT350 and CT384. Of these, CT350 and CT384 are predicted to be secreted by the bacteria according to secretion prediction algorithms (Table 5.5).

To confirm whether the prediction of secretion of CT350 and CT384 is correct, and so whether these chlamydial proteins are capable of being effectors, antibodies could be raised against CT350 and CT384 to detect their presence in the host cell during infection. For this approach, purified protein should be produced to immunise a host, serum should be collected and antibodies should be tested. However, as demonstrated by efforts in the Hayward laboratory (Dumoux et al., 2015; McMahon, In preparation), production of purified chlamydial proteins is not a trivial process and requires a significant time investment, therefore an alternative method was adopted. Historically, the secretion of *Chlamydia* effectors has been demonstrated by expressing proteins of interest in *Yersinia enterocolitica*, which encodes a heterologous type III secretion system (Fields and Hackstadt, 2000; Clifton et al., 2004). However, during the course of this work attempts were made to transform *C. trachomatis* using the new genetic tools that became available, as this additionally allows the study of endogenous localisation of target proteins (Wang et al., 2011). These methods were successfully used by Bauler and Hackstadt (2014) to demonstrate the secretion of IncD, an inclusion membrane effector. Other effectors genetically tagged with a FLAG sequence have also been expressed and properly translocated into the host cell (Agaisse and Derré, 2014). In brief, the pTrl2 vector (a kind gift from Professor. Scott Hefty), derived from the endogenous *C. trachomatis* plasmid, was introduced into *C. trachomatis* EBs by transformation in a $CaCl_2$ buffer (Wickstrum et al., 2013). pTrl2 encodes beta-lactamase conferring bacterial resistance to penicillin G. Rounds of antibiotic selection were then performed using increasing concentrations of penicillin G. Successful transformants constitutively express red fluorescent protein, and so are visible by fluorescence microscopy. Expression of the tagged protein of

interest is controlled by a tetracycline repressor, and is inducible by the addition of anhydrotetracycline (Wickstrum et al., 2013). Although *C. trachomatis* LGV2 was successfully transformed in the Hayward laboratory using the original pTRL2 cloning vector, transformation experiments using vector with CT384-3xFLAG inserted at the multiple cloning site were to date unsuccessful. Modifications to the transformation protocol, for example by using lower concentrations of antibiotic during initial rounds of selection, may be used in the future to confirm secretion of the identified proteins.

Whilst localisation of CT384 during chlamydial infection remains to be confirmed, preliminary data suggests CT384-GFP is enriched in the nucleus when ectopically expressed in HeLa cells, and that there is an apparent induction of aberrant nuclear architecture reminiscent of nuclei in *Chlamydia*-infected cells as shown in chapter 3 (Figs 5.5 and 5.6). Further experiments are necessary to examine the impact of expression levels on this nuclear localisation, and quantification of the frequency of aberrant nuclear architecture is required. Nevertheless, experiments to observe the different compartments of the nucleus such as the NE, the nucleoli, the nuclear speckles and heterochromatin in these transfected cells may reveal further insights into CT384 function, and might be linked to the previous investigations in chapters 3 and 4. Should transformation of *Chlamydia* with pTRL2 vector encoding for CT384-3xFLAG be successful, coimmunoprecipitation and mass spectrometry studies could be conducted with *Chlamydia*-infected lysates using antibodies to the FLAG tag to identify which protein or proteins are interacting with CT384. As CT384 is predicted to have an α-solenoid fold that may be mimicking the NTRs, it would be interesting to determine if CT384 interacts with NUE, as the mechanism by which NUE traffics to the nucleus is unknown (Pennini et al., 2010). Similarly, these approaches could be used for other potential effectors such as CT350.

Finally, it would be interesting to apply the bioinformatics approach developed here to determine whether other chlamydial proteins have eukaryotic domains. The remote sequence homology and fold recognition approach used in this work is specific, requiring an intermediate protein to be present in another prokaryote, and so may not be as suitable for such searches. The proteomic approach based on SSE prediction may be more transferable, as it does not require any sequence homology between the query protein and chlamydial proteins for identification. Indeed, during the course of this work a proteomic approach was also used by Fournier et al. (2013) to identify α-solenoid proteins from a broad range of eukaryotic, archaeal and prokaryotic proteomes. In their approach, a neural network was trained on known α-solenoid protein sequences to identify the linker between two α-helices of

a repeat unit, and three such identifications were required to predict a protein sequence as containing an α-solenoid (Fournier et al., 2013). For the *Chlamydiae*, 155 α-solenoids were identified from 103375 protein sequences, a frequency of 0.15% (Fournier et al., 2013). When compared to the 894 ORFs of the *C. trachomatis* genome, a frequency of 0.15% predicts 1.34 α-solenoid-containing proteins, less than the three proteins found in this work predicted to have an α-solenoid fold. These data indicate that *C. trachomatis* may encode a higher than average number of α-solenoid proteins than other members of the *Chlamydiae*. Nevertheless, the analysis by Fournier et al. (2013) supports the predictions of α-solenoid-containing *Chlamydia* proteins presented in this chapter, and validates the use of a broad, proteome-based method. It would be interesting to use the proteomic approach to search for other chlamydial proteins that may mimic eukaryotic folds, such as, for example, the SUN or KASH domains of the LINC proteins in the NE, which are involved in the regulation of nuclear positioning and movement (Burke and Roux, 2009).

Chapter 6 – Discussion

The results presented in this thesis demonstrate a novel and unique interaction between *Chlamydia trachomatis* and the host nucleus. During infection, the nucleus appears polarised with the formation of a specific domain proximal to the inclusion, leading to gross architectural changes to the entire nucleus, whereby the shape of the nuclear envelope (NE) becomes increasingly lobulated (Fig 6.1). Indeed, the NE proximal to the inclusion exhibits an enrichment of lamin A/C, termed a 'lamin A/C patch', whereas the region of the NE distal to the inclusion exhibits depletion of lamin A/C (Figs 3.7-3.10). This lamin A/C patch is coincident with a reduction in lamin B (Figs 3.11 and 3.12) and corresponding depletion of NPCs (termed an 'NPC gap') (Figs 3.14 and 3.15), which is only observed at the inclusion-proximal face of the NE with no additional disruption occurring around the remainder of the NE. These *Chlamydia*-induced NE modifications are distinct from endogenous cellular pore-free islands, as the ER is not excluded from the region closely surrounding them, and no characteristic enrichment in emerin is present (Figs 3.24-3.26) (Maeshima et al., 2006). *C. trachomatis* drives the enrichment of lamin A/C (Figs 4.2-4.4), and the lamin A/C patch was demonstrated to be necessary for the depletion of NPCs by using a *LMNA*$^{-/-}$ cell line (Figs 4.17 and 4.19). Furthermore, these changes in lamin A/C induced a specific enrichment of heterochromatin at the inclusion-proximal face of the nucleus (Figs 4.13-4.15 and 4.18-4.19). This nuclear reorganisation led to an absence of transport at the nuclear-proximal face of the inclusion but failed to discernibly redistribute global cellular mRNA (Figs 4.7 and 4.9-4.10). Finally, chlamydial infection in the absence of lamin A/C permitted increased bacterial replication (Fig 4.22).

Figure 6.1. Summary of the *Chlamydia*-induced modifications to nuclear architecture in infected wild-type and *LMNA*$^{-/-}$ cells. (A) In wild-type (WT) cells infected with *C. trachomatis* LGV2 or *C. trachomatis* A a specific domain is formed proximal to the inclusion, characterised by enriched lamin A/C (red), depletion of NPCs (green) and enrichment of heterochromatin (blue). The inclusion-distal face of the nuclear envelope (black) becomes lobulated. (B) In *LMNA*$^{-/-}$ cells infected with *C. trachomatis* LGV2 a domain of depleted NPCs and enriched heterochromatin is not formed, although the inclusion-distal face of the nuclear envelope remains lobulated. However, the inclusion is larger and more bacterial progeny are produced. EBs: elementary bodies. RBs: reticulate bodies.

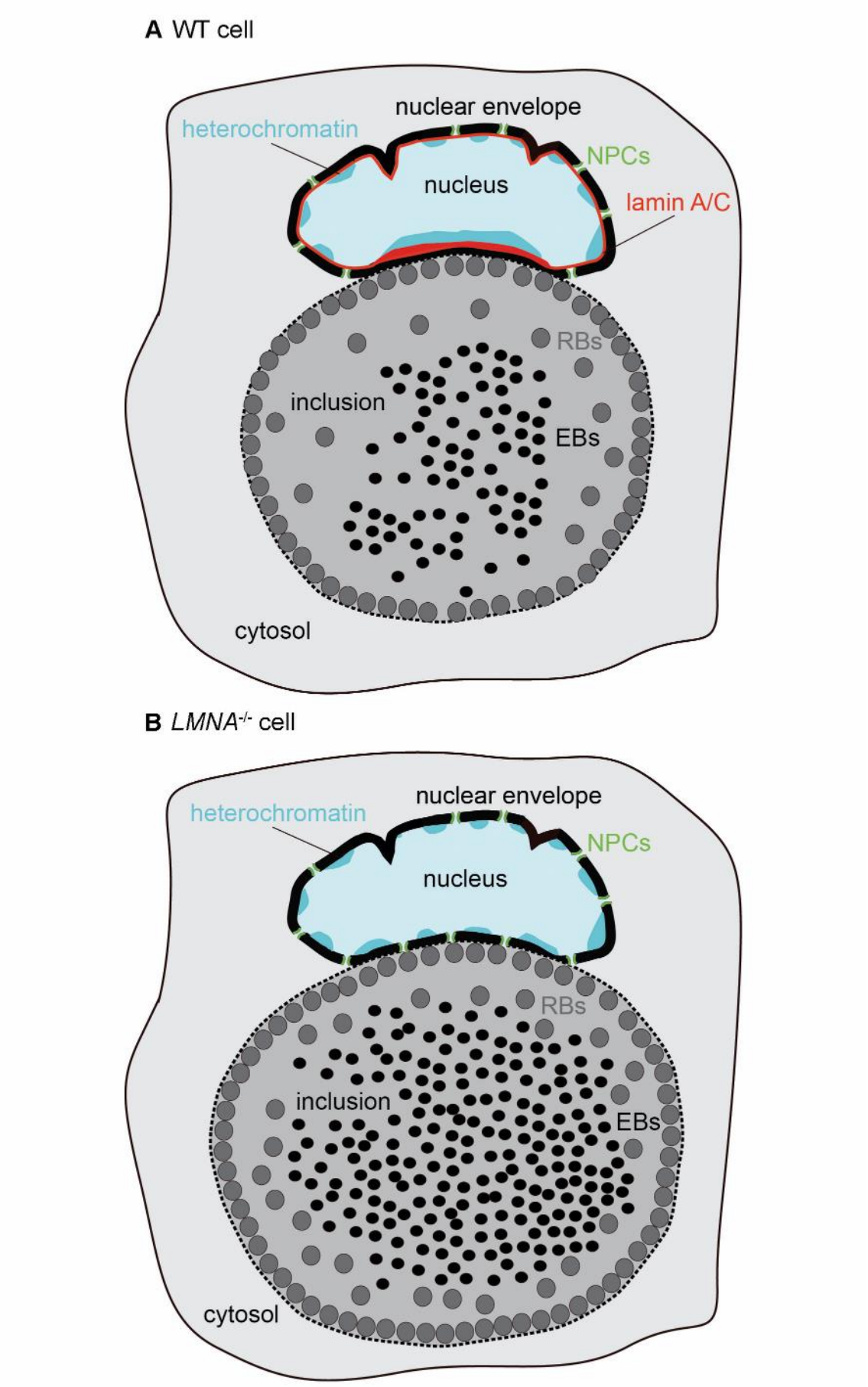
A WT cell
nuclear envelope
heterochromatin
NPCs
nucleus
lamin A/C
RBs
inclusion
EBs
cytosol
B LMNA-/- cell
nuclear envelope
heterochromatin
NPCs
nucleus
RBs
inclusion
EBs
cytosol

The *Chlamydia*-induced alterations involve the depletion of lamin A/C from the inclusion-distal region of the NE, and simultaneous stabilisation or enrichment at the inclusion-proximal face (Figs 3.7-3.10). It is unlikely that a single bacterial effector mediates both depletion and stabilisation of lamin A/C, and so two distinct pathways likely account for these alterations. Lamin A/C is removed from the NE via two cellular processes. Firstly, cyclin dependent kinase 1 (Cdk1) phosphorylates both serine 22 in the head domain and serine 392 in the tail domain of lamin A/C to induce depolymerisation and the consequent disassembly of the NL during mitosis (Heald and McKeon, 1990; Peter et al., 1990). Secondly, caspase-6 is activated during apoptosis and can cleave lamin A/C (Orth et al., 1996; Takahashi et al., 1996). Immunoblotting experiments demonstrated that lamin A and lamin C levels are reduced during infection (Fig 3.10), suggesting lamin A/C is depleted rather than disassembled and rearranged. Caspase-6 is therefore one candidate capable of mediating the depletion of lamin A/C during infection. Caspase-6 can be activated by caspases 1, 3, 7 and 9 (Guo et al., 2006; Inoue et al., 2009; Akpan et al., 2011), or by self-activation upon over-expression (Klaiman et al., 2009). Conversely, caspase-6 activity is reduced by interaction with the transcription factor Sox11 (Waldron-Roby et al., 2015). Chlamydial subversion of caspase-6 regulation is therefore a possible pathway by which lamin A/C levels are depleted during infection. Alternatively, *Chlamydia* also secretes proteases, including CT441 and HtrA, to degrade substrates such as the p65/RelA subunit of the heterodimeric NF-κB complex (CT441) (Lad et al., 2007a; Wu et al., 2011). It is therefore possible that *Chlamydia* encodes an effector that targets lamin A/C directly. Type II secretion can be blocked using arylomycin C16, an inhibitor of the Sec-dependent pathway peptidase I, and so whether the likely T2S protease HtrA may be involved in degradation of lamin A/C could be determined (Wu et al., 2011). Should neither capsase-6 nor chlamydial proteases be involved in the lamin A/C degradation, a broader approach may be required to identify *Chlamydia* effectors required for lamin A/C depletion, such as screening of a library of *C. trachomatis* mutants to identify a strain that does not induce depletion of lamin A/C (Kokes et al., 2015).

Analysis of lamin A/C fluorescence around the nuclear periphery demonstrated that lamin A/C levels are equal to or greater at the inclusion-proximal face of the NE than lamin A/C levels in non-infected cells (Fig 3.9). It could be argued that these changes represent a stabilisation of pre-existing lamin A/C. Indeed, in Hutchinson-Gilford progeria syndrome (HGPS) cells the thickening of the lamin A/C network at the nuclear periphery is attributed solely to the accumulation of a truncated form of lamin A, LAΔ50, as the normal processing and turnover of this truncate is disrupted (Goldman et al., 2004). Alternatively, lamin A/C could be re-localised

from elsewhere in the nucleus into this inclusion-proximal region of the NE. Such a rearrangement occurs during human cytomegalovirus (HCMV) infection (Camozzi et al., 2008). This viral pathogen redirects both lamin A/C and lamin B into regions of HCMV protein UL53 accumulation at late stages of infection, resulting in a ruffled staining pattern of lamins at the nuclear rim. This rearrangement was also dependent on the viral protein UL50, but no variations in the total amount of nuclear lamins were detected during HCMV infection (Camozzi et al., 2008). Thus, *C. trachomatis* likely secretes an effector or effectors that direct the specific stabilisation or enrichment of lamin A/C on the inclusion-proximal face of the NE. The *C. psittaci* SINC effector localises to the inner face of the NE adjacent to the inclusion, and localises in close proximity to NL proteins including lamin A/C. However these authors could not identify a homologue of SINC encoded by *C. trachomatis* (Mojica et al., 2015). Immunoprecipitation experiments may yet reveal the identity of *Chlamydia* effectors in complex with lamin A/C.

A key feature of the lamin A/C patch was its location in close proximity to the inclusion membrane. Analysis of electron micrographs of infected cells revealed the IM closely follows the contours of the NE (Fig 3.4), and across this region there is an increase in electron density in the IM suggesting the IM may be modified, for example, with specific Inc proteins. Furthermore, the distance between the IM and NE is consistent, hinting at the presence of complexes between these membranes which maintain the separation. Cryo-electron tomography techniques such as those used by Nans and colleagues (2014) may yet reveal electron densities between the IM and NE. Nevertheless, the lamin A/C patch may represent a novel junction between the nucleus and the inclusion mediated by chlamydial proteins. Precedent exists for such junctions between the inclusion and host organelles, as membrane contact sites (MCSs) between the *C. psittaci* RB envelope, the IM and mitochondria, and between the *C. trachomatis* RB envelope, the IM and the ER have previously been reported (Matsumoto, 1981; Dumoux et al., 2012). However, in both of these examples RBs are frequently located in the inclusion lumen at the contact site, which was not observed where the IM and the NE are adjacent. Furthermore, the distance between the IM and the mitochondria, or the IM and the ER at these MCSs is approximately 10-30 nm, significantly less than the 163 nm distance observed between the IM and the NE. These data therefore suggest if a junction does exist between the IM and NE where lamin A/C is enriched, it is likely structurally distinct from MCSs observed previously, and warrants further investigation.

NPCs are also depleted and lamin B is reduced in the region of the NE where the lamin A/C patch is located (Figs 3.11-3.15). A similar phenotype is observed in cellular pore-free islands, which are present on the nuclear surface of proliferating cells and are also characterised by an enrichment in lamin A/C, and the depletion of lamin B and NPCs (Maeshima et al., 2006). As discussed previously, the nuclei of HGPS cells also exhibit a thickening of lamin A/C, resulting in abnormal pore distribution and depletion of lamin B in regions of increased lobulation (Goldman et al., 2004). It is therefore likely that the NPC gap and lamin B reduction are a cellular response to the enrichment of lamin A/C, rather than being specifically induced by *Chlamydia*. Heterochromatin was also enriched proximal to the inclusion and is dependent on the presence of lamin A/C (Figs 4.13-4.15, 4.18 and 4.19). Maeshima and colleagues (2006) did not investigate heterochromatin with respect to PFIs, but Goldman and co-workers (2004) observed a complete loss of peripheral heterochromatin in HGPS nuclei, a phenotype counter to that evident in *Chlamydia*-infected cells. There may therefore be another *Chlamydia* effector that drives the lamin A/C-associated redistribution of heterochromatin. NUE exhibits *in vitro* histone methyltransferase activity via a SET domain, and localises to the nucleus when ectopically expressed in mammalian cells (Pennini et al., 2010). Methylation of histone H3 lysine 9 has a role in targeting and anchoring chromatin to the NE, and so NUE could potentially function in the reorganisation of heterochromatin (Towbin et al., 2013). The endogenous localisation of NUE is yet to be determined in infected cells, but with recent advances in the genetic manipulation of *Chlamydia*, it is now feasible to generate a strain expressing epitope-tagged NUE to study this (Weber et al., 2015). Parallel experiments conducted in the Hayward laboratory by Dr. Maud Dumoux have shown that nucleoplasmic lamin A/C is depleted during late (48-72 hpi) *C. trachomatis* infection in addition to the depletion from the NE presented in this thesis (Dumoux and Hayward, unpublished data). A recent study by Gesson and co-workers (2016) demonstrated that nucleoplasmic lamin A/C interacts with euchromatic regions bound by LAP2α in addition to heterochromatic lamina-associated domains, and so depletion of nucleoplasmic lamin A/C may have consequences for the epigenetic regulation of both gene activation and gene repression in infected cells (Gesson et al., 2016).

In chapter 4 experiments were conducted to determine the functional impact of *C. trachomatis* induced NE alterations. As NPCs were depleted, host nucleocytoplasmic transport was assessed. The NTR importin-β was excluded from a region of the nuclear periphery proximal to the inclusion (Fig 4.7), suggesting transport of proteins is blocked in this area as observed at pore-free islands (Appendix 6.1). This correlates with the absence of NPCs

at the inclusion-proximal face of the NE, demonstrating that host nucleocytoplasmic transport does not occur in regions of the NE lacking NPCs. However, given that the NPC gap is likely an indirect consequence of the formation of the lamin A/C patch, it is difficult to speculate as to how the local absence of host nucleocytoplasmic transport is advantageous to the chlamydial lifecycle. Changes to total nuclear mRNA levels were not detected during infection, suggesting global mRNA export is not significantly impaired, and so the functional consequences of NPC gap formation remain unclear (Fig 4.10). The speckle-like pattern of nuclear mRNA fluorescence did however appear more clustered in infected cells (Fig 4.9). Compaction of the nuclear area in the xy-plane due to the distortion of nuclear shape may account for these changes, but nevertheless it would be interesting to investigate the behaviour of the nuclear speckles, the mRNA splicing compartments of the nucleus, in infected cells. Nuclear speckles become enlarged and rounded during inhibitor induced, or heat-shock induced, transcriptional inhibition, and speckles compact when transcription levels are high such as during viral infection (Lamond and Spector, 2003). Thus, the morphology of nuclear speckles during chlamydial infection may be an indicator of host transcription levels, the study of which could reveal novel mechanisms by which *Chlamydia* targets the host nucleus.

In addition to the nuclear speckles, the host nucleus contains many other structures that mediate specialised nuclear functions from transcription to DNA repair. Given the architectural and compositional changes in the NE and the associated reorganisation of heterochromatin, studying these other major compartments and structures of the nucleus such as the chromosome territories and the nucleoli could determine the extent to which *Chlamydia* is hijacking this major organelle. Chromosome territories describe the non-random distribution of chromosomes within the nucleus, in which both highly transcribed and poorly transcribed regions are segregated, allowing for co-regulation of the activation or repression of expression of specific genes (Cremer and Cremer, 2010). Changes in the distribution of chromosome territories have been described during viral infection. Epstein-Barr virus infection induced alterations in the radial position of chromosome 17, whereas the localisation of chromosome 18 remained stable (Li et al., 2010). However, the consequences of positional changes in chromosome 17 were not determined. In the context of the results presented in this thesis, the chromosome territories would be interesting to study to identify whether any clusters of genes are specifically relocated to the enriched region of heterochromatin on the inclusion-proximal face of the nucleus, and so explain why it is advantageous for the bacteria to reorganise the heterochromatin to this location.

The impact of the changes in lamin A/C on nuclear shape, stability and stiffness should also be considered. A-type lamins are the main proponents in providing mechanical support to the nucleus from lamin A/C located in both the nucleoplasm and the nuclear periphery (Dahl et al., 2004). Additionally, A-type lamins allow the cell to modulate gene expression in response to extracellular or cytoskeletal forces in a process termed mechanotransduction (Crisp et al., 2006; Dahl et al., 2008). Inclusion-distal depletion of lamin A/C likely results in the increased lobulation of nuclei during *Chlamydia* infection (Fig 4.2), as the nuclei of infected cells lacking lamin A/C were similarly lobulated (Fig 4.20). These observations correlate with increased lobulation of nuclei in granulocytes, a phenotype also linked to the depletion of lamins (Olins et al., 2001), but contrast with progeria cells, in which accumulation of truncated lamin AΔ50 also induces nuclear lobulation (Goldman et al., 2004). Nevertheless, the inclusion-distal depletion and inclusion-proximal stabilisation of lamin A/C likely differentially impact the flexibility of nuclei. Lamin A/C is enriched on the inclusion-proximal face of the nucleus, and thus the stiffness of this region of the NE is likely increased. One could hypothesise that this reinforced region of the NE would provide a platform for the inclusion to support its expansion and maintain its shape. However, inclusions within infected *LMNA*$^{-/-}$ mouse embryonic fibroblasts (MEFs) were similarly shaped and were also larger than those formed within WT MEFs (Fig 4.21). The functional consequences of the stabilisation of lamin A/C proximal to the inclusion are therefore unlikely to be related to the flexibility of the NE in this region.

Conversely, the NE distal to the inclusion is likely more flexible, as cells lacking lamin A/C exhibit reduced nuclear stiffness, but also misshapen nuclei and increased nuclear and cellular fragility due to a loss of connectivity between the nucleus and the cytoskeleton (Broers et al., 2004; Lammerding et al., 2004). The reduction in lamin A/C may therefore increase cellular sensitivity to mechanical stress caused by, for example, the expanding inclusion, which could contribute to the lytic pathway of *Chlamydia* exit from the host cell. One could also consider the *in vivo* scenario, in which pressure would be applied on the *Chlamydia*-infected cell by the surrounding cells of the epithelium, promoting lysis once the inclusion expands to a critical point. As a starting point to investigating these possibilities, the propensity for bacterial exit via the lytic pathway in cells lacking lamin A/C could be analysed. Furthermore, it would also be intriguing to consider whether the infection model typically used for studying *Chlamydia* infection may also have an impact on the architectural changes to the nucleus and nuclear envelope. *In vivo, C. trachomatis* preferentially infects the columnar epithelium, an organised layer of polarised rectangular epithelial cells. In comparison to infection of HeLa or MEF cell lines, numerous infection characteristics are altered during infection of these polarised

epithelial cells, including entry and exit mechanisms, infectious progeny, infection kinetics and a number of innate immune pathways (Wyrick and Bavoil, 2006). As an initial avenue to investigating whether characteristics such as cell shape or orientation impact on the observed changes to lamin A/C and nuclear shape, infection of polarised epithelial cells such as the A2EN human endocervical epithelial cell line could therefore be studied (Buckner et al., 2013).

Finally, *LMNA*$^{-/-}$ MEFs were utilised in experiments presented in this thesis in the context of examining the effects on the *Chlamydia* lifecycle. As previously described, in infected cells lacking lamin A/C inclusions are significantly larger and more infectious progeny are produced (Figs 4.21 and 4.22). This challenged the understanding of the functionality of the lamin A/C patch. Ongoing work in the laboratory has shown that inclusion size and infectious progeny are also increased in HGPS cells infected with *C. trachomatis* (Dumoux and Hayward, unpublished data). While *LMNA*$^{-/-}$ cells and HGPS cells exhibit an absence and stabilisation of lamin A/C at the NE respectively, a clear decrease in nucleoplasmic lamin A/C can be observed in both. This highlights the potential importance for nucleoplasmic lamin A/C-mediated reorganisation of heterochromatin and the potential effects on gene expression. It would be interesting to study the effect on the *Chlamydia* lifecycle when the degradation of inclusion-distal lamin A/C is prevented. If the reverse phenotype occurs, then a smaller inclusion and less infectious progeny may be expected.

In conclusion, the data presented in this thesis have demonstrated a novel mechanism by which a pathogenic intracellular bacterium interacts with and manipulates the host nucleus. *C. trachomatis* polarises the nucleus towards the inclusion by inducing major architectural changes to the nuclear envelope. The polarisation of heterochromatin likely generates an environment whereby *C. trachomatis* can better manipulate host gene expression in order to enhance aspects of infection not related to inclusion enlargement and bacterial replication, for example, the inhibition of host responses to infection such as immune signalling or apoptosis. These observations are distinct from the known interactions of intracellular pathogenic bacteria with the nucleus, that can be broadly categorised into three groups (Bierne and Cossart, 2012): bacterial proteins that manipulate chromatin structure, including *C. tra*chomatis NUE, which can methylate histones H2B, H3 and H4 *in vitro* (Pennini et al., 2010), and the *L. pneumophila* protein RomA, which methylates H3K14 to repress host gene expression (Rolando et al., 2013); bacterial proteins that target nuclear regulators of gene expression such as the *Shigella flexneri* effector OspF, which inhibits MAPK signalling to block activation of pro-inflammatory genes (Arbibe et al., 2007; Brennan and Barford, 2009); and

bacterial proteins that manipulate the cell cycle, for example *E. coli* Cif_{Ec} which induces arrest at G1/S or G2/M by stabilising cyclin-dependent kinase inhibitors (Samba-Louaka et al., 2008). The work presented here demonstrates that in addition to manipulating nuclear function with effectors such as NUE, *C. trachomatis* targets the nucleus on a more global level than is known for other bacterial pathogens, inducing a major reorganisation of nuclear architecture with potential impact on gene expression, chromosome organisation and mechanotransduction. These findings reveal exciting avenues for further research into the relationship between *Chlamydia trachomatis* and nuclear architecture and function.

Appendix Chapter 3

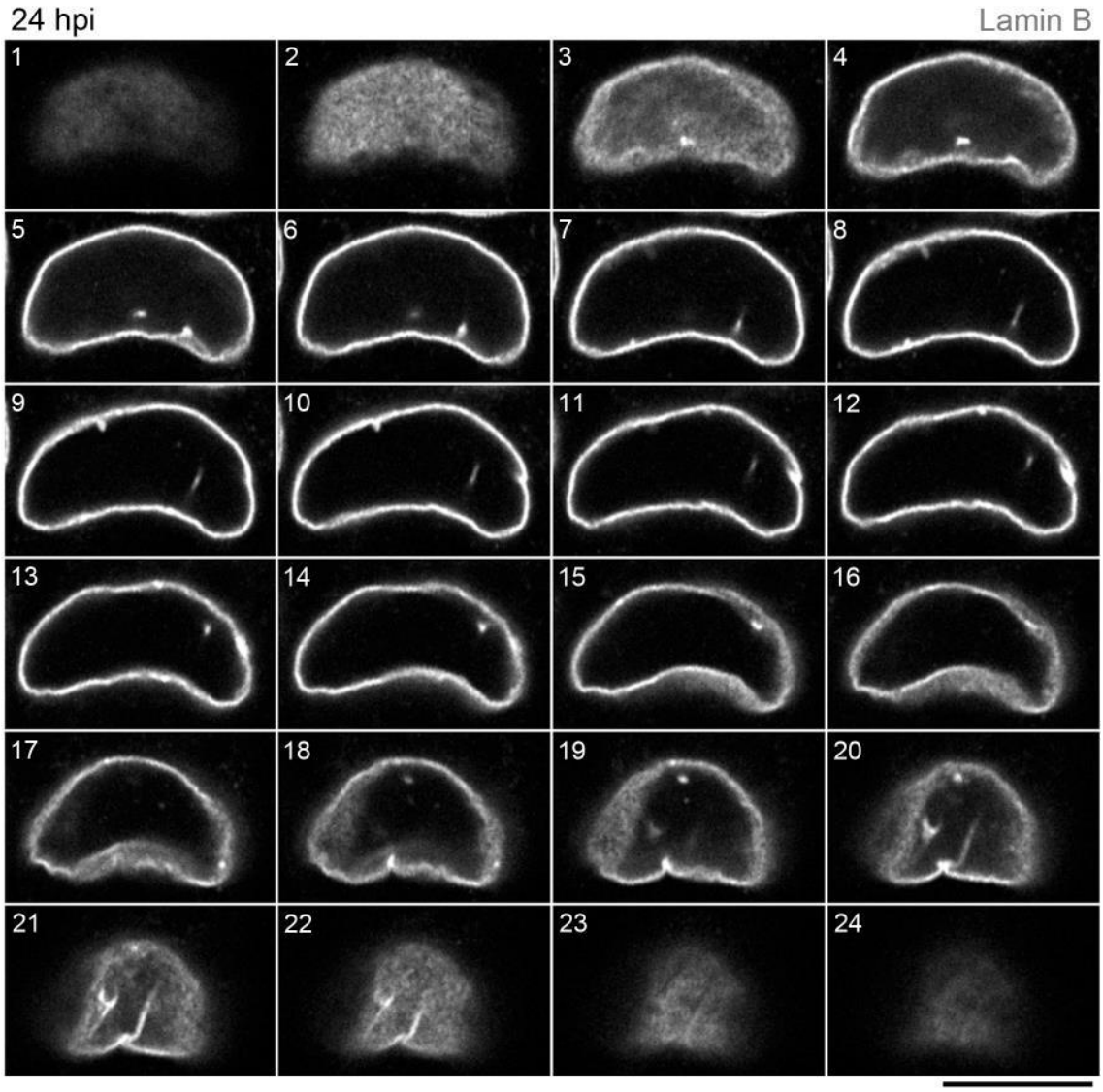

Appendix 3.1. Full z-stack of the nucleus of the cell shown in figure 3.11A infected with *C. trachomatis* for 24 hours. HeLa cells were infected with *C. trachomatis* LGV2, fixed at 24 hours post infection (hpi) and stained with anti-lamin B1 primary antibody and an AlexaFluor® 546-conjugated secondary antibody (grey) to visualise lamin B. Panels show confocal xy-sections of the nucleus, ascending in the z dimension through the cell (1-24) with a step of 0.34 µm. Scale bars, 10 µm.

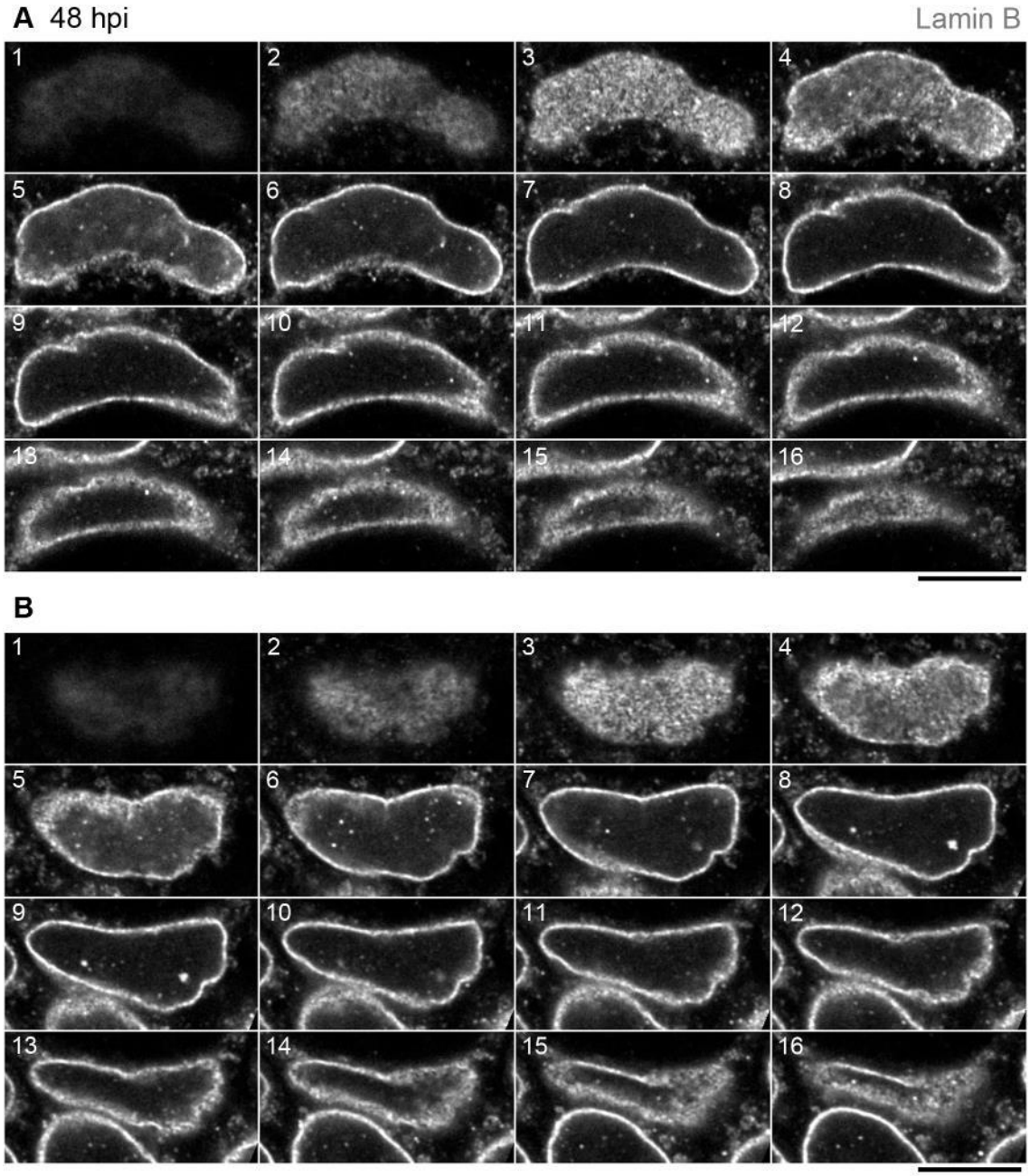

Appendix 3.2. Full z-stacks of the nuclei of the cell shown in figure 3.11B infected with *C. trachomatis* for 48 hours. HeLa cells were infected with *C. trachomatis* LGV2, fixed at 48 hours post infection (hpi) and stained with anti-lamin B1 primary antibody and an AlexaFluor® 546-conjugated secondary antibody (grey) to visualise lamin B. Panels show confocal xy-sections of the nuclei, ascending in the z dimension through the cell (1-16) with a step of 0.34 µm. (A) Nucleus equivalent to the upper panel in figure 3.11B. (B) Nucleus equivalent to the lower panel in figure 3.11B. Scale bars, 10 µm.

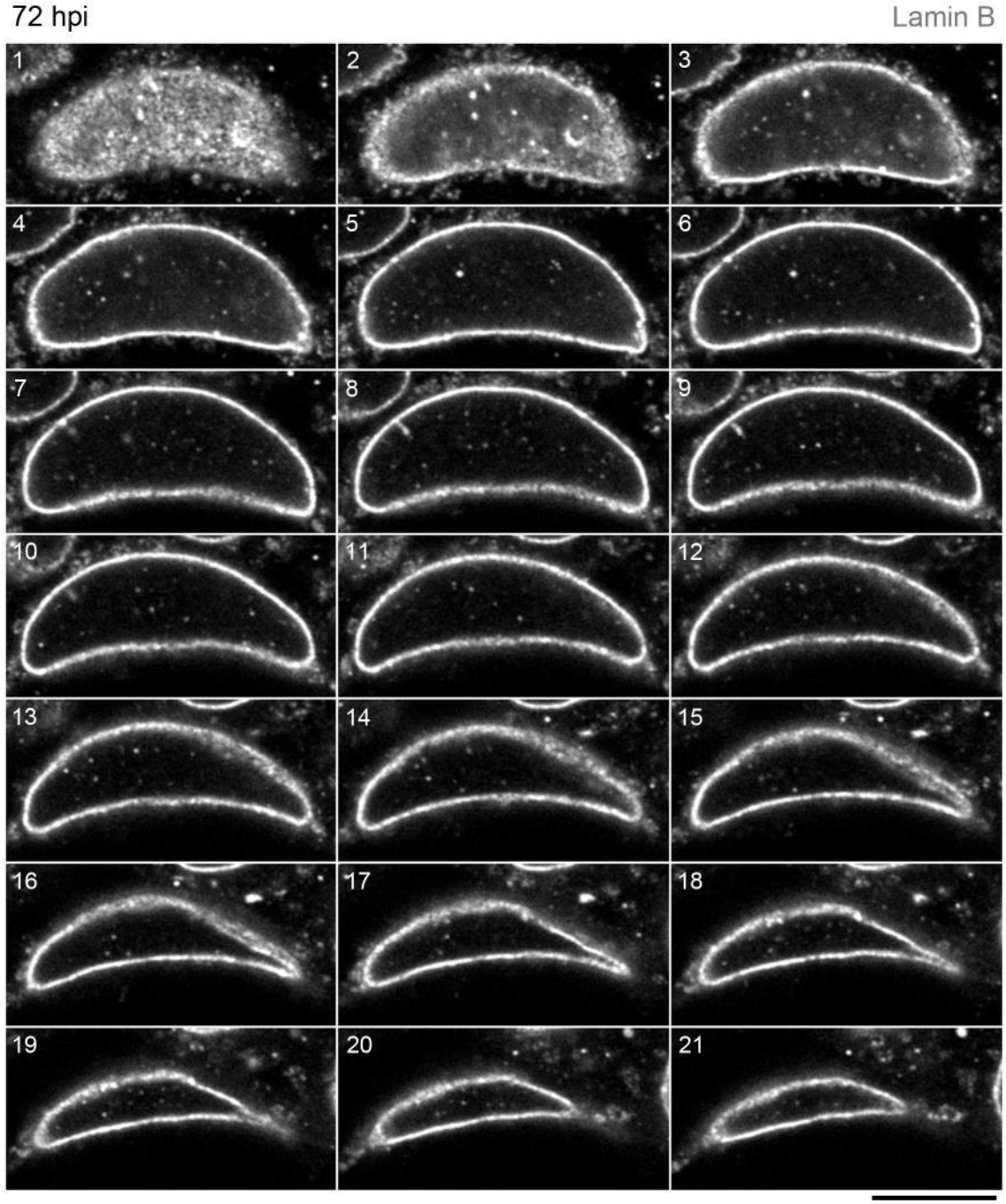

Appendix 3.3. Full z-stack of the nucleus of the cell shown in the upper panel of figure 3.11C infected with *C. trachomatis* for 72 hours. HeLa cells were infected with *C. trachomatis* LGV2, fixed at 72 hours post infection (hpi) and stained with anti-lamin B1 primary antibody and an AlexaFluor® 546-conjugated secondary antibody (grey) to visualise lamin B. Panels show confocal xy-sections of the nuclei, ascending in the z dimension through the cell (1-21) with a step of 0.34 µm. Scale bars, 10 µm.

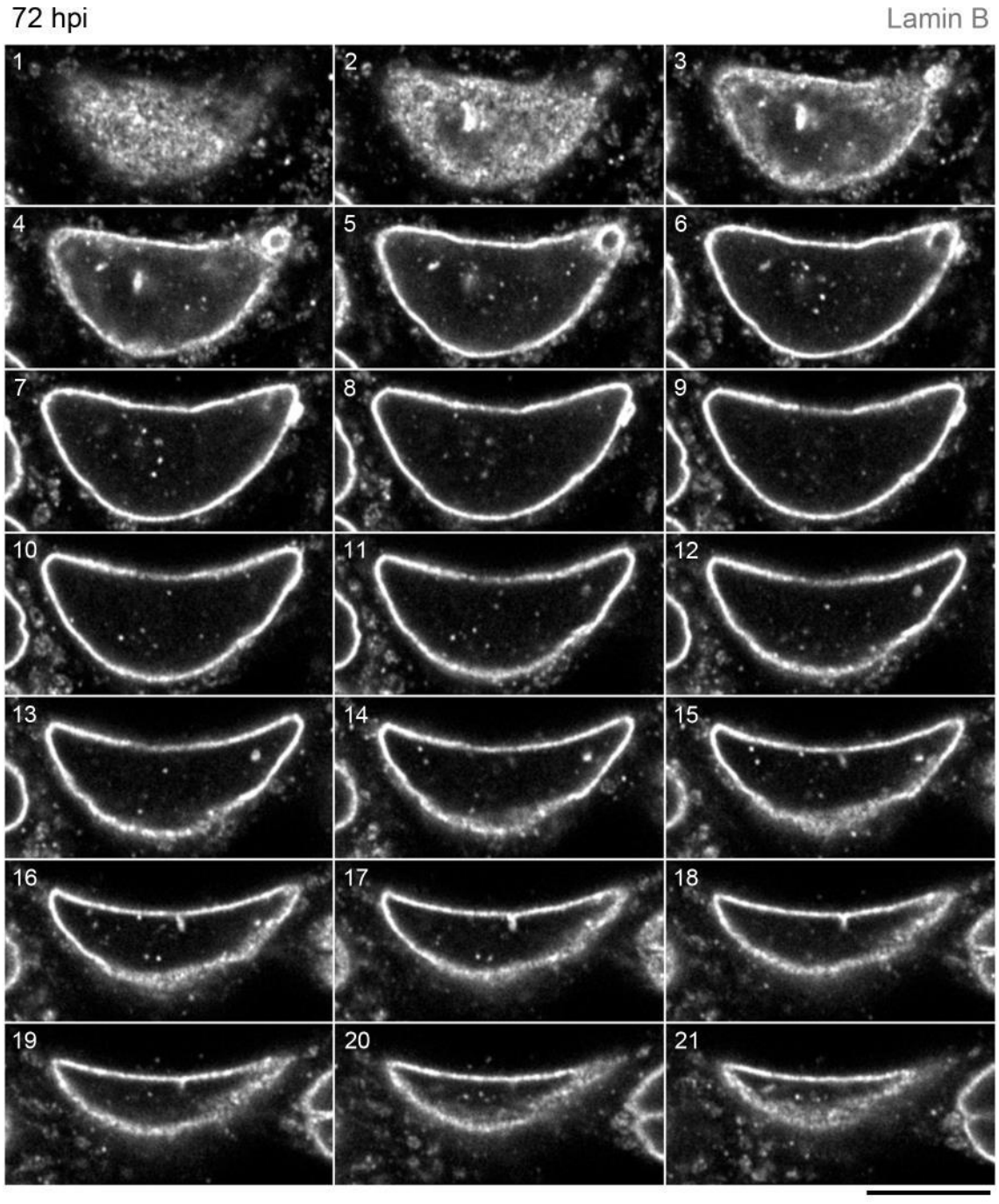

Appendix 3.4. Full z-stack of the nucleus of the cell shown in the lower panel of figure 3.11C infected with *C. trachomatis* for 72 hours. HeLa cells were infected with *C. trachomatis* LGV2, fixed at 72 hours post infection (hpi) and stained with anti-lamin B1 primary antibody and an AlexaFluor® 546-conjugated secondary antibody (grey) to visualise lamin B. Panels show confocal xy-sections of the nuclei, ascending in the z dimension through the cell (1-21) with a step of 0.34 µm. Scale bars, 10 µm.

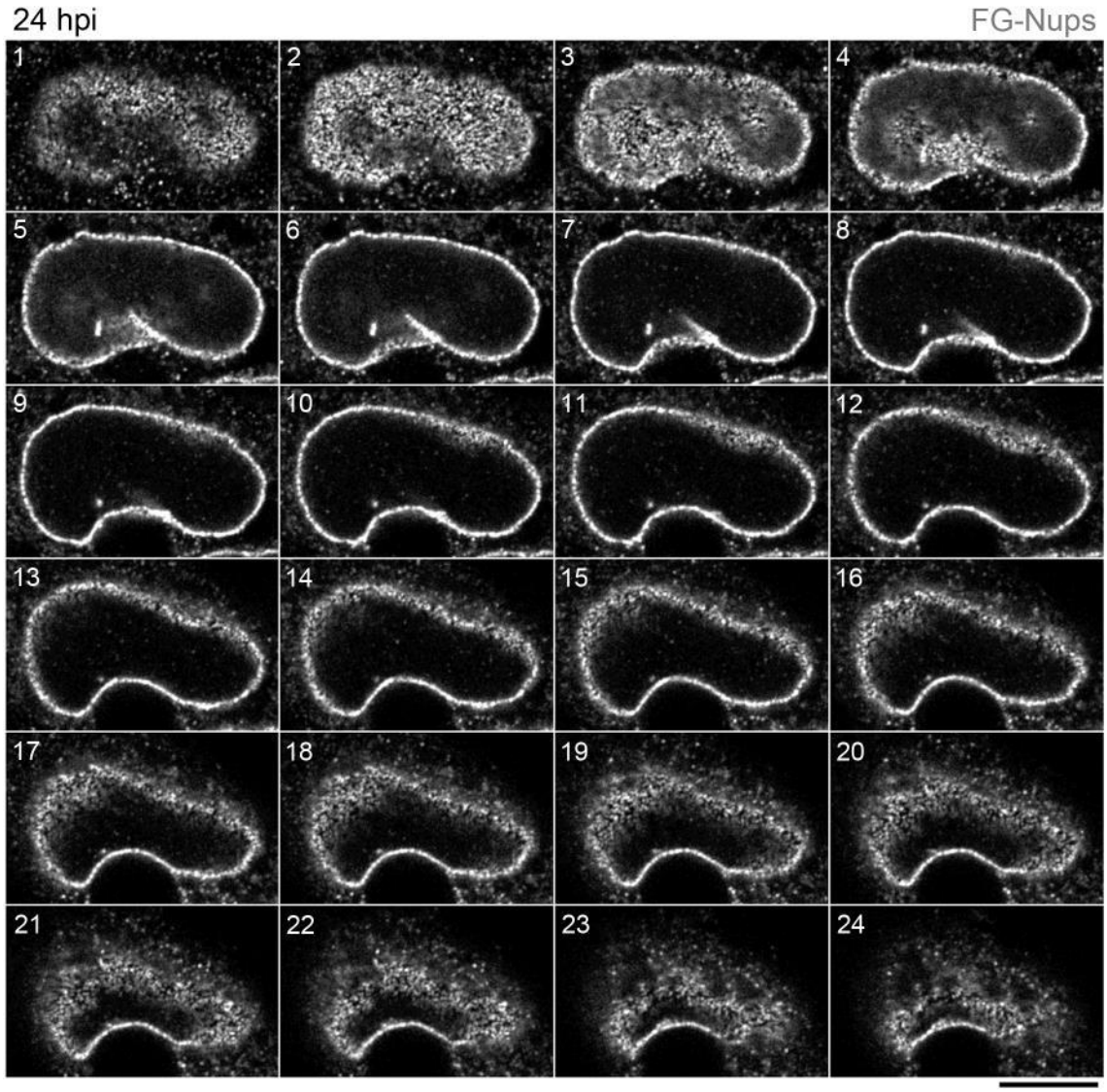

Appendix 3.5. Full z-stack of the nucleus of the cell shown in figure 3.14A infected with *C. trachomatis* for 24 hours. HeLa cells were infected with *C. trachomatis* LGV2, fixed at 24 hours post infection (hpi) and stained with mAb414 primary antibody and an AlexaFluor® 488-conjugated secondary antibody (grey) to visualise phenylalanine glycine-containing nucleoporins (FG-Nups). Panels show confocal xy-sections of the nuclei, ascending in the z dimension through the cell (1-24) with a step of 0.34 µm. Scale bars, 10 µm.

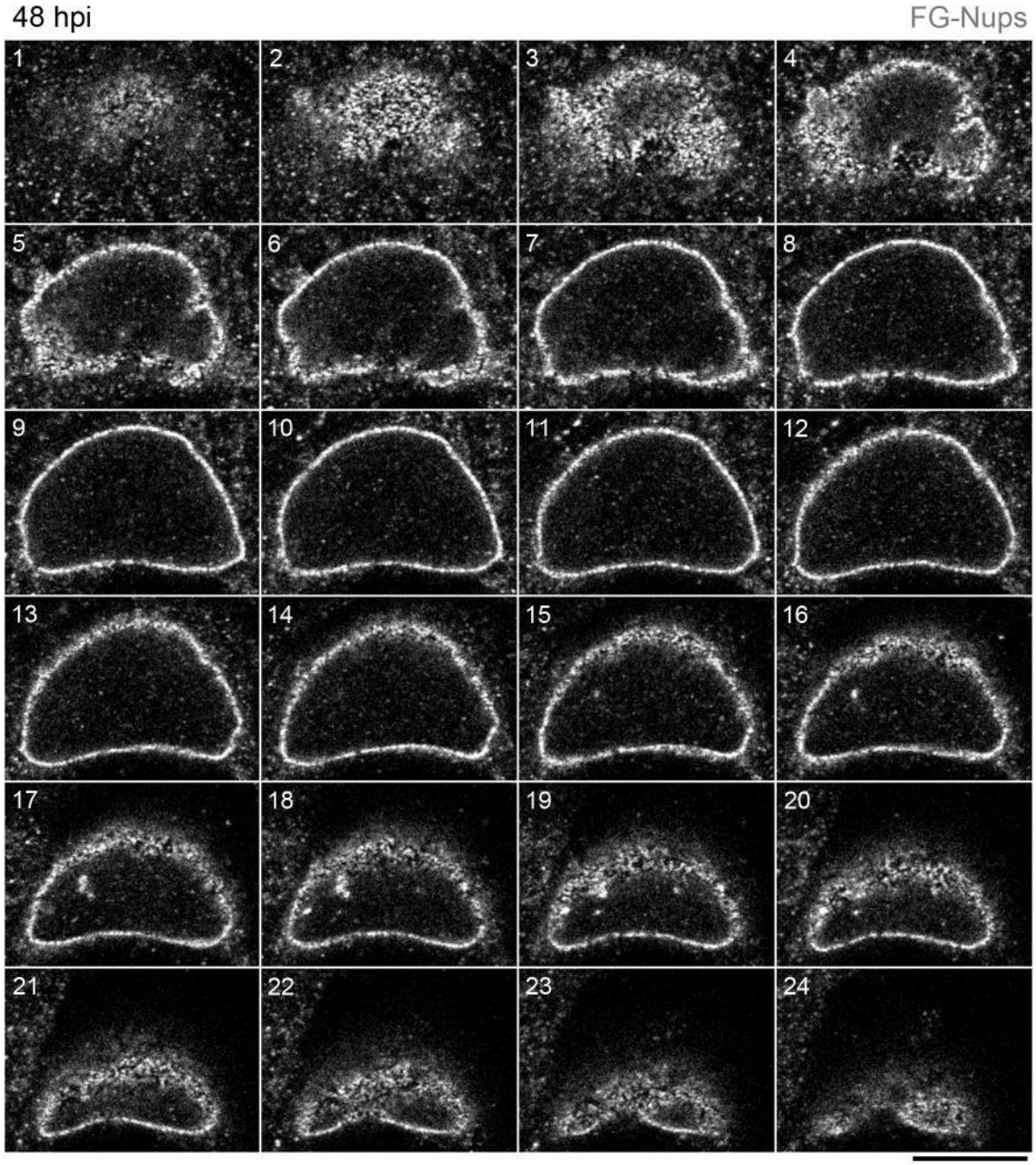

Appendix 3.6. Full z-stack of the nucleus of the cell shown in the upper panel of figure 3.14B infected with *C. trachomatis* for 48 hours. HeLa cells were infected with *C. trachomatis* LGV2, fixed at 48 hours post infection (hpi) and stained with mAb414 primary antibody and an AlexaFluor® 488-conjugated secondary antibody (grey) to visualise phenylalanine glycine-containing nucleoporins (FG-Nups). Panels show confocal xy-sections of the nuclei, ascending in the z dimension through the cell (1-24) with a step of 0.34 µm. Scale bars, 10 µm.

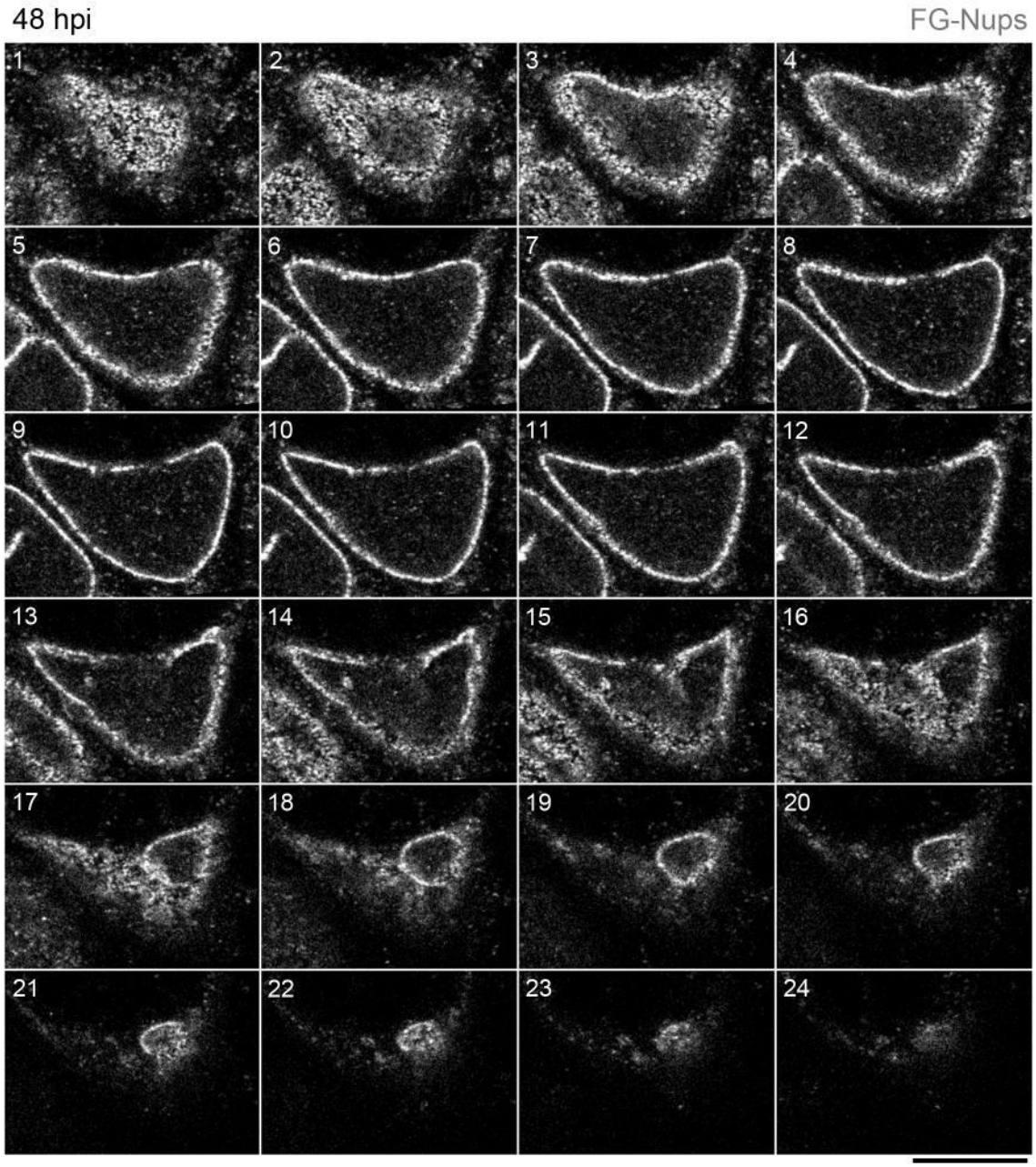

Appendix 3.7. Full z-stack of the nucleus of the cell shown in the lower panel of figure 3.14B infected with *C. trachomatis* for 48 hours. HeLa cells were infected with *C. trachomatis* LGV2, fixed at 48 hours post infection (hpi) and stained with mAb414 primary antibody and an AlexaFluor® 488-conjugated secondary antibody (grey) to visualise phenylalanine glycine-containing nucleoporins (FG-Nups). Panels show confocal xy-sections of the nuclei, ascending in the z dimension through the cell (1-24) with a step of 0.34 µm. Scale bars, 10 µm.

Appendix 3.8. Full z-stacks of the nuclei of the cell shown in figure 3.14C infected with *C. trachomatis* for 72 hours. HeLa cells were infected with *C. trachomatis* LGV2, fixed at 72 hours post infection (hpi) and stained with mAb414 primary antibody and an AlexaFluor® 488-conjugated secondary antibody (grey) to visualise phenylalanine glycine-containing nucleoporins (FG-Nups). Panels show confocal xy-sections of the nuclei, ascending in the z dimension through the cell (1-24) with a step of 0.34 µm. (A) Nucleus equivalent to the upper panel in figure 3.14C. (B) Nucleus equivalent to the lower panel in figure 3.14C .Scale bars, 10 µm.

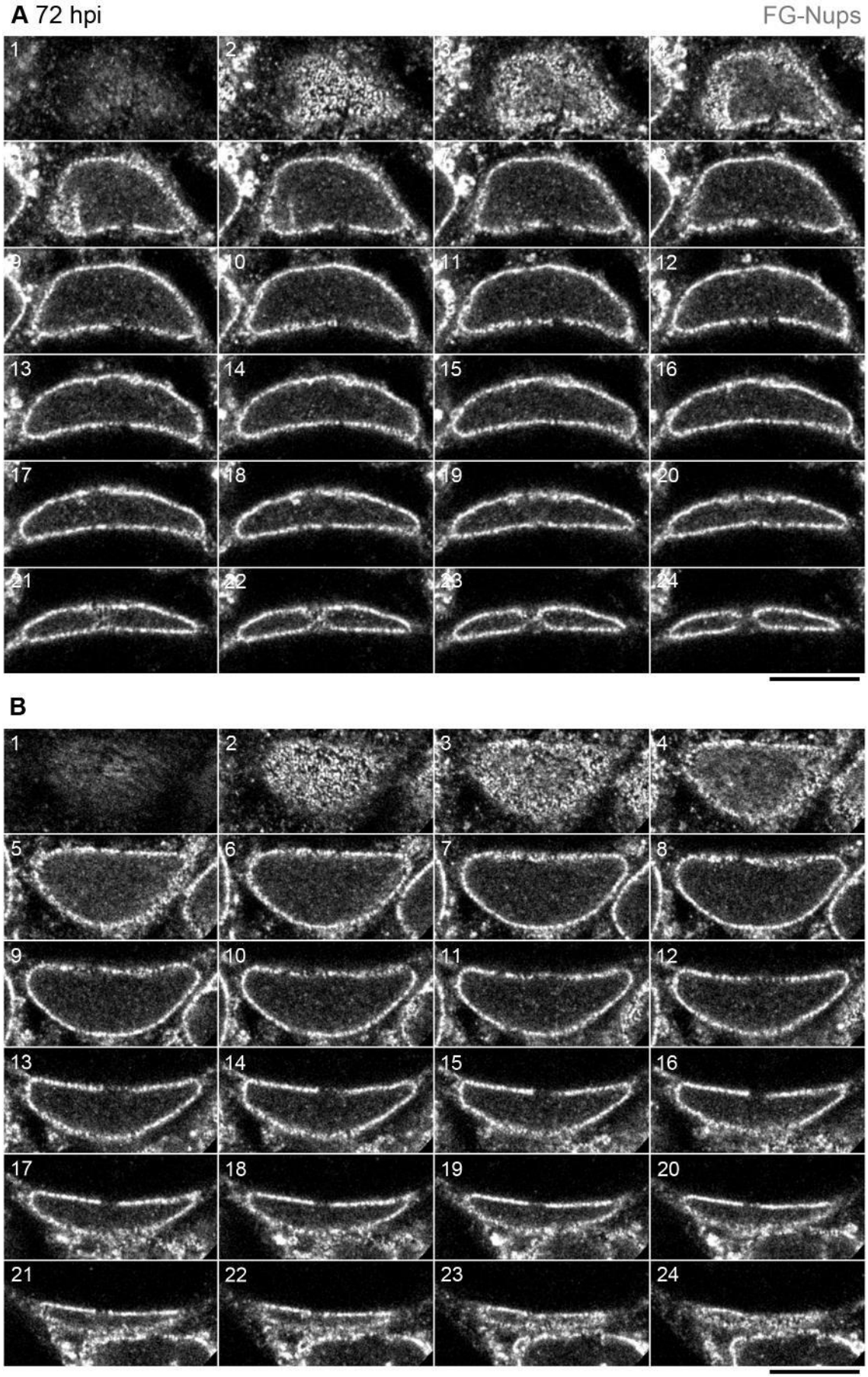
A 72 hpi
FG-Nups
1
2
3
4
5
6
7
8
9
10
11
12
13
14
15
16
17
18
19
20
21
22
23
24
B
1
2
3
4
5
6
7
8
9
10
11
12
13
14
15
16
17
18
19
20
21
22
23
24

Appendix Chapter 5

Species	Gene Identifier (IMG database)	Encoded protein name
Blastopirellula marina	638976093	probable L-sorbosone dehydrogenase
	638976556	glucose dehydrogenase-B [pyrroloquinoline-quinone] precursor-like protein
	638978984	hypothetical protein
	638979435	Cytochrome c-like protein
	638979470	hypothetical protein
	638980220	hypothetical protein
	638980641	hypothetical protein
	638980874	hypothetical protein
	638980886	L-sorbosone dehydrogenase-like protein
	638981029	hypothetical protein
	638981356	hypothetical protein
	638981358	glucose dehydrogenase-B [pyrroloquinoline-quinone] precursor-like protein
Chthoniobacter flavus	642908240	heme-binding protein
	642910918	membrane-bound dehydrogenase domain protein
	642911202	glucose dehydrogenase-B (pyrroloquinoline-quinone) (precursor)-like protein
	642911438	membrane-bound dehydrogenase domain protein
	642911451	heme-binding protein
	642911540	membrane-bound dehydrogenase domain protein
	642911638	coagulation factor 5/8 type domain protein
	642911643	heme-binding protein
	642913322	membrane-bound dehydrogenase domain protein
	642913358	heme-binding protein
	642913419	membrane-bound dehydrogenase domain protein
	642913493	heme-binding protein
	642913495	membrane-bound dehydrogenase domain protein
	642913861	heme-binding protein
Gemmata obscuriglobus	642220721	hypothetical protein
	642221071	hypothetical protein
	642225323	hypothetical protein
	642225569	hypothetical protein
	642225867	hypothetical protein
	642226015	hypothetical protein
	642226674	hypothetical protein
	642227083	probable L-sorbosone dehydrogenase
Lentisphaera araneosa	641128129	hypothetical protein
	641128534	probable cytochrome c precursor
	641128545	hypothetical protein
	641129208	hypothetical protein
	641131688	hypothetical protein
	641131908	hypothetical protein
	641132248	hypothetical protein
	641132354	hypothetical protein
	641132994	hypothetical protein
Pedosphaera parvula	642468634	heme-binding protein
	642469007	heme-binding protein

	642469316	membrane-bound dehydrogenase domain protein
	642472080	heme-binding protein
	642472266	membrane-bound dehydrogenase domain protein
	642472454	membrane-bound dehydrogenase domain protein
	642473041	membrane-bound dehydrogenase domain protein
	642474024	membrane-bound dehydrogenase domain protein
	642474746	membrane-bound dehydrogenase domain protein
Planctomyces maris	641107130	hypothetical protein
	641108038	hypothetical protein
	641110955	hypothetical protein
	641110980	probable L-sorbosone dehydrogenase
	641111294	hypothetical protein
	641111761	hypothetical protein
	641112091	hypothetical protein
	641112369	hypothetical protein
	641112478	hypothetical protein
	641112544	hypothetical protein
	641112798	quinoprotein glucose dehydrogenase
Rhodopirellula baltica	637433005	similar to L-sorbosone dehydrogenase
	637433385	conserved hypothetical protein-putative cytochrome c
	637434028	similar to glucose dehydrogenase-B
	637438096	conserved hypothetical protein-possibly contains sugar binding site
	637438335	probable L-sorbosone dehydrogenase
Verrucomicrobium spinosum	642329454	hypothetical protein
	642329771	hypothetical protein
	642329814	hypothetical protein
	642332150	hypothetical protein
	642332272	hypothetical protein
	642332458	hypothetical protein
	642333361	hypothetical protein
	642333382	hypothetical protein
	642333400	probable L-sorbosone dehydrogenase
	642333437	probable secreted glycosyl hydrolase
	642333450	hypothetical protein
	642333699	hypothetical protein
	642333971	hypothetical protein
	642334466	hypothetical protein
	642334781	hypothetical protein
	642334798	hypothetical protein

Appendix 5.1. Membrane coat-like (MC) proteins of the *Planctomycetes-Verrucomicrobia-Chlamydiae* (PVC) superphylum used for remote homology detection. Gene identifiers of genes encoding for MC proteins detected by Santarella-Mellwig et al. (2010) correspond to entries in the Integrated Microbial Genomes & Microbiome Samples (IMG) database, available at https://img.jgi.doe.gov.

```
class SSparse:
    def __init__(self):
        # Confirm script started correctly
        import sys
        self.path = sys.argv[1]
        if len(sys.argv) != 2:
            sys.exit('Script requires 2 arguements, %i given. Example script:\
 user$ python LOCATION_OF_SCRIPT LOCATION_OF_INPUT_FILES'%(len(sys.argv)))
        else:
            pass
        # Dictionary containing scalebar text position information
        self.d = {0:'\n-22 90 moveto\n( 0 ) show' , 100:'\n76 90 moveto\n( 100 ) show',
        200:'\n188 90 moveto\n( 200 ) show',
             300:'\n300 90 moveto\n( 300 ) show', 400:'\n412 90 moveto\n( 400 ) show',
             500:'\n524 90 moveto\n( 500 ) show',
             600:'\n636 90 moveto\n( 600 ) show', 700:'\n748 90 moveto\n( 700 ) show',
             800:'\n860 90 moveto\n( 800 ) show',
             900:'\n972 90 moveto\n( 900 ) show', 1000:'\n1074 90 moveto\n( 1000 ) show',
             1100:'\n1186 90 moveto\n( 1100 ) show',
             1200:'\n1298 90 moveto\n( 1200 ) show', 1300:'\n1410 90 moveto\n( 1300 ) show',
             1400:'\n1522 90 moveto\n( 1400 ) show',
             1500:'\n1634 90 moveto\n( 1500 ) show', 1600:'\n1746 90 moveto\n( 1600 ) show',
             1700:'\n1858 90 moveto\n( 1700 ) show',
             1800:'\n1970 90 moveto\n( 1800 ) show', 1900:'\n2082 90 moveto\n( 1900 ) show',
             2000:'\n2194 90 moveto\n( 2000 ) show\n\n'}
    def mkdirs(self):
        import subprocess
        try:    # Creates temporary folders at start of script
            subprocess.Popen(['mkdir',self.path+'parse'])
            subprocess.Popen(['mkdir',self.path+'merge'])
            subprocess.Popen(['mkdir',self.path+'consensus'])
            subprocess.Popen(['mkdir','-p',self.path+'Consensus_preds'])
        except OSError:
            pass
    def deldirs(self):
        import subprocess
        try:    # Removes temporary folders at end of script
            subprocess.Popen(['rm', '-rf',self.path+'parse'])
            subprocess.Popen(['rm', '-rf',self.path+'merge'])
            subprocess.Popen(['rm', '-rf',self.path+'consensus'])
        except OSError:
            print 'Directory not deleted'
    def runscript(self):    # Runs all other classes. Path set by user.
        import subprocess
        print 'Raw data file formatting as follows: ProteinSoftware.txt, where:-\
        \nProtein = Input protein\
        \nSoftware = Software used (PSIPRED/RaptorX/Jnet)'
        subprocess.Popen(['mkdir','-p',self.path+'results'])
        pathout = self.path+'results/'
        pathmerge = self.path+'parse/'
        pathcons = self.path+'merge/'
        pathps = self.path+'consensus/'
        self.inputloop = raw_input('Include loop regions in image? (y/n) ')
        self.filename(self.path)
        self.pred(self.path, pathmerge)
        print 'Predicted secondary structure extracted...'
        self.conf(self.path, pathmerge)
        print 'Predicted confidence values extracted...'
        self.seq(self.path, pathmerge)
        print 'Amino acid sequences extracted...'
        self.join(pathmerge, pathcons)
        print 'All information merged...'
        self.consensus(self.path, pathcons, pathps)
        print 'Consensus sequences created...'
        self.ps(pathps, pathout)
        print 'Postscript graphics created from consensus sequences...'
        self.psmerge(pathout)
        print 'Individual graphics merged into MergeFilemanual.ps...'
        print 'Cleaning up...'
```

```
        self.deldirs()
        print 'Done!'
    def filename(self, path):    # Retrieves and stores name of each file
        import os
        listfile = []
        file_dict = {}

        dirs = os.listdir(path)
        for inputfile in dirs:
            if inputfile.endswith('.txt'):
                inputfile = inputfile.replace('_Jpred.txt','')
                inputfile = inputfile.replace('_RaptorX.txt','')
                inputfile = inputfile.replace('_Psipred.txt', '')
                listfile.append(inputfile)
        for item in sorted(set(listfile)):
            file_dict[item] = listfile.count(item)
        self.file_dict = file_dict
        listfile = list(set(listfile))
        self.listfile = listfile
    def pred (self, path, pathmerge):    # Retrieves and stores each SS prediction in one file
        import os
        parseseq = ''
        method = ['Psipred', 'RaptorX', 'Jpred']
        methodtitle = ''

        dirs = os.listdir(path)

        for inputfile in dirs:
            if inputfile.endswith('.txt'):
                f = open(path+inputfile,'r').readlines()
                outfilename = inputfile.replace('.txt','SSparse.txt')
                out_file = open(pathmerge+outfilename,'w')
                for line in f:
                    if line.startswith('Pred'):
                        segs = line.split()
                        try:
                            parseseq += segs[1]
                        except:
                            pass
                for string in method:
                    if string in inputfile:
                        methodtitle = string
                out_file.write(methodtitle+'\t'+parseseq)
                out_file.close()
                parseseq = ''
    def conf(self, path, pathmerge):    # Retrieves and scores confidence values for each SS
    prediction in one file
        import os
        parseseq = ''
        method = ['Psipred', 'RaptorX', 'Jpred']
        methodtitle = ''

        dirs = os.listdir(path)

        for inputfile in dirs:
            if inputfile.endswith('txt'):
                f = open(path+inputfile,'r').readlines()
                for line in f:
                    if line.startswith('Conf'):
                        segs = line.split()
                        try:
                            parseseq += segs[1]
                        except:
                            pass
                for string in method:
                    if string in inputfile:
                        methodtitle = string
                outfilename = inputfile.replace('.txt','SSxconf.txt')
                out_file = open(pathmerge+outfilename,'w')
```

```
            out_file.write(methodtitle+'\t'+parseseq)
            out_file.close()
            parseseq = ''
def seq(self, path, pathmerge):     # Retrieves and stores amino acid sequence of each
protein
    import os
    parseseq = ''
    subtitle = 'AA_seq'

    dirs = os.listdir(path)

    for inputfile in dirs:
        if inputfile.endswith('Psipred.txt'):
            f = open(path+inputfile,'r').readlines()
            for line in f:
                if line.startswith('  AA'):
                    segs = line.split()
                    try:
                        parseseq += segs[1]
                    except:
                        pass
            outfilename = inputfile.replace('Psipred','AA_seq')
            out_file = open(pathmerge+outfilename,'w')
            out_file.write(subtitle+'\t'+parseseq)
            out_file.close()
            parseseq = ''
def join(self, pathmerge, pathcons):    # Merges information previously stored in one
file in format:
    import os                           # AA_seq, SS pred, conf values, SS pred, conf
    values etc.

    filestart = self.listfile
    sumlines = ''

    dirs = os.listdir(pathmerge)

    for string in filestart:
        out_file = open(pathcons+string[:-4]+'merge.txt','w')
        for inputfile in dirs:
            if string[:-4] in inputfile:
                f = open(pathmerge+inputfile,'r').readlines()
                for line in f:
                    sumlines += line+'\n'
        out_file.write(sumlines)
        out_file.close()
        sumlines = ''
def consensus(self, path, pathcons, pathps):# Determines consensus sequence between
different prediction softwares
    import os                                   # Writes consensus sequence in table with
    format: loop, helix, strand, with confidence
                                                # score for each at that position.
    d = {}
    outfilename = ''
    confpercent = ''
    conflist = ''
    counter = 0

    dirs = os.listdir(pathcons)

    if '.DS_Store' in dirs:
        dirs.remove('.DS_Store')
    for inputfile in dirs:
        if inputfile.endswith('merge.txt'):
            outfilename = inputfile.replace('merge.txt','consensus.txt')
            openfile = open(pathcons+inputfile,'r')
            for line in openfile:
                line = line.split()
                if line[0]=='AA_seq':
                    pass
```

```
                else:
                    characters = list(line[1])
                    for i, v in enumerate(characters[0:]):
                        i += 1
                        if d.has_key(i):
                            d[i].append(v)
                        else:
                            d[i] = list(v)
            for key in sorted(d.iterkeys()):
                conf = {'C':0.0, 'H':0.0,'E':0.0}
                for i in xrange(0,len(d[key]),2):
                    conf[d[key][i]] = conf[d[key][i]]+int(d[key][i+1])
                vals = [val for key, val in conf.iteritems()]
                for key2 in sorted(conf.iteritems()):
                    if sum(vals) == 0:
                        confpercent = '0.00'
                    else:       # Divides confidence value by number of prediction
                    softwares to give consensus confidence value
                        confpercent = '%.2f'%((float(key2[1])/2))
                    conflist += confpercent+'\t'
                    counter += 1
                    if counter == 3:
                        conflist += '\n'
                        counter = 0
            ssorder = 'C\tE\tH\n'
            out_file = open (pathps+outfilename,'w')
            out_file2 = open(path+'Consensus_preds/'+outfilename,'w')
            out_file.write(ssorder+conflist)
            out_file2.write(ssorder+conflist)
            out_file.close()
            out_file2.close()
            conflist = ''
            d = {}
def ps(self, pathps, pathout):      # Writes scores into postscript file. Takes highest
score and divides by total of all scores
                                    # to give the height of the bar.
    import os, sys
    position = 0.00
    proteinname = ''
    posstring = ''
    sstype = ''
    conf = 0
    outstring = ''
    linecount = 0

    # coil colour values are 1, 0.7, 0.25
    # helix colour values are 0, 0.3921, 1
    # sheet colour values are .922, 0.13, .922
    if self.inputloop == 'y':
        colour = {0:'1' '\t' '0.7' '\t' '0.25', 1:'0' '\t' '0.3921' '\t' '1', 2:'0.922'
        '\t' '0.13' '\t' '0.922'}
    elif self.inputloop == 'n':
        colour = {0:'1' '\t' '1' '\t' '1', 1:'0' '\t' '0.3921' '\t' '1', 2:'0.922' '\t'
        '0.13' '\t' '.922'}
    else:
        print 'Incorrect input, correct input is y or n.\nScript terminating.'
        sys.exit()
    self.legendpos = 1
    scalebar = ''

    dirs = os.listdir(pathps)

    for inputfile in dirs:
        if inputfile.endswith('.txt'):
            proteinname = inputfile.replace('consensus.txt', '')
            openfile = open(pathps+inputfile,'r')
            self.legendpos += 1
            prev = 100000
            for line in openfile:
```

```
    if line.startswith('C'):
        pass
    else:
        line = line.split()
        line = [float(i) for i in line]
        linecount += 1
        conf = max(line)
        if prev == 100000:
            sstype = line.index(max(line))
            prev = sstype
        elif (line[0] == line[1]) and (line[0] == max(line)) and (line[1] ==
        max(line)):
            sstype = prev
        elif (line[0] == line[2]) and (line[0] == max(line)) and (line[2] ==
        max(line)):
            sstype = prev
        elif (line[1] == line[2]) and (line[1] == max(line)) and (line[2] ==
        max(line)):
            sstype = prev
        else:
            sstype = line.index(max(line))
            prev = sstype
        posstring +=
        '%.2f'%(conf)+'\t'+'%.2f'%(position)+'\t'+colour[sstype]+'\t'+'sstr'+'
        \n'
        position += 1.12
openfile.close()

textpos = -22-(len(proteinname)*22.166666666)
linelength = position
for k in sorted(self.d):
    if linecount > k:
        sb = k+100
        scalebar += self.d[k]
    else:
        pass
scalebar += self.d[sb]
scaleline = scalebar.split()
scalelineno = int(scaleline[len(scaleline)-7])+48
if self.inputloop == 'y':
    legendbox = '%i'%(scalelineno-430)+' -100 1 0.7 0.25
    rectangle\n%i'%(scalelineno-430)+' -150 0 0.3921 1
    rectangle\n%i'%(scalelineno-430)+' -200 .922 0.13 .922 rectangle\n'
    legendtext = '%i'%(scalelineno-335)+' -95 moveto\n( = Random Coil)
    show\n%i'%(scalelineno-335)+' -145 moveto\n( = Beta Sheet)
    show\n%i'%(scalelineno-335)+' -195 moveto\n( = Alpha Helix) show\n\n\n'
if self.inputloop == 'n':
    legendbox = '%i'%(scalelineno-430)+' -100 1 1 1
    rectangle\n%i'%(scalelineno-430)+' -150 0 0.3921 1
    rectangle\n%i'%(scalelineno-430)+' -200 .922 0.13 .922 rectangle\n'
    legendtext = '%i'%(scalelineno-335)+' -95 moveto\n()
    show\n%i'%(scalelineno-335)+' -145 moveto\n( = Beta Sheet)
    show\n%i'%(scalelineno-335)+' -195 moveto\n( = Alpha Helix) show\n\n\n'
template = '%!PS% definning sec str\n/sstr {\nsetcolor\n0 moveto\ndup\n0
exch 3 mul rlineto\
\nneg\n0 exch rmoveto\nstroke\n} def\n\n/rectangle {\nsetcolor\
\nmoveto\n0 30 rlineto\n80 0 rlineto\n0 -30 rlineto\nclosepath\nfill\nstroke\
\n} def\n\n%-90 rotate\n/DeviceRGB setcolorspace\n\ngsave\nnewpath\n90 rotate\
\n100 -95 translate\n0.3 .5 scale\n\n'+legendbox+'0 0 0 setcolor\n1
setlinewidth\n\n/Arial findfont\n25 scalefont\nsetfont\n\
\n'+legendtext+'%i'%(scalelineno)+' 50 moveto\n0 50 lineto\n0 56 %i'\
%(scalelineno)+'{\n50 moveto\n0 30 rlineto\n0 -30 rlineto\n}
for\n\nstroke\n\n/Arial findfont\
\n25 scalefont\nsetfont\n'+scalebar+'\n\n'
outstring = '% '+proteinname+'\n'+'0 0 0 setcolor\n'+'1 setlinewidth\n'+'0 0
translate\n\n'\
+'% Protein Name\n'+'%f'%(textpos)+' 5 moveto\n'+'/Arial findfont\n'+'35
scalefont\n'+'setfont\n'+\
'( '+proteinname+' ) show\n'+'%.2f '%(linelength+25)+'5
```

```
            moveto\n'+'(%i'%(linecount)+') show\n\n\n'+'%lgt\n'+\
            '0 0 moveto\n\n'+'%.2f'%(linelength)+' 0 rlineto\n'+'stroke\n'+'3
            setlinewidth\n'+posstring+'\n'
            out_file = open(pathout+proteinname+'.ps','w')
            out_file.write(template+'\n'+outstring)
            out_file.close()
            posstring = ''
            position = 0
            linecount = 0
            scalebar = ''
            sb = 0
def psmerge(self, pathout):     # Merges individual postscript files in numerical then
alphabetical order
    import os

    dirs = os.listdir(pathout)
    output = ''
    translate = 0
    x = 0
    y = 0
    aalength = 0
    z = []
    scalebar = ''
    sb = 0
    legendpos = (self.legendpos-1)*50

    if 'MergeFilemanual.ps' in dirs:
        dirs.remove('MergeFilemanual.ps')
    if '.DS_Store' in dirs:
        dirs.remove('.DS_Store')
    for inputfile in dirs:
        if inputfile.endswith('auto.ps'):
            pass
        elif inputfile.endswith('noloop.ps'):
            pass
        else:
            proteinname = inputfile.replace('.ps','')
            addon = '% '+proteinname+'\n0 0 0 setcolor\n1 setlinewidth\n0 %i
            translate\n\n'%(translate)
            output = output + addon
            openfile = open(pathout+inputfile,'r')
            for i, line in enumerate(openfile):
                if line == '% Protein Name\n':
                    x = i-1
                    y = i+7
                if x == 0:
                    pass
                else:
                    if i > x:
                        output += line
                    if y == i:
                        aalength = line.split()[0]
                        z.append(int(str(aalength).replace('(','').replace(')','')))
                    else:
                        pass

            for k in sorted(self.d):
                if max(z) > k:
                    sb = k+100
                    scalebar += self.d[k]
                else:
                    pass
            openfile.close()
            translate = -50
        scalebar += self.d[sb]
        scaleline = scalebar.split()
        scalelineno = int(scaleline[len(scaleline)-7])+48
        if self.inputloop == 'y':
            legendbox = '%i'%(scalelineno-430)+' %i'%(-legendpos)+' 1 0.7 0.25
```

```
            rectangle\n%i'%(scalelineno-430)+' %i'%(-legendpos-50)+' 0 0.3921 1
            rectangle\n%i'%(scalelineno-430)+' %i'%(-legendpos-100)+' .922 0.13 .922
            rectangle\n'
            legendtext = '%i'%(scalelineno-335)+' %i'%(-legendpos+5)+' moveto\n( =
            Random Coil) show\n%i'%(scalelineno-335)+' %i'%(-legendpos-45)+' moveto\n( =
            Beta Sheet) show\n%i'%(scalelineno-335)+' %i'%(-legendpos-95)+' moveto\n( =
            Alpha Helix) show\n\n\n'
        if self.inputloop == 'n':
            legendbox = '%i'%(scalelineno-430)+' %i'%(-legendpos)+' 1 1 1
            rectangle\n%i'%(scalelineno-430)+' %i'%(-legendpos-50)+' 0 0.3921 1
            rectangle\n%i'%(scalelineno-430)+' %i'%(-legendpos-100)+' .922 0.13 .922
            rectangle\n'
            legendtext = '%i'%(scalelineno-335)+' %i'%(-legendpos+5)+' moveto\n()
            show\n%i'%(scalelineno-335)+' %i'%(-legendpos-45)+' moveto\n( = Beta Sheet)
            show\n%i'%(scalelineno-335)+' %i'%(-legendpos-95)+' moveto\n( = Alpha Helix)
            show\n\n\n'

        template = '%!PS% definning sec str\n/sstr {\nsetcolor\n0 moveto\ndup\n0 exch 3
        mul rlineto\
        \nneg\n0 exch rmoveto\nstroke\n} def\n\n/rectangle {\nsetcolor\
        \nmoveto\n0 30 rlineto\n80 0 rlineto\n0 -30 rlineto\nclosepath\nfill\nstroke\
        \n} def\n\n%-90 rotate\n/DeviceRGB setcolorspace\n\ngsave\nnewpath\n90 rotate\
        \n100 -95 translate\n0.3 .5 scale\n\n'+legendbox+'0 0 0 setcolor\n1
        setlinewidth\n\n/Arial findfont\n25 scalefont\nsetfont\n\
        \n'+legendtext+'%i'%(scalelineno)+' 50 moveto\n0 50 lineto\n0 56\
        %i'%(scalelineno)+' {\n50 moveto\n0 30 rlineto\n0 -30 rlineto\n}
        for\n\nstroke\n\n/Arial findfont\
        \n25 scalefont\nsetfont\n'+scalebar+'\n\n\n'

        outputfile = open(pathout+'MergeFilemanual.ps','w')
        outputfile.write(template+output)
        outputfile.close()
        x = 0
        scalebar = ''

first = SSparse()
first.deldirs()
first.mkdirs()
first.runscript()
```

Appendix 5.2. Python code for the secondary structure element (SSE) consensus and visual output tool. To run, navigate to the directory where the predicted SSE sequences are located (in text format with Psipred syntax) using the Unix command-line interpreter and execute the script using Python. The tool will output the consensus SSE sequence as a .txt file and in a visual format (for an example, refer to Figure 5.1) which can be read using a PostScript viewing software.

```
class identifyMC:
    def __init__(self):
        import os, subprocess
        self.path =
        '/Users/omarti03-2/Desktop/Rotation_2/Ct_genome_ss_pred/L2_serovar/textfiles/Consensus
        _preds/'
        self.dirs = os.listdir(self.path)
        subprocess.Popen(['mkdir','-p', self.path+'mcprots2'])
    def firstpass(self):
        import subprocess
        subprocess.Popen(['mkdir','-p', self.path+'failed2'])
        for inputfile in self.dirs:
            if inputfile.endswith('consensus.txt'):
                openfile = open(self.path+inputfile,'r')
                for i, l in enumerate(openfile):
                    pass
                if i < 450:
                    subprocess.Popen(['mv', self.path+inputfile, self.path+'failed2/'])
    def solenoid(self):                 #FOR ALPHA SOLENOID
        import os, subprocess
        subprocess.Popen(['mkdir','-p', self.path+'pass2'])
        self.dirs = os.listdir(self.path)
        for inputfile in self.dirs:
            if inputfile.endswith('consensus.txt'):
                count = 0
                length = 0
                Ecount = 0
                Xcount = 0
                prev = []
                openfile = open(self.path+inputfile,'r')
                for line in openfile:
                    if line.startswith('C'):
                        pass
                    else:
                        line = line.split()
                        if Ecount > 0:
                            count += 1
                            prev = line
                            if line.index(max(line)) == 1:
                                Ecount += 1
                                if Ecount > 10:
                                    count = 0
                            if count > length:
                                length = count
                            if Xcount > 20:
                                Ecount = 0
                                Xcount = 0
                            if line.index(max(line)) == 0:
                                Xcount += 1
                            if line.index(max(line)) == 2:
                                Xcount += 1
                        elif line.index(max(line)) == 1:
                            if prev.index(max(prev)) == 0:
                                prev = line
                            elif prev.index(max(prev)) == 2:
                                prev = line
                            else:
                                prev = line
                                Ecount += 1
                                if Ecount > 10:
                                    count = 0
                        else:
                            count += 1
                            prev = line
                            if count > length:
                                length = count
                if length > 200:
                    if length < 1000:
                        subprocess.Popen(['mv', self.path+inputfile, self.path+'pass2/'])
```

```
    def solenoid2(self):
        outfile = open(self.path+'mcprots2/Loop_helix_hits.txt','w')
        import os
        self.dirs = os.listdir(self.path+'pass2')
        file_count = 0
        for inputfile in self.dirs:
            if inputfile.endswith('consensus.txt'):
                helix_count = 0
                loop_count = 0
                total_count = 0
                openfile = open(self.path+'pass2/'+inputfile,'r')
                for line in openfile:
                    if line.startswith('C'):
                        pass
                    else:
                        total_count += 1
                        line = line.split()
                        if line.index(max(line)) == 0:
                            loop_count += 1
                        if line.index(max(line)) == 2:
                            helix_count += 1
                if ((float(loop_count)+float(helix_count))/float(total_count))*100 > 90:
                    if (float(helix_count)/float(total_count))*100 > 40:
                        outfile.write(inputfile.replace('consensus.txt','')+'\n')
                        openfile.close()
runit = identifyMC()
runit.firstpass()
runit.solenoid()
runit.solenoid2()
```

Appendix 5.3. Python code for filtering consensus secondary structure element (SSE) sequences to identify α-solenoid proteins. To run, replace the object self.path with the location of the directory where the consensus SSE sequences generated from the SSE consensus tool are located in .txt format, and execute the script using Python. The tool will generate a list of the input proteins whose SSE sequences conform to the parameters defined in Figure 5.2.

Appendix 5.4. Consensus secondary structure sequences of predicted α-solenoid proteins following filtering of the *C. trachomatis* proteome. The consensus secondary structure element (SSE) sequence was determined for each protein in the *C. trachomatis* proteome from three prediction algorithms, PsiPred, Jpred and RaptorX. The SSE sequences were then filtered for proteins with an α-solenoid fold using parameters (as defined in figure 5.2) devised from analysis of the secondary structure sequence of structural Nups and importin-β. The SSE sequences of the 55 remaining proteins are shown. Accession identifiers correspond to entries in the UniParc database. β-sheets are represented in blue, α-helixes in pink, whilst coil residues are not shown. Vertical scale bar, confidence (Conf) scored from 0-9. Horizontal scale bar, residue number.

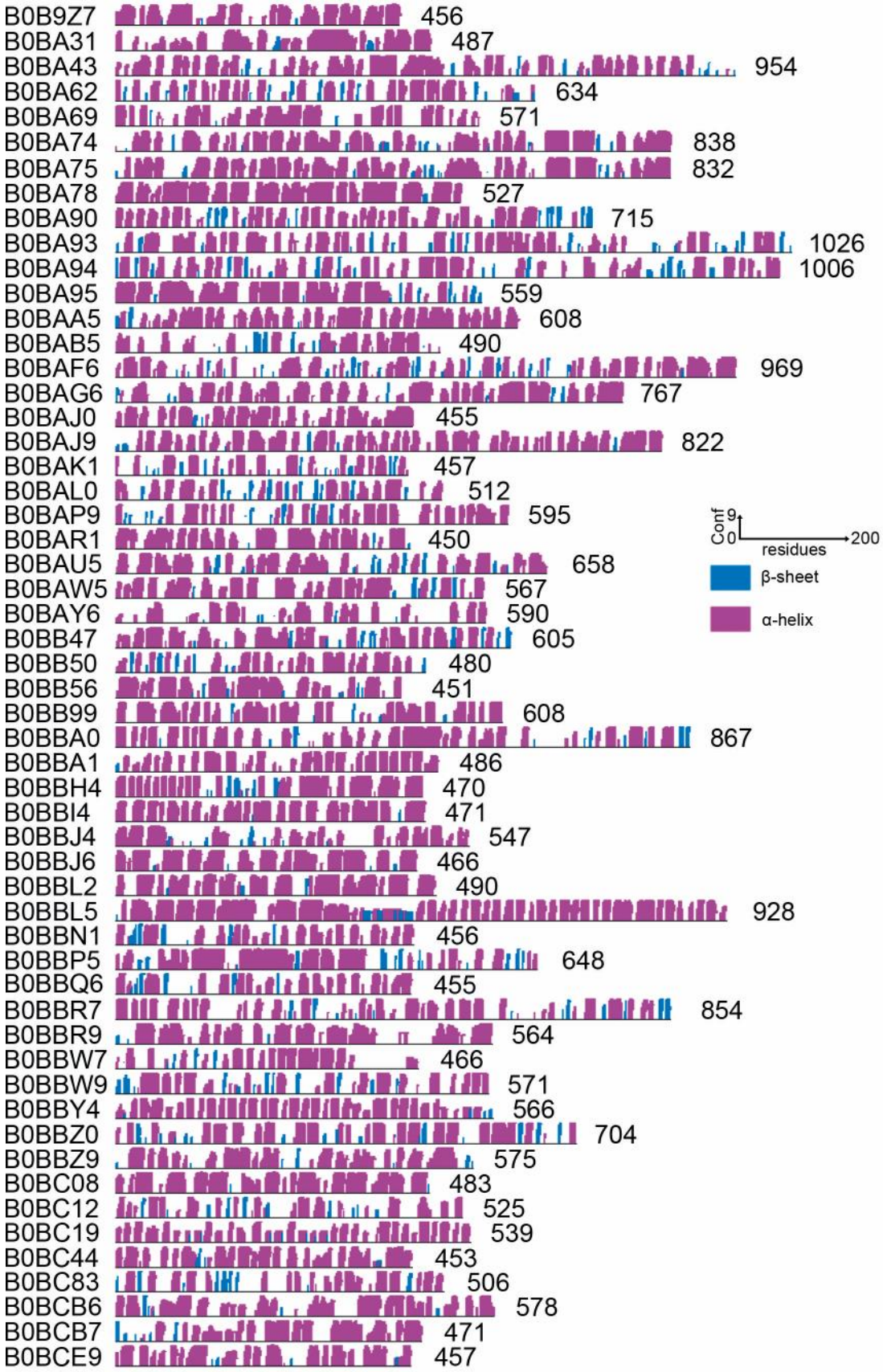
B0B9Z7 456
B0BA31 487
B0BA43 954
B0BA62 634
B0BA69 571
B0BA74 838
B0BA75 832
B0BA78 527
B0BA90 715
B0BA93 1026
B0BA94 1006
B0BA95 559
B0BAA5 608
B0BAB5 490
B0BAF6 969
B0BAG6 767
B0BAJ0 455
B0BAJ9 822
B0BAK1 457
B0BAL0 512
B0BAP9 595
B0BAR1 450
B0BAU5 658
B0BAW5 567
B0BAY6 590
B0BB47 605
B0BB50 480
B0BB56 451
B0BB99 608
B0BBA0 867
B0BBA1 486
B0BBH4 470
B0BBI4 471
B0BBJ4 547
B0BBJ6 466
B0BBL2 490
B0BBL5 928
B0BBN1 456
B0BBP5 648
B0BBQ6 455
B0BBR7 854
B0BBR9 564
B0BBW7 466
B0BBW9 571
B0BBY4 566
B0BBZ0 704
B0BBZ9 575
B0BC08 483
B0BC12 525
B0BC19 539
B0BC44 453
B0BC83 506
B0BCB6 578
B0BCB7 471
B0BCE9 457
Conf
9
0
200
residues
β-sheet
α-helix

>CT234 (O84237)
MLLFYKGSGSLRALRFLLSLRRGEEKRALLFLLLGLIWSVACYGSLALGESLFLEEIGAE
KLPFAYLGASFFLCFISCLILYNLSRKRVSPKALFLSFISCVLICNLYLFWHLAIHKGVS
GTPTFLYRILIWGLTILCYANFWGFIDQFFNIQDAKRHFCIFNAITFCGDFLGARIVNQI
QYLGAELILLAFIVVITFIFPLVHYISSSLKELSEDHNLFLDTGYPPSTKQTLKLCLKDK
YTFYLVSFYFLMQLLVVFTEFNYLKIFDAQFGNAETCELTENFTKYSSWISLGNMFFALF
AYSRVITRFGINNIILFAPICFFSLFCCWSIKTSVFIATMGMIAREGLAYALDDNNLQLL
IYGIPNKIRNQVRIAIESFVEPAGMFICALLCLFIPHQYVLCIIISAVCILLAILLRTHY
SKAILRNLSLESIHRRRSIREWFADMNDTEKRQAEILLLTHLKNPQERNQMFAFQHLLNL
KNRAVLPNLLLHMNKLGLSGKLKTLNMLKNSVWAKDFLTLELLKRWSSLPQHPTIAAALH
LYFVEHDLLHVSDIADDLYDQSGDRLFAAVLIVRKHKPSGEYQALAEKHLSEILESEDPE
LIIKGLSILALERSPSNFPIILPFLTHPNEQVFLQACLSLETCADKQYAQYGRTVLNTLK
KTKDTQAAQALLNTLAALLDASLVYEFVLASVQLKNVLRKLAETILASLPKECIPILIEM
VADHSLHNSCRIMAAKALSHIDSRQLKRLALKILKSKAAKTLFYDYHKNFIQKRYPRYDL
HLLIESLEANYQAEVNFMLAFLAIVGSSDYADVLIRSLTGKNLKARAQALESLEKDCENH
LFTLVTPFVYRDKHTSDEKYYMKKGVEPLAIEELLNRLEQTPFLFSKLIAQQLKEELSLC
DAEFSSALQSFAKKQKTSILSREYITSS

>CT350 (O84354)
MGLSRLAFISFLSFTLSASCDFPSSVSQRILFSCRKSVPQALEAYLEASATYQQHDFSVL
RVIAESYLQQSFLSEDTYIRKSAIIGAGLSGSSEALELLSEAIETQDLYEQLLILNAATS
QLSKTSDKLLFKGLTASHPVIRLEAAYRLACMKNSKVSDYLYSFIYKLPEEIQNLAATIF
LQLETEEADAYIHHLLSSPNNLTRNYVAYLIGEYKQKRFLPTLRSLLTSASPLDQEGALY
ALGKLEDSGSYPRIKALSSRSNPEVVLAAAQTLLFLEKEEEALPILTNLCQQKLLRALYT
ARFLSQEKGEELLLPIFYNATQEEIRLNTALALVHQGCTDPQVLHYLTEILESKVLHRIF
LPTHSTGKAIQFWKECTTFPLMSQEDKMRTLAMYRVAEDTILSALLKLPNDAYLPYLERI
LASQKTILAAKAIAFLSVTAHPQALSLVSKAALTPGDPIIRAYANLALYTMTKDPEKKAV
LYRYAEQLIEDTILFTDAENPLPSPSSSYLRYQVSPETRTQLMLAILETLVSSKTDEDIR
VFLSLMKKTHYKNIPILSGLLMRIVE

>CT384 (O84389)
MCCVDGSNSIQQRMRFCEYRTAAQEAKTSLSSDCSLLEARLALRALAKHHEYSAWREAFL
RSQERFPSLEADRDIHEDLAASLLQKNIRHSSLTVRVITILAVGMARDYRLVPIVLQALS
DDSDTVREIAVQVAVMYGSSCLLRAVGDLAKNDSSIQVRITAYRAAAVLEIQDLVPHLRV
VVQNTQLDGTERREAWRSLCVLTRPHSGVLTGIDQALMTCEMLKEYPEKCTEEQIRTLLA
ADHPEVQVATLQIILRGGRVFRSSSIMESVQKLACNSLSARVQMQAAAILYLEGDPFGED
KLTEGLSATSSILCEAASEAVCSLGIHGVHLAGRFLSKVQGMRSRVNLAFALLVSREKVE
EAGDVVASFIHRIEPCRAIEQFLCEDQKIFVASSPLQVEIMKRDLAKKIIRLLVAAQYSK
AKMVVAQYLAGQQVGWSFCSEVFWEEGDSEDFVEPLQEESFAFALEKALSFLQREGGEAG
LHAVISLYPHSRWQDKLTILEAIAYSENRIATCFLRERCLQEAASLQSAAAGAVFALFK

Appendix 5.5. Amino acid sequences and UniProt database accession numbers of identified *C. trachomatis* α-solenoid proteins in FASTA format.

Appendix Chapter 6

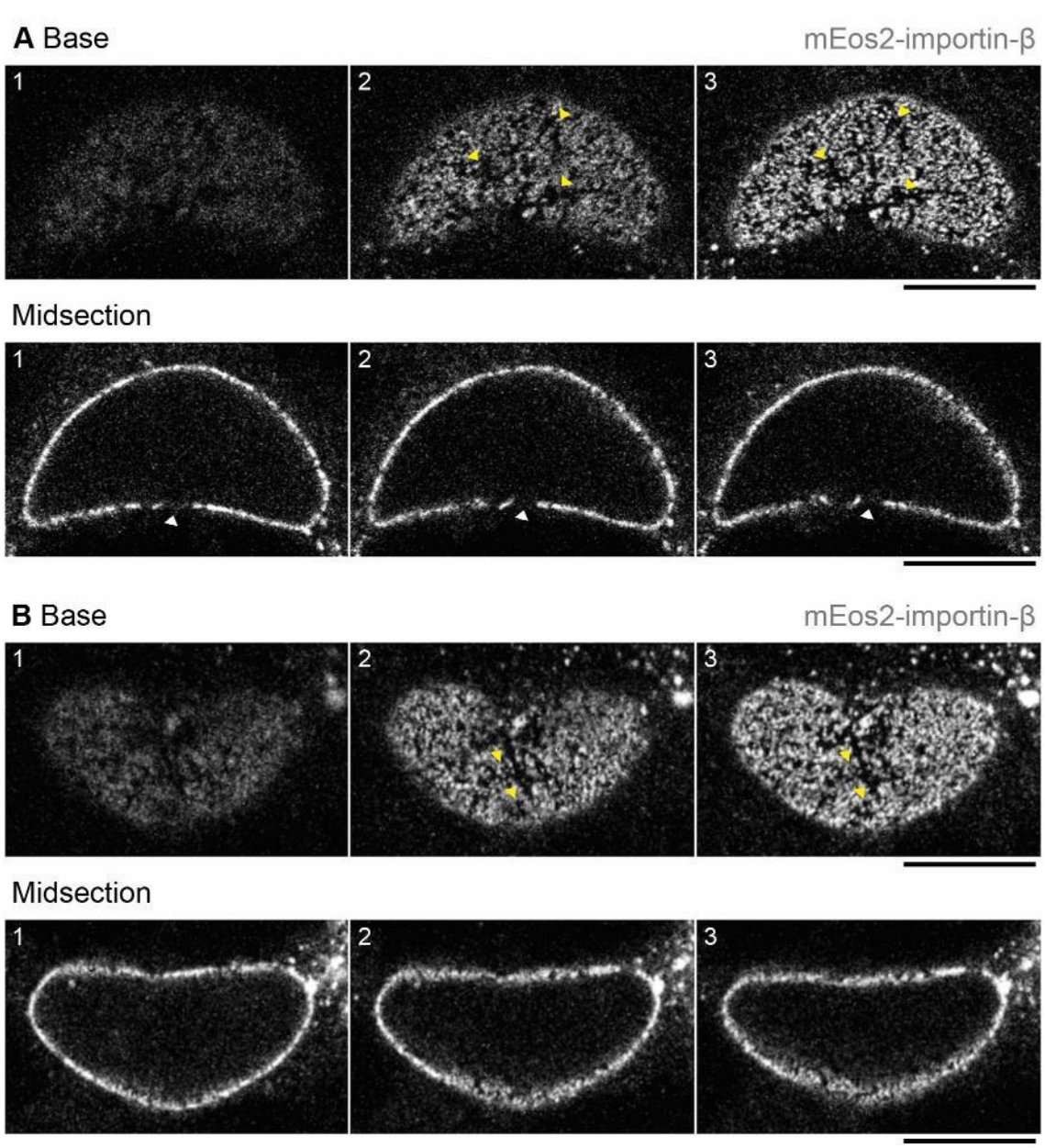

Appendix 6.1. Regions lacking mEos2-importin-β equivalent to pore-free islands are present at the nuclear surface in *Chlamydia*-infected cells. HeLa cells transiently expressing mEos2-importin-β (grey) were infected with *C. trachomatis* LGV2 and fixed at 48 hours post infection. Panels at the base and midsection of the nuclei are shown, ascending in the z dimension through the cell (1-3) with a step of 0.34 µm. (A) Nucleus equivalent to the upper panels in figure 4.7B. (B) Nucleus equivalent to the lower panels in figure 4.7B. Pore-free islands in the nuclei are indicated by yellow arrowheads, areas of importin-β depletion are highlighted by white arrowheads. Scale bars, 10 µm.

Bibliography

Agaisse, H. and Derré, I. (2014). "Expression of the effector protein IncD in *Chlamydia trachomatis* mediates recruitment of the lipid Transfer protein CERT and the endoplasmic reticulum-resident protein VAPB to the inclusion membrane." **Infection and immunity.** 82 (5): 2037-2047.

Ajonuma, C. L., Fok, L. K., Ho, S. L., et al. (2010). "CFTR is required for cellular entry and internalization of *Chlamydia trachomatis*." **Cell Biology International.** 34 (6): 593-600.

Akpan, N., Serrano-Saiz, E., Zacharia, B. E., et al. (2011). "Intranasal delivery of caspase-9 inhibitor reduces caspase-6-dependent axon/neuron loss and improves neurological function after stroke." **The Journal of neuroscience : the official journal of the Society for Neuroscience.** 31 (24): 8894-8904.

Al-Younes, H. M., Al-Zeer, M. A., Khalil, H., et al. (2011). "Autophagy-independent function of MAP-LC3 during intracellular propagation of *Chlamydia trachomatis*." **Autophagy.** 7 (8): 814-828.

Al-Zeer, M. A., Al-Younes, H. M., Kerr, M., et al. (2014). "*Chlamydia trachomatis* remodels stable microtubules to coordinate Golgi stack recruitment to the chlamydial inclusion surface." **Molecular microbiology.** 94 (6): 1285-1297.

Al Haboubi, T., Shumaker, D., Köser, J., et al. (2011). "Distinct association of the nuclear pore protein Nup153 with A- and B-type lamins." **Nucleus.** 2 (5): 500-509.

Alber, F., Dokudovskaya, S., Veenhoff, L., et al. (2007). "The molecular architecture of the nuclear pore complex." **Nature.** 450 (7170): 695-701.

Alzhanov, D., Weeks, S., Burnett, J., et al. (2009). "Cytokinesis is blocked in mammalian cells transfected with *Chlamydia trachomatis* gene CT223." **BMC Microbiology.** 9: 2-2.

Amendola, M. and van Steensel, B. (2014). "Mechanisms and dynamics of nuclear lamina–genome interactions." **Current Opinion in Cell Biology.** 28: 61-68.

Andrade, M. A., Perez-Iratxeta, C. and Ponting, C. P. (2001). "Protein Repeats: Structures, Functions, and Evolution." **Journal of structural biology.** 134 (2–3): 117-131.

Andrew, S. (2014). Potassium homeostasis during intracellular *Chlamydia* development. PhD Thesis. Institute of Structural and Molecular Biology, **University College London**.

Arbibe, L., Kim, D. W., Batsche, E., et al. (2007). "An injected bacterial effector targets chromatin access for transcription factor NF-[kappa]B to alter transcription of host genes involved in immune responses." **Nat Immunol.** 8 (1): 47-56.

Armstrong, J. A. and Reed, S. E. (1964). "NATURE AND ORIGIN OF INITIAL BODIES IN LYMPHOGRANULOMA VENEREUM." **Nature.** 201: 371-373.

Arnold, R., Brandmaier, S., Kleine, F., et al. (2009). "Sequence-based prediction of type III secreted proteins." **PLoS Pathogens.** 5 (4).

Arnold, R., Brandmaier, S., Kleine, F., et al. (2009). "Sequence-Based Prediction of Type III Secreted Proteins." **Plos Pathogens.** 5 (4): e1000376.

Babbio, F., Castiglioni, I., Cassina, C., et al. (2012). "Knock-down of methyl CpG-binding protein 2 (MeCP2) causes alterations in cell proliferation and nuclear lamins expression in mammalian cells." **BMC cell biology.** 13: 19-19.

Bannantine, Griffiths, Viratyosin, et al. (2000). "A secondary structure motif predictive of protein localization to the chlamydial inclusion membrane." **Cellular Microbiology.** 2 (1): 35-47.

Bannantine, J. P., Stamm, W. E., Suchland, R. J., et al. (1998). "*Chlamydia trachomatis* IncA is localized to the inclusion membrane and is recognized by antisera from infected humans and primates." **Infection and immunity.** 66 (12): 6017-6021.

Barker, J. R., Koestler, B. J., Carpenter, V. K., et al. (2013). "STING-dependent recognition of cyclic di-AMP mediates type I interferon responses during *Chlamydia trachomatis* infection." **mBio.** 4 (3): e00018-00013.

Bártová, E., Krejčí, J., Harničarová, A., et al. (2008). "Histone modifications and nuclear architecture: A review." **Journal of Histochemistry and Cytochemistry.** 56 (8): 711-721.

Baud, D., Regan, L. and Greub, G. (2008). "Emerging role of *Chlamydia* and *Chlamydia*-like organisms in adverse pregnancy outcomes." **Current opinion in infectious diseases.** 21 (1): 70-76.

Bauler, L. D. and Hackstadt, T. (2014). "Expression and targeting of secreted proteins from *Chlamydia trachomatis*." **Journal of Bacteriology.** 196 (7): 1325-1334.

Beatty, W. L. (2006). "Trafficking from CD63-positive late endocytic multivesicular bodies is essential for intracellular development of *Chlamydia trachomatis*." **Journal of Cell Science.** 119 (2): 350-359.

Beatty, W. L. (2007). "Lysosome repair enables host cell survival and bacterial persistence following *Chlamydia trachomatis* infection." **Cellular Microbiology.** 9 (9): 2141-2152.

Beatty, W. L., Belanger, T. A., Desai, A. A., et al. (1994). "Tryptophan depletion as a mechanism of gamma interferon-mediated chlamydial persistence." **Infection and immunity.** 62 (9): 3705-3711.

Bébéar, C. and de Barbeyrac, B. (2009). "Genital *Chlamydia trachomatis* infections." **Clinical microbiology and infection.** 15 (1): 4-10.

Bedson, S. P. and Gostling, J. V. T. (1954). "A STUDY OF THE MODE OF MULTIPLICATION OF PSITTACOSIS VIRUS." **British Journal of Experimental Pathology.** 35 (3): 299-308.

Bell, E. S. and Lammerding, J. (2016). "Causes and consequences of nuclear envelope alterations in tumour progression." **European journal of cell biology.**

Belland, R. J., Zhong, G., Crane, D. D., et al. (2003). "Genomic transcriptional profiling of the developmental cycle of *Chlamydia trachomatis*." **Proceedings of the National Academy of Sciences of the United States of America.** 100 (14): 8478-8483.

Ben-Efraim, I., Frosst, P. and Gerace, L. (2009). "Karyopherin binding interactions and nuclear import mechanism of nuclear pore complex protein Tpr." **BMC cell biology.** 10: 74-74.

Ben-Harush, K., Wiesel, N., Frenkiel-Krispin, D., et al. (2009). "The supramolecular organization of the *C. elegans* nuclear lamin filament." **Journal of molecular biology.** 386 (5): 1392-1402.

Bernardi, R. and Pandolfi, P. (2007). "Structure, dynamics and functions of promyelocytic leukaemia nuclear bodies." **Nature reviews. Molecular cell biology.** 8 (12): 1006-1016.

Bernstein-Hanley, I., Coers, J., Balsara, Z. R., et al. (2006). "The p47 GTPases Igtp and Irgb10 map to the *Chlamydia trachomatis* susceptibility locus Ctrq-3 and mediate cellular resistance in mice." **Proceedings of the National Academy of Sciences of the United States of America.** 103 (38): 14092-14097.

Bierne, H. and Cossart, P. (2012). "When bacteria target the nucleus: the emerging family of nucleomodulins." **Cellular Microbiology.** 14 (5): 622-633.

Boiko, E., Maltsev, D., Savicheva, A., et al. (2015). "Infection of human retinal pigment epithelium with *Chlamydia trachomatis*." **Plos One.** 10 (11): e0141754.

Boisvert, F. o.-M., van Koningsbruggen, S., NavascuÃƒs, J. n., et al. (2007). "The multifunctional nucleolus." **Nature reviews. Molecular cell biology.** 8 (7): 574-585.

Booth-Gauthier, Elizabeth A., Alcoser, Turi A., Yang, G., et al. (2012). "Force-induced changes in subnuclear movement and rheology." **Biophysical journal.** 103 (12): 2423-2431.

Brennan, D. F. and Barford, D. (2009). "Eliminylation: a post-translational modification catalyzed by phosphothreonine lyases." **Trends in Biochemical Sciences.** 34 (3): 108-114.

Brinkworth, A. J., Malcolm, D. S., Pedrosa, A. T., et al. (2011). "*Chlamydia trachomatis* Slc1 is a type III secretion chaperone that enhances the translocation of its invasion effector substrate TARP." **Molecular microbiology.** 82 (1): 131-144.

Broers, J. L., Machiels, B. M., van Eys, G. J., et al. (1999). "Dynamics of the nuclear lamina as monitored by GFP-tagged A-type lamins." **Journal of Cell Science.** 112 (20): 3463-3475.

Broers, J. L. V., Peeters, E. A. G., Kuijpers, H. J. H., et al. (2004). "Decreased mechanical stiffness in *LMNA*−/− cells is caused by defective nucleo-cytoskeletal integrity: implications for the development of laminopathies." **Human Molecular Genetics.** 13 (21): 2567-2580.

Brown, H. M., Knowlton, A. E. and Grieshaber, S. S. (2012). "Chlamydial infection induces host cytokinesis failure at abscission." **Cellular Microbiology.** 14 (10): 1554-1567.

Brown, H. M., Knowlton, A. E., Snavely, E., et al. (2014). "Multinucleation during *C. trachomatis* infections is caused by the contribution of two effector pathways." **Plos One.** 9 (6): e100763.

Buckner, L., Lewis, M., Greene, S., et al. (2013). "*Chlamydia trachomatis* infection results in a modest pro-inflammatory cytokine response and a decrease in T cell chemokine secretion in human polarised endocervical epithelial cells." **Cytokine.** 63 (2): 151-165.

Burke, B. and Roux, K. J. (2009). "Nuclei take a position: managing nuclear location." **Developmental Cell.** 17 (5): 587-597.

Burke, B. and Stewart, C. L. (2002). "Life at the edge: the nuclear envelope and human disease." **Nat Rev Mol Cell Biol.** 3 (8): 575-585.

Caldwell, H. D., Kromhout, J. and Schachter, J. (1981). "Purification and partial characterization of the major outer membrane protein of *Chlamydia trachomatis*." **Infection and immunity.** 31 (3): 1161-1176.

Camozzi, D., Pignatelli, S., Valvo, C., et al. (2008). "Remodelling of the nuclear lamina during human cytomegalovirus infection: role of the viral proteins pUL50 and pUL53." **Journal of General Virology.** 89 (3): 731-740.

Capmany, A. and Damiani, M. T. (2010). "*Chlamydia trachomatis* intercepts Golgi-derived sphingolipids through a Rab14-mediated transport required for bacterial development and replication." **Plos One.** 5 (11): e14084.

Carabeo, R. A., Grieshaber, S. S., Fischer, E., et al. (2002). "*Chlamydia trachomatis* induces remodeling of the actin cytoskeleton during attachment and entry into HeLa cells." **Infection and immunity.** 70 (7): 3793-3803.

Carabeo, R. A., Grieshaber, S. S., Hasenkrug, A., et al. (2004). "Requirement for the Rac GTPase in *Chlamydia trachomatis* invasion of non-phagocytic cells." **Traffic.** 5 (6): 418-425.

Carpenter, A. E., Jones, T. R., Lamprecht, M. R., et al. (2006). "CellProfiler: image analysis software for identifying and quantifying cell phenotypes." **Genome Biology.** 7 (10): R100-R100.

Castelló, A., Izquierdo, J. M., Welnowska, E., et al. (2009). "RNA nuclear export is blocked by poliovirus 2A protease and is concomitant with nucleoporin cleavage." **Journal of Cell Science.** 122 (20): 3799-3809.

Caturegli, P., Asanovich, K. M., Walls, J. J., et al. (2000). "ankA: an *Ehrlichia phagocytophila* group gene encoding a cytoplasmic protein antigen with ankyrin repeats." **Infection and immunity.** 68 (9): 5277-5283.

Chang, J., Chen, J. and Zhou, D. (2005). "Delineation and characterization of the actin nucleation and effector translocation activities of *Salmonella* SipC." **Molecular microbiology.** 55 (5): 1379-1389.

Chen, A. L., Johnson, K. A., Lee, J. K., et al. (2012). "CPAF: A chlamydial protease in search of an authentic substrate." **PLoS Pathogens.** 8 (8): e1002842.

Chen, D., Lei, L., Lu, C., et al. (2010). "Secretion of the chlamydial virulence factor CPAF requires the Sec-dependent pathway." **Microbiology.** 156 (Pt 10): 3031-3040.

Choo, K. H., Tan, T. W. and Ranganathan, S. (2009). "A comprehensive assessment of N-terminal signal peptides prediction methods." **BMC bioinformatics.** 10 (Suppl 15): S2-S2.

Chumduri, C., Gurumurthy, Rajendra K., Zadora, Piotr K., et al. (2013). "*Chlamydia* infection promotes host DNA damage and proliferation but impairs the DNA damage response." **Cell Host & Microbe.** 13 (6): 746-758.

Clark, R. B., Schatzki, P. F. and Dalton, H. P. (1982). "Ultrastructural analysis of the effects of erythromycin on the morphology and developmental cycle of *Chlamydia trachomatis* HAR-13." **Archives of Microbiology.** 133 (4): 278-282.

Clarke, I. N. (2011). "Evolution of *Chlamydia trachomatis*." **Annals of the New York Academy of Sciences.** 1230 (1): E11-E18.

Clausen, J. D., Christiansen, G., Holst, H. U., et al. (1997). "*Chlamydia trachomatis* utilizes the host cell microtubule network during early events of infection." **Molecular microbiology.** 25 (3): 441-449.

Clifton, D., Fields, K., Grieshaber, S., et al. (2004). "A chlamydial type III translocated protein is tyrosine-phosphorylated at the site of entry and associated with recruitment of actin." **Proceedings of the National Academy of Sciences of the United States of America.** 101 (27): 10166-10171.

Clifton, D. R., Fields, K. A., Grieshaber, S. S., et al. (2004). "A chlamydial type III translocated protein is tyrosine-phosphorylated at the site of entry and associated with recruitment of actin." **Proceedings of the National Academy of Sciences of the United States of America.** 101 (27): 10166-10171.

Cocchiaro, J. L., Kumar, Y., Fischer, E. R., et al. (2008). "Cytoplasmic lipid droplets are translocated into the lumen of the *Chlamydia trachomatis* parasitophorous vacuole." **Proceedings of the National Academy of Sciences.** 105 (27): 9379-9384.

Coles, A. (1930). "MICRO-ORGANISMS IN PSITTACOSIS." **The Lancet.** 215 (5567): 1011-1012.

Coles, A. M., Reynolds, D. J., Harper, A., et al. (1993). "Low-nutrient induction of abnormal chlamydial development: A novel component of chlamydial pathogenesis?" **FEMS Microbiology Letters.** 106 (2): 193-200.

Costa, T. R. D., Felisberto-Rodrigues, C., Meir, A., et al. (2015). "Secretion systems in Gram-negative bacteria: structural and mechanistic insights." **Nat Rev Micro.** 13 (6): 343-359.

Cremer, T. and Cremer, M. (2010). "Chromosome territories." **Cold Spring Harbor perspectives in biology.** 2 (3): a003889.

Crisp, M., Liu, Q., Roux, K., et al. (2006). "Coupling of the nucleus and cytoplasm: role of the LINC complex." **The Journal of cell biology.** 172 (1): 41-53.

Croft, J. A., Bridger, J. M., Boyle, S., et al. (1999). "Differences in the localization and morphology of chromosomes in the human nucleus." **The Journal of cell biology.** 145 (6): 1119-1131.

Cronshaw, J. M., Krutchinsky, A. N., Zhang, W., et al. (2002). "Proteomic analysis of the mammalian nuclear pore complex." **The Journal of cell biology.** 158 (5): 915-927.

Cuff, J. A., Clamp, M. E., Siddiqui, A. S., et al. (1998). "JPred: a consensus secondary structure prediction server." **Bioinformatics.** 14 (10): 892-893.

Dahl, K. N., Kahn, S. M., Wilson, K. L., et al. (2004). "The nuclear envelope lamina network has elasticity and a compressibility limit suggestive of a molecular shock absorber." **Journal of Cell Science.** 117 (20): 4779-4786.

Dahl, K. N., Ribeiro, A. J. S. and Lammerding, J. (2008). "Nuclear shape, mechanics, and mechanotransduction." **Circulation research.** 102 (11): 1307-1318.

Dahl, K. N., Scaffidi, P., Islam, M. F., et al. (2006). "Distinct structural and mechanical properties of the nuclear lamina in Hutchinson–Gilford progeria syndrome." **Proceedings of the National Academy of Sciences of the United States of America.** 103 (27): 10271-10276.

de las Heras, J. I., Batrakou, D. G. and Schirmer, E. C. (2013). "Cancer biology and the nuclear envelope: A convoluted relationship." **Seminars in Cancer Biology.** 23 (2): 125-137.

Dechat, T., Gajewski, A., Korbei, B., et al. (2004). "LAP2α and BAF transiently localize to telomeres and specific regions on chromatin during nuclear assembly." **Journal of Cell Science.** 117 (25): 6117-6128.

Dehoux, P., Flores, R., Dauga, C., et al. (2011). "Multi-genome identification and characterization of chlamydiae-specific type III secretion substrates: the Inc proteins." **BMC Genomics.** 12: 109-109.

Delevoye, C., Nilges, M., Dehoux, P., et al. (2008). "SNARE Protein Mimicry by an Intracellular Bacterium." **PLoS Pathogens.** 4 (3): e1000022.

Derré, I., Swiss, R. and Agaisse, H. (2011). "The lipid transfer protein CERT interacts with the *Chlamydia* inclusion protein IncD and participates to ER-*Chlamydia* inclusion membrane contact sites." **PLoS Pathogens.** 7 (6): e1002092.

Devos, D., Dokudovskaya, S., Alber, F., et al. (2004). "Components of coated vesicles and nuclear pore complexes share a common molecular architecture." **PLoS biology.** 2 (12).

Devos, D., Dokudovskaya, S., Williams, R., et al. (2006). "Simple fold composition and modular architecture of the nuclear pore complex." **Proceedings of the National Academy of Sciences of the United States of America.** 103 (7): 2172-2177.

Devos, D. P. (2012). "Regarding the presence of membrane coat proteins in bacteria: Confusion? What confusion?" **BioEssays.** 34 (1): 38-39.

Ding, H., Gong, S., Tian, Y., et al. (2013). "Transformation of sexually transmitted infection-causing serovars of *Chlamydia trachomatis* using blasticidin for selection." **Plos One.** 8 (11): e80534.

Dingwall, C. and Laskey, R. A. (1991). "Nuclear targeting sequences — a consensus?" **Trends in Biochemical Sciences.** 16: 478-481.

Ditsworth, D., Zong, W.-X. and Thompson, C. B. (2007). "Activation of poly(ADP)-ribose polymerase (PARP-1) induces release of the pro-inflammatory mediator HMGB1 from the nucleus." **Journal of Biological Chemistry.** 282 (24): 17845-17854.

Donahue, D. A., Amraoui, S., di Nunzio, F., et al. (2016). "SUN2 overexpression deforms nuclear shape and inhibits HIV." **Journal of Virology.**

Dong, F., Pirbhai, M., Xiao, Y., et al. (2005). "Degradation of the proapoptotic proteins Bik, Puma, and Bim with Bcl-2 domain 3 homology in *Chlamydia trachomatis*-infected cells." **Infection and immunity.** 73 (3): 1861-1864.

Dong, X., Lu, X. and Zhang, Z. (2015). "BEAN 2.0: an integrated web resource for the identification and functional analysis of type III secreted effectors." **Database: The Journal of Biological Databases and Curation.** 2015: bav064.

Dorner, D., Gotzmann, J. and Foisner, R. (2007). "Nucleoplasmic lamins and their interaction partners, LAP2α, Rb, and BAF, in transcriptional regulation." **FEBS Journal.** 274 (6): 1362-1373.

Dreuillet, C., Tillit, J., Kress, M., et al. (2002). "In vivo and in vitro interaction between human transcription factor MOK2 and nuclear lamin A/C." **Nucleic acids research.** 30 (21): 4634-4642.

Dumoux, M., Clare, D. K., Saibil, H. R., et al. (2012). "*Chlamydiae* assemble a pathogen synapse to hijack the host endoplasmic reticulum." **Traffic.** 13 (12): 1612-1627.

Dumoux, M., Le Gall, S. M., Habbeddine, M., et al. (2013). "Penicillin kills *Chlamydia* following the fusion of bacteria with lysosomes and prevents genital inflammatory lesions in *C. muridarium*-infected mice." **Plos One.** 8 (12): e83511.

Dumoux, M., Menny, A., Delacour, D., et al. (2015). "A *Chlamydia* effector recruits CEP170 to reprogram host microtubule organization." **Journal of Cell Science.**

Eggert Kruse, W., Weltin, M. and Strowitzki, T. (2011). "Are chlamydial lipopolysaccharide-directed antibodies in seminal plasma or serum clinically significant during investigation of male infertility?" **Urology.** 77 (5): 1101-1106.
Elwell, C. A., Ceesay, A., Kim, J. H., et al. (2008). "RNA interference screen identifies Abl kinase and PDGFR signaling in *Chlamydia trachomatis* entry." **PLoS Pathogens.** 4 (3): e1000021.
Elwell, C. A., Jiang, S., Kim, J. H., et al. (2011). "*Chlamydia trachomatis* co-opts GBF1 and CERT to acquire host sphingomyelin for distinct roles during intracellular development." **PLoS Pathogens.** 7 (9): e1002198.
Eriksson, M., Brown, W. T., Gordon, L. B., et al. (2003). "Recurrent de novo point mutations in lamin A cause Hutchinson-Gilford progeria syndrome." **Nature.** 423 (6937): 293-298.
Eskandarian, H., Impens, F., Nahori, M.-A., et al. (2013). "A role for SIRT2-dependent histone H3K18 deacetylation in bacterial infection." **Science.** 341 (6145): 1238858-1238858.
Everett, K. D. E., Bush, R. M. and Andersen, A. A. (1999). "Emended description of the order *Chlamydiales*, proposal of *Parachlamydiaceae* fam. nov. and *Simkaniaceae* fam. nov., each containing one monotypic genus, revised taxonomy of the family *Chlamydiaceae*, including a new genus and five new species, and standards for the identification of organisms." **International Journal of Systematic Bacteriology.** 49: 415-440.
Fan, T., Lu, H., Hu, H., et al. (1998). "Inhibition of apoptosis in *Chlamydia*-infected cells: blockade of mitochondrial cytochrome c release and caspase activation." **The Journal of Experimental Medicine.** 187 (4): 487-496.
Fatica, A. and Tollervey, D. (2002). "Making ribosomes." **Current Opinion in Cell Biology.** 14 (3): 313-318.
Fedorchak, G. R., Kaminski, A. and Lammerding, J. (2014). "Cellular mechanosensing: getting to the nucleus of it all." **Progress in biophysics and molecular biology.** 115 (0): 76-92.
Fields, K. and Hackstadt, T. (2002). "The chlamydial inclusion: escape from the endocytic pathway." **Annual review of cell and developmental biology.** 18: 221-245.
Fields, K. A. and Hackstadt, T. (2000). "Evidence for the secretion of *Chlamydia trachomatis* CopN by a type III secretion mechanism." **Molecular microbiology.** 38 (5): 1048-1060.
Filloux, A. (2004). "The underlying mechanisms of type II protein secretion." **Biochimica et Biophysica Acta (BBA) - Molecular Cell Research.** 1694 (1–3): 163-179.
Finlan, L. E., Sproul, D., Thomson, I., et al. (2008). "Recruitment to the nuclear periphery can alter expression of genes in human cells." **PLoS Genetics.** 4 (3): e1000039.
Fischer, S. F., Schwarz, C., Vier, J., et al. (2001). "Characterization of antiapoptotic activities of *Chlamydia pneumoniae* in human cells." **Infection and immunity.** 69 (11): 7121-7129.
Fisher, D. Z., Chaudhary, N. and Blobel, G. (1986). "cDNA sequencing of nuclear lamins A and C reveals primary and secondary structural homology to intermediate filament proteins." **Proceedings of the National Academy of Sciences of the United States of America.** 83 (17): 6450-6454.
Foeger, N., Wiesel, N., Lotsch, D., et al. (2006). "Solubility properties and specific assembly pathways of the B-type lamin from *Caenorhabditis elegans*." **Journal of structural biology.** 155 (2): 340-350.
Ford, C. (2016). Mechanisms of *Chlamydia trachomatis* entry in eukaryotic cells. PhD Thesis. Institute of Structural and Molecular Biology, **Birkbeck, University of London**.
Fournier, D., Palidwor, G. A., Shcherbinin, S., et al. (2013). "Functional and genomic analyses of alpha-solenoid proteins." **Plos One.** 8 (11): e79894.
Fried, H. and Kutay, U. (2003). "Nucleocytoplasmic transport: taking an inventory." **Cellular and Molecular Life Sciences CMLS.** 60 (8): 1659-1688.
Fu, Y. and Galán, J. E. (1999). "A salmonella protein antagonizes Rac-1 and Cdc42 to mediate host-cell recovery after bacterial invasion." **Nature.** 401 (6750): 293-297.

Fukushi, H. and Hirai, K. (1992). "Proposal of *Chlamydia pecorum* sp. nov. for *Chlamydia* strains derived from ruminants." **International Journal of Systematic Bacteriology.** 42 (2): 306-308.

Funakoshi, T., Maeshima, K., Yahata, K., et al. (2007). "Two distinct human POM121 genes: Requirement for the formation of nuclear pore complexes." **FEBS Letters.** 581 (25): 4910-4916.

Furukawa, K. and Hotta, Y. (1993). "cDNA cloning of a germ cell specific lamin B3 from mouse spermatocytes and analysis of its function by ectopic expression in somatic cells." **The EMBO journal.** 12 (1): 97-106.

Gall, J. G. (2000). "Cajal bodies: the first 100 years." **Annual review of cell and developmental biology.** 16: 273-300.

Galy, V., Olivo Marin, J. C., Scherthan, H., et al. (2000). "Nuclear pore complexes in the organization of silent telomeric chromatin." **Nature.** 403 (6765): 108-112.

Gambarte Tudela, J., Capmany, A., Romao, M., et al. (2015). "The late endocytic Rab39a GTPase regulates the interaction between multivesicular bodies and chlamydial inclusions." **Journal of Cell Science.** 128 (16): 3068-3081.

Gehre, L., Gorgette, O., Perrinet, S., et al. (2016). "Sequestration of host metabolism by an intracellular pathogen." **eLife.** 5: e12552.

Gerace, L., Blum, A. and Blobel, G. (1978). "Immunocytochemical localization of the major polypeptides of the nuclear pore complex-lamina fraction. Interphase and mitotic distribution." **The Journal of cell biology.** 79 (2): 546-566.

Gerace, L. and Burke, B. (1988). "Functional Organization of the Nuclear Envelope." **Annual review of cell biology.** 4 (1): 335-374.

Gesson, K., Rescheneder, P., Skoruppa, M. P., et al. (2016). "A-type lamins bind both hetero- and euchromatin, the latter being regulated by lamina-associated polypeptide 2 alpha." **Genome Research.** 26 (4): 462-473.

Ghosh, P. (2004). "Process of Protein Transport by the Type III Secretion System." **Microbiology and Molecular Biology Reviews.** 68 (4): 771-795.

Goldberg, M. W. and Allen, T. D. (1992). "High resolution scanning electron microscopy of the nuclear envelope: demonstration of a new, regular, fibrous lattice attached to the baskets of the nucleoplasmic face of the nuclear pores." **The Journal of cell biology.** 119 (6): 1429-1440.

Goldman, R. D., Shumaker, D. K., Erdos, M. R., et al. (2004). "Accumulation of mutant lamin A causes progressive changes in nuclear architecture in Hutchinson–Gilford progeria syndrome." **Proceedings of the National Academy of Sciences of the United States of America.** 101 (24): 8963-8968.

González, E., Rother, M., Kerr, M. C., et al. (2014). "*Chlamydia* infection depends on a functional MDM2-p53 axis." **Nature Communications.** 5: 5201.

Gordon, F. B. and Quan, A. L. (1965). "OCCURENCE OF GLYCOGEN IN INCLUSIONS OF THE PSITTACOSIS-LYMPHOGRANULOMA VENEREUM-TRACHOMA AGENTS." **The Journal of infectious diseases.** 115: 186-196.

Görlich, D. and Kutay, U. (1999). "Transport between the cell nucleus and the cytoplasm." **Annual review of cell and developmental biology.** 15: 607-660.

Grayston, J. T., Wang, S. P., Kuo, C. C., et al. (1989). "Current knowledge on *Chlamydia pneumoniae*, strain TWAR, an important cause of pneumonia and other acute respiratory diseases." **European journal of clinical microbiology & infectious diseases.** 8 (3): 191-202.

Greene, W. and Zhong, G. (2003). "Inhibition of host cell cytokinesis by *Chlamydia trachomatis* infection." **Journal of Infection.** 47 (1): 45-51.

Grieshaber, S. S., Grieshaber, N. A. and Hackstadt, T. (2003). "*Chlamydia trachomatis* uses host cell dynein to traffic to the microtubule-organizing center in a p50 dynamitin-independent process." **Journal of Cell Science.** 116 (18): 3793-3802.

Guan, T., Kehlenbach, R. H., Schirmer, E. C., et al. (2000). "Nup50, a nucleoplasmically oriented nucleoporin with a role in nuclear protein export." **Molecular and Cellular Biology.** 20 (15): 5619-5630.

Guelen, L., Pagie, L., Brasset, E., et al. (2008). "Domain organization of human chromosomes revealed by mapping of nuclear lamina interactions." **Nature.** 453 (7197): 948-951.

Guo, H., Pétrin, D., Zhang, Y., et al. (2006). "Caspase-1 activation of caspase-6 in human apoptotic neurons." **Cell Death and Differentiation.** 13 (2): 285-292.

Guo, Y. and Zheng, Y. (2015). "Lamins position the nuclear pores and centrosomes by modulating dynein." **Molecular Biology of the Cell.** 26 (19): 3379-3389.

Hackstadt, T., Scidmore-Carlson, M. A., Shaw, E. I., et al. (1999). "The *Chlamydia trachomatis* IncA protein is required for homotypic vesicle fusion." **Cellular Microbiology.** 1 (2): 119-130.

Hackstadt, T., Scidmore, M. A. and Rockey, D. D. (1995). "Lipid metabolism in *Chlamydia trachomatis*-infected cells: directed trafficking of Golgi-derived sphingolipids to the chlamydial inclusion." **Proceedings of the National Academy of Sciences.** 92 (11): 4877-4881.

Hall, J. V., Schell, M., Dessus-Babus, S., et al. (2011). "The multifaceted role of oestrogen in enhancing *Chlamydia trachomatis* infection in polarized human endometrial epithelial cells." **Cellular Microbiology.** 13 (8): 1183-1199.

Haque, F., Lloyd, D. J., Smallwood, D. T., et al. (2006). "SUN1 interacts with nuclear lamin A and cytoplasmic nesprins to provide a physical connection between the nuclear lamina and the cytoskeleton." **Molecular and Cellular Biology.** 26 (10): 3738-3751.

Hatch, T. P., Allan, I. and Pearce, J. H. (1984). "Structural and polypeptide differences between envelopes of infective and reproductive life cycle forms of *Chlamydia* spp." **Journal of Bacteriology.** 157 (1): 13-20.

Hauser, M., Mayer, C. E. and Söding, J. (2013). "kClust: fast and sensitive clustering of large protein sequence databases." **BMC bioinformatics.** 14: 248-248.

Heald, R. and McKeon, F. (1990). "Mutations of phosphorylation sites in lamin A that prevent nuclear lamina disassembly in mitosis." **Cell.** 61 (4): 579-589.

Hefty, P. S. and Stephens, R. S. (2007). "Chlamydial type III secretion system is encoded on ten operons preceded by sigma 70-like promoter elements." **Journal of Bacteriology.** 189 (1): 198-206.

Heinzen, R. A. and Hackstadt, T. (1997). "The *Chlamydia trachomatis* parasitophorous vacuolar membrane is not passively permeable to low-molecular-weight compounds." **Infection and immunity.** 65 (3): 1088-1094.

Helle, S. C. J., Kanfer, G., Kolar, K., et al. (2013). "Organization and function of membrane contact sites." **Biochimica et Biophysica Acta (BBA) - Molecular Cell Research.** 1833 (11): 2526-2541.

Heuer, D., Lipinski, A. R., Machuy, N., et al. (2009). "*Chlamydia* causes fragmentation of the Golgi compartment to ensure reproduction." **Nature.** 457 (7230): 731-U738.

Hildebrand, A., Remmert, M., Biegert, A., et al. (2009). "Fast and accurate automatic structure prediction with HHpred." **Proteins: Structure, Function, and Bioinformatics.** 77 (S9): 128-132.

Hoffmann, K., Sperling, K., Olins, A. L., et al. (2007). "The granulocyte nucleus and lamin B receptor: avoiding the ovoid." **Chromosoma.** 116 (3): 227-235.

Hogan, R. J., Mathews, S. A., Mukhopadhyay, S., et al. (2004). "Chlamydial persistence: beyond the biphasic paradigm." **Infection and immunity.** 72 (4): 1843-1855.

Hozak, P., Sasseville, A. M., Raymond, Y., et al. (1995). "Lamin proteins form an internal nucleoskeleton as well as a peripheral lamina in human cells." **Journal of Cell Science.** 108 (2): 635-644.

Hybiske, K. and Stephens, R. S. (2007). "Mechanisms of host cell exit by the intracellular bacterium Chlamydia." **Proceedings of the National Academy of Sciences.** 104 (27): 11430-11435.

Hybiske, K. and Stephens, R. S. (2007). "Mechanisms of host cell exit by the intracellular bacterium Chlamydia." **Proceedings of the National Academy of Sciences of the United States of America.** 104 (27): 11430-11435.

Idahl, A., Abramsson, L., Kumlin, U., et al. (2007). "Male serum *Chlamydia trachomatis* IgA and IgG, but not heat shock protein 60 IgG, correlates with negatively affected semen characteristics and lower pregnancy rates in the infertile couple." **International journal of andrology.** 30 (2): 99-107.

Imbalzano, K. M., Cohet, N., Wu, Q., et al. (2013). "Nuclear shape changes are induced by knockdown of the SWI/SNF ATPase BRG1 and are independent of cytoskeletal connections." **Plos One.** 8 (2): e55628.

Inoue, S., Browne, G., Melino, G., et al. (2009). "Ordering of caspases in cells undergoing apoptosis by the intrinsic pathway." **Cell Death and Differentiation.** 16 (7): 1053-1061.

Ivorra, C., Kubicek, M., González, J. M., et al. (2006). "A mechanism of AP-1 suppression through interaction of c-Fos with lamin A/C." **Genes & development.** 20 (3): 307-320.

Iyer, K V., Pulford, S., Mogilner, A., et al. (2012). "Mechanical activation of cells induces chromatin remodeling preceding MKL nuclear transport." **Biophysical journal.** 103 (7): 1416-1428.

Jewett, T. J., Fischer, E. R., Mead, D. J., et al. (2006). "Chlamydial TARP is a bacterial nucleator of actin." **Proceedings of the National Academy of Sciences.** 103 (42): 15599-15604.

Jiwani, S., Ohr, R. J., Fischer, E. R., et al. (2012). "Chlamydia trachomatis Tarp cooperates with the Arp2/3 complex to increase the rate of actin polymerization." **Biochemical and Biophysical Research Communications.** 420 (4): 816-821.

Johnson, B. R., Nitta, R. T., Frock, R. L., et al. (2004). "A-type lamins regulate retinoblastoma protein function by promoting subnuclear localization and preventing proteasomal degradation." **Proceedings of the National Academy of Sciences of the United States of America.** 101 (26): 9677-9682.

Johnson, F. W. A. and Hobson, D. (1977). "The effect of penicillin on genital strains of *Chlamydia trachomatis* in tissue culture." **Journal of Antimicrobial Chemotherapy.** 3 (1): 49-56.

Jorgensen, I., Bednar, M. M., Amin, V., et al. (2011). "The *Chlamydia* protease CPAF regulates host and bacterial proteins to maintain pathogen vacuole integrity and promote virulence." **Cell Host & Microbe.** 10 (1): 21-32.

Joyee, A. G. and Yang, X. (2008). "Role of toll-like receptors in immune responses to chlamydial infections." **Current pharmaceutical design.** 14 (6): 593-600.

Källberg, M., Wang, H., Wang, S., et al. (2012). "Template-based protein structure modeling using the RaptorX web server." **Nature protocols.** 7 (8): 1511-1522.

Kalman, S., Mitchell, W., Marathe, R., et al. (1999). "Comparative genomes of *Chlamydia pneumoniae* and *C. trachomatis*." **Nat Genet.** 21 (4): 385-389.

Karunakaran, K. P., Noguchi, Y., Read, T. D., et al. (2003). "Molecular analysis of the multiple GroEL proteins of *Chlamydiae*." **Journal of Bacteriology.** 185 (6): 1958-1966.

Kawaguchi, A., Asaka, M. N., Matsumoto, K., et al. (2015). "Centrosome maturation requires YB-1 to regulate dynamic instability of microtubules for nucleus reassembly." **Scientific Reports.** 5: 8768.

Kawana, K., Quayle, A. J., Ficarra, M., et al. (2007). "CD1d degradation in *Chlamydia trachomatis*-infected epithelial cells is the result of both cellular and chlamydial proteasomal activity." **Journal of Biological Chemistry.** 282 (10): 7368-7375.

Kim, J. F. (2001). "Revisiting the chlamydial type III protein secretion system: clues to the origin of type III protein secretion." **Trends in genetics.** 17 (2): 65-69.

Kimura, H. (2013). "Histone modifications for human epigenome analysis." **J Hum Genet.** 58 (7): 439-445.
Klaiman, G., Champagne, N. and LeBlanc, A. C. (2009). "Self-activation of Caspase-6 in vitro and in vivo: Caspase-6 activation does not induce cell death in HEK293T cells." **Biochimica et Biophysica Acta (BBA) - Molecular Cell Research.** 1793 (3): 592-601.
Knittler, M. R., Berndt, A., Böcker, S., et al. (2014). "*Chlamydia psittaci*: New insights into genomic diversity, clinical pathology, host–pathogen interaction and anti-bacterial immunity." **International Journal of Medical Microbiology.** 304 (7): 877-893.
Kobe, B. and Kajava, A. V. (2000). "When protein folding is simplified to protein coiling: the continuum of solenoid protein structures." **Trends in Biochemical Sciences.** 25 (10): 509-515.
Kokes, M., Dunn, J. D., Granek, J. A., et al. (2015). "Integrating chemical mutagenesis and whole genome sequencing as a platform for forward and reverse genetic analysis of *Chlamydia*." **Cell Host & Microbe.** 17 (5): 716-725.
Kong, L., Schäfer, G., Bu, H., et al. (2012). "Lamin A/C protein is overexpressed in tissue-invading prostate cancer and promotes prostate cancer cell growth, migration and invasion through the PI3K/AKT/PTEN pathway." **Carcinogenesis.** 33 (4): 751-759.
Korotkov, K. V., Sandkvist, M. and Hol, W. G. J. (2012). "The type II secretion system: biogenesis, molecular architecture and mechanism." **Nature reviews. Microbiology.** 10 (5): 336-351.
Krull, S., Dörries, J., Boysen, B., et al. (2010). "Protein Tpr is required for establishing nuclear pore-associated zones of heterochromatin exclusion." **The EMBO journal.** 29 (10): 1659-1673.
Kumar, Y., Cocchiaro, J. and Valdivia, R. H. (2006). "The obligate intracellular pathogen *Chlamydia trachomatis* targets host lipid droplets." **Current biology : CB.** 16 (16): 1646-1651.
Kumar, Y. and Valdivia, R. H. (2008). "Actin and intermediate filaments stabilize the *Chlamydia trachomatis* vacuole by forming dynamic structural scaffolds." **Cell Host & Microbe.** 4 (2): 159-169.
Kumar, Y. and Valdivia, R. H. (2008). "Reorganization of the host cytoskeleton by the intracellular pathogen *Chlamydia trachomatis*." **Communicative & Integrative Biology.** 1 (2): 175-177.
Kuss, S., Mata, M., Zhang, L., et al. (2013). "Nuclear imprisonment: viral strategies to arrest host mRNA nuclear export." **Viruses.** 5 (7): 1824-1849.
Lad, S. P., Li, J., da Silva Correia, J., et al. (2007a). "Cleavage of p65/RelA of the NF-κB pathway by *Chlamydia*." **Proceedings of the National Academy of Sciences of the United States of America.** 104 (8): 2933-2938.
Lad, S. P., Yang, G., Scott, D. A., et al. (2007b). "Chlamydial CT441 is a PDZ domain-containing tail-specific protease that interferes with the NF-κB pathway of immune response." **Journal of Bacteriology.** 189 (18): 6619-6625.
Lammerding, J., Fong, L. G., Ji, J. Y., et al. (2006). "Lamins A and C but not Lamin B1 regulate nuclear mechanics." **Journal of Biological Chemistry.** 281 (35): 25768-25780.
Lammerding, J., Hsiao, J., Schulze, P. C., et al. (2005). "Abnormal nuclear shape and impaired mechanotransduction in emerin-deficient cells." **The Journal of cell biology.** 170 (5): 781-791.
Lammerding, J., Schulze, P. C., Takahashi, T., et al. (2004). "Lamin A/C deficiency causes defective nuclear mechanics and mechanotransduction." **Journal of Clinical Investigation.** 113 (3): 370-378.
Lamond, A. I. and Spector, D. L. (2003). "Nuclear speckles: a model for nuclear organelles." **Nat Rev Mol Cell Biol.** 4 (8): 605-612.
Lane, B. J., Mutchler, C., Al Khodor, S., et al. (2008). "Chlamydial entry involves Tarp binding of guanine nucleotide exchange factors." **PLoS Pathogens.** 4 (3): e1000014.

Le Negrate, G., Krieg, A., Faustin, B., et al. (2008). "ChlaDub1 of *Chlamydia trachomatis* suppresses NF-κB activation and inhibits IκBα ubiquitination and degradation." **Cellular Microbiology.** 10 (9): 1879-1892.

Lebreton, A., Job, V., Ragon, M., et al. (2014). "Structural basis for the inhibition of the chromatin repressor BAHD1 by the bacterial nucleomodulin LntA." **mBio.** 5 (1): e00775-00713.

Lee, K. K., Haraguchi, T., Lee, R. S., et al. (2001). "Distinct functional domains in emerin bind lamin A and DNA-bridging protein BAF." **Journal of Cell Science.** 114 (24): 4567-4573.

Lei, L., Dong, X., Li, Z., et al. (2013). "Identification of a novel nuclear localization signal sequence in *Chlamydia trachomatis*-secreted hypothetical protein CT311." **Plos One.** 8 (5): e64529-e64529.

Levsky, J. M. and Singer, R. H. (2003). "Fluorescence in situ hybridization: past, present and future." **Journal of Cell Science.** 116 (14): 2833-2838.

Li, C., Shi, Z., Zhang, L., et al. (2010). "Dynamic changes of territories 17 and 18 during EBV-infection of human lymphocytes." **Molecular Biology Reports.** 37 (5): 2347-2354.

Li, Z., Chen, C., Chen, D., et al. (2008). "Characterization of fifty putative inclusion membrane proteins encoded in the *Chlamydia trachomatis* genome." **Infection and immunity.** 76 (6): 2746-2757.

Liechti, G., Kuru, E., Hall, E., et al. (2014). "A new metabolic cell wall labeling method reveals peptidoglycan in *Chlamydia trachomatis*." **Nature.** 506 (7489): 507-510.

Lin, F. and Worman, H. J. (1993). "Structural organization of the human gene encoding nuclear lamin A and nuclear lamin C." **Journal of Biological Chemistry.** 268 (22): 16321-16326.

Lin, H. S. and Moulder, J. W. (1966). "Patterns of response to sulfadiazine, D-cycloserine and D-alanine in members of the psittacosis group." **The Journal of infectious diseases.** 116 (3): 372-376.

Lipinski, A. R., Heymann, J., Meissner, C., et al. (2009). "Rab6 and Rab11 regulate *Chlamydia trachomatis* development and Golgin-84-dependent Golgi fragmentation." **PLoS Pathogens.** 5 (10): e1000615.

Liu, J., Ben-Shahar, T. R., Riemer, D., et al. (2000). "Essential roles for *Caenorhabditis elegans* lamin gene in nuclear organization, cell cycle progression, and spatial organization of nuclear pore complexes." **Molecular Biology of the Cell.** 11 (11): 3937-3947.

Liu, Q., Pante, N., Misteli, T., et al. (2007). "Functional association of Sun1 with nuclear pore complexes." **The Journal of cell biology.** 178 (5): 785-798.

Lloyd, D. J., Trembath, R. C. and Shackleton, S. (2002). "A novel interaction between lamin A and SREBP1: implications for partial lipodystrophy and other laminopathies." **Human Molecular Genetics.** 11 (7): 769-777.

Lombardi, M. L. and Lammerding, J. (2011). "Keeping the LINC: the importance of nucleo-cytoskeletal coupling in intracellular force transmission and cellular function." **Biochemical Society transactions.** 39 (6): 1729-1734.

Lowe, A. R., Siegel, J. J., Kalab, P., et al. (2010). "Selectivity mechanism of the nuclear pore complex characterized by single cargo tracking." **Nature.** 467 (7315): 600-603.

Lowe, A. R., Tang, J. H., Yassif, J., et al. (2015). "Importin-β modulates the permeability of the nuclear pore complex in a Ran-dependent manner." **eLife.** 4: e04052.

Löwer, M. and Schneider, G. (2009). "Prediction of type III secretion signals in genomes of Gram-negative bacteria." **Plos One.** 4 (6): e5917.

Lu, C., Lei, L., Peng, B., et al. (2013). "*Chlamydia trachomatis* GlgA is secreted into host cell cytoplasm." **Plos One.** 8 (7): e68764.

Lu, W., Gotzmann, J., Sironi, L., et al. (2008). "Sun1 forms immobile macromolecular assemblies at the nuclear envelope." **Biochimica et Biophysica Acta (BBA) - Molecular Cell Research.** 1783 (12): 2415-2426.

Lussi, Y. C., Hügi, I., Laurell, E., et al. (2011). "The nucleoporin Nup88 is interacting with nuclear lamin A." **Molecular Biology of the Cell.** 22 (7): 1080-1090.

Lutter, E. I., Barger, A. C., Nair, V., et al. (2013). "*Chlamydia trachomatis* inclusion membrane protein CT228 recruits elements of the myosin phosphatase pathway to regulate release mechanisms." **Cell reports.** 3 (6): 1921-1931.

Lutter, E. I., Bonner, C., Holland, M. J., et al. (2010). "Phylogenetic analysis of *Chlamydia trachomatis* Tarp and correlation with clinical phenotype." **Infection and immunity.** 78 (9): 3678-3688.

Luz, J. M. and Lennarz, W. J. (1996). "Protein disulfide isomerase: a multifunctional protein of the endoplasmic reticulum." **Experientia Supplementum.** 77: 97-117.

Lyons, J. M., Ito, J. I., Peña, A. S., et al. (2005). "Differences in growth characteristics and elementary body associated cytotoxicity between *Chlamydia trachomatis* oculogenital serovars D and H and *Chlamydia muridarum*." **Journal of Clinical Pathology.** 58 (4): 397-401.

Maeshima, K., Yahata, K., Sasaki, Y., et al. (2006). "Cell-cycle-dependent dynamics of nuclear pores: pore-free islands and lamins." **Journal of Cell Science.** 119 (21): 4442-4451.

Makatsori, D., Kourmouli, N., Polioudaki, H., et al. (2004). "The inner nuclear membrane protein lamin B receptor forms distinct microdomains and links epigenetically marked chromatin to the nuclear envelope." **Journal of Biological Chemistry.** 279 (24): 25567-25573.

Maniotis, A. J., Chen, C. S. and Ingber, D. E. (1997). "Demonstration of mechanical connections between integrins, cytoskeletal filaments, and nucleoplasm that stabilize nuclear structure." **Proceedings of the National Academy of Sciences of the United States of America.** 94 (3): 849-854.

Margueron, R. and Reinberg, D. (2011). "The Polycomb complex PRC2 and its mark in life." **Nature.** 469 (7330): 343-349.

Mariotti, S. P., Pascolini, D. and Rose Nussbaumer, J. (2009). "Trachoma: global magnitude of a preventable cause of blindness." **British journal of ophthalmology.** 93 (5): 563-568.

Martin, R. M., Leonhardt, H. and Cardoso, M. C. (2005). "DNA labeling in living cells." **Cytometry Part A.** 67A (1): 45-52.

Martins, R. P., Finan, J. D., Guilak, F., et al. (2012). "MECHANICAL REGULATION OF NUCLEAR STRUCTURE AND FUNCTION." **Annual Review of Biomedical Engineering.** 14: 431-455.

Matsumoto, A. (1981). "Isolation and electron microscopic observations of intracytoplasmic inclusions containing *Chlamydia psittaci*." **Journal of Bacteriology.** 145 (1): 605-612.

Matsuura, Y. and Stewart, M. (2005). "Nup50/Npap60 function in nuclear protein import complex disassembly and importin recycling." **The EMBO journal.** 24 (21): 3681-3689.

Maul, G. G., Negorev, D., Bell, P., et al. (2000). "Review: properties and assembly mechanisms of ND10, PML bodies, or PODs." **Journal of structural biology.** 129 (2-3): 278-287.

McClelland, M., Sanderson, K. E., Spieth, J., et al. (2001). "Complete genome sequence of *Salmonella enterica* serovar Typhimurium LT2." **Nature.** 413 (6858): 852-856.

McCord, R. P., Nazario-Toole, A., Zhang, H., et al. (2013). "Correlated alterations in genome organization, histone methylation, and DNA–lamin A/C interactions in Hutchinson-Gilford progeria syndrome." **Genome Research.** 23 (2): 260-269.

McGee, M. D., Rillo, R., Anderson, A. S., et al. (2006). "UNC-83 is a KASH protein required for nuclear migration and is recruited to the outer nuclear membrane by a physical interaction with the SUN protein UNC-84." **Molecular Biology of the Cell.** 17 (4): 1790-1801.

McGuffin, L. J., Bryson, K. and Jones, D. T. (2000). "The PSIPRED protein structure prediction server." **Bioinformatics.** 16 (4): 404-405.

McInerney, J. O., Martin, W. F., Koonin, E. V., et al. (2011). "*Planctomycetes* and eukaryotes: a case of analogy not homology." **BioEssays : news and reviews in molecular, cellular and developmental biology.** 33 (11): 810-817.

McMahon, E. (In preparation). Structural functional characterisation of *Chlamydia* inclusion membrane proteins. PhD Thesis. Institute of Structural and Molecular Biology, **Birkbeck, University of London**.

Meinke, P., Mattioli, E., Haque, F., et al. (2014). "Muscular dystrophy-associated SUN1 and SUN2 variants disrupt nuclear-cytoskeletal connections and myonuclear organization." **PLoS Genetics.** 10 (9): e1004605.

Melčák, I., Cermanová, Š., Jirsová, K., et al. (2000). "Nuclear pre-mRNA compartmentalization: trafficking of released transcripts to splicing factor reservoirs." **Molecular Biology of the Cell.** 11 (2): 497-510.

Mirrashidi, Kathleen M., Elwell, Cherilyn A., Verschueren, E., et al. (2015). "Global mapping of the Inc-human interactome reveals that retromer restricts *Chlamydia* infection." **Cell Host & Microbe.** 18 (1): 109-121.

Mital, J., Lutter, E. I., Barger, A. C., et al. (2015). "*Chlamydia trachomatis* inclusion membrane protein CT850 interacts with the dynein light chain DYNLT1 (Tctex1)." **Biochemical and Biophysical Research Communications.** 462 (2): 165-170.

Mital, J., Miller, N. J., Dorward, D. W., et al. (2013). "Role for chlamydial inclusion membrane proteins in inclusion membrane structure and biogenesis." **Plos One.** 8 (5): e63426.

Mital, J., Miller, N. J., Fischer, E. R., et al. (2010). "Specific chlamydial inclusion membrane proteins associate with active Src family kinases in microdomains that interact with the host microtubule network." **Cellular Microbiology.** 12 (9): 1235-1249.

Miyairi, I., Mahdi, O. S., Ouellette, S. P., et al. (2006). "Different growth rates of *Chlamydia trachomatis* biovars reflect pathotype." **Journal of Infectious Diseases.** 194 (3): 350-357.

Moelleken, K. and Hegemann, J. H. (2008). "The *Chlamydia* outer membrane protein OmcB is required for adhesion and exhibits biovar-specific differences in glycosaminoglycan binding." **Molecular microbiology.** 67 (2): 403-419.

Mohr, D., Frey, S., Fischer, T., et al. (2009). "Characterisation of the passive permeability barrier of nuclear pore complexes." **Embo Journal.** 28 (17): 2541-2553.

Moir, R. D., Yoon, M., Khuon, S., et al. (2000). "Nuclear lamins A and B1: different pathways of assembly during nuclear envelope formation in living cells." **The Journal of cell biology.** 151 (6): 1155-1168.

Mojica, S. A., Hovis, K. M., Frieman, M. B., et al. (2015). "SINC, a type III secreted protein of *Chlamydia psittaci*, targets the inner nuclear membrane of infected cells and uninfected neighbors." **Molecular Biology of the Cell.** 26 (10): 1918-1934.

Monroe, K. M., McWhirter, S. M. and Vance, R. E. (2010). "Induction of type I interferons by bacteria." **Cellular Microbiology.** 12 (7): 881-890.

Mosavi, L. K., Cammett, T. J., Desrosiers, D. C., et al. (2004). "The ankyrin repeat as molecular architecture for protein recognition." **Protein Science : A Publication of the Protein Society.** 13 (6): 1435-1448.

Moulder, J. W. (1966). "RELATION OF PSITTACOSIS GROUP (CHLAMYDIAE) TO BACTERIA AND VIRUSES." **Annual Review of Microbiology.** 20: 107-&.

Moulder, J. W. (1991). "Interaction of *Chlamydiae* and host cells in vitro." **Microbiological Reviews.** 55 (1): 143-190.

Mount, D. (2004). Bioinformatics: Sequence and Genome Analysis, **Cold Spring Harbor Laboratory Press**.

Muschiol, S., Bailey, L., Gylfe, Å., et al. (2006). "A small-molecule inhibitor of type III secretion inhibits different stages of the infectious cycle of *Chlamydia trachomatis*." **Proceedings of the National Academy of Sciences.** 103 (39): 14566-14571.

Musich, P. R. and Zou, Y. (2009). "Genomic instability and DNA damage responses in progeria arising from defective maturation of prelamin A." **Aging (Albany NY).** 1 (1): 28-37.

Nanagara, R., Li, F., Beutler, A., et al. (1995). "Alteration of *Chlamydia trachomatis* biologic behavior in synovial membranes suppression of surface antigen production in reactive arthritis and Reiter's syndrome." **Arthritis & Rheumatism.** 38 (10): 1410-1417.

Nans, A., Kudryashev, M., Saibil, H. R., et al. (2015). "Structure of a bacterial type III secretion system in contact with a host membrane in situ." **Nature Communications.** 6: 10114.

Nans, A., Saibil, H. R. and Hayward, R. D. (2014). "Pathogen–host reorganization during *Chlamydia* invasion revealed by cryo-electron tomography." **Cellular Microbiology.** 16 (10): 1457-1472.

National Chlamydia Screening Programme. (2012). "*Chlamydia* testing data for 15-24 year olds in England, January to December 2012." National Chlamydia Screening Programme. Retrieved 28/03/2014, from http://www.chlamydiascreening.nhs.uk/ps/resources/data-tables/CTAD_Data_Tables_2012.pdf.

Neefjes, J., Jongsma, M. L. M., Paul, P., et al. (2011). "Towards a systems understanding of MHC class I and MHC class II antigen presentation." **Nat Rev Immunol.** 11 (12): 823-836.

Nelson, D. E., Virok, D. P., Wood, H., et al. (2005). "Chlamydial IFN-γ immune evasion is linked to host infection tropism." **Proceedings of the National Academy of Sciences of the United States of America.** 102 (30): 10658-10663.

Noble, K., Tran, E., Alcazar-Romn, A., et al. (2011). "The Dbp5 cycle at the nuclear pore complex during mRNA export II: nucleotide cycling and mRNP remodeling by Dbp5 are controlled by Nup159 and Gle1." **Genes & development.** 25 (10): 1065-1077.

Nunes, A. and Gomes, J. P. (2014). "Evolution, phylogeny, and molecular epidemiology of *Chlamydia*." **Infection, Genetics and Evolution.** 23: 49-64.

Ojcius, D. M., Degani, H., Mispelter, J., et al. (1998). "Enhancement of ATP levels and glucose metabolism during an infection by *Chlamydia* : NMR STUDIES OF LIVING CELLS." **Journal of Biological Chemistry.** 273 (12): 7052-7058.

Olins, A. L., Herrmann, H., Lichter, P., et al. (2001). "Nuclear envelope and chromatin compositional differences comparing undifferentiated and retinoic acid- and phorbol ester-treated HL-60 cells." **Experimental Cell Research.** 268 (2): 115-127.

Olins, A. L. and Olins, D. E. (2004). "Cytoskeletal influences on nuclear shape in granulocytic HL-60 cells." **BMC cell biology.** 5: 30-30.

Olins, A. L., Rhodes, G., Welch, D. B. M., et al. (2010). "Lamin B receptor: Multi-tasking at the nuclear envelope." **Nucleus.** 1 (1): 53-70.

Olins, A. L., Zwerger, M., Herrmann, H., et al. (2008). "The human granulocyte nucleus: unusual nuclear envelope and heterochromatin composition." **European journal of cell biology.** 87 (5): 279-290.

Orth, K., Chinnaiyan, A. M., Garg, M., et al. (1996). "The CED-3/ICE-like protease Mch2 is activated during apoptosis and cleaves the death substrate lamin A." **Journal of Biological Chemistry.** 271 (28): 16443-16446.

Padberg, I., Janßen, S. and Meyer, T. F. (2013). "*Chlamydia trachomatis* inhibits telomeric DNA damage signaling via transient hTERT upregulation." **International Journal of Medical Microbiology.** 303 (8): 463-474.

Padmakumar, V. C., Libotte, T., Lu, W., et al. (2005). "The inner nuclear membrane protein Sun1 mediates the anchorage of Nesprin-2 to the nuclear envelope." **Journal of Cell Science.** 118 (15): 3419-3430.

Park, J., Kim, K. J., Choi, K.-s., et al. (2004). "*Anaplasma phagocytophilum* AnkA binds to granulocyte DNA and nuclear proteins." **Cellular Microbiology.** 6 (8): 743-751.

Peipert, J. (2003). "Clinical practice. Genital chlamydial infections." **The New England journal of medicine.** 349 (25): 2424-2430.

Pemberton, L. F. and Paschal, B. M. (2005). "Mechanisms of receptor-mediated nuclear import and nuclear export." **Traffic.** 6 (3): 187-198.

Pennini, M., Perrinet, S., Dautry-Varsat, A., et al. (2010). "Histone methylation by NUE, a novel nuclear effector of the intracellular pathogen Chlamydia trachomatis." **Plos Pathogens.** 6 (7).

Pennini, M. E., Perrinet, S., Dautry-Varsat, A., et al. (2010). "Histone methylation by NUE, a novel nuclear effector of the intracellular pathogen *Chlamydia trachomatis*." **PLoS Pathogens.** 6 (7).

Peter, M., Kitten, G. T., Lehner, C. F., et al. (1989). "Cloning and sequencing of cDNA clones encoding chicken lamins A and B1 and comparison of the primary structures of vertebrate A- and B-type lamins." **Journal of molecular biology.** 208 (3): 393-404.

Peter, M., Nakagawa, J., Dorée, M., et al. (1990). "In vitro disassembly of the nuclear lamina and M phase-specific phosphorylation of lamins by cdc2 kinase." **Cell.** 61 (4): 591-602.

Peters, J., Wilson, D. P., Myers, G., et al. (2007). "Type III secretion à la *Chlamydia*." **Trends in Microbiology.** 15 (6): 241-251.

Petersen, T. N., Brunak, S., von Heijne, G., et al. (2011). "SignalP 4.0: discriminating signal peptides from transmembrane regions." **Nat Meth.** 8 (10): 785-786.

Pilhofer, M., Aistleitner, K., Ladinsky, M. S., et al. (2014). "Architecture and host interface of environmental *Chlamydiae* revealed by electron cryotomography." **Environmental Microbiology.** 16 (2): 417-429.

Poleshko, A., Mansfield, K. M., Burlingame, C. C., et al. (2013). "The human protein PRR14 tethers heterochromatin to the nuclear lamina during interphase and mitotic exit." **Cell reports.** 5 (2): 10.1016/j.celrep.2013.1009.1024.

Prunuske, A. J. and Ullman, K. S. (2006). "The nuclear envelope: form and reformation." **Current Opinion in Cell Biology.** 18 (1): 108-116.

Rajalingam, K., Sharma, M., Lohmann, C., et al. (2008). "Mcl-1 is a key regulator of apoptosis resistance in *Chlamydia trachomatis*-infected cells." **Plos One.** 3 (9): e3102.

Rajalingam, K., Sharma, M., Paland, N., et al. (2006). "IAP-IAP complexes required for apoptosis resistance of *C. trachomatis*–infected cells." **PLoS Pathogens.** 2 (10): e114.

Rake, G., Shaffer, M. F. and Thygeson, P. (1942). "Relationship of agents of trachoma and inclusion conjunctivitis to those of lymphogranuloma-psittacosis group." **Proceedings of the Society for Experimental Biology and Medicine.** 49: 545-547.

Razafsky, D. and Hodzic, D. (2009). "Bringing KASH under the SUN: the many faces of nucleo-cytoskeletal connections." **The Journal of cell biology.** 186 (4): 461-472.

Rea, S., Eisenhaber, F., O'Carroll, D., et al. (2000). "Regulation of chromatin structure by site-specific histone H3 methyltransferases." **Nature.** 406 (6796): 593-599.

Read, T. D., Brunham, R. C., Shen, C., et al. (2000). "Genome sequences of *Chlamydia trachomatis* MoPn and *Chlamydia pneumoniae* AR39." **Nucleic acids research.** 28 (6): 1397-1406.

Reichelt, R., Holzenburg, A., Buhle, E. L., et al. (1990). "Correlation between structure and mass distribution of the nuclear pore complex and of distinct pore complex components." **The Journal of cell biology.** 110 (4): 883-894.

Remmert, M., Biegert, A., Hauser, A., et al. (2011). "HHblits: lightning-fast iterative protein sequence searching by HMM-HMM alignment." **Nat Meth.** 9 (2): 173-175.

Reynolds, A. E., Liang, L. and Baines, J. D. (2004). "Conformational changes in the nuclear lamina induced by Herpes Simplex Virus Type 1 require genes U(L)31 and U(L)34." **Journal of Virology.** 78 (11): 5564-5575.

Rockey, D., Scidmore, M., Bannantine, J., et al. (2002). "Proteins in the chlamydial inclusion membrane." **Microbes and infection.** 4 (3): 333-340.

Rockey, D. D., Grosenbach, D., Hruby, D. E., et al. (1997). "*Chlamydia psittaci* IncA is phosphorylated by the host cell and is exposed on the cytoplasmic face of the developing inclusion." **Molecular microbiology.** 24 (1): 217-228.

Rolando, M., Sanulli, S., Rusniok, C., et al. (2013). "*Legionella pneumophila* effector RomA uniquely modifies host chromatin to repress gene expression and promote intracellular bacterial replication." **Cell Host & Microbe.** 13 (4): 395-405.
Roshick, C., Wood, H., Caldwell, H. D., et al. (2006). "Comparison of gamma interferon-mediated antichlamydial defense mechanisms in human and mouse cells." **Infection and immunity.** 74 (1): 225-238.
Rout, M. P., Aitchison, J. D., Suprapto, A., et al. (2000). "The yeast nuclear pore complex: composition, architecture, and transport mechanism." **The Journal of cell biology.** 148 (4): 635-652.
Roux, K. J., Crisp, M. L., Liu, Q., et al. (2009). "Nesprin 4 is an outer nuclear membrane protein that can induce kinesin-mediated cell polarization." **Proceedings of the National Academy of Sciences of the United States of America.** 106 (7): 2194-2199.
Rusconi, B. and Greub, G. (2011). "*Chlamydiales* and the innate immune response: friend or foe?" **FEMS Immunology & Medical Microbiology.** 61 (3): 231-244.
Rzomp, K. A., Moorhead, A. R. and Scidmore, M. A. (2006). "The GTPase Rab4 interacts with *Chlamydia trachomatis* inclusion membrane protein CT229." **Infection and immunity.** 74 (9): 5362-5373.
Rzomp, K. A., Scholtes, L. D., Briggs, B. J., et al. (2003). "Rab GTPases are recruited to chlamydial inclusions in both a species-dependent and species-independent manner." **Infection and immunity.** 71 (10): 5855-5870.
Saka, H. A., Thompson, J. W., Chen, Y.-S., et al. (2015). "*Chlamydia trachomatis* infection leads to defined alterations to the lipid droplet proteome in epithelial cells." **Plos One.** 10 (4): e0124630.
Saka, H. A. and Valdivia, R. H. (2010). "Acquisition of nutrients by *Chlamydiae*: unique challenges of living in an intracellular compartment." **Current Opinion in Microbiology.** 13 (1): 4-10.
Samba-Louaka, A., Nougayrède, J.-P., Watrin, C., et al. (2008). "Bacterial cyclomodulin Cif blocks the host cell cycle by stabilizing the cyclin-dependent kinase inhibitors p21waf1 and p27kip1." **Cellular Microbiology.** 10 (12): 2496-2508.
Sandilands, E. and Frame, M. C. (2008). "Endosomal trafficking of Src tyrosine kinase." **Trends in Cell Biology.** 18 (7): 322-329.
Sandoz, K. and Rockey, D. (2010). "Antibiotic resistance in *Chlamydiae*." **Future microbiology.** 5 (9): 1427-1442.
Santarella-Mellwig, R., Franke, J., Jaedicke, A., et al. (2010). "The compartmentalized bacteria of the *Planctomycetes-Verrucomicrobia-Chlamydiae* superphylum have membrane coat-like proteins." **PLoS biology.** 8 (1): e1000281.
Sasseville, A. M.-J. and Langelier, Y. (1998). "In vitro interaction of the carboxy-terminal domain of lamin A with actin." **FEBS Letters.** 425 (3): 485-489.
Scaffidi, P. and Misteli, T. (2006). "Lamin A-dependent nuclear defects in human aging." **Science.** 312 (5776): 1059-1063.
Schachter, J., Stephens, R. S., Timms, P., et al. (2001). "Radical changes to chlamydial taxonomy are not necessary just yet." **International journal of systematic and evolutionary microbiology.** 51 (1): 249-243.
Schautteet, K., De Clercq, E. and Vanrompay, D. (2011). "*Chlamydia trachomatis* vaccine research through the years." **Infectious diseases in obstetrics and gynecology.** 2011: 963513-963513.
Schindelin, J., Arganda-Carreras, I., Frise, E., et al. (2012). "Fiji - an Open Source platform for biological image analysis." **Nature methods.** 9 (7): 10.1038/nmeth.2019.
Schneider, C. A., Rasband, W. S. and Eliceiri, K. W. (2012). "NIH Image to ImageJ: 25 years of image analysis." **Nat Meth.** 9 (7): 671-675.
Schneider, R., Bannister, A. J., Myers, F. A., et al. (2004). "Histone H3 lysine 4 methylation patterns in higher eukaryotic genes." **Nat Cell Biol.** 6 (1): 73-77.

Schulz, I. (1990). Permeabilizing cells: Some methods and applications for the study of intracellular processes. **Methods in Enzymology**, Academic Press. Volume 192**:** 280-300.

Scidmore, M. A. and Hackstadt, T. (2001). "Mammalian 14-3-3β associates with the *Chlamydia trachomatis* inclusion membrane via its interaction with IncG." **Molecular microbiology.** 39 (6): 1638-1650.

Seshacharyulu, P., Pandey, P., Datta, K., et al. (2013). "Phosphatase: PP2A structural importance, regulation and its aberrant expression in cancer." **Cancer letters.** 335 (1): 9-18.

Sharma, A., Takata, H., Shibahara, K.-i., et al. (2010). "Son is essential for nuclear speckle organization and cell cycle progression." **Molecular Biology of the Cell.** 21 (4): 650-663.

Shilatifard, A. (2006). "Chromatin modifications by methylation and ubiquitination: implications in the regulation of gene expression." **Annual review of biochemistry.** 75 (1): 243-269.

Shinkura, N. and Forrester, W. (2002). "Pushing the envelope: chromatin boundaries at the nuclear pore." **Molecular Cell.** 9 (6): 1156-1158.

Siebenlist, U., Franzoso, G. and Brown, K. (1994). "Structure, regulation and function of NF-kappaB." **Annual review of cell biology.** 10 (1): 405-455.

Silva, J., Cerqueira, F. and Medeiros, R. (2014). "*Chlamydia trachomatis* infection: implications for HPV status and cervical cancer." **Archives of Gynecology and Obstetrics.** 289 (4): 715-723.

Skilton, R. J., Cutcliffe, L. T., Barlow, D., et al. (2009). "Penicillin induced persistence in *Chlamydia trachomatis*: high quality time lapse video analysis of the developmental cycle." **Plos One.** 4 (11): e7723.

Skowasch, D., Yeghiazaryan, K., Schrempf, S., et al. (2003). "Persistence of *Chlamydia pneumoniae* in degenerative aortic valve stenosis indicated by heat shock protein 60 homologues." **The Journal of heart valve disease.** 12 (1): 68-75.

Snavely, E. A., Kokes, M., Dunn, J. D., et al. (2014). "Reassessing the role of the secreted protease CPAF in *Chlamydia trachomatis* infection through genetic approaches." **Pathogens and disease.** 71 (3): 336-351.

Söding, J. (2004). "Protein homology detection by HMM–HMM comparison." **Bioinformatics.** 21 (7): 951-960.

Söding, J. (2005). "Protein homology detection by HMM-HMM comparison." **Bioinformatics.** 21 (7): 951-960.

Söding, J., Biegert, A. and Lupas, A. (2005). "The HHpred interactive server for protein homology detection and structure prediction." **Nucleic acids research.** 33 (Web Server issue): 8.

Söding, J., Biegert, A. and Lupas, A. N. (2005). "The HHpred interactive server for protein homology detection and structure prediction." **Nucleic acids research.** 33 (Web Server issue): W244-W248.

Solovei, I., Wang, Audrey S., Thanisch, K., et al. (2013). "LBR and lamin A/C sequentially tether peripheral heterochromatin and inversely regulate differentiation." **Cell.** 152 (3): 584-598.

Sosa, B. A., Rothballer, A., Kutay, U., et al. (2012). "LINC complexes form by binding of three KASH peptides to the interfaces of trimeric SUN proteins." **Cell.** 149 (5): 1035-1047.

Spector, D. and Lamond, A. (2011). "Nuclear speckles." **Cold Spring Harbor perspectives in biology.** 3 (2).

Spector, D. L. (1993). "Macromolecular domains within the cell nucleus." **Annual review of cell biology.** 9: 265-315.

Spector, D. L. (1993). "Nuclear organization of pre-mRNA processing." **Current Opinion in Cell Biology.** 5 (3): 442-447.

Spector, D. L., Fu, X. D. and Maniatis, T. (1991). "Associations between distinct pre-mRNA splicing components and the cell nucleus." **The EMBO journal.** 10 (11): 3467-3481.
Sperschneider, J., Gardiner, D. M., Dodds, P. N., et al. (2015). "EffectorP: predicting fungal effector proteins from secretomes using machine learning." **New Phytologist.** 210 (2): 743-761.
Stamm, W. E. (1999). "*Chlamydia trachomatis* infections: progress and problems." **The Journal of infectious diseases.** 179 Suppl 2: S380-S383.
Starr, D. A. and Fridolfsson, H. N. (2010). "Interactions between nuclei and the cytoskeleton are mediated by SUN-KASH nuclear envelope bridges." **Annual review of cell and developmental biology.** 26: 421-444.
Stavru, F., Nautrup-Pedersen, G., Cordes, V. C., et al. (2006). "Nuclear pore complex assembly and maintenance in POM121-and gp210-deficient cells." **The Journal of cell biology.** 173 (4): 477-483.
Stebbins, C. E. and Galan, J. E. (2001). "Structural mimicry in bacterial virulence." **Nature.** 412 (6848): 701-705.
Stebbins, C. E. and Galán, J. E. (2000). "Modulation of host signaling by a bacterial mimic: structure of the Salmonella effector SptP bound to Rac1." **Molecular Cell.** 6 (6): 1449-1460.
Stephens, R., Myers, G., Eppinger, M., et al. (2009). "Divergence without difference: phylogenetics and taxonomy of *Chlamydia* resolved." **FEMS immunology and medical microbiology.** 55 (2): 115-119.
Stephens, R. S., Kalman, S., Lammel, C., et al. (1998). "Genome sequence of an obligate intracellular pathogen of humans: *Chlamydia trachomatis*." **Science.** 282 (5389): 754-759.
Strambio-De-Castillia, C., Niepel, M. and Rout, M. P. (2010). "The nuclear pore complex: bridging nuclear transport and gene regulation." **Nat Rev Mol Cell Biol.** 11 (7): 490-501.
Subtil, A., Wyplosz, B., Balañá, M. E., et al. (2004). "Analysis of *Chlamydia caviae* entry sites and involvement of Cdc42 and Rac activity." **Journal of Cell Science.** 117 (17): 3923-3933.
Suchland, R. J., Rockey, D. D., Bannantine, J. P., et al. (2000). "Isolates of *Chlamydia trachomatis* that occupy nonfusogenic inclusions lack IncA, a protein localized to the inclusion membrane." **Infection and immunity.** 68 (1): 360-367.
Sullivan, T., Escalante-Alcalde, D., Bhatt, H., et al. (1999). "Loss of A-type lamin expression compromises nuclear envelope integrity leading to muscular dystrophy." **The Journal of cell biology.** 147 (5): 913-920.
Sun, H. S., Sin, A. T. W., Poirier, M. B., et al. (2016). "*Chlamydia trachomatis* inclusion disrupts host cell cytokinesis to enhance its growth in multinuclear cells." **Journal of Cellular Biochemistry.** 117 (1): 132-143.
Sun, H. S., Wilde, A. and Harrison, R. E. (2011). "*Chlamydia trachomatis* inclusions induce asymmetric cleavage furrow formation and ingression failure in host cells." **Molecular and Cellular Biology.** 31 (24): 5011-5022.
Szymborska, A., de Marco, A., Daigle, N., et al. (2013). "Nuclear pore scaffold structure analyzed by super-resolution microscopy and particle averaging." **Science.** 341 (6146): 655-658.
Takahashi, A., Alnemri, E. S., Lazebnik, Y. A., et al. (1996). "Cleavage of lamin A by Mch2 alpha but not CPP32: multiple interleukin 1 beta-converting enzyme-related proteases with distinct substrate recognition properties are active in apoptosis." **Proceedings of the National Academy of Sciences of the United States of America.** 93 (16): 8395-8400.
Takeuchi, O. and Akira, S. (2010). "Pattern recognition receptors and inflammation." **Cell.** 140 (6): 805-820.

Tan-Wong, S., Wijayatilake, H. and Proudfoot, N. (2009). "Gene loops function to maintain transcriptional memory through interaction with the nuclear pore complex." **Genes & development.** 23 (22): 2610-2624.

Tan Wong, S., Wijayatilake, H. and Proudfoot, N. (2009). "Gene loops function to maintain transcriptional memory through interaction with the nuclear pore complex." **Genes & development.** 23 (22): 2610-2624.

Taylor Robinson, D. and Thomas, B. J. (1980). "The role of *Chlamydia trachomatis* in genital-tract and associated diseases." **Journal of Clinical Pathology.** 33 (3): 205-233.

Tessarz, P. and Kouzarides, T. (2014). "Histone core modifications regulating nucleosome structure and dynamics." **Nat Rev Mol Cell Biol.** 15 (11): 703-708.

Thalmann, J., Janik, K., May, M., et al. (2010). "Actin re-organization induced by *Chlamydia trachomatis* Serovar D - evidence for a critical role of the effector protein CT166 targeting Rac." **Plos One.** 5 (3): e9887.

Tjaden, J., Winkler, H. H., Schwöppe, C., et al. (1999). "Two nucleotide transport proteins in *Chlamydia trachomatis*, one for net nucleoside triphosphate uptake and the other for transport of energy." **Journal of Bacteriology.** 181 (4): 1196-1202.

Towbin, Benjamin D., González-Aguilera, C., Sack, R., et al. (2012). "Step-wise methylation of histone H3K9 positions heterochromatin at the nuclear periphery." **Cell.** 150 (5): 934-947.

Towbin, B. D., Gonzalez-Sandoval, A. and Gasser, S. M. (2013). "Mechanisms of heterochromatin subnuclear localization." **Trends in Biochemical Sciences.** 38 (7): 356-363.

Tucker, K. E., Berciano, M. T., Jacobs, E. Y., et al. (2001). "Residual Cajal bodies in coilin knockout mice fail to recruit Sm snRNPs and SMN, the spinal muscular atrophy gene product." **The Journal of cell biology.** 154 (2): 293-308.

Tzur, Y. B., Wilson, K. L. and Gruenbaum, Y. (2006). "SUN-domain proteins: 'Velcro' that links the nucleoskeleton to the cytoskeleton." **Nat Rev Mol Cell Biol.** 7 (10): 782-788.

Vaquerizas, J. M., Suyama, R., Kind, J., et al. (2010). "Nuclear pore proteins Nup153 and megator define transcriptionally active regions in the *Drosophila* genome." **PLoS Genetics.** 6 (2): e1000846.

Verbeke, P., Welter-Stahl, L., Ying, S., et al. (2006). "Recruitment of BAD by the *Chlamydia trachomatis* vacuole correlates with host-cell survival." **PLoS Pathogens.** 2 (5): e45.

Vidak, S., Kubben, N., Dechat, T., et al. (2015). "Proliferation of progeria cells is enhanced by lamina-associated polypeptide 2α (LAP2α) through expression of extracellular matrix proteins." **Genes & development.** 29 (19): 2022-2036.

von Moeller, H., Basquin, C. and Conti, E. (2009). "The mRNA export protein DBP5 binds RNA and the cytoplasmic nucleoporin NUP214 in a mutually exclusive manner." **Nature structural & molecular biology.** 16 (3): 247-254.

Vorburger, K., Lehner, C. F., Kitten, G. T., et al. (1989). "A second higher vertebrate B-type lamin." **Journal of molecular biology.** 208 (3): 405-415.

Voulhoux, R., Ball, G., Ize, B., et al. (2001). "Involvement of the twin-arginine translocation system in protein secretion via the type II pathway." **The EMBO journal.** 20 (23): 6735-6741.

Voulhoux, R., Taupiac, M.-P., Czjzek, M., et al. (2000). "Influence of deletions within domain II of exotoxin A on its extracellular secretion from *Pseudomonas aeruginosa*." **Journal of Bacteriology.** 182 (14): 4051-4058.

Walde, S. and Kehlenbach, R. (2010). "The part and the whole: functions of nucleoporins in nucleocytoplasmic transport." **Trends in Cell Biology.** 20 (8): 461-469.

Waldron-Roby, E., Hoerauf, J., Arbez, N., et al. (2015). "Sox11 Reduces Caspase-6 Cleavage and Activity." **Plos One.** 10 (10): e0141439.

Walther, T. C. and Farese, R. V. (2012). "Lipid droplets and cellular lipid metabolism." **Annual review of biochemistry.** 81: 687-714.

Wang, H., Wang, L., Erdjument-Bromage, H., et al. (2004). "Role of histone H2A ubiquitination in Polycomb silencing." **Nature.** 431 (7010): 873-878.
Wang, Y., Kahane, S., Cutcliffe, L. T., et al. (2011). "Development of a transformation system for *Chlamydia trachomatis*: restoration of glycogen biosynthesis by acquisition of a plasmid shuttle vector." **PLoS Pathogens.** 7 (9): e1002258.
Wang, Y., Sun, M. a., Bao, H., et al. (2013). "Effective identification of bacterial type III secretion signals using joint element features." **Plos One.** 8 (4): e59754.
Wang, Y., Zhang, Q., Sun, M.-a., et al. (2011). "High-accuracy prediction of bacterial type III secreted effectors based on position-specific amino acid composition profiles." **Bioinformatics.** 27 (6): 777-784.
Weber, M. M., Bauler, L. D., Lam, J., et al. (2015). "Expression and Localization of Predicted Inclusion Membrane Proteins in Chlamydia trachomatis." **Infection and immunity.** 83 (12): 4710-4718.
Weber, M. M., Noriea, N. F., Bauler, L. D., et al. (2016). "A functional core of IncA is required for *Chlamydia trachomatis* inclusion fusion." **Journal of Bacteriology.** 198 (8): 1347-1355.
Webster, M., Witkin, K. L. and Cohen-Fix, O. (2009). "Sizing up the nucleus: nuclear shape, size and nuclear-envelope assembly." **Journal of Cell Science.** 122 (10): 1477-1486.
White, J. (2009). "Manifestations and management of lymphogranuloma venereum." **Current opinion in infectious diseases.** 22 (1): 57-66.
Wickramasinghe, V. O., McMurtrie, P. I. A., Mills, A. D., et al. (2010). "mRNA export from mammalian cell nuclei Is dependent on GANP." **Current Biology.** 20 (1): 25-31.
Wickstrum, J., Sammons, L. R., Restivo, K. N., et al. (2013). "Conditional gene expression in *Chlamydia trachomatis* using the Tet system." **Plos One.** 8 (10): e76743.
Wilson, D. P., Timms, P., Mcelwain, D. L. S., et al. (2006). "Type III secretion, contact-dependent model for the intracellular development of *Chlamydia*." **Bulletin of Mathematical Biology.** 68 (1): 161-178.
Wilson, D. P., Whittum-Hudson, J. A., Timms, P., et al. (2009). "Kinematics of intracellular *Chlamydiae* provide evidence for contact-dependent development." **Journal of Bacteriology.** 191 (18): 5734-5742.
Wilson, K. L. and Foisner, R. (2010). "Lamin-binding proteins." **Cold Spring Harbor perspectives in biology.** 2 (4): a000554.
Winstanley, C. and Hart, C. A. (2001). "Type III secretion systems and pathogenicity islands." **Journal of medical microbiology.** 50 (2): 116-126.
Wolf, K., Betts, H. J., Chellas-Géry, B., et al. (2006). "Treatment of *Chlamydia trachomatis* with a small molecule inhibitor of the Yersinia type III secretion system disrupts progression of the chlamydial developmental cycle." **Molecular microbiology.** 61 (6): 1543-1555.
Wooten-Blanks, L. G., Song, P., Senkal, C. E., et al. (2007). "Mechanisms of ceramide-mediated repression of the human telomerase reverse transcriptase promoter via deacetylation of Sp3 by histone deacetylase 1." **The FASEB Journal.** 21 (12): 3386-3397.
Wu, X., Lei, L., Gong, S., et al. (2011). "The chlamydial periplasmic stress response serine protease cHtrA is secreted into host cell cytosol." **BMC Microbiology.** 11: 87-87.
Wu, Z., Wu, L., Weng, D., et al. (2009). "Reduced expression of lamin A/C correlates with poor histological differentiation and prognosis in primary gastric carcinoma." **Journal of Experimental & Clinical Cancer Research.** 28 (1): 1-12.
Wyrick, P. and Bavoil, P. (2006). *Chlamydia* Genomic and Pathogenesis, **Horizon Bioscience.**
Ying, S., Seiffert, B. M., Häcker, G., et al. (2005). "Broad degradation of proapoptotic proteins with the conserved Bcl-2 homology domain 3 during infection with *Chlamydia trachomatis*." **Infection and immunity.** 73 (3): 1399-1403.
Yu, H., Schwarzer, K., Förster, M., et al. (2010). "Role of high-mobility group box 1 protein and poly(ADP-Ribose) polymerase 1 degradation in *Chlamydia trachomatis*-induced cytopathicity." **Infection and immunity.** 78 (7): 3288-3297.

Zeidler, H. and Hudson, A. (2014). "New insights into *Chlamydia* and arthritis. Promise of a cure?" **Annals of the Rheumatic Diseases.** 73 (4): 637-644.

Zhang, J. P. and Stephens, R. S. (1992). "Mechanism of *C. trachomatis* attachment to eukaryotic host cells." **Cell.** 69 (5): 861-869.

Zhong, G., Fan, T. and Liu, L. (1999). "*Chlamydia* inhibits interferon γ–inducible major histocompatibility complex class II expression by degradation of upstream stimulatory factor 1." **The Journal of Experimental Medicine.** 189 (12): 1931-1938.

Zhong, G., Liu, L., Fan, T., et al. (2000). "Degradation of transcription factor Rfx5 during the inhibition of both constitutive and interferon γ–inducible major histocompatibility complex class I expression in *Chlamydia*-infected cells." **The Journal of Experimental Medicine.** 191 (9): 1525-1534.

Zöllner, B., Feucht, H. H., Laufs, R., et al. (1993). "Isolation of *Chlamydia trachomatis* from the lower digestive tract." **Infection.** 21 (5): 318-320.

Zullo, Joseph M., Demarco, Ignacio A., Piqué-Regi, R., et al. (2012). "DNA sequence-dependent compartmentalization and silencing of chromatin at the nuclear lamina." **Cell.** 149 (7): 1474-1487.